

University of Windsor

Scholarship at UWindsor

Electronic Theses and Dissertations

Theses, Dissertations, and Major Papers

1994

Thermal analysis and bearing capacity of piles embedded in frozen uniform soils

Issa F. Assali
University of Windsor

Follow this and additional works at: <https://scholar.uwindsor.ca/etd>

Recommended Citation

Assali, Issa F., "Thermal analysis and bearing capacity of piles embedded in frozen uniform soils" (1994).
Electronic Theses and Dissertations. 4371.
<https://scholar.uwindsor.ca/etd/4371>

This online database contains the full-text of PhD dissertations and Masters' theses of University of Windsor students from 1954 forward. These documents are made available for personal study and research purposes only, in accordance with the Canadian Copyright Act and the Creative Commons license—CC BY-NC-ND (Attribution, Non-Commercial, No Derivative Works). Under this license, works must always be attributed to the copyright holder (original author), cannot be used for any commercial purposes, and may not be altered. Any other use would require the permission of the copyright holder. Students may inquire about withdrawing their dissertation and/or thesis from this database. For additional inquiries, please contact the repository administrator via email (scholarship@uwindsor.ca) or by telephone at 519-253-3000ext. 3208.



National Library
of Canada

Bibliothèque nationale
du Canada

Acquisitions and
Bibliographic Services Branch

Direction des acquisitions et
des services bibliographiques

395 Wellington Street
Ottawa, Ontario
K1A 0N4

395, rue Wellington
Ottawa (Ontario)
K1A 0N4

Your file *Votre référence*

Our file *Notre référence*

NOTICE

AVIS

The quality of this microform is heavily dependent upon the quality of the original thesis submitted for microfilming. Every effort has been made to ensure the highest quality of reproduction possible.

La qualité de cette microforme dépend grandement de la qualité de la thèse soumise au microfilmage. Nous avons tout fait pour assurer une qualité supérieure de reproduction.

If pages are missing, contact the university which granted the degree.

S'il manque des pages, veuillez communiquer avec l'université qui a conféré le grade.

Some pages may have indistinct print especially if the original pages were typed with a poor typewriter ribbon or if the university sent us an inferior photocopy.

La qualité d'impression de certaines pages peut laisser à désirer, surtout si les pages originales ont été dactylographiées à l'aide d'un ruban usé ou si l'université nous a fait parvenir une photocopie de qualité inférieure.

Reproduction in full or in part of this microform is governed by the Canadian Copyright Act, R.S.C. 1970, c. C-30, and subsequent amendments.

La reproduction, même partielle, de cette microforme est soumise à la Loi canadienne sur le droit d'auteur, SRC 1970, c. C-30, et ses amendements subséquents.

Canada

**THERMAL ANALYSIS AND BEARING CAPACITY
OF PILES EMBEDDED IN FROZEN
UNIFORM SOILS**

by

Issa F. Assali

**A Thesis
submitted to the Faculty of Graduate Studies and Research through
the Department of Civil and Environmental Engineering
in Partial Fulfilment of the Requirements for the
degree of Master of Applied Science at the
University of Windsor**

**Windsor, Ontario, Canada
1994**



National Library
of Canada

Acquisitions and
Bibliographic Services Branch

395 Wellington Street
Ottawa, Ontario
K1A 0N4

Bibliothèque nationale
du Canada

Direction des acquisitions et
des services bibliographiques

395, rue Wellington
Ottawa (Ontario)
K1A 0N4

Your file *Votre référence*

Our file *Notre référence*

THE AUTHOR HAS GRANTED AN IRREVOCABLE NON-EXCLUSIVE LICENCE ALLOWING THE NATIONAL LIBRARY OF CANADA TO REPRODUCE, LOAN, DISTRIBUTE OR SELL COPIES OF HIS/HER THESIS BY ANY MEANS AND IN ANY FORM OR FORMAT, MAKING THIS THESIS AVAILABLE TO INTERESTED PERSONS.

L'AUTEUR A ACCORDE UNE LICENCE IRREVOCABLE ET NON EXCLUSIVE PERMETTANT A LA BIBLIOTHEQUE NATIONALE DU CANADA DE REPRODUIRE, PRETER, DISTRIBUER OU VENDRE DES COPIES DE SA THESE DE QUELQUE MANIERE ET SOUS QUELQUE FORME QUE CE SOIT POUR METTRE DES EXEMPLAIRES DE CETTE THESE A LA DISPOSITION DES PERSONNE INTERESSEES.

THE AUTHOR RETAINS OWNERSHIP OF THE COPYRIGHT IN HIS/HER THESIS. NEITHER THE THESIS NOR SUBSTANTIAL EXTRACTS FROM IT MAY BE PRINTED OR OTHERWISE REPRODUCED WITHOUT HIS/HER PERMISSION.

L'AUTEUR CONSERVE LA PROPRIETE DU DROIT D'AUTEUR QUI PROTEGE SA THESE. NI LA THESE NI DES EXTRAITS SUBSTANTIELS DE CELLE-CI NE DOIVENT ETRE IMPRIMES OU AUTREMENT REPRODUITS SANS SON AUTORISATION.

ISBN 0-612-01385-5

Canada

Name ISSA FAWZI ASSALI

Dissertation Abstracts International is arranged by broad, general subject categories. Please select the one subject which most nearly describes the content of your dissertation. Enter the corresponding four-digit code in the spaces provided.

CIVIL ENGINEERING

SUBJECT TERM

0543

U-M-I

SUBJECT CODE

Subject Categories

THE HUMANITIES AND SOCIAL SCIENCES

COMMUNICATIONS AND THE ARTS	
Architecture	0729
Art History	0377
Cinema	0900
Dance	0378
Fine Arts	0357
Information Science	0723
Journalism	0391
Library Science	0399
Mass Communications	0708
Music	0413
Speech Communication	0459
Theater	0465
EDUCATION	
General	0515
Administration	0514
Adult and Continuing	0516
Agricultural	0517
Art	0273
Bilingual and Multicultural	0282
Business	0688
Community College	0275
Curriculum and Instruction	0727
Early Childhood	0518
Elementary	0524
Finance	0277
Guidance and Counseling	0519
Health	0680
Higher	0745
History of	0520
Home Economics	0278
Industrial	0521
Language and Literature	0279
Mathematics	0280
Music	0522
Philosophy of	0998
Physical	0523

Psychology	0525
Reading	0535
Religious	0527
Sciences	0714
Secondary	0533
Social Sciences	0534
Sociology of	0340
Special	0529
Teacher Training	0530
Technology	0710
Tests and Measurements	0288
Vocational	0747

LANGUAGE, LITERATURE AND LINGUISTICS

Language	
General	0679
Ancient	0289
Linguistics	0290
Modern	0291
Literature	
General	0401
Classical	0294
Comparative	0295
Medieval	0297
Modern	0298
African	0316
American	0591
Asian	0305
Canadian (English)	0352
Canadian (French)	0355
English	0593
Germanic	0311
Latin American	0312
Middle Eastern	0315
Romance	0313
Slavic and East European	0314

PHILOSOPHY, RELIGION AND THEOLOGY

Philosophy	0422
Religion	
General	0318
Biblical Studies	0321
Clergy	0319
History of	0320
Philosophy of	0322
Theology	0469

SOCIAL SCIENCES

American Studies	0323
Anthropology	
Archaeology	0324
Cultural	0326
Physical	0327
Business Administration	
General	0310
Accounting	0272
Banking	0770
Management	0454
Marketing	0338
Canadian Studies	0385
Economics	
General	0501
Agricultural	0503
Commerce-Business	0505
Finance	0508
History	0509
Labor	0510
Theory	0511
Folklore	0358
Geography	0366
Gerontology	0351
History	
General	0578

Ancient	0579
Medieval	0581
Modern	0582
Black	0328
African	0331
Asia, Australia and Oceania	0332
Canadian	0334
European	0335
Latin American	0336
Middle Eastern	0333
United States	0337
History of Science	0585
Law	0398
Political Science	
General	0615
International Law and Relations	0616
Public Administration	0617
Recreation	0814
Social Work	0452
Sociology	
General	0626
Criminology and Penology	0627
Demography	0938
Ethnic and Racial Studies	0631
Individual and Family Studies	0628
Industrial and Labor Relations	0629
Public and Social Welfare	0630
Social Structure and Development	0700
Theory and Methods	0344
Transportation	0709
Urban and Regional Planning	0999
Women's Studies	0453

THE SCIENCES AND ENGINEERING

BIOLOGICAL SCIENCES

Agriculture	
General	0473
Agronomy	0285
Animal Culture and Nutrition	0475
Animal Pathology	0476
Food Science and Technology	0359
Forestry and Wildlife	0478
Plant Culture	0479
Plant Pathology	0480
Plant Physiology	0817
Range Management	0777
Wood Technology	0746
Biology	
General	0306
Anatomy	0287
Biostatistics	0308
Botany	0309
Cell	0379
Ecology	0329
Entomology	0353
Genetics	0369
Limnology	0793
Microbiology	0410
Molecular	0307
Neuroscience	0317
Oceanography	0416
Physiology	0433
Radiation	0821
Veterinary Science	0778
Zoology	0472
Biophysics	
General	0786
Medical	0760
EARTH SCIENCES	
Biogeochemistry	0425
Geochemistry	0996

Geodesy	0370
Geology	0372
Geophysics	0373
Hydrology	0388
Mineralogy	0411
Paleobotany	0345
Paleoecology	0426
Paleontology	0418
Paleozoology	0985
Palynology	0427
Physical Geography	0368
Physical Oceanography	0415

HEALTH AND ENVIRONMENTAL SCIENCES

Environmental Sciences	0768
Health Sciences	
General	0566
Audiology	0300
Chemotherapy	0992
Dentistry	0567
Education	0350
Hospital Management	0769
Human Development	0758
Immunology	0982
Medicine and Surgery	0564
Mental Health	0347
Nursing	0569
Nutrition	0570
Obstetrics and Gynecology	0380
Occupational Health and Therapy	0354
Ophthalmology	0381
Pathology	0571
Pharmacology	0419
Pharmacy	0572
Physical Therapy	0382
Public Health	0573
Radiology	0574
Recreation	0575

Speech Pathology	0460
Toxicology	0383
Home Economics	0386

PHYSICAL SCIENCES

Pure Sciences	
Chemistry	
General	0485
Agricultural	0749
Analytical	0486
Biochemistry	0487
Inorganic	0488
Nuclear	0738
Organic	0490
Pharmaceutical	0491
Physical	0494
Polymer	0495
Radiation	0754
Mathematics	0405
Physics	
General	0605
Acoustics	0986
Astronomy and Astrophysics	0606
Atmospheric Science	0608
Atomic	0748
Electronics and Electricity	0607
Elementary Particles and High Energy	0798
Fluid and Plasma	0759
Molecular	0609
Nuclear	0610
Optics	0752
Radiation	0756
Solid State	0611
Statistics	0463
Applied Sciences	
Applied Mechanics	0346
Computer Science	0984

Engineering	
General	0537
Aerospace	0538
Agricultural	0539
Automotive	0540
Biomedical	0541
Chemical	0542
Civil	0543
Electronics and Electrical	0544
Heat and Thermodynamics	0348
Hydraulic	0545
Industrial	0546
Marine	0547
Materials Science	0794
Mechanical	0548
Metallurgy	0743
Mining	0551
Nuclear	0552
Packaging	0549
Petroleum	0765
Sanitary and Municipal	0554
System Science	0790
Geotechnology	0428
Operations Research	0796
Plastics Technology	0795
Textile Technology	0994

PSYCHOLOGY

General	0621
Behavioral	0384
Clinical	0622
Developmental	0620
Experimental	0623
Industrial	0624
Personality	0625
Physiological	0989
Psychobiology	0349
Psychometrics	0632
Social	0451



© ————— 1994
Issa F. Assali
All Rights Reserved

Approved by:

W. J. ...

R. ...

M. C. Temple

G. Abdul-Samed

I hereby declare that I am the sole author of this document.

I authorize the University of Windsor to lend this document to other institutions or individuals for the purpose of scholarly research.

Issa F. Assali

I further authorize the University of Windsor to reproduce the document by photocopying or by other means, in total or in part, at the request of other institutions or individuals for the purpose of scholarly research.

Issa F. Assali

THE UNIVERSITY OF WINDSOR requires the signatures of all persons using or photocopying this document.

Please sign below, and give address and date.

ABSTRACT

The objective of this research is the analysis of propagation of the thawing front in frozen soils induced by the periodical change of temperature acting on the top boundaries. This problem appears to be important in determination of the maximum depth of thawing zone arising around the piles. The negligence of the thawing depth in analysis of deep foundations embedded in frozen soils leads to excessive settlements and finally can result in very costly repairs of the structures. Consequently, this problem is very important in calculations of the bearing capacity of the piles supporting various structures (e.g. bridge structures). Where piles are installed in frozen soil, a bond is developed between the pile and frozen earth at the ground surface, transferring uplift forces to the pile.

The formulation of the heat transfer problem including phase change for fixed domain is based on the law of conservation of energy. This law determines the weak form of the problem including all possible thermal boundary conditions. With respect to time variables, the incremental decomposition concept is used. The finite element method is used with respect to spatial variables. Integration with respect to time is obtained by the application of the Euler backward scheme. In order to increase the accuracy of the solution, the Newton-Raphson equilibrium iterations are used at each time step.

The term connected with phase change on the moving boundary is treated in a special way. The moving phase-change interface is simulated by curvilinear finite

element intersecting the original finite element in arbitrary fashion. The proposed numerical algorithm enables one to analyze multi-phase media with appearing and disappearing phases. Several modelling problems dealing with evolution of the thawing depth around pile embedded in frozen soil are presented and discussed.

A comparative analysis with the theoretical equation formulated by Franz Neumann and modified by Nixon and McRoberts is conducted. The comparative analysis shows the differences between the numerical solution and the existing one-dimensional problem.

After the determination of the maximum depth of thaw defining the active layer, uplift or heaving forces that result from adfreezing on deep foundation in frozen soil are investigated. Laboratory experiments are conducted to estimate the adfreeze bond strength at the side of a pile in contact with a soil sample. A graphical solution using the output data of each sample, in terms of loads and displacements, and curves of τ_a versus displacement are presented. Then, τ_a is plotted as a function of temperature for a fixed water content for each sample. These curves will serve later to determine the bearing capacity of the pile embedded in sand, clay, and peat for both summer and winter conditions. A design method to solve for the governing condition is presented and a discussion on the complexity of the solution involving the crucial effect of the uplift heaving forces on winter conditions, is carried out.

Finally, a conclusion will summarize the various aspects of the thermal and physical properties of the soil and their interbalancing effects to design a pile embedded in frozen soil.

TO MY MOTHER, MARGUERITE
&
MY BROTHER, CHARBEL, IN BELGIUM

ACKNOWLEDGEMENTS

The author wishes to express his deep sincere thanks to his advisor, *Dr. Barbara Budkowska* for her continuous support, encouragement and valuable recommendations without which this work would have not been accomplished.

The author also wishes to thank the civil engineering faculty members and staff.

Special thanks are due to *Mr. Richard Clark* and *Mr. Greg Kuhun* for their technical help and assistance during the experimental laboratory work of this study. The author is also grateful to *Mrs. Noran Eissa* for her help during the editorial phase of this study.

Finally, the financial support provided by the Natural Sciences and Engineering Research Council of Canada (NSERC) is gratefully acknowledged.

TABLE OF CONTENTS

ABSTRACT	vi
ACKNOWLEDGEMENTS	ix
LIST OF TABLES	xv
LIST OF FIGURES	xvii
NOMENCLATURE	xxvi

CHAPTER

I- INTRODUCTION	1
II- MECHANISMS OF HEAT TRANSFER IN SOILS	6
2.1 Introduction	6
2.2 Thermal Properties of Soil	7
2.2.1 Thermal Conductivity	7
2.2.2 Heat Capacity	10
2.2.3 Thermal Diffusivity	11
2.2.4 Latent Heat in Soils	12
2.2.5 Enthalpy and Heat Capacity	13
2.3 Thermal Analysis	15
2.3.1 Thermal Conduction	16
2.3.2 Convective Heat Transfer in Soil	17
2.3.3 Radiations in Soils	18
2.4 Neumann Problem Considerations	20
III- HEAT TRANSFER WITH PHASE CHANGE IN SOILS	25
3.1 Literature Review	25

3.2	Strong Formulation of Heat Transfer Problem with Phase Change	29
3.3	Boundary Conditions	32
3.3.1	Temperature Boundary Conditions	32
3.3.2	Heat Flow Boundary Conditions	32
3.3.3	Convective Boundary Conditions	33
3.3.4	Phase Change Interface Conditions	33
3.4	Integral Formulation Employing the Energy Conservation Equation	34
3.5	The Weighted Residual Method as an Approximation to Integral Formulation	38
3.6	Implicit Time Integration	40
3.7	Numerical Strategy to Include Latent Heat Term and Temperature Dependent Material Properties	46
IV-	MODELLING PROBLEMS AND RESULTS	48
4.1	Numerical Assumptions and Configurations	48
4.2	Modelling of Geotechnical Problems	50
4.2.1	Global Numerical Assumptions	50
4.2.2	Results Presentation and Observation	52
4.3	Problem # 1, Pile in Sandy Soil	54
4.3.1	Neumann Solution for Sand with $w = 15\%$	55
4.3.2	Neumann Solution for Sand with $w = 20\%$	57
4.4	Problem # 2, Pile in Clayey Soil	58
4.4.1	Neumann Solution for Clay with $w = 15\%$	59
4.4.2	Neumann Solution for Clay with $w = 30\%$	60
4.5	Problem # 3, Pile in Peat Soil	61
4.5.1	Neumann Solution for Peat with $w = 80\%$	62
4.5.2	Neumann Solution for Peat with $w = 120\%$	63
4.6	Problem # 4 Pile in Sandy Soil with Gravel on Top	63
4.6.1	Observations and Conclusions	64
4.6.2	Neumann Problem for Sand with Gravel on Top	65
4.7	Problem # 5 Pile in Clayey Soil with Gravel on Top	67
4.7.1	Neumann Problem for Clay with Gravel on Top	67
4.8	Problem # 6 Pile in Peat Soil with Gravel on Top	69
4.8.1	General Observations	69
4.8.2	Neumann Problem for Peat with Gravel on Top	70
V-	FROST ACTIONS AND FOUNDATIONS	73

5.1	Introduction	73
5.2	Frost Action Process	74
5.3	Frost-Heaving Forces on Foundations	75
5.4	Frost Heave and Adfreezing Forces	76
5.5	Experimental Studies Using Sand, Peat and Clay	77
5.6	Control of Frost Heave	78
VI-	PILE FOUNDATION AND ADFREEZE SHEAR STRENGTH	80
6.1	Introduction	80
6.2	Pile Types	81
6.2.1	Timber Piles	81
6.2.2	Steel Piles	82
6.2.3	Concrete Piles	82
6.3	Installation of Piles	83
6.4	Design for Vertical Loads	84
6.4.1	Adfreeze Strength and Pile Capacity	84
6.4.2	Experimental Procedure	86
6.4.2.1	Pertinent Factors Affecting Pile Capacity	87
A-	Effect of Soil Temperature	87
B-	Effects of Pile Surface and Size	88
C-	Effect of Soil Water Content	89
6.4.2.2	Testing Procedure	90
6.4.2.3	Soil Description	91
6.4.3	Experimental Results	93
6.4.3.1	General	93
6.4.3.2	Effect of Temperature and Water Content on Adfreeze Strength	94
6.4.3.3	Pile Performance and Adfreeze Strength	97
VII-	BEARING CAPACITY OF PILES EMBEDDED IN FROZEN SOIL	99
7.1	Introduction	99
7.2	Summer Conditions	100
7.3	Pile Embedded in Sand	101
7.3.1	Problem 1 a	103
7.3.2	Problem 2 a	104
7.4	Pile Embedded in Clay	106
7.4.1	Problem 3 a	108

7.4.2 Problem 4 a	110
7.5 Pile in Peat Soil	111
7.5.1 Problem 5 a	111
7.5.2 Problem 6 a	112
7.6 Determination of the Bearing Capacity of the Pile for Winter Condition	113
7.6.1 Ultimate Capacity with Heave Considered in the Active Layer	114
7.6.2 Ultimate Capacity without Heave Considered in the Active Layer	116
7.7 Problem 1.b	116
7.7.1 Case 1: Heave is Considered in the Analysis	117
7.7.2 Case 2: Heave is Neglected in the Analysis	117
7.8 Problem 2.b	118
7.8.1 Case 1: Heave is Considered in the Analysis	118
7.8.2 Case 2: Heave is Neglected in the Analysis	119
7.9 Problem 3.b	120
7.9.1 Case 1: Heave is Considered in the Analysis	120
7.9.2 Case 2: Heave is Neglected in the Analysis	121
7.10 Problem 4.b	121
7.10.1 Case 1: Heave is Considered in the Analysis	121
7.10.2 Case 2: Heave is Neglected in the Analysis	122
7.11 Problem 5.b	123
7.11.1 Case 1: Heave is Considered in the Analysis	123
7.11.2 Case 2: Heave is Neglected in the Analysis	126
7.12 Problem 6.b	124
7.12.1 Case 1: Heave is Considered in the Analysis	124
7.12.2 Case 2: Heave is Neglected in the Analysis	126
7.13 Determination of the Design Load Capacity of Pile Embedded in Soil	126
7.13.1 Definitions and Assumptions	126
A- Heave Force	127
B- Suppression of Heave	127
7.13.2 Problem 7	130
A- Sand with Water Content, $w = 15\%$	131
B- Sand with Water Content, $w = 20\%$	133
7.13.3 Problem 8	134
7.13.4 Problem 9	136
7.14 Summary	138

VIII- SUMMARY, CONCLUSIONS AND RECOMMENDATIONS	140
8.1 Summary	143
8.2 Conclusions	142
8.3 Recommendations for Further Research	147
TABLES	148
FIGURES	175
REFERENCES	322
VITA AUCTORIS	328

LIST OF TABLES

<u>Table</u>	<u>Page</u>
2.1 Thermal Conductivity for Sand	148
2.2 Thermal Conductivity for Clay	149
2.3 Thermal Conductivity for Peat	150
2.4 Volumetric Heat Capacity for Sand	151
2.5 Volumetric Heat Capacity for Clay	152
2.6 Volumetric Heat Capacity for Peat	153
2.7 Thermal Properties of Common Materials	154
2.8 Volumetric Latent Heat in Soil: A- for sand and Clay B- for Peat	155
4.1 Comparative Analysis for Sand with $w = 15\%$	156
4.2 Comparative Analysis for Sand with $w = 20\%$	157
4.3 Comparative Analysis for Clay with $w = 15\%$	158
4.4 Comparative Analysis for Clay with $w = 30\%$	159
4.5 Comparative Analysis for Peat with $w = 80\%$	160
4.6 Comparative Analysis for Peat with $w = 120\%$	161
4.7 Comparative Analysis for Sand with Gravel on Top, Sand Water Content, $w = 20\%$	162
4.8 Comparative Analysis for Clay with Gravel on Top, Clay Water Content, $w = 30\%$	163
4.9 Comparative Analysis for Peat with Gravel on Top, Peat Water Content, $w = 120\%$	164

6.1	Nomenclature for Experimental Procedure	165
6.2	Summary for Experimental Results	166
7.1	Pile Capacity in Sand for Summer Condition	167
7.2	Pile Capacity in Clay for Summer Condition	168
7.3	Pile Capacity in Peat for Summer Condition	169
7.4	The Results of Bearing Capacity Analysis for Summer Condition (August 20)	170
7.5	Pile Capacity in Sand for Winter Condition	171
7.6	Pile Capacity in Clay for Winter Condition	172
7.7	Pile Capacity in Peat for Winter Condition	173
7.8	The Results of Bearing Capacity Analysis for Summer Condition (August 20)	174

LIST OF FIGURES

<u>Figure</u>		<u>Page</u>
2.1	Constitution of Frozen Soil	175
2.2	Average Thermal Conductivity for Sand as a Function of Water Content and Bulk Dry Density. FROZEN. (After Kersten, 1949)	176
2.3	Average Thermal Conductivity for Sand as a Function of Water Content and Bulk Dry Density. UNFROZEN. (After Kersten, 1949)	177
2.4	Average Thermal Conductivity for Clay as a Function of Water Content and Bulk Dry Density. FROZEN. (After Kersten, 1949)	178
2.5	Average Thermal Conductivity for Clay as a Function of Water Content and Bulk Dry Density. UNFROZEN. (After Kersten, 1949)	179
2.6	Average Thermal Conductivity for Peat as a Function of Water Content and Bulk Dry Density. FROZEN. (After Kersten, 1949)	180
2.7	Average Thermal Conductivity for Peat as a Function of Water Content and Bulk Dry Density. UNFROZEN. (After Kersten, 1949)	181
2.8	Enthalpy versus Temperature for Continuum Medium	182
2.9	Enthalpy for Melting Procedure of Medium with Phase Change	183
2.10	Enthalpy for Melting Procedure of Medium with Phase Change Straight Line Approximation	184
2.11	The Neumann Problem. (After Nixon and McRoberts, 1973)	185
2.12	Graphical Solution of the Neumann Equation. (After Nixon and McRoberts, 1973)	186
2.13	Phase Change Seasons for Air and Surface Temperatures (after Lunardini, 1981)	187

3.1	Control Volume with Moving Interface Boundary	188
3.2	Discontinuity Surface (after Eringen, 1967)	189
3.3	Types of Intersection of Interface Layer	190
3.4a	First Group of Intersection for the Interface Position in the Finite Element	191
3.4b	Second Group of Intersection for the Interface Position in the Finite Element	192
4.1a	Geometry of Mesh # 1	193
4.1b	Idealization of the Axisymmetrical Finite Elements for Mesh # 1	194
4.2a	Geometry of Mesh # 2	195
4.2b	Idealization of the Axisymmetrical Finite Elements for Mesh # 2	196
4.3	Temperature Distribution at the Boundary of the Soil for a Period of One Year	197
4.4	Temperature Fields Distribution around Pile Foundation in sand with Water Content, $w = 15 \%$	198
4.5	Temperature Fields Distribution around Pile Foundation in sand with Water Content, $w = 20 \%$	199
4.6	Zero Isotherm propagation around Pile in Sand with Water Content, $w = 15 \%$	200
4.7	Zero Isotherm propagation around Pile in Sand with Water Content, $w = 15 \%$	201
4.8	Plots of Isotherms: -2, -1, +1, +2 for sand with Water Content, $w = 15 \%$	202
4.9	Plots of Isotherms: -2, -1, +1, +2 for sand with Water Content, $w = 20 \%$	203
4.10	The Comparative Analysis between the Numerical and Neumann Solutions for Thawing Penetration in Sand with $w = 15 \%$	204
4.11	Percentage of Error between the Numerical and the Neumann Solutions for Sand with $W = 15 \%$	205

4.12	The Comparative Analysis between the Numerical and Neumann Solutions for Thawing Penetration in Sand with $w = 20\%$	206
4.13	Percentage of Error between the Numerical and the Neumann Solutions for Sand with $W = 20\%$	207
4.14	Temperature Distribution Fields around Pile Foundation in Clay with Water Content, $w = 15\%$	208
4.15	Temperature Fields Distribution around Pile Foundation in Clay with Water Content, $w = 30\%$	209
4.16	Zero Isotherm propagation around Pile in Clay with Water Content, $w = 15\%$	210
4.17	Zero Isotherm propagation around Pile in Clay with Water Content, $w = 30\%$	211
4.18	Plots of Isotherms: -2, -1, +1, +2 for Clay with Water Content, $w = 15\%$	212
4.19	Plots of Isotherms: -2, -1, +1, +2 for Clay with Water Content, $w = 30\%$	213
4.20	The Comparative Analysis between the Numerical and Neumann Solutions for Thawing Penetration in Clay with $w = 15\%$	214
4.21	Percentage of Error between the Numerical and the Neumann Solutions for Clay with $w = 15\%$	215
4.22	The Comparative Analysis between the Numerical and Neumann Solutions for Thawing Penetration in Clay with $w = 30\%$	216
4.23	Percentage of Error between the Numerical and the Neumann Solutions for Clay with $w = 30\%$	217
4.24	Temperature Distribution fields around Pile Foundation in Peat with Water Content, $w = 80\%$	218
4.25	Temperature Distribution fields around Pile Foundation in Peat with Water Content, $w = 120\%$	219
4.26	Zero Isotherm propagation around Pile in Peat with Water Content, $w = 80\%$	220

4.27	Zero Isotherm propagation around Pile in Peat with Water Content, w = 120 %	221
4.28	Plots of Isotherms: -2, -1, +1, +2 for Peat with Water Content, w = 80 %	222
4.29	Plots of Isotherms: -2, -1, +1, +2 for Peat with Water Content, w = 120 %	223
4.30	The Comparative Analysis between the Numerical and Neumann Solutions for Thawing Penetration in Peat with w = 80 %	224
4.31	Percentage of Error between the Numerical and the Neumann Solutions for Peat with w = 80 %	225
4.32	The Comparative Analysis between the Numerical and Neumann Solutions for Thawing Penetration in Peat with w = 120 %	226
4.33	Percentage of Error between the Numerical and the Neumann Solutions for Peat with w = 120 %	227
4.34	Temperature Distribution for April 20 in Sand with Gravel on Top	228
4.35	0° C Isotherm Propagation in Sand with Gravel on Top	229
4.36	Comparative Analysis between the Numerical and Neumann Solutions for Pile Foundation in Sand with Gravel on Top	230
4.37	Percentage of Error between the Numerical and the Neumann Solutions for Sand with Gravel on Top	231
4.38	Temperature Distribution for April 20 in Clay with Gravel on Top	232
4.39	0° C Isotherm Propagation in Clay with Gravel on Top	233
4.40	Comparative Analysis between the Numerical and Neumann Solutions for Pile Foundation in Clay with Gravel on Top	234
4.41	Percentage of Error between the Numerical and the Neumann Solutions for Clay with Gravel on Top	235
4.42	Temperature Distribution for April 20 in Peat with Gravel on Top	236
4.43	0° C Isotherm Propagation in Peat with Gravel on Top	237

4.44	Comparative Analysis between the Numerical and Neumann Solutions for Pile Foundation in Peat with Gravel on Top	238
4.45	Percentage of Error between the Numerical and the Neumann Solutions for Peat with Gravel on Top	239
4.46	Comparative Analysis between the Numerical and Neumann Solutions for Pile Founded in Sand with Gravel on Top, as semi-infinite medium	240
4.47	Comparative Analysis between the Numerical and Neumann Solutions for Pile Founded in Clay with Gravel on Top, as semi-infinite medium	241
4.48	Comparative Analysis between the Numerical and Neumann Solutions for Pile Founded in Peat with Gravel on Top, as semi-infinite medium	242
6.1	Large Building on Pile Foundations.	243
6.2	Guyed Communication Tower	244
6.3	Unsuccessful Attempt to Drive 8 m Long Wood Piles	245
6.4	Forces Acting on Pile Embedded in Sand for Summer and Winter Conditions	246
6.5	Forces Acting on Pile Embedded in Clay for Summer and Winter Conditions	247
6.6	Forces Acting on Pile Embedded in Peat for Summer and Winter Conditions	248
6.7	Ultimate Short-Term and Sustained Adfreeze Strengths for Wood and Steel Piles in Frozen Clays and Silts (after Johnston, Edition 1981)	249
6.8	Recommended Adfreeze Strength for Soil Interface, Modified from Johnston, 1981 (after Phukan, 1985)	250
6.9	Tentative Ultimate Adfreeze Bond Strength in Creep for Saturated Soils. (Adapted from Sanger, 1959)	251
6.10	Adfreeze Strength Frame Loading System	252
6.11	Laboratory Testing Disposition for Pile Embedded in Sand, Clay and Peat Soil	253

6.12	Grain Size Distribution for Sand Samples	254
6.13	Adfreeze Shear Strength for Sample # 8	255
6.14	Adfreeze Shear Strength for Sample # 9	256
6.15	Adfreeze Shear Strength for Sample # 10 - L Curve	257
6.16	Adfreeze Shear Strength for Sample # 10 - R Curve	258
6.17	Adfreeze Shear Strength for Sample # 11	259
6.18	Adfreeze Shear Strength for Sample # 12	260
6.19	Adfreeze Shear Strength for Sample # 13	261
6.20	Adfreeze Strength for Sample # 14 - L Curve	262
6.21	Adfreeze Strength for Sample # 14 - R Curve	263
6.22	Adfreeze Shear Strength for Sample # 15	264
6.23	Adfreeze Strength for Sample # 16 - L Curve	265
6.24	Adfreeze Strength for Sample # 16 - R Curve	266
6.25	Adfreeze Shear Strength for Sample # 17 - L Curve	267
6.26	Adfreeze Shear Strength for Sample # 17 - R Curve	268
6.27	Adfreeze Shear Strength for Sample # 19	269
6.28	Adfreeze Shear Strength for Sample # 20 - L Curve	270
6.29	Adfreeze Shear Strength for Sample # 20 - R Curve	271
6.30	Adfreeze Shear Strength for Sample # 21	272
6.31	Adfreeze Shear Strength for Sample # 22	273
6.32	Adfreeze Shear Strength for Sample # 24 - L Curve	274
6.33	Adfreeze Shear Strength for Sample # 24 - R Curve	275

6.34	Adfreeze Shear Strength for Sample # 25	276
6.35	Adfreeze Shear Strength for Sample # 26	277
6.36	Adfreeze Shear Strength for Sample # 27 - Curve	278
6.37	Adfreeze Shear Strength for Sample # 27 - R Curve	279
6.38	Adfreeze Strength, Function of Temperature, for Sand with $w = 7.9\%$	280
6.39	Adfreeze Strength, Function of Temperature, for Sand with $w = 11.5\%$	281
6.40	Adfreeze Strength, Function of Temperature, for Sand with $w = 14.2\%$	282
6.41	Adfreeze Strength, Function of Temperature, for Peat with $w = 275\%$	283
6.42	Adfreeze Strength, Function of Temperature, for Peat with $w = 412.5\%$	284
6.43	Adfreeze Strength, Function of Temperature, for Sand soil with Variable Water Contents	285
6.44	Adfreeze Strength, Function of Temperature, for Peat Soil with Variable Water Contents	286
6.45	Adfreeze Shear Strength for Pile Foundation Embedded in Clayey Soil with Variable Water Content	287
6.46	Adfreeze Strength for Sand with Experimental Result after Study done by Biggar, K. and Sego, D. (1993)	288
6.47	Steel Model Piles for Laboratory Testing.	289
6.48	High Power Hydraulic Pump with Max. Pressure 10000 psi (700 bars) Used to Transmit Loads on Top of the Pile Through the Flat Load Cell	290
6.49	Data Acquisition System Used to Monitor Pre-and-Post-Tests Processing Data Including Temperature, Settlements, and Corresponding Loads. The Megadac and the PC computer are Shown	291

6.50	Samples of Peat Soil Used for Laboratory Testing	292
6.51	Test # 16: Sand Sample with Water Content $w = 14.2\%$, $T = -4.52^\circ\text{C}$	293
6.52	Test # 17: Sand Sample with Water Content $w = 14\%$, $T = -4.86^\circ\text{C}$	294
6.53	Test # 26: Peat Sample with Water Content $w = 272\%$, $T = -4.26^\circ\text{C}$	295
6.54	Test # 27: Peat Sample with Water Content $w = 273\%$, $T = -4.39^\circ\text{C}$	296
6.55	Mode of Failure for Test # 24 to 27: Concentric Rupture Circles Appearing around the Pile Surface	297
6.56	Foam Material Used as a Separating Surface between Wet and Dry Peat Sample for Test # 19 to 27	298
6.57	Disposition Set Up for Tests with Peat	299
7.1	System of Forces Acting on the Pile Embedded in: a) sand, b) Clay, c) Peat	300
7.2	Distribution of the Adfreeze Strength along the Pile Embedded in Sandy Soil with Water Content, $w = 15\%$, for Summer Condition	301
7.3	Distribution of the Adfreeze Strength along the Pile Embedded in Sandy Soil with Water Content, $w = 20\%$, for Summer Condition	302
7.4	Distribution of the Adfreeze Strength along the Pile Embedded in Clayey Soil with Water Content, $w = 15\%$, for Summer Condition	303
7.5	Distribution of the Adfreeze Strength along the Pile Embedded in Clayey Soil with Water Content, $w = 30\%$, for Summer Condition	304
7.6	Distribution of the Adfreeze Strength along the Pile Embedded in Peat Soil with Water Content, $w = 80\%$, for Summer Condition	305
7.7	Distribution of the Adfreeze Strength along the Pile Embedded in Peat Soil with Water Content, $w = 120\%$, for Summer Condition	306
7.8	System of Forces Acting on the Pile Embedded in Sand, Clay and Peat for Winter Condition: a) with Heave, b) without Heave	307
7.9	Distribution of the Adfreeze Strength along the Pile Embedded in Sandy Soil with $w = 15\%$, for Winter Condition with Heaving	308

7.10	Distribution of the Adfreeze Strength along the Pile Embedded in Sandy Soil with $w = 15\%$, for Winter Condition without Heaving	309
7.11	Distribution of the Adfreeze Strength along the Pile Embedded in Sandy Soil with $w = 20\%$, for Winter Condition with Heaving	310
7.12	Distribution of the Adfreeze Strength along the Pile Embedded in Sandy Soil with $w = 20\%$, for Winter Condition without Heaving	311
7.13	Distribution of the Adfreeze Strength along the Pile Embedded in Clayey Soil with $w = 15\%$, for Winter Condition with Heaving	312
7.14	Distribution of the Adfreeze Strength along the Pile Embedded in Clayey Soil with $w = 15\%$, for Winter Condition without Heaving	313
7.15	Distribution of the Adfreeze Strength along the Pile Embedded in Clayey Soil with $w = 30\%$, for Winter Condition with Heaving	314
7.16	Distribution of the Adfreeze Strength along the Pile Embedded in Clayey Soil with $w = 30\%$, for Winter Condition without Heaving	315
7.17	Distribution of the Adfreeze Strength along the Pile Embedded in Peat Soil with $w = 80\%$, for Winter Condition with Heaving	316
7.18	Distribution of the Adfreeze Strength along the Pile Embedded in Peat Soil with $w = 80\%$, for Winter Condition without Heaving	317
7.19	Distribution of the Adfreeze Strength along the Pile Embedded in Peat Soil with $w = 120\%$, for Winter Condition with Heaving	318
7.20	Distribution of the Adfreeze Strength along the Pile Embedded in Peat Soil with $w = 120\%$, for Winter Condition without Heaving	319
7.21	Proposed Linear Adfreeze Strength versus Load in the Permafrost Zone	320
7.22	Equilibrium Conditions for Winter	321

NOMENCLATURE

B	matrix of shape function gradient
c	specific heat (heat capacity per unit mass)
$C^{(t)}$	Incremental capacity matrix for time instant t
$C^{(t+\Delta t)}$	additional incremental capacity matrix for time instant t + Δt
dA	infinitesimal area
$\frac{D}{Dt} ()$	material derivative
k	thermal conductivity
k_n	thermal conductivity in n direction
$K_c^{(t)}$	incremental convection matrix for time instant t
$K_k^{(t)}$	incremental conductivity matrix for time instant t
L	latent heat per unit mass
n	outward normal vector to the bounding surface
n_i	i^{th} component of outward normal vector to the bounding surface
N	matrix of shape functions
p	internal pressure
q	heat flux

q_B	generated heat rate per unit volume
q'	prescribed heat flow input on $\partial \Omega_q$
$Q^{(t)}$	balanced heat flow vector for time instant t
$Q^{(t+\Delta t)}$	heat flow vector for time instant $(t + \Delta t)$
$Q_c^{(t+\Delta t)}$	convective heat transfer rate vector for time instant $(t + \Delta t)$
$Q_L^{(t+\Delta t)}$	heat flow vector due to phase-change effects for time instant $(t + \Delta t)$
$Q_{LM}^{(t+\Delta t)}$	modified heat flow vector due to phase-change effects for time instant $(t + \Delta t)$
$Q_L^{*(t+\Delta t)}$	heat flow vector due to phase change in the region with prescribed temperature for time instant $(t + \Delta t)$
t	time
T	approximated temperature field
\vec{T}	vector of nodal temperature increment
u	specific internal energy
u	orthogonal vector to v lying in phase-change interface
v	phase-change interface velocity vector
v_i	i^{th} component of phase-change interface velocity vector
x_1, x_2, x_3	coordinates of global cartesian coordinate system
x	vector in three dimensional space

Greek Symbols

α_c	convective heat transfer coefficient
δ_{ij}	Kronecker symbol
ϵ	specific enthalpy per unit mass
$\Gamma(t)$	phase change interface for time instant t
$\Gamma(t+\Delta t)$	phase change interface for time instant $(t + \Delta t)$
ρ or γ	density
θ	temperature field
θ_f	phase change temperature
θ_s	surface temperature
θ_∞	ambient temperature
$\dot{\theta}$	rate of temperature field
θ^*	prescribed temperature field on the surface $\partial\Omega_T$
ω	weighing function
Ω	control volume
Ω_1	solidus volume
Ω_2	liquidus volume
$\partial\Omega$	fixed boundary of control volume Ω

$\partial\Omega_1$	fixed solidus boundary
$\partial\Omega_2$	fixed liquidus boundary
$\partial\Omega_c$	boundary of prescribed convection
$\partial\Omega_q$	boundary of prescribed heat flux
$\partial\Omega_T$	boundary of prescribed temperature

Subscripts

$(i-1), (i)$	$(i-1)^{\text{th}}$ and i^{th} iteration number for time increment Δt in Newton-Raphson method
ij	component of tensor of second order
i, j	vector component in three-dimensional space

Superscripts

h	discretized approximation
$(t), (t+\Delta t)$	current time instant (t) and next time instant $(t + \Delta t)$
T	transposition

Other symbols

$\ \nabla\theta\ $	temperature gradient at time instant $(t + \Delta t)$
$(\dot{\quad})$	rate
$(\quad)^*$	prescribed volume

Δ	increment
∇	Nabla operator
{ }	matrix of specified components
()	solidus side
() ⁺	liquidus side

XXX

CHAPTER I

INTRODUCTION

The important aspect in the design of structures in cold regions is the analysis of thermal effects on the overall behaviour of the structure. The applied load must be transferred to the soil medium such to ensure safe and reliable performance of the structure during its life time. The supporting soil medium consists of the mixture of soil grains, water, ice and air. These constituents affect substantially the thermal properties of the entire medium. In particular, the factors which are very important in thermal analysis are soil dry unit weight and the water content.

The investigation of the thermal effects of the soil medium on the behaviour of the structures embedded in frozen soil is a complex problem. This is caused by arbitrary variable changes of temperature affecting medium with complex geometry which is subjected to phase change. Consequently, the evolution of temperature field directly affects the strength of the soil defining the performance of the structure. It is essential for the structure, in cold regions, embedded in soils to have reliable information about effects of thermal changes for arbitrary time. Knowing the temperature distribution, one can determine the summer and winter conditions, estimate the adfreeze bond strength

between the soil and the pile interface, then decide on the weakest supporting conditions which governs the design of the structure. Improper estimation for the weakest supporting conditions can produce even failure of the structure. For the deep foundations the determination of the evolution of the thawing zone and then its maximum depth is of primary importance. The most pronounced determination of the support conditions is connected with changes of temperature during summer season.

Unfortunately, there exist only limited number of exact solutions which are valid within rigorously satisfied assumptions (Carslaw and Jaeger 1959, Nixon and McRoberts 1973, Jumikis 1977, Andersland and Anderson 1978, Lunardini 1981, Phukan 1985). The development of the numerical methods constitutes the powerful tool which enables one to tackle the wide range of problems of practical importance with complex geometry, properties of the medium and arbitrary thermal conditions (Comini Del. Guidece, Lewis, Zienkiewicz 1974, Morgan, Lewis Zienkiewicz 1978). In the thesis, the theoretical formulation of the heat transfer problem with phase change is presented. It is based on the law of conservation of energy for the medium with thermal properties (Eringer 1967), which takes into account the prescribed arbitrary temperature conditions. The energy conservation formulation in integral form leads to the weak form of the problem. Consequently, the Galerkin-Bubnov approach combined with the assumed piece-wise representation of the temperature functions provides the basis for the implementation of the finite element method with respect to spatial variables (Bathe 1982, Hughes 1987, Zienkiewicz 1977, Rubinsky and Cravahlo 1981).

The transient heat transfer problem requires integration with respect to time. In

discrete form, it is done by application of Euler backward method (Lunardini 1981, Ralston 1965, Dalhuijsen and Segal 1986). The sequential dependence of the solution and the thermal quantities for the current time instant in relation to the previous time instant is obtained by introducing the incremental decomposition procedure (Bathe 1982). Special treatment was introduced in order to take into account the conditions existing on the moving phase-change interface and to determine its position and shape (Bell and Wood 1983, Tacke 1985, Mackinnon and Garey 1987, Storti, Crivelli and Idelsohn 1988). This special approach is connected with involvement of the temperature gradient in the description of the conditions existing on the moving phase-change front.

The numerical simulation of the propagation of the phase-change interface by means of the finite element method is done by introducing curvilinear finite element intersecting the original finite element in arbitrary fashion. In order to improve the accuracy of the solution, Newton-Raphson and modified Newton-Raphson iterative procedure are applied (Zienkiewicz 1977, Kleiber 1985). By means of the presented formulation and the proposed numerical algorithm, several modelling examples are computed and analyzed.

The analyses of the results determine the evolution of the temperature field around deep foundation embedded in frozen soils subjected to the arbitrary changes of temperature on its top boundary. Special attention is paid to the determination of the propagation of the zero isotherm which defines the temperature of phase change for various soils (Sand, Clay and Peat) with different water content. The obtained distributions of temperature fields are used for comparative analysis with Neumann

problem (Nixon and McRoberts 1973) as well as the determination of the active layer where uplift heaving force develops during the winter. Uplift resulting from the freezing process in frozen soils is a serious stability problem for various structures, such as unheated building foundations, transmission towers, utility poles for telephone and power lines and transforming and distribution stations. Uplift forces caused by frost heaving in the active layer of frozen soils have been shown to be substantial and various investigators (Penner, 1972 and 1974, Hoekstra et al., 1965, Crory and Reed, 1965, Kinoshita and Ono, 1963, Vyalov, 1959; Tsytovich, 1975) have studied the uplift or heaving forces that result from adfreezing on different foundations in frost-susceptible soils.

Laboratory studies are conducted to estimate the adfreeze bond strength of a cylindrical steel pile embedded in frozen soils (sand, clay and peat) with variable water contents and freezing temperatures. For each type of soil with fixed water content, the adfreeze strength at the soil-pile interface varies linearly with temperature then moves constantly after the temperature has dropped below -5°C . These results will constitute input data to determine the bearing capacity of the deep foundation, defined by the mathematical model, for both summer and winter conditions. Special attention will be given to account for the uplift heaving stresses developed in the active layer when writing the equation of static equilibrium for the winter conditions. A solution method is presented and assumptions are made considering all aspects that contribute to the stability of the structure. Finally the bearing capacity of the pile embedded in frozen soil is determined following a discussion on the governing condition of the design for different

types of soil (sand, clay and peat), (Johnston, 1981, Andersland and Anderson, 1978, Phukan, 1985).

The most important features of the theoretical as well as numerical analysis combined with the conclusions followed from numerical examples are presented in Chapter VIII of the thesis.

CHAPTER II

MECHANISMS OF HEAT TRANSFER IN SOILS

2.1 Introduction

The thermal properties of soil are of great importance in many engineering projects such as buildings, roads, airports, pipelines in frozen ground. It is also important to determine the position of the interface boundary between the thawed and frozen soil with respect to the ground surface for an arbitrary surface temperature. The position of thaw or frost penetration is dependent on the thermal properties of soils and the factors influencing them. Also, thermal properties constitute the basic parameters to solve analytically problems dealing with ground heat-transfer. The basic thermal properties of soils are thermal conductivity, heat capacity, thermal diffusivity and latent heat. Kersten (1949), Johansen (1975), and Farouki (1981) have published information on various aspects of thermal properties of soils. The thermal properties of soils vary with phase composition as shown in Fig. 2.1.

These phases are:

1- Solid phase or soil particles. These are mineral particles (silicates), organic or both.

2- Plastic-viscous phase or ice:

Their properties depend strongly on the material below-freezing temperature and the magnitude and duration of load applied.

3- Liquid phase or unfrozen water: Water molecules fill parts or all of the voids between the soil particles

4- Gaseous phase: Air vapor fills voids that are not occupied by liquid. For saturated soils, with water or ice, this phase will vanish as V_A tends to zero as shown in Fig. 2.1.

2.2 Thermal Properties of soil

2.2.1 Thermal Conductivity

The thermal conductivity, k , which characterizes the ability of a material to transmit heat by conduction is defined as the amount of heat passing in unit time through a unit cross-sectional area of the material under a unit temperature gradient applied in the direction of the heat flow. Considering a prismatic element of a material having a cross sectional area A at right angles to the heat flow q , the thermal conductivity k is given by:

$$k = \frac{q}{A(T_2 - T_1)L} \quad (2.6)$$

where the temperature drops from T_2 to T_1 over a length L of the element. Its units are

$$\frac{\text{Btu}}{\text{hr ft}^2} \quad \text{or} \quad \frac{W}{mK}$$

The relationship between thermal conductivity and water content in soil was explored by Kersten (1949) and Figs. 2.2 to 2.7 present his experimental data on the thermal conductivity of both unfrozen and frozen soils at different dry densities and water contents. His empirical equations showed that the thermal conductivity is linearly related to the logarithm of the moisture content at a constant dry density.

For unfrozen silt and clay containing 50 % of silt and clay the equation of thermal conductivity is

$$k = (0.9 \log w + 0.4)10^{0.01\gamma_d} \quad \text{for } w \geq 7\% \quad (2.7 \text{ a})$$

and, for unfrozen sandy soils (clean sand), it is

$$k = (0.7 \log w + 0.4) 10^{0.01\gamma_d} \quad \text{for } w \geq 1\% \quad (2.7 \text{ b})$$

where k = thermal conductivity in Btu in./ft².

w = moisture content in percent.

γ_d = dry density in lb/ft³.

Equations (2.7 a) and (2.7 b) can be rewritten as

$$k = 0.00144 \times 10^{1.373\gamma_d} + 0.01226 \times 10^{0.499\gamma_d w} \quad \text{for silt and clay} \quad (2.8 \text{ a})$$

$$k = 0.01096 \times 10^{1.373\gamma_d} + 0.00461 \times 10^{0.9115\gamma_d w} \text{ for sand} \quad (2.8 \text{ b})$$

where k is in W/mK,

γ_d is in g/cm^3 , and,

w is in percent.

Johansen (1975) introduced the concept of the Kersten number k_e to calculate the thermal conductivity k of soil at partial saturation from known values of the conductivity in the saturated state (k_{sat}) and that in the dry state (k_{dry}) by the following relationship:

$$k_e = \frac{k - k_{dry}}{k_{sat} - k_{dry}}$$

and

$$k = (k_{sat} - k_{dry})k_e + k_{dry} \quad (2.9)$$

The thermal conductivity of ice is about four times that of water. Therefore the thermal conductivity of frozen soils (k_f) may be expected to be greater than that of unfrozen soil (k_u). This is the case for saturated soils and soils with high saturation. For soils with a low degree of saturation, k_f may be less than k_u .

Tables 2.1 to 2.3 present different values of the thermal conductivities k_u and k_f for sandy soils, silt and clay, and peat as a function of the bulk dry density and water content.

A value of $k = 0.928$ W/mK will be adopted as a conductivity coefficient for the

concrete pile embedded in the soil used for the numerical analysis.

2.2.2 Heat Capacity

Heat capacity is defined as the quantity of heat necessary to raise the temperature of given material by 1° C. When expressed on a unit volume basis, the quantity is known as the volumetric heat capacity, and when expressed on a unit weight basis, the quantity is referred to as the specific heat capacity.

The volumetric heat capacity is given by:

$$c = c_1 \gamma_d \quad (2.10)$$

and its units are:

$$\frac{Btu}{ft^3 F} \quad or \quad \frac{J}{m^3 K} \quad or \quad \frac{Wd}{m^3 K}$$

where c = volumetric heat capacity

$$c_1 = \text{specific heat capacity, in } \frac{Btu}{lb^{\circ}F} \quad or \quad \frac{J}{Kg^{\circ}K} \quad or \quad \frac{Wd}{kg^{\circ}K}$$

$$\gamma_d = \text{dry unit weight of soil, in pcf or } kg/m^3$$

Using metric units, the specific heat capacity of soil grains usually lies between 0.17 and 0.2, an average value of 0.18 is adopted below, (Anderson and Andersland, 1978; Farouki, 1981). For moist unfrozen soil,

$$c_u = \frac{\gamma_d}{\gamma_w} \left(0.18 + 1.0 \frac{w}{100} \right) c_w \quad (2.11)$$

and for moist frozen soils,

$$c_f = \frac{\gamma_d}{\gamma_w} \left(0.18 + 0.5 \frac{w}{100} \right) c_w \quad (2.12)$$

where c_w = volumetric heat capacity of water,

γ_w = water unit weight = 1000kg/m³, and,

w = water content of the soil expressed in percent of dry weight.

The volumetric heat capacity for frozen soils, c_f and for unfrozen soils c_u , including sand, silt and clay, and peat soils are presented in Tables 2.4 to 2.6 as a function of the water content and the bulk dry density of soils.

The thermal conductivity and volumetric heat capacity for a number of common materials of particular relevance to cold-region engineering are given in Table. 2.7

2.2.3 Thermal Diffusivity

For unsteady state heat transfer, the thermal behavior of a soil is governed not only by its thermal conductivity k but also by its heat capacity c . The ratio of the two properties is termed as the thermal diffusivity, κ , which becomes the governing parameter in the transient state and is given by:

$$\kappa = \frac{k}{c} \quad (2.13)$$

Its units are ft²/hr or mm²/s or m²/day.

A high value for the thermal diffusivity implies a capacity for rapid and considerable changes in temperature. The diffusivity of ice is about eight times that of liquid water, and consequently the diffusivity of frozen soil is much higher than that of the same soil in thawed condition.

2.2.4 Latent Heat in Soils

The volumetric latent heat of fusion L of soil is the amount of heat required to melt the ice or freeze the water in a unit volume of soil without a change in temperature.

When ice melts, it absorbs heat from the air with which it is in contact and the same amount of heat must be added to ice to transform it to water without a change in temperature.

Its units are Btu/ft³ or J/m³ or Wd/m³.

The latent heat of the soil is dominated by water content and given by:

$$L = \gamma_d w (1 - w_{uw}) L' \quad (2.14)$$

or

$$L = \gamma_d w L' \quad \text{for } w_{uw} = 0 \quad (2.15)$$

where $L' = 79.6 \text{ cal/g}$, or 143.4 Btu/lb or 333 kJ/kg or 3.854 Wday/kg for water.

Theoretically at 0° C at atmospheric pressure, with no temperature change during crystallization, the amount of heat energy removed from water is equal to 79.6 cal/g or 143.4 Btu/lb or 3.854 Wd/kg . Table (2.8) presents values of volumetric latent heat as a function of the bulk dry density and the water content for the soil.

2.2.5 Enthalpy and Heat Capacity

For unsteady state, the enthalpy is the thermodynamic function which is related mathematically to heat capacity in the following way:

$$\frac{\partial}{\partial t}(\rho\epsilon) = \rho c \frac{\partial \theta}{\partial t} \quad (2.16)$$

where ϵ = enthalpy expressed in J/kg ,

$\rho\epsilon$ = volumetric enthalpy function expressed in J/m^3 or Wd/m^3 ,

$\frac{\partial \theta}{\partial t}$ = temperature gradient with respect to time, and,

ρc = volumetric heat capacity in $\text{J/m}^3\text{ }^\circ\text{K}$ or $\text{Wd/m}^3\text{ }^\circ\text{K}$.

Multiplying both sides of eq. (2.16) by Δt , leads to:

$$\partial(\rho\epsilon) = \rho c \partial \theta \quad (2.17 \text{ a})$$

or

$$\frac{\partial(\rho\epsilon)}{\partial\theta} = \rho c \quad (2.17 \text{ b})$$

For the material without phase change, the enthalpy is a function of the temperature as shown in Fig. 2.8.

From equation (2.17 b), it follows that, ρc is also a function of temperature.

For material with phase change, i.e. soil, the mushed region is defined as the region where phase change occurs (melting or solidification) between two temperatures θ_1 and θ_2 as shown in Fig. 2.9. Also Fig. 2.9 shows that ρc is a curvilinear function of the temperature. (Steven, G.P., 1982).

Figure 2.10 presents an interpretation of the enthalpy function assumed as a linear function with respect to temperature and therefore, ρc will become a step function. From Fig. 2.10, it follows:

$$\text{if } \Delta\theta = \theta_1 - \theta_2 \rightarrow 0, \quad [\rho c] \rightarrow \infty \text{ and } [\rho\epsilon] = \rho L \quad (2.18)$$

The Heaviside function $H(t)$ is defined as follows:

$$H(t) = 1 \quad \text{for } t > 0$$

$$H(t) = 0 \quad \text{for } t \leq 0$$

The Dirac delta function $\delta(t)$ is defined as follows:

$$\delta(t) = \infty \quad \text{for } t = 0$$

$$\delta(t) = 0 \quad \text{for } t \neq 0$$

and

$$\int_a^b \delta(t) dt = 1$$

The relationship between the Heaviside function and the Dirac delta function is :

$$\frac{d H(t)}{dt} = \delta(t) \quad (2.19)$$

Knowing that at the discontinuity jump $[\rho \epsilon] = \rho L$,

Homologously, using equation (2.19), Eq. (2.17 b) leads to:

$$\frac{\partial}{\partial \theta} (\rho \epsilon) = \rho c = \infty$$

Therefore, at the phase change interface, the heat transfer equation cannot be mathematically possible and must be replaced by the energy balance equation to complete the equilibrium.

2.3 Thermal Analysis

Thermal analysis between the structure and ground can be made by considering boundary conditions including temperature distribution and thermal properties of the ground. The basic heat transfer of energy is due to conduction, convection, and radiation. They must be considered in doing heat-flow calculations.

2.3.1 Thermal Conduction

The principal mechanism for heat transport in soils in most engineering applications involving thawing and freezing is conduction. Conduction is the transfer of heat by the passage of energy from particle to particle or through the soil pore fluids. Conduction, as such, is independent of mass transfer process, (Incropera and Dewitt, 1985)

Because conduction is the principal mode of heat transfer, most analytical techniques developed for the prediction of rates and depths of thawing and freezing have been based on heat conduction theory.

The governing equation of the one-dimensional heat transfer in a material by conduction assuming no phase change is:

$$\frac{\partial \theta}{\partial t} = \kappa \frac{\partial^2 \theta}{\partial x^2} \quad (2.20)$$

where T = temperature in °C,

t = time in days or seconds, and

κ = thermal diffusivity k/c , where k and c are the thermal conductivity in W/mK and the volumetric heat capacity in Wd/m³K, respectively.

x = depth in m

or by means of the generalized Fourier law,

$$q_i = k_{ij} \frac{\partial \theta}{\partial x_j} \quad (2.21)$$

where q_i = heat flux generated in W/m^2 ,

k_{ij} = coefficient of thermal conductivity in W/mK , and

x_j = depth along the ordinate j , in m.

For the most general case, the three dimensional problem represents a tensor of conductivity coefficients in three dimensional cartesian coordinate system and k would be replaced by a matrix of the form:

$$[k] = \begin{bmatrix} k_{xx} & k_{xy} & k_{xz} \\ & k_{yy} & k_{yz} \\ & & k_{zz} \end{bmatrix} \quad (2.22)$$

For isotropic material, the matrix will be reduced to a scalar factor, k . The transient heat transfer problem with phase change, including change of temperature in time will be examined and discussed in chapters III and IV.

2.3.2 Convective Heat Transfer in Soil

Convection is defined as the transmission of heat by mass movement of the heated particles. It is, also, defined as the energy transfer in the presence of the bulk motion of the body referring to fluid. The governing law of convection is presented by Newton's cooling law as:

$$q_c = h_c(\theta_s - \theta_\infty) \quad (2.23)$$

where q_c = heat flux generated by convection only (W/m^2)

h_c = coefficient of convection ($W/m^2 \text{ } ^\circ K$), also denoted by α_c .

θ_s = surface temperature in $^\circ C$, and,

θ_∞ = environmental temperature in $^\circ C$.

This is not a basic law but merely a definition of h_c (or α_c). The surface coefficient is a complex function of the fluid flow conditions and the geometric and thermal conditions of the solid and fluid. In general, h_c may vary from point to point on the surface and also may vary in time. It should be emphasized that h_c (or α_c) is not a fluid property, as k . It is merely a convenient parameter defined by equation (2.23) and it varies very greatly even for one fluid. Some typical values of h_c (or α_c) are given below:

Convective mode	h_c (or α_c), $W/m^2 \text{ } K$
Free Convection:	5 - 25.
Forced convection:	
1- Gases	25 - 50.
2- Liquid	50 - 20,000.

A value of $\alpha_c = 20 \text{ } W/m^2 \text{ } K$ will be adopted later for the numerical analysis.

2.3.3 Radiations in Soils

The thermal radiation is defined as the emission of energy. This emission is associated with the change in atomic configuration of the elements. The transport of

thermal radiation energy is made by electromagnetic waves. The governing law of thermal radiation is represented by Stefan-Bolzman law as:

$$q = \sigma \cdot \theta_s^4 \quad (2.24)$$

where q = heat flux generated by radiation, in W/m^2 ,

σ = Stefan-Bolzman constant, defining a perfect black body,

= $5.67 \times 10^{-8} W/m^2 K^4$, and,

θ_s = surface temperature in $^\circ K$.

The net rate of radiation heat exchange with the surroundings having the temperature θ_{sur} is given by the following law:

$$q = \epsilon \sigma (\theta_s^4 - \theta_{sur}^4) \quad (2.25)$$

where ϵ = coefficient of emissivity, and is less than or equal to one.

θ_{sur} = surrounding temperature in $^\circ K$.

The law is usually used in a similar form to Newton's cooling law with:

$$q = \alpha_r (\theta_s - \theta_{sur}) \quad (2.26)$$

where α_r = coefficient of radiation calculated to be as:

$$\alpha_r = \epsilon \sigma (\theta_s + \theta_{sur}) (\theta_s^2 + \theta_{sur}^2) \quad (2.27)$$

Goodling and Khadar (1974) numerically evaluated the freezing of a sphere with convection and radiation at the surface of the sphere. The numerical results were too limited to reproduce but, if

$$\sigma \cdot \epsilon \theta_f^3 \frac{r_o}{k} < \frac{1}{3} B_i^2 \quad (2.28)$$

where θ_f = freezing temperature, in ° K,

r_o = surface radius of the sphere, in m,

k = coefficient of thermal conductivity, in W/mK,

σ = Stefan-Bolzman constant = 5.67×10^{-8} W/m²K²,

ϵ = coefficient of emissivity, is less than or equal to one, and,

B_i = Biot number = $\alpha_c r_o/k$,

α_c = coefficient of convection, in W/m² °K.,

the solidification line with radiation will exceed 90 % of the time with only convection.

Thus, for soil system, it can be anticipated that surface radiation will not be significant (Lunardini, 1981).

2.4 Neumann Problem Considerations

Estimation of depth of thaw or frost penetration in soils is one of the most important thermal calculations in frozen ground engineering. Solutions are needed to estimate the rate and depth of the active layer in permafrost area, rates of thermal degradation or deepening of the active layer following surface disturbances, depth of frost

or thaw under highways and airstrips, rates of frost or thaw advance beneath chilled or warm buried pipelines and many other engineering areas.

Neumann (in about 1860) derived the solution for determining the depth of thaw or frost and Carslaw and Jaeger (1959) have presented Neumann's solution. As illustrated in Fig. 2.11, a uniform homogeneous frozen soil is subjected to step increase in temperature T_g in the ground to T_s at the surface. Assuming that properties of the frozen and thawed zones are independent of temperature and are homogeneous, the Neumann formulation leads to

$$X_t = \alpha\sqrt{t} \quad (2.29)$$

where X_t = depth of thaw, and

α = constant determined as the root of the transcendental equation

$$\frac{e^{-\alpha^2/4\kappa_u}}{\text{erf}[\alpha/2(\kappa_u)^{1/2}]} - \frac{T_g K_f (\kappa_u)^{1/2}}{T_s K_u \kappa_f} \frac{e^{-\alpha^2/4\kappa_f}}{\text{erfc}[\alpha/2(\kappa_f)^{1/2}]} = \frac{L\pi^{1/2}\alpha}{2(\kappa_u)^{1/2}c_u T_s} \quad (2.30)$$

where $\text{erf} []$ = error function = $\frac{2}{\sqrt{\pi}} \int e^{-\beta^2} d\beta$

$\text{erfc} []$ = 1- $\text{erf} []$,

κ_u, κ_f = diffusivity of unfrozen and frozen soil, in m^2/s or m^2/d ,

c_u, c_f = volumetric heat capacities of unfrozen and frozen soil, $\text{J}/\text{m}^3\text{K}$ or

Wd/m³K,

L = volumetric latent heat of soil, J/m³ or Wd/m³.

T_g = (uniform) initial ground temperature, °C below freezing,

T_s = applied constant surface temperature > T_g, °C.

As the diffusivity of a zone is simply the conductivity divided by the volumetric heat capacity for that zone, α_c is defined as a function of seven variables:

$$\alpha_c = f(k_u, k_f, c_u, c_f, T_g, T_s, L)$$

As shown by Nixon and McRoberts (1973), Eq. (2.30) can be rewritten so that only three dimensionless variables remain:

$$\frac{\alpha}{2(\kappa_u)^{1/2}} = f \left\{ Ste, \left[-\frac{T_g k_f}{T_s k_u} \left(\frac{\kappa_u}{\kappa_f} \right)^{1/2} \right], \left(\frac{\kappa_u}{\kappa_f} \right)^{1/2} \right\} \quad (2.31)$$

where "Ste" is the Stefan number, defined as the ratio of sensible heat to latent heat by:

$$Ste = \frac{c_u T_s}{L} \quad (2.32)$$

The results are almost independent of the ratio (κ_u/κ_f)^{1/2}. The results for the normalized thaw rate α/2(κ_u)^{1/2} are presented in Fig. 2.12 as a function of the two significant variables,

$$Ste \text{ and } -\frac{T_g}{T_s} \frac{k_f}{k_u} \left(\frac{\kappa_u}{\kappa_f} \right)^{1/2}$$

This chart represents a complete and accurate solution to the Neuman problem with no assumption other than those inherent in the original formulation, (McRoberts and Nixon, 1973). The range of the parameter

$$-\frac{T_g}{T_s} \frac{k_f}{k_u} \left(\frac{\kappa_u}{\kappa_f}\right)^{1/2}$$

shown in Fig. 2.20 is extreme. It usually lies between 0.0 and 0.4.

To apply Neumann solution to practical field cases where the surface temperature varies arbitrarily, the average surface temperature for the thawing period is T_s and T_a is taken as the mean air or ground temperature T_g . With these assumptions, Eq. (2.29) is referred to as the Berggren equation. The average surface temperature may be estimated from the air-temperature thawing index, I_a , using an n-factor correlation as shown in Fig. 2.13. The thawing index, I_t , is defined as the number of degree-days above freezing integrated over the time during which the surface is above freezing.

The factor n is defined as the ratio between the surface index and air index as follows:

$$n = \frac{I_t}{I_a} = \frac{\int_0^{\theta_s} (T_f - T_s) dt}{\int_0^{\theta_a} (T_f - T_a) dt} \quad (2.33)$$

For thawing conditions, an n factor of 1.0 is suggested for turf surfaces and an n factor of 1.5 to 2.0 for sand and gravel surfaces. Using the average thawed and frozen

values for the thermal properties and two dimensionless parameters as follows:

$$\alpha = \text{thermal ratio} = \frac{T_a - T_f}{T_s - T_f} = \frac{(T_a - T_p)_t}{I_t} = \frac{T_a - T_f}{V_s} \quad (2.34)$$

where $T_f = 0^\circ \text{C}$

V_s = surface thawing index divided by the length of the thawing season

$$\lambda = \alpha \sqrt{\frac{L}{k_a(T_s - T_p)}} \quad (2.35)$$

where k_a = average thermal conductivity of soil, (Eq. 2.29) becomes

$$X_t = \lambda \sqrt{\frac{2k}{L} I_t} \quad (2.36)$$

which is the equation recommended by Aldrich and Paynter (1953) and is known as the *modified Berggren equation*.

The modified Berggren equation and the graphical Neumann solution illustrated in Fig. 2.12 will be used as a comparative analysis to the solution of the three-dimensional transient problem employing the finite element method with respect to the spatial variables and the backward Euler integrations with respect to time variable as will be discussed later in the following chapter.

CHAPTER III

FORMULATION OF HEAT TRANSFER WITH PHASE CHANGE IN SOILS

3.1 Literature Review

A characteristic of heat transfer problems dealing with phase change is the existence of an interface separating the phases. On this interface, the latent heat, liberated or absorbed, is a consequence of the heat transfer process in the two phases, and creates a discontinuity in the material properties as the conductivity progresses in time. Extensive reviews on methods solving heat transfer problems with phase change have been presented by many authors (Carslaw and Jaeger, 1959, Nixon and McRoberts, 1973, Jumikis, 1977, Andersland and Anderson, 1978, Lunardini, 1981 and Phukan, 1985). The development of the numerical methods constitutes the powerful tools to tackle a wide range of problems with complex geometry, variable properties of the medium and arbitrary thermal conditions.

Rubinsky and Cravahlo in 1981, developed a finite element method for the analysis of one-dimensional change of phase that occurs at a specific temperature. To

illustrate the method, the position of a phase front and the temperature distribution were found for a slab of water with an initial temperature of -20°C is applied on the outer surface. The slab was modelled by using 10 two-node elements with a time step of 4000 s. The results show that for short times, the method of solution presented gives an almost identical solution to Neumann's solution.

Roose and Storrer, in 1984, presented an algorithm to solve two-dimensional phase change problems, which are highly non-linear. They used the concept of fictitious heat flow to define the latent heat in the conservation of energy equation. The fictitious heat flow defined at any node, of the finite element, was positive when solidification occurred, negative when melting occurred, and zero when no phase change occurred. The concept of the area associated with nodes was developed and some practical values for the weight coefficients are recommended. In order to improve the stability and convergence of the problem, relaxation techniques were used in the iterative procedure. This method allowed the study of phase change problems for pure bodies, for which the phenomenon occurred at a precise temperature. Some inconveniences, however, should be mentioned:

- 1- The method used the concept of associated area with node, which was not easy to define.
- 2- Approximations were necessary to compute the evolution of the thermal properties of the material during the phase change.
- 3- The progression of the phase change front was not continuous, but defined at the mesh nodes, pertaining to one or another phase.

Crivelli and Idelsohn, in 1986, described a finite element procedure for solving

multi-dimensional phase change problems. The algorithm combined a temperature formulation with a finite element treatment of the differential equation and discontinuous integration within the two-phase elements to avoid the necessity of regularization.

The solution was obtained in terms of temperature and its main feature was that there was no need for an explicit smoothing of the temperature-enthalpy relationship. Here, any convergence criterion based on the relation between the enthalpy at a given node and the total latent heat associated with that node did not account for the convergence out of the phase-change region. To insure stability of the iterative process, an adequate correction of the iteration matrix was devised. A useful heuristic estimation of the proper time step associated with the spatial mesh used was established. The disadvantage of this method was that it has emphasised the use of linear finite elements scheme whose phase change region always lied inside one element. The interface was defined by a straight line dividing the quadrilateral element into two polygons, depending on whether it cut two adjacent or two opposite sides. This is not the case when coarse meshes are used. Steven, in 1982, described internally discontinuous finite elements for moving interface problems. His work presented and developed the characteristics matrices for two such elements, namely a quadratic triangular with an internal interface modelled by two straight lines and a quadratic isoparametric element. Both these elements were tested against an analytical solution to simple Poisson equation. Such tests have revealed the performance of the proposed elements to be satisfactory except for the definitions of the gradients near the interface.

MacKinnon and Carey, in 1987, considered finite element analysis of problems

with discontinuous material coefficients. For applications in which the material interface crosses an element, they developed special elements with an embedded flux constraints at the interface. These special elements comprised subelements in which the interface flux balance was enforced locally in consistent sense with the weak integral statement of the problem. This approach was then extensively tested against computations with the standard finite element method and with the method proposed by Steven in 1982. The numerical solutions, undertaken, demonstrated that the proposed method yields similar accuracy and the same asymptotic rate of convergence as the standard method. Further, it produced superconvergent fluxes in certain situation. Accordingly, Steven's method was less accurate and converged at suboptimal rates. This method has proposed a curvilinear interface dividing the element into biquadratic quadrilateral subelements. However, a disadvantage with this approach is that subelements are true elements, and ill-conditioning may be induced if a subelement is small relatively to its neighbour elements. In the following sections of this chapter, a numerical algorithm will be presented to formulate the transient heat transfer problem with phase change. It is based on the law of conservation of energy for the medium with thermal properties, taking into account the arbitrary temperature conditions. The energy conservation formulation in integral form will be expressed in terms of enthalpy. Then, the Galerkin-Bubnov approach combined with the assumed piece-wise representation of the temperature functions provides the basis for the implementation of the finite element method with respect to special variables and lead to the weak formulation of the problem (Bathe, 1982 and Zienkiewicz, 1977).

The transient heat transfer problem is integrated with respect to time. In discrete form, it is done by the application of Euler backward method (Lunardini, 1981, Ralston, 1965, Dalhuijsen and Segal, 1986). Special approach is introduced to determine the position and the shape of the moving phase-change interface (MacKinnon and Carey, 1987, Crivelli and Idelsohn, 1988). The numerical simulation of the propagation of the phase change interface by means of finite element methods, is done by introducing curvilinear finite element intersecting the original finite element in arbitrary fashion. Numerically, the interface position is defined by means of three points, since the shape functions used for eight-noded elements are quadratic. The six types of intersection considered for the analysis as shown in Fig. 3.4. In order to improve the accuracy of the solution, Newton-Raphson and modified Newton-Raphson iterative procedures are applied (Kleiber, 1985). In order to speed up the convergence of the problem an under relaxation factor is used in the iterative procedure starting from the second iteration (Patankar, 1981). By means of the presented formulations and the proposed numerical algorithm, several modelling problems of pile embedded in frozen uniform and layered soil are computed and analyzed. The analysis will determine the evolution of the temperature field around the pile and the propagation of the zero isotherm, defining thawing, in time. The computation and related discussion is carried out in Chapter IV.

3.2 Strong Formulation of the Heat Transfer Problem with Phase Change

We consider a control volume Ω with a fixed boundary $\partial\Omega$. The control volume Ω is divided by moving interface boundary $\Gamma(t)$ into two regions Ω_1

and Ω_2 each of different phase as shown in Fig 3.1.

That is the following condition is satisfied.

$$\Omega = \Omega_1 \cup \Omega_2, \quad \Omega_1 \cap \Omega_2 = 0 \quad \text{and} \quad \partial\Omega = \partial\Omega_1 \cup \partial\Omega_2 \quad (3.1)$$

Volume : $\Omega = \Omega_1 \cup \Omega_2$,

Boundary: $\partial\Omega_1 \cup \partial\Omega_2$, and,

Interface: $\Gamma(t)$

The equation of conservation of energy considered in this study may be written in a Cartesian space as:

$$-\frac{\partial q_i}{\partial x_i} + q_B = \rho c \frac{\partial \Theta}{\partial t} \quad (3.2)$$

where:

ρ or γ = the mass density,

ρc = volumetric heat capacity,

Θ = temperature,

q_B = the rate of heat generated per unit volume,

q_i = the heat flux in the x_i direction.

The heat flow conducted by unit area q_i is related to the gradient of temperature, θ by means of the generalized Fourier law (refer to Eq. 2.21).

$$q_i = -k_{ij} \frac{\partial \Theta}{\partial x_j} \quad (3.3)$$

The minus sign means that the heat flows from higher to lower temperature where k_{ij} is the thermal conductivity tensor, which in the most general case, can be the function of position and temperature, i.e. (refer to Eq. 2.22)

$$k_{ij} = k_{ij}(x, \Theta)$$

and

$$k_{ij} = k_{ji} \quad (3.4)$$

Assuming x_i and x_j are directed along the principal direction of the thermal conductivity tensor, we have:

$$k_{ij}(x, \Theta) = k(x, \Theta) \delta_{ij} \quad (3.5)$$

where δ_{ij} = Kronecker symbol and is defined as follows:

$$\delta_{ij} = \begin{cases} 1 & \text{where } i=j \\ 0 & \text{where } i \neq j \end{cases} \quad (3.6)$$

combining 3.3 and 3.5, the equation 3.2 will be written as:

$$\frac{\partial}{\partial x_i} (k_{ij} \frac{\partial \Theta}{\partial x_j}) = \rho c \dot{\Theta} - q_B \quad (3.6)$$

or

$$\nabla (k \nabla \Theta) = \rho c \dot{\Theta} - q_B$$

where ∇ = Nabla operator, and in cartesian coordinates;

$$\nabla = \frac{\partial}{\partial x}(\)\vec{i} + \frac{\partial}{\partial y}(\)\vec{j} + \frac{\partial}{\partial z}(\)\vec{k}$$

The sought solution of eq. 3.6 should satisfy the prescribed boundary conditions.

3.3 Boundary Conditions

3.3.1 Temperature Boundary Conditions:

The temperature can be prescribed at specific points and surfaces of the body, i.e.

$$\Theta = \Theta^* \text{ on } \partial\Omega_T \quad (3.7)$$

3.3.2 Heat Flow Boundary Conditions:

The heat flow inputs can be given at specific points and surfaces of the body, like e.g.

$$k_n \frac{\partial \Theta}{\partial n} = q^* \text{ on } \partial\Omega_q \quad (3.8)$$

where:

n = the direction of the outward normal vector to the bounding surface,

k_n = the normal conductivity in the direction of n ,

q^* = the prescribed heat flow input.

3.2.3. Convective Boundary Conditions

The Convective boundary conditions are of the same types as heat flow conditions:

$$k_n \frac{\partial \Theta}{\partial n} = \alpha_c (\Theta_\infty - \Theta_s) \text{ on } \partial\Omega_c \quad (3.9)$$

where:

α_c = coefficient of convection (can be temperature dependent), as defined in section 2.2.2

θ_∞ = environmental temperature,

θ_s = surface temperature.

3.2.4 Phase Change Interface Condition:

For the phase change interface $\Gamma(t)$, the following condition must be satisfied:

$$\Theta = \Theta_f \text{ and } [k \nabla \Theta] \cdot n + \rho L v \cdot n = 0 \quad (3.10)$$

where:

θ_f = phase change temperature,

L = latent heat (per unit mass of the material currently converted),

ρL = volumetric latent heat (noted as L in Chapter IV, for simplicity),

v = the phase change interface velocity vector,

[] = the jump of the enclosed quantity across $\Gamma(t)$, i.e.

$$[k\nabla\Theta] = (k\nabla\Theta)^+ - (k\nabla\Theta)^- \quad (3.11)$$

where

()⁺ = the estimated values at positive side of \mathbf{n} of $\Gamma(t)$,

()⁻ = the estimated values at negative side of \mathbf{n} of $\Gamma(t)$.

It should be pointed out that the positive direction of \mathbf{n} assumed in Eq. (3.10) is from solidus (Ω_1) toward liquidus (Ω_2).

The direction of the normal to the phase change interface $\Gamma(t)$ is the outnormal with respect to Ω_2 so that $\mathbf{n} = \mathbf{n}^+ = -\mathbf{n}^-$. The velocity vector \mathbf{v} governing the kinematics of the interfacial surface is obtained by differentiation of the equation of the interface $\Gamma(t)$ with respect to time.

3.4 Integral Formulation Employing the Energy Conservation Equation

The energy conservation law for thermal problems states that: The rate of increase of the energy content of control volume Ω with time is equal to heat influx conducted into Ω plus the internal heat generation rate.

$$\frac{D}{Dt} \int_{\Omega} \rho u \, dV = \int_{\partial\Omega} k\nabla\Theta \cdot \mathbf{n} \, dA + \int_{\Omega} q_B \, dV \quad (3.12)$$

where u = the specific internal energy.

Introducing the specific internal enthalpy ϵ , the internal energy can be written as:

$$\rho u = \rho \epsilon - p$$

and

$$\frac{D}{Dt} \int_{\Omega} \rho u \, dV = \frac{D}{Dt} \int_{\Omega} \rho \epsilon \, dV - \int_{\Omega} p \, dV \quad (3.13)$$

where p = the internal pressure.

In the absence of motion, the internal pressure is independent of time, i.e.

$$\frac{D}{Dt} \int_{\Omega} p \, dV = 0 \quad (3.14)$$

Taking into account the condition (3.14) and substitution of Eq. (3.13) into Eq. (3.12) gives that the law of conservation of energy can be expressed in terms of enthalpy, i.e.

$$\frac{D}{Dt} \int_{\Omega} \rho \epsilon \, dV = \int_{\partial \Omega} k \nabla \Theta \cdot n \, dA + \int_{\Omega} q_B \, dV \quad (3.15)$$

Following Eringen (1967), the material derivative on the left hand side of Eq. 3.15 can be written as:

$$\frac{D}{Dt} \int_{\Omega} \rho \epsilon \, dV = \int_{\Omega} \frac{\partial}{\partial t} (\rho \epsilon) \, dV - \int_{\Gamma} [\rho \epsilon] v \cdot n \, dA \quad (3.16)$$

where \mathbf{v} = velocity vector of the moving phase-change interface.

The first term on the right hand side of Eq. 3.15 according to Green-Gauss theorem for discontinuous region (what is shown in Fig. 3.2), is written in the following way:

$$\int_{\partial\Omega} k\nabla\Theta \cdot n dA = \int_{\Omega} \nabla \cdot (k\nabla\Theta) dV + \int_{\Gamma} [k\nabla\Theta] \cdot n dA \quad (3.17)$$

Combining 3.16 and 3.17, we obtain the new form of equation 3.15, i.e.

$$\begin{aligned} \int_{\Omega} \frac{\partial}{\partial t} (\rho\epsilon) dV - \int_{\Gamma} [\rho\epsilon]\mathbf{v} \cdot \mathbf{n} dA = \\ \int_{\Omega} \nabla \cdot (k\nabla\Theta) dV + \int_{\Gamma} [k\nabla\Theta] \cdot \mathbf{n} dA + \int_{\Omega} q_B dV \end{aligned} \quad (3.18)$$

Assuming that Ω_2 denotes liquidus and Ω_1 stands for solidus, the following condition is satisfied on the moving interface (Eq. 2.18)

$$[\rho\epsilon] = \rho L \quad (3.19)$$

In the other points of Ω_1 or Ω_2 the relation between specific enthalpy and the heat capacity using Eq. (2.16) is as follows:

$$\frac{\partial}{\partial t}(\rho\epsilon) = \rho c \frac{\partial\Theta}{\partial t} = \rho c \dot{\Theta} \quad (3.20)$$

The dot over temperature Θ means the partial differentiation with respect to time. Substituting the relationships 3.19 and 3.20 into 3.18 and after regrouping all terms into the left hand side, we get the following equation:

$$\int_{\Omega} (\rho c \dot{\Theta} - \nabla \cdot (k \nabla \Theta) - q_B) dV - \int_{\Gamma} ([k \nabla \Theta] + \rho L v) \cdot n dA = 0 \quad (3.21)$$

The first integrand of Eq. 3.21 is Eq. 3.6 and Eq. 3.10 is the second integrand.

Introducing now a new function ω from the variational space, such that ω satisfies boundary conditions for Θ , the weak form of the heat transfer problem including phase change can be written as:

$$\begin{aligned} \int_{\Omega} \omega \rho c \dot{\Theta} dV - \int_{\Omega} \omega \nabla \cdot (k \nabla \Theta) dV - \int_{\Omega} \omega q_B dV \\ - \int_{\Gamma} \omega \rho L v \cdot n dA - \int_{\Gamma} \omega [k \nabla \Theta] \cdot n dA = 0 \end{aligned} \quad (3.22)$$

Integrating by parts the second integrand of Eq. 3.22 and using Gauss's Divergence theorem, we have:

$$\begin{aligned} \int_{\Omega} \omega \nabla \cdot (k \nabla \Theta) dV = \int_{\partial \Omega} \omega k \nabla \Theta \cdot n dA \\ - \int_{\Gamma} \omega [k \nabla \Theta] \cdot n dA - \int_{\Omega} \nabla \omega \cdot (k \nabla \Theta) dV \end{aligned} \quad (3.23)$$

Taking into account the prescribed flow input and according to boundary

conditions defined by Eqs. 3.8 and 3.9 we get:

$$\int_{\partial\Omega} \omega k \nabla \Theta \cdot n \, dA = \int_{\partial\Omega_c} \omega \alpha_c (\Theta_w - \Theta_s) dA + \int_{\partial\Omega_q} \omega q^* \, dA \quad (3.24)$$

where $\partial\Omega_c$ and $\partial\Omega_q$ refer to the surface along which either the convective flux or the specified flux boundary conditions are applied respectively.

Combining the relationships 3.24 and 3.23 with equation 3.22, leads to:

$$\begin{aligned} \int_{\Omega} \rho c \dot{\Theta} \, dV + \int_{\Omega} \nabla \omega \cdot (k \nabla \Theta) \, dV + \int_{\partial\Omega_c} \omega \alpha_c \Theta_s \, dA = \\ \int_{\Omega} \omega q_B \, dV + \int_{\partial\Omega_c} \omega \alpha_c \Theta_w \, dA + \int_{\partial\Omega_q} \omega q^* \, dA + \int_{\Gamma} \omega \rho L v \cdot n \, dA \end{aligned} \quad (3.25)$$

The above equation constitutes the weak form of the heat transfer analysis including phase change. It describes thermal behaviour of the control volume in time and in general, all terms in equation 3.25 can be time dependent.

3.5 The Weighted Residual Method as an Approximation to Integral Formulation

The equation (3.25) should be solved with respect to the unknown temperature Θ . Regarding further discretization, the unknown function Θ is replaced by its discretized approximation Θ^h , as well as variation ω by ω^h , and also assume that:

$$\Theta^h = T^h + \Theta^{*h} \quad (3.26)$$

where Θ^h satisfies at least in the approximate sense the prescribed temperature boundary conditions defined by Eq. (3.7) and

$$T^h = 0 \quad \text{on} \quad \partial\Omega_T \quad (3.27)$$

If the approximation Θ^h can be described by the expansion:

$$\Theta^h = \sum_{i=1}^n N_i \Theta_i = \sum_{i=1}^n N_i T_i + \sum_{i=1}^n N_i \Theta_i^* \quad (3.28)$$

where N_i are the shape functions, we put a finite set of arbitrary weighing functions ω_j for $j = 1, 2, 3, \dots, n$ in place of any function ω^h . As a result, a set of n equations of the following form will be obtained as:

$$\begin{aligned} & \int_{\Omega} \omega_j \rho c \dot{T}^h dV + \int_{\Omega} \nabla \omega_j \cdot (k \nabla T^h) dV + \int_{\partial\Omega_c} \omega_j \alpha_c T_s^h dA = \\ & \int_{\Omega} \omega_j q_B dV + \int_{\partial\Omega_c} \omega_j \alpha_c \Theta_{\infty} dA + \int_{\partial\Omega_q} \omega_j q^* dA + \int_{\Gamma} \omega_j \rho L v \cdot n dA \quad (3.29) \\ & - \int_{\Omega} \omega_j \rho c \dot{\Theta}^{*h} dV - \int_{\Omega} \nabla \omega_j \cdot (k \nabla \Theta^{*h}) dV - \int_{\partial\Omega_c} \omega_j \alpha_c \Theta_s^{*h} dA \end{aligned}$$

It is seen, that the above equation contains derivatives of the unknown function and requires integration with respect to time.

3.6 Implicit Time Integration

To solve Eq. 3.29, an implicit integration scheme is employed with the following assumptions:

- 1) The conditions at time t are known,
- 2) The temperatures at time $(t + \Delta t)$ are to be determined.

The discretization of Eq. 3.29 with respect to time gives the following relationship:

$$\begin{aligned}
 & \int_{\Omega} \omega_j \rho^{(t+\Delta t)} c^{(t+\Delta t)} \dot{T}^{(t+\Delta t)} dV + \int_{\Omega} \nabla \omega_j \cdot k \nabla (T^{(t+\Delta t)}) dV \\
 & + \int_{\partial \Omega_c} \omega_j \alpha_c^{(t+\Delta t)} T_s^{(t+\Delta t)} dA = \int_{\Omega} \omega_j \rho_B^{(t+\Delta t)} dV + \int_{\partial \Omega_c} \omega_j \alpha_c^{(t+\Delta t)} \Theta_{\infty}^{(t+\Delta t)} dA \\
 & + \int_{\partial \Omega_q} \omega_j q^{*(t+\Delta t)} dA + \int_{\Gamma(t+\Delta t)} \omega_j \rho^{(t+\Delta t)} L v^{(t+\Delta t)} \cdot n^{(t+\Delta t)} dA \quad (3.30) \\
 & - \int_{\Omega} \omega_j \rho^{(t+\Delta t)} c^{(t+\Delta t)} \Theta^{*(t+\Delta t)} dV - \int_{\Omega} \nabla \omega_j \cdot k^{(t+\Delta t)} \nabla (\Theta^{*(t+\Delta t)}) dV \\
 & - \int_{\partial \Omega_c} \omega_j \alpha_c^{(t+\Delta t)} \Theta_s^{*(t+\Delta t)} dA
 \end{aligned}$$

For any time dependent quantity appearing in Eq. 3.30, the relationship between the current time instant and the previous time instant is described by the incremental decomposition procedure Eq. (3.25) written as:

$$T^{(t+\Delta t)} = T^{(t)} + \vec{T} \quad (3.31)$$

and

$$\nabla(T^{(t+\Delta t)}) = \nabla(T^{(t)}) + \nabla \vec{T} \quad (3.32)$$

where \tilde{T} denotes the increment of T. Employing the linearization assumption, the dot products of time dependent quantities appearing in Eq. 3.30 are approximated as shown below:

$$k^{(t+\Delta t)} \nabla(T^{(t+\Delta t)}) = k^{(t)} \nabla(T^{(t)}) + k^{(t)} \nabla \tilde{T} \quad (3.33)$$

$$\alpha_c^{(t+\Delta t)} (\Theta_\infty^{(t+\Delta t)} - T_s^{(t+\Delta t)}) = \alpha_c^{(t)} (\Theta_\infty^{(t+\Delta t)} - T_s^{(t)} - \tilde{T}_s) \quad (3.34)$$

Integration with respect to time is obtained by implementation of the Euler backward integration method according to the following formula:

$$\dot{T}^{(t+\Delta t)} = \frac{T^{(t+\Delta t)} - T^{(t)}}{\Delta t} = \frac{\tilde{T}}{\Delta t} \quad (3.35)$$

Combining the Euler backward formula with linearization assumption, the dot product of time dependent quantities containing derivative of the unknown variable is approximated as:

$$\rho^{(t+\Delta t)} c^{(t+\Delta t)} \dot{T}^{(t+\Delta t)} = \rho^{(t)} c^{(t)} \frac{\tilde{T}}{\Delta t} \quad (3.36)$$

Following the Bubnov-Galerkin method, weighing functions ω_j are taken in the form of original shape functions N_j i. e.

$$\omega_j = N_j \quad (3.37)$$

Introducing the relationships 3.31 through 3.37 into Eq. 3.30, the incremental equilibrium equation, written in a matrix form, finally is:

$$\left[\frac{1}{\Delta t} \mathbf{C}^{(t)} + \mathbf{K}_k^{(t)} + \mathbf{K}_c^{(t)} \right] \tilde{\mathbf{T}} = \mathbf{Q}^{(t+\Delta t)} + \mathbf{Q}_c^{(t+\Delta t)} + \mathbf{Q}_L^{(t+\Delta t)} - \mathbf{Q}^{*(t+\Delta t)} - \mathbf{Q}^{(t)} \quad (3.38)$$

where

$\tilde{\mathbf{T}} = \{T_i\}$ = the vector of nodal temperature increment for time step Δt ,

$\mathbf{C}^{(t)}$ = the incremental capacity matrix,

$$\mathbf{C}^{(t)} = \int_{\Omega} \mathbf{N}^T \rho^{(t)} c^{(t)} \mathbf{N} dV \quad (3.39)$$

$\mathbf{K}_k^{(t)}$ = the incremental conductivity matrix,

$$\mathbf{K}_k^{(t)} = \int_{\Omega} \mathbf{B}^T k^{(t)} \mathbf{B} dV \quad (3.40)$$

$\mathbf{K}_c^{(t)}$ = the incremental convection matrix,

$$K_c^{(t)} = \int_{\partial\Omega_c} N^T \alpha_c^{(t)} N dA \quad (3.41)$$

$Q^{(t+\Delta t)}$ = the heat flow vector for time $(t+\Delta t)$

$$Q^{(t+\Delta t)} = \int_{\Omega} N^T q_B^{(t+\Delta t)} dV + \int_{\partial\Omega_q} N^T q^{*(t+\Delta t)} dA \quad (3.42)$$

$Q_c^{(t+\Delta t)}$ = the convective heat transfer rate vector

$$Q_c^{(t+\Delta t)} = \int_{\partial\Omega_c} N^T \alpha_c^{(t)} (\Theta_{\infty}^{(t+\Delta t)} - T_s^{(t)}) dA \quad (3.43)$$

$Q^{*(t+\Delta t)}$ = the vector of heat flow due to temperature boundary conditions,

$$Q^{*(t+\Delta t)} = \int_{\Omega} N^T \rho^{(t)} c^{(t)} \dot{\Theta}^{*(t+\Delta t)} dV + \int_{\Omega} B^T k^{(t)} \nabla(\Theta^{*(t+\Delta t)}) dV + \int_{\partial\Omega_c} N^T \alpha_c^{(t)} \Theta_s^{*(t+\Delta t)} dA \quad (3.44)$$

$Q_L^{(t+\Delta t)}$ = the vector of heat flow due to phase-change effect,

$$Q_L^{(t+\Delta t)} = \int_{\Gamma^{(t+\Delta t)}} N^T \rho^{(t+\Delta t)} L v^{(t+\Delta t)} \bullet n^{(t+\Delta t)} dA \quad (3.45)$$

$Q^{(t)}$ = the vector of "balanced heat flow" at the time instant t .

$$Q^{(t)} = \int_{\Omega} B^T k^{(t)} \nabla (T^{(t)}) dV \quad (3.46)$$

where:

$N = \{N_i\}$ = the vector of shape functions,

$B = \{B_{ij}\} = \left\{ \frac{\partial N_j}{\partial x_i} \right\}$ = the matrix of shape functions gradients.

The superscript T denotes the operation of transposition of a matrix.

It should be stressed that according to previously made linearization assumptions, the obtainable solution in discrete form is simply an approximation to the exact solution. In order to increase the accuracy of the results, Newton-Raphson equilibrium iterations are employed at each time step, according to the following formula:

$$\tilde{T}_{(0)}^{(t+\Delta t)} = \tilde{T}_{(i-1)}^{(t+\Delta t)} + \Delta \tilde{T}_{(0)} \quad (3.47a)$$

with initial conditions:

$$\tilde{T}_{(0)}^{(t+\Delta t)} = \tilde{T}^{(t)} \quad \text{and} \quad \Delta \tilde{T}_{(1)} = \tilde{T} \quad (3.47b)$$

The application of the full Newton-Raphson equilibrium iterations to the Eq. 3.38 gives:

$$\left[\frac{1}{\Delta t} C_{(i-1)}^{(t+\Delta t)} + K_{k(i-1)}^{(t+\Delta t)} + K_{c(i-1)}^{(t+\Delta t)} \right] \Delta \tilde{T}_{(i-1)} = \quad (3.48)$$

$$Q_{(i-1)}^{(t+\Delta t)} + Q_{c(i-1)}^{(t+\Delta t)} + Q_{L(i-1)}^{(t+\Delta t)} - Q_{(i-1)}^{*(t+\Delta t)} - Q_{(i-1)}^{(t+\Delta t)}$$

where

$$C_{(i-1)}^{(t+\Delta t)} = \int_{\Omega} N^T \rho_{(i-1)}^{(t+\Delta t)} c_{(i-1)}^{(t+\Delta t)} N dV \quad (3.49)$$

$$K_{k(i-1)}^{(t+\Delta t)} = \int_{\Omega} B^T k_{(i-1)}^{(t+\Delta t)} B dV \quad (3.50)$$

$$K_{c(i-1)}^{(t+\Delta t)} = \int_{\partial\Omega_c} N^T \alpha_{c(i-1)}^{(t+\Delta t)} N dA \quad (3.51)$$

$$Q_{c(i-1)}^{(t+\Delta t)} = \int_{\partial\Omega_c} N^T \alpha_{c(i-1)}^{(t+\Delta t)} (\Theta_{-}^{(t+\Delta t)} - T_{s(i-1)}^{(t+\Delta t)}) dA \quad (3.52)$$

$$Q_{(i-1)}^{*(t+\Delta t)} = \int_{\Omega} N^T \rho_{(i-1)}^{(t+\Delta t)} c_{(i-1)}^{(t+\Delta t)} \dot{\Theta}^{*(t+\Delta t)} dV$$

$$+ \int_{\Omega} B^T k_{(i-1)}^{(t+\Delta t)} \nabla(\Theta^{*(t+\Delta t)}) dV + \int_{\partial\Omega_c} N^T \alpha_{c(i-1)}^{(t+\Delta t)} \Theta_s^{*(t+\Delta t)} dA \quad (3.53)$$

$$Q_{L(i-1)}^{(t+\Delta t)} = \int_{\Gamma(t+\Delta t)} N^T \rho_{(i-1)}^{(t+\Delta t)} L v_{(i-1)}^{(t+\Delta t)} \cdot n_{(i-1)}^{(t+\Delta t)} dA \quad (3.54)$$

$$\begin{aligned}
Q_{(i-1)}^{(t+\Delta t)} &= \int_{\Omega} \mathbf{B}^T k_{(i-1)}^{(t+\Delta t)} \nabla T_{(i-1)}^{(t+\Delta t)} dV + \\
&\int_{\Omega} \mathbf{N}^T \rho_{(i-1)}^{(t+\Delta t)} c_{(i-1)}^{(t+\Delta t)} \bar{T}_{(i-1)}^{(t+\Delta t)} dV
\end{aligned} \tag{3.55}$$

For the modified Newton-Raphson method, for which the iterations are performed with the coefficient matrix constant during the entire time step, Eq. 3.48 gives:

$$\begin{aligned}
& \left[\frac{1}{\Delta t} C^{(i)} + K_k^{(i)} + K_c^{(i)} \right] \Delta \bar{T}_{(i)} \\
& = Q^{(t+\Delta t)} + Q_{c(i-1)}^{(t+\Delta t)} + Q_{L(i-1)}^{(t+\Delta t)} - Q_{(i-1)}^{*(t+\Delta t)} - Q_{(i-1)}^{(t+\Delta t)}
\end{aligned} \tag{3.56}$$

3.7 Numerical Strategy to Include Latent Heat Term and Temperature Dependent Material Properties

For the element which is intersected by the phase-change interface, the special treatment should be employed due to the discontinuities in the material properties and the temperature gradient. It is assumed, that the domain and mesh are fixed and the discontinuity surface moves through the interior of the elements. A simple procedure is implemented to detect the existence of the phase-change interface. When the phase change in the finite element is confirmed, the position and the shape of the interface is determined by special routine. Numerically, the interface position is defined by means of three points, since the shape functions used for eight-nodded elements are quadratic. The six types of intersections shown in Fig. 3.3 are considered in the analysis.

The type one and two can be classified as case one, since the numerical treatment of both types is similar and the difference is in the procedure defining the sequence of nodes associated with the finite element.

Similarly, the third, fourth, fifth and sixth types form the second case. For the first group (type 1 and 2), the finite element is divided into two parts such, that each part can be modelled by an eight noded quadrilateral subelement which is shown in Fig. 3.4a.

In this group, the matrices of coefficients and flow vectors are evaluated for each subelement and for the three-noded one dimensional interface element. Considering the second group of elements, we have to employ two six-node triangular isoparametric subelements and one eight-noded quadrilateral subelement as shown in Fig. 3.4b.

The strategy as described above provides that an independent interpolation is implemented for both material phases inside each element. The nine-point Gauss-Legendre numerical quadrature is employed to obtain matrices and vectors for the quadrilateral subelements and the seven point scheme for the triangular subelement.

CHAPTER IV

MODELLING PROBLEMS AND RESULTS

4.1 Numerical Assumptions and Configurations

The moving phase-change interface intersecting the finite element introduces discontinuity in the shape functions defining incremental conductivity matrix, incremental heat capacity matrix, and constant value of latent heat associated with phase-change. This, of course, violates the assumptions made for the definition of the shape functions and necessitates the introduction of a special approach. As it has been discussed in section 3.7 of the present thesis, the phase change interface is simulated by a curvilinear finite element which intersects in an arbitrary fashion the original finite element in sub-elements (Figs 3.4 a and 3.4 b). In this way, each of the subelements is described by continuous shape functions, which satisfies the requirements of F.E.M. The numerical elaboration of the phase change interface involves the temperature gradient and leads to the additional heat capacity matrix conjugated with phase-change front. Regarding spatial variables, the proposed algorithm enables us to analyze plane as well as axisymmetrical three-dimensional problems.

Considering thermal properties of the medium, the following **MODELS** can be analyzed and investigated by means of the presented algorithm:

- 1- Medium with temperature independent properties without phase change.
- 2- Medium with temperature dependent properties without phase change.
- 3- Medium with temperature independent properties with phase change.
- 4- Medium with temperature dependent properties with phase change.

The combination of two or more models can also be investigated as well. For instance, the pile embedded in the soil is considered as the combination of Model 1, the pile, and Model 4, the soil.

Due to the high nonlinearity of the problem basically caused by the large value of the latent heat appearing on the phase-change interface, the numerical formulation employs the Newton-Raphson method as well as the modified Newton-Raphson Method (Zienkiewicz, 1977, Kleiber, 1985).

In the analyzed modelling problems, the applied temperature distribution with time is presented in Fig. 4.3 (Jumikis, 1977), and the applied increment of time is equal to one day. The computational process requires special attention to the situation when the phase change interface coincides with the boundaries of the finite element. That is, when the moving front travels down into the soil, leaves the previous element and enters the next one. Then the dramatic reduction of increment of time is required, to satisfy the requirements of the convergence. The incremental time steps used in this iterative procedure are 1/10 day, 1/100 day, 1/1000 day.

To improve and accelerate the convergence of the solution, a relaxation factor

equals to 0.75 was introduced starting from the second iteration (Patankar, 1980). This factor is useful when the solution reaches a steady oscillatory convergence.

After the moving phase-change interface crosses the boundary of the finite element, the solution starts to stabilize, the iterative computational process will gradually returns to the initially applied increment of time, one day.

4.2 Modelling of Geotechnical Problems

For the theoretical formulation and the proposed numerical algorithm, the analysis of several modelling problems are investigated. They represent the solution for a concrete pile of diameter, $\phi = 0.40$ m, embedded in uniform soil including sand, clay and peat with different water contents and also in layered with a gravel layer overlying the same uniform soil.

4.2.1 Global Numerical Assumptions

1- The pile embedded in the soil is a concrete pile of diameter, $\phi = 0.40$ m, and length, $L = 5.50$ m, having constant thermal properties for both frozen and unfrozen states.

$$k = 0.928 \text{ W/mK} \quad c = 25.23 \text{ W day/m}^3 \text{ K.}$$

$$L = 0 \text{ (No latent heat to be considered } \equiv \text{ Model 1).}$$

- 2- The uniform soil medium is, initially, frozen at a temperature $\theta = -2^\circ \text{ C}$.
- 3- On the bottom boundary, the temperature is maintained constant during the entire process of computation and is equal to the initial temperature $\theta = -2^\circ \text{ C}$.

4- The geometry of the finite element meshes are presented in Fig. 4.1 and Fig. 4.2, depending on the type of the soil used in the analysis. The axis of the pile is considered as the axis of symmetry of the geometry and the cylindrical coordinates are reduced to two-dimensional system: radial (r or y) and elevation (z or x) and having the tangential ordinate maintained constant.

5- The adiabatic conditions are imposed on the external vertical side and on the vertical axis of the pile (see Fig. 4.1 and Fig. 4.2) due to axial symmetry.

6- On the top boundary, the available air temperature distribution presented in Fig. 4.3 (Jumikis, 1977) is applied.

7- The following uniform soil types will be investigated:

I- Sand with $\gamma_{dry} = 1400 \text{ kg/m}^3$

$w = 15 \%$ and $w = 20 \%$.

II- Clay with $\gamma_{dry} = 1200 \text{ kg/m}^3$

$w = 15 \%$ and $w = 30 \%$.

II- Peat with $\gamma_{dry} = 400 \text{ kg/m}^3$

$w = 80 \%$ and $w = 120 \%$.

8- The following layered soil types will be investigated in comparison with uniform soils described in 7.

I- Sand with gravel on top

$\gamma_{dry, sand} = 1400 \text{ kg/m}^3$ and $w = 20 \%$

depth of gravel = 2.4 m.

II- Clay with gravel on top

$$\gamma_{\text{dry, clay}} = 1200 \text{ kg/m}^3 \text{ and } w = 30 \%$$

depth of gravel $d = 2.4 \text{ m}$.

III- Peat with gravel on top

$$\gamma_{\text{dry, peat}} = 400 \text{ kg/m}^3 \text{ and } w = 12\% \text{ }$$

depth of gravel $d = 2.5 \text{ m}$.

The unit weight of the layer of gravel overtopping the uniform soil is

$$\gamma_{\text{gravel}} = 1800 \text{ kg/m}^3$$

9- The subscript u refers to unfrozen state.

The subscript f refers to frozen state.

10- The solution of the problem constitutes the evolution of the temperature fields which enables us to prepare and draw the diagrams of the temperature distribution with depth around the pile shaft and determine analytically the location of the permafrost surface (or table) in each soil.

4.2.2 Results Presentation and Observation

The obtained results are presented graphically for each type of soil separately.

They represent:

1- the distributions of temperature for February 20, April 20, June 20, August 20, October 20, December 22. The reason for such choices is based on the following:

a- February 20 shows the results of a pure heat transfer problem before the appearance of the phase-change interface on the surface of the soil.

b- April 20 shows the results at the beginning of propagation of thawing at the soil

surface. These results are important to calculate the ground temperature, T_g for the Neuman problem.

c- June 20 and August 20 indicate the process of propagation of the thawing depth to the permafrost table. August 20 defines the depth of the active layer for the calculation of the pile bearing capacity for summer conditions (Chapter VII).

d- October 20 exemplifies the process of formation of multi-phase medium, solid-liquid-solid taken from the surface of the soil, down, and how the inclusion of the thawing zone changes as the result of the application of variable temperature.

e- December 22 displays the temperature distribution right after the complete merge of the 2 interfaces of the multi-phase change zone. At this time, the freezing front reaches the permafrost table and the soil exerts heaving pressure on the pile. December 22 constitutes a very important data when, later in this thesis, we attempt to calculate the pile bearing capacity for winter conditions.

- 2- The evolution of the 0°C isotherm which defines the propagation of the thawing depth in a period of one year. This graph defines the thickness of the thawed zone, also called the active layer.
- 3- The evolution of the isotherms -2°C , -1°C , $+1^\circ\text{C}$, $+2^\circ\text{C}$, with depth plotted during the period of one year. These data are important to determine boundary conditions for future analytical problems.
- 4- Finally the comparison of the analytical results with the Neumann solution (modified by Nixon and McRoberts, 1973). The modified Berggren Equation (Eq. 2.36) together with the graphical solution of the Neumann equation presented in

Fig. 2.20 are used to make the comparison. The surface temperature, T_s , was calculated from Fig. 4.3, as the ratio of the thawing index, I_T , expressed in degree.days interval of time in days to the ΔT where temperature were above freezing value,

$$T_s = \frac{I_T}{\Delta_T} = \frac{1895.775}{169.62} = 11.18^\circ \text{ C} \quad (4.1)$$

4.3 Problem # 1, Pile in Sandy Soil

The thermal properties for sand which are water-dependent are presented below and the geometry of the problem is taken as Mesh 1 with total depth of soil $d = 9.5$ m.

<u>Sand</u>	$w = 15 \%$	$w = 20 \%$
	$\gamma_d = 1400 \text{ kg/m}^3$	$\gamma_d = 1400 \text{ kg/m}^3$
From Table 2.1a	$K_f = 1.52 \text{ W/mK}$	$K_f = 1.97 \text{ W/mK}$
From Table 2.1b	$K_u = 1.33 \text{ W/mK}$	$K_u = 1.43 \text{ W/mK}$
From Table 2.4a	$C_f = 17.24 \text{ Wday/m}^3\text{K}$	$C_f = 18.98 \text{ Wday/m}^3\text{K}$
From Table 2.4b	$C_u = 24.42 \text{ Wday/m}^3\text{K}$	$C_u = 25.69 \text{ Wday/m}^3\text{K}$
Eq. 2.15 gives	$L = 809.38 \text{ Wday/m}^3$	$L = 1079.17 \text{ Wday/m}^3$

The evolution of temperature for February 20, April 20, June 20, August 20, October 20, and December 22 are presented in the diagram of Figs. 4.4 respectively for $w = 15 \%$ and in Figs. 4.5 and f for $w = 20 \%$. Then the 0° C isotherm evolution in the period of one year is plotted in Fig. 4.6 for $w = 15 \%$ and Fig. 4.7 for $w = 20 \%$.

Comparing Fig. 4.6 and Fig. 4.7, the thermal analysis shows that the thawing propagation is slower for higher water content. For $w = 15\%$, the maximum depth of thaw is approximately 2.25 m while for $w = 20\%$, it is also approximately 2.0 m resulting in a decrease of 11 % for an increase of 33 % water content. As a matter of fact this result was expected because the more moisture the soil contains, the more saturated with ice it becomes in the winter and the slower the process of thawing will propagate in the summer.

Figures 4.8 and 4.9 represent the evolution of isotherms -2, -1, +1, +2, for $w = 15\%$ and $w = 20\%$, respectively. The comparison with the Neumann problem will be carried out in section 4.3.1 and 4.3.2 for both water contents, $w = 15\%$ and 20% , respectively.

4.3.1 Neumann Solution for Sand with $w = 15\%$

The average ground temperature T_g is calculated from the diagram of Fig. 4.4 (April 20), as the ratio of the area enclosing the temperature curve with depth to the total depth of soil considered for the analysis. Hence,

$$T_g = \sum_{i=1} \frac{T_i + T_{i+1}}{2} * \frac{d_i}{d} \quad (4.2)$$

where: T_i = temperature for the i^{th} elevation, in °C,

T_{i+1} = temperature for the $(i+1)^{\text{th}}$ elevation, in °C,

d_i = depth interval between consecutive elevations, in m

d = total depth of soil, in m.

From Eq. 4.2, T_g was found to be equal to -3.67 °C. (4.3)

From Eq. 4.1, $T_s = 11.18$ °C.

Using the thermal properties data for both frozen and unfrozen state and substituting in Eq. (2.13), we get:

$$\kappa_f = \frac{K_f}{C_f} = \frac{1.52}{17.24} = 0.088 \quad (4.4)$$

and

$$\kappa_u = \frac{K_u}{C_u} = \frac{1.33}{24.42} = 0.054 \quad (4.5)$$

Equation (2.32) gives,

$$Ste = \frac{C_u T_s}{L} = \frac{24.42 \times 11.18}{809.38} = 0.337$$

Using the graphical solution of the Neumann equation in Fig. 2.20 to determine the normalised thaw parameter $\alpha/2 (\kappa_u)^{1/2}$,

$$-\frac{T_g}{T_s} \frac{k_f}{k_u} \left(\frac{\kappa_u}{\kappa_f}\right)^{\frac{1}{2}} = \frac{3.67}{11.18} \times \frac{1.52}{1.33} \left(\frac{0.54}{0.088}\right)^{\frac{1}{2}} = 0.295$$

Interpolating between graphs of 0.2 and 0.4 for $Ste = 0.337$, we get;

$$\frac{\alpha}{2(\kappa_u)^{1/2}} = 0.344$$

and

$$\alpha = 0.344 \times 2 \times \sqrt{0.054} = 0.161 \quad (4.6)$$

Substituting Eq. (4.6) into Eq. (2.29), the thawing depth, function of the square root of time for temperatures above 0° C is:

$$X = 0.161 \sqrt{t-110.38} \quad \text{for } 110.38 \leq t \leq 280 \text{ days} \quad (4.7)$$

where X = thawing depth, in m.

t = time in days.

The results of both the numerical analysis and Neumann problem with the percentage of error calculated with respect to Neumann solution are summarized in Table 4.1. Equation (4.7) and the outcoming results of the numerical analysis are graphically plotted as a function of time, in days, during the thawing period and are shown in Fig. 4.10. When the thawing depth reaches its maximum near the end of the warm season, the Neumann approach underpredicts its value by a remarkable margin. Therefore, the use of Neumann solution is confined to a short period of time only.

4.3.2 Neumann Solution for Sand with w = 20 %

$$\text{Using Fig. 4.5 (April 20) and Eq. (4.2), } T_g = -4.84 \text{ }^\circ\text{C} \quad (4.8)$$

Following the same steps of section 4.3.1, the thawing depth for sand with water content, w = 20 % is:

$$X (m) = 0.144 \sqrt{t-110.38} \text{ for } 110.38 \leq t \leq 280.00 \text{ days} \quad (4.9)$$

The comparative results of the numerical and Neumann problems are summarized in Table 4.2.

Figure 4.12 displays graphically the outcoming results of both numerical and Neumann problems. Once again, the thawing process is overestimated at the beginning and underestimated later when the thawing is deepening with time.

The relative error with respect to the Neumann solution (Col. 5 of Table 4.2) is presented in the bar diagram of Fig. 4.13.

Comparing Figs. 4.11 and 4.13, the growth of error is practically the same for both diagrams. The thawing depth is overestimated at the beginning, then, overestimated at the end of the thawing period for the considered boundary condition.

4.4 Problem # 2 Pile in Clayey Soil

The thermal properties of clay are presented below and the geometry of the analytical problem is taken as mesh 2 with a total depth of soil, $d = 11.5$ m.

<u>Clay</u>	$w = 15 \%$	$w = 30 \%$
	$\gamma_{dry} = 1200 \text{ kg/m}^3$	$\gamma_{dry} = 1200 \text{ kg/m}^3$
From Table 2.2a	$K_f = 0.80 \text{ W/mK}$	$K_f = 1.50 \text{ W/mK}$
From Table 2.2b	$K_u = 0.69 \text{ W/mK}$	$K_u = 0.93 \text{ W/mK}$
From Table 2.5a	$C_f = 14.81 \text{ Wday/m}^3\text{K}$	$C_f = 19.21 \text{ Wday/m}^3\text{K}$
From Table 2.5b	$C_u = 19.21 \text{ Wday/m}^3\text{K}$	$C_u = 27.89 \text{ Wday/m}^3\text{K}$

Eq. 2.15 gives $L = 693.75 \text{ Wday/m}^3$ $L = 1387.50 \text{ Wday/m}^3$

The evolution of temperature for February 20, April 20, June 20, August 20, October 20 and December 22 are presented in Figs. 4.14, for $w = 15 \%$ and Figs. 4.15 for $w = 30 \%$. Then, the $0 \text{ }^\circ\text{C}$ isotherm evolution in the period of one year is plotted in Figs. 4.16 and 4.17 for $w = 15 \%$ and $w=30 \%$, respectively.

Figures 4.16 and 4.17 show that the maximum depths of thaw are approximately 1.75 m for $w = 15 \%$ and 1.50 m for $w = 30 \%$. A decrease of only 14 % was observed for an increase of 100 % in water content. Consequently, the process of thawing is always slower for higher water contents. Comparing these results with those of problem # 1, we can conclude that the rate of thawing in sand is much higher than in clay 11 % decrease in depth was observed for an increase of 33 % in water content for sand and only 14 % decrease in depth for an increase of 100 % in water content for clay.

Figure 4.18 and 4.19 represent the evolution of isotherms -2, -1, +1, +2 for $w=15\%$ and $w = 30 \%$, respectively.

The comparisons with the Neumann problem are carried out in sections 4.4.1 and 4.4.2 for both water contents, $w = 15 \%$ and $w = 30 \%$, respectively.

4.4.1 Neumann Solution for Clay with $w = 15 \%$

Using Fig. 4.14 (April 20) and Eq. (4.2), $T_g = -3.797 \text{ }^\circ\text{C}$ (4.10)

Comparing Eq. (4.10) and (4.3), the ground temperature, as defined by Eq. (4.2), is almost the same for both sand and clay with water content, $w = 15 \%$. That is, the distribution of T_g provided the same boundary condition for the Neumann problem independently of

the type of soil involved in the analysis.

Following the same step of section 4.3.1, the thawing depth is as:

$$X(m) = 0.129 \sqrt{t-110.38} \text{ for } 110.38 \leq t \leq 280.00 \text{ days} \quad (4.11)$$

the comparative results of both numerical and Neumann Problems are summarized in table 4.3.

The comparison between the numerical solution resulting from the thermal analysis and the Neumann equation is shown in Fig 4.20. The percentage of error to the Neumann equation is shown in the bar diagram of Fig. 4.21.

4.4.2 Neumann Solution for clay with w = 30 %

$$\text{Using Fig. 4.15 (April 20) and Eq. 4.2, } T_g = -3.998 \text{ }^\circ\text{C} \quad (4.12)$$

Comparing Eq. (4.12) to Eq. (4.10) for clay with w = 15 %, it follows that the boundary condition in terms of temperature is practically invariant with water content for clay since the difference in the ground temperature is only = 0.2 °C when the water content has doubled in quantity.

Following the same steps of section 4.3.1, the thawing depth is estimated as:

$$X(m) = 0.106 \sqrt{t-110.38} \text{ for } 110.38 \leq t \leq 280.00 \text{ days} \quad (4.13)$$

The comparative results of both numerical and Neumann problems are summarized in Table 4.4.

The graphical comparison between both solutions is plotted in Fig. 4.2.1. The

percentage of error is shown in the bar diagram of Fig. 4.23. Observing graphs of Fig. 4.23 and Fig. 4.21, the Neumann solution appears to overestimate the depth of thaw for approximately the first 70 days then underestimates it later for both graphs with water contents, $w = 15\%$ and $w = 30\%$.

By analogy with the results from sand (section 4.4.1 and 4.4.2), we can say that the Neumann problem has presented a proportional margin of error for both soils. Consequently, a practical solution of thawing for piles embedded in frozen sand or clay would be to apply the Neumann Equation up to 70 days approximately then later the analytical solution to the end of the period when the freezing process has been completed reaching the permafrost table.

4.5 Problem # 3 Pile in Peat Soil

The thermal properties of peat with $w = 80\%$ and 120% are presented below. The geometry of finite element problem is considered to be Mesh 2 with total depth of soil, $d = 11.5$ m.

<u>Peat</u>	$w = 80\%$	$w = 120\%$
	$\gamma_d = 400 \text{ kg/m}^3$	$\gamma_d = 400 \text{ kg/m}^3$
From Table 2.3a	$K_f = 0.32 \text{ W/mK}$	$K_f = 0.60 \text{ W/mK}$
From Table 2.3b	$K_u = 0.22 \text{ W/mK}$	$K_u = 0.35 \text{ W/mK}$
From Table 2.6a	$C_f = 11.22 \text{ Wday/m}^3\text{K}$	$C_f = 15.04 \text{ Wday/m}^3\text{K}$
From Table 2.6b	$C_u = 18.96 \text{ Wday/m}^3\text{K}$	$C_u = 26.74 \text{ Wday/m}^3\text{K}$
Eq. 2.15 gives	$L = 1233.33 \text{ Wday/m}^3$	$L = 1850.00 \text{ Wday/m}^3$

The evolution of temperature for February 20, April 20, June 20, August 20, October 20 and December 22 are presented in Figs. 4.24, for $w = 80\%$ and Figs. 4.25 for $w = 120\%$. Then, the $0\text{ }^{\circ}\text{C}$ isotherm evolution in the period of one year is plotted in Figs. 4.26 and 4.27 for $w = 80\%$ and $w=120\%$, respectively. Both figures show that the depth of thaw at the end of the thawing period, are almost equal with a very small decrease of 2.9% when the water content increased by 50% . Therefore, a foreseeing difference in peat problems would be expected with higher water contents, 200% to 400% because of the high absorption capacity of peat to water and its lighter unit weight. The evolution of isotherms $-2, -1, +1, +2\text{ }^{\circ}\text{C}$ for both water contents, $w = 80\%$ and $w = 120\%$ are presented in Figs. 4.28 and 4.29, respectively.

The comparison with the Neumann problems are carried out in the following sections, 4.5.1 and 4.5.2.

4.5.1 Neumann Solution for Peat with $w = 80\%$

$$\text{Using Fig. 4.24 (April 20) and Eq. 4.2, } T_g = -3.395^{\circ}\text{C} \quad (4.14)$$

Following the same steps of section 4.3.1, the thawing depth is estimated as:

$$X = 0.0566 \sqrt{t-110.38} \text{ for } 110.38 \leq t \leq 280.00 \text{ days} \quad (4.15)$$

Table 4.5 summarizes the comparative results of Eq. 4.15 and the numerical problem. The graphical comparison between both solutions is plotted in Fig. 4.30. The percentage of error with respect to the Neumann problem is also plotted and shown in Fig. 4.31.

At the end of the thawing period, the Neumann problem underestimates the

thawing depth by 24 % as shown in Table 4.5, or by 17.8 cm as shown in Fig. 4.30.

4.5.2 Neumann Problem for Peat with $w = 120$ %

Using Fig. 4.25 (April 20) and Eq. 4.2, $T_g = -3.538^\circ \text{C}$ (4.16)

Following the same steps of section 4.3.1, the thawing depth is estimated as:

$$X(m) = 0.0577 \sqrt{t-110.38} \text{ for } 110.38 \leq t \leq 280.00 \text{ days} \quad (4.17)$$

Table 4.6 summarizes the comparative results of Eq. 4.17 and the numerical solution. The graphical comparison between both solutions is plotted in Fig. 4.32. The percentage of error with respect to the Neumann problem is also plotted and shown in Fig. 4.33.

At the end of the thawing period, the Neumann problem underestimates the thawing depth by 18 % as shown in Table 4.6, or by 13.8 cm as shown in Fig. 4.32.

Comparing diagrams of Figs. 4.33 and 4.31, the rate of error flows quite proportionally for both graphs, meets at almost 150 days (≈ 40 days from the beginning of the thawing period) and then diverges at the end of the thawing period with an error difference of approximately 6 % in depth between the two graphs. Therefore, a good estimate of the thawing depth using Neumann Equation is effective only in the first 40 days of the considered thawing period.

4.6 Problem #4: Pile in Sandy Soil with Gravel on Top

In this section, a gravel pad of depth, $d = 2.40$ m has been introduced to insulate the active layer where thawing in the summer and freezing in the winter have taken place.

The gravel layer will be considered as Model 2 for the thermal analysis with temperature-dependent variables and without the inclusion of latent heat.

The thermal properties for sand are shown in section 4.3 for $w = 20 \%$, and for gravel below;

<u>Gravel</u>	$w = 0.0 \%$
	$\gamma_d = 1800 \text{ kg/m}^3$
From Table 2.1a	$K_f = 0.13 \text{ W/mK}$
From Table 2.1b	$K_u = 0.10 \text{ W/mK}$
From Table 2.4a	$C_f = 10.42 \text{ Wday/m}^3\text{K}$
From Table 2.4b	$C_u = 10.42 \text{ Wday/m}^3\text{K}$
Eq. 2.15 gives	$L = 0.0 \text{ Wday/m}^3$

Keeping the total depth of soil for mesh 1, $d = 9.50 \text{ m}$, the depth of sand underlying the gravel is : $9.5 - 2.4 = 7.10 \text{ m}$.

The evolution of temperature distribution for April 20 is shown in Fig. 4.34. This figure will be utilized to determine T_g for the Neumann problem developed in section 4.6.2.

The 0° C isotherm evolution in the period of one year is plotted in Fig. 4.35.

4.6.1 Observations and Conclusions

In comparison with Fig. 4.7 for homogeneous sandy soil, the following observations can be noticed:

- 1- The thaw deepening is faster in gravel than in sand resulting in a smoother curve

and an earlier occurrence of freeze back. A difference of 50 days is noticed between the two curves at the time the freeze back of the soil has started.

2- the maximum depth of thaw is almost the same for both graphs, and approximately equal to 2.0 m. This result indicates that the layer of gravel has been adequately introduced to the depth where thawing has reached its maximum before reaching the underlain sand layer.

These observations were expected for the following reasons:

a- The introduced pad of gravel is completely dry with water content, $w = 0.0\%$ accelerating the process of heat transfer.

b- From Eq. (2.15), it resulted that the volumetric latent heat of gravel is: $L = 0.0$, meaning that a pure heat transfer was conducted in the medium without phase change.

4.6.2 Neumann Problem for Sand with Gravel on Top

From Fig. 4.34, Eq. (4.2), the initial ground temperature is:

$$T_g = -2.748^\circ \text{C}. \quad (4.18)$$

Since the Neumann problem deals only with uniform soil medium, it is necessary to find a mathematical approach to solve for the case of a surficial layer of gravel of height 2.40 m overlaying a 7.10 m of sandy soil. This approach is called "The Equivalent Parameters Approach". It simply consists of replacing the layered medium by a uniform medium having weighted thermal properties with respect to the depth of each layer. The thermal conductivity and volumetric heat capacity for both frozen and unfrozen states, as

well as the volumetric latent heat are expressed as follows:

$$K_f = \frac{0.13 \times 2.4 + 1.97 \times 7.1}{9.5} = 1.505 \text{ W/mK}$$

$$K_u = \frac{0.10 \times 2.4 + 1.43 \times 7.1}{9.5} = 1.094 \text{ W/mK}$$

$$C_f = \frac{10.42 \times 2.4 + 18.98 \times 7.1}{9.5} = 16.815 \text{ W.day/m}^3\text{K}$$

$$C_u = \frac{10.42 \times 2.4 + 25.69 \times 7.1}{9.5} = 21.832 \text{ W.day/m}^3\text{K}$$

$$L = \frac{1079.17}{9.5} \times 7.1 = 806.538 \text{ W.day/m}^3$$

Following the same concept of problem # 1 (section 4.3.2), the thawing depth using the Equivalent Parameters is estimated as:

$$X(m) = 0.163 \sqrt{t-110.38} \text{ for } 110.38 \leq t \leq 280.00 \text{ days} \quad (4.19)$$

The comparative results of both analytical and Neuman problems are summarized in Table 4.7. Figure 4.36 displays graphically the outcoming results of both analytical and

Neumann problems, and Fig. 4.37 represents the relative error with respect to the Neumann solution. In this particular case, the Neumann Equation using the equivalent Parameters Approach, represents a good estimate of the thawing depth in time because the percentage error is small compared to the analytical results and therefore could be utilized as characteristic solution and Eq. 4.19 could be used.

4.7 Problem # 5 Pile in Clayey Soil with Gravel on top

The geometry of the finite element problem is considered as mesh 2. the total depth of soil is 11.50 m, divided into 2.50 m for the gravel layer on top and 9.00 m for the clay layer in the bottom. the thermal properties of clay are determined in section 4.4 for $w = 30\%$, and of gravel in section 4.6. The evolution of temperature distribution for April 20 is shown in Fig. 4.38. The movement of the 0°C isotherm in the period of one year is plotted in Fig. 4.39. The same observations for sand can be seen here for clay with the gravel on top, except for the maximum depth of thaw is approximately 0.50 m deeper for this case than for the uniform clay shown in Fig. 4.17. Consequently, in the soil, the higher the water content is, the higher the contribution of the soil to conduct heat and therefore the deeper the thawing propagation moves.

4.7.1 Neumann Problem for Clay with Gravel on Top

From Fig. 4.38, and Eq. (4.2), $T_g = -2.742^\circ\text{C}$ (4.20)

The Equivalent Parameters Approach will be used to determine the thawing depth function of the square root of time for this case. The equivalent uniform medium has the

following thermal properties:

$$K_f = 1.202 \text{ W/mK}$$

$$K_u = 0.750 \text{ W/mK}$$

$$C_f = 17.299 \text{ W.day/m}^3\text{K}$$

$$C_u = 24.092 \text{ W.day/m}^3\text{K}$$

$$L = 1085.87 \text{ W.day/m}^3.$$

These values were calculated similarly to those in section 4.6.1, but with depth of gravel 2.5 m and a depth of clay 9.00 m.

Following the same concept of problem # 1 (section 4.3.2), the thawing depth using the Equivalent Parameters Approach is estimated as follows:

$$X(m) = 0.114 \sqrt{t-110.38} \text{ for } 110.38 \leq t \leq 280.00 \text{ days} \quad (4.21)$$

The comparative results of both numerical and Neumann problems are summarized in Table 4.8.

Figure 4.40 displays graphically the comparative analysis between the two solution and Fig. 4.41 represents the relative error with respect to the Neumann problem. These figures indicate that the Neumann solution underestimates the thawing at the end of the thawing period by 0.63 m or 42 % with respect to the analytical solution. The maximum depth estimated was approximately as 1.5 m meaning that a height of 1.5 m of gravel would be sufficient to insulate the top layer where thawing and freezing activities took place. The percentage of error for a pile embedded in frozen clay with gravel on top is much higher than for frozen sand with gravel on top, as shown in Fig. 4.37. Therefore,

a better approximation of the Neumann solution to estimate the thawing (or freezing) would be in sandy rather than clayey soils.

4.8 Problem # 6, Pile in Peat Soil with Gravel on Top

The geometry of the finite element problem is considered as mesh 2. The total depth of soil is 11.5 m, divided into 2.5 m for the gravel layer on top and 9.00 m for the peat in the bottom. The thermal properties of peat are determined in section 4.5 for $w=120\%$ and of gravel in section 4.6.

The evolution of temperature distribution for April 20 is shown in Fig. 4.42. The movement of the 0°C isotherm in a period of one year is plotted in Fig. 4.43. The maximum depth of thaw resulting from this analysis is approximately 1.00 m deeper than that produced by the uniform peat medium as shown in Fig. 4.27.

4.8.1 General Observations

Comparing Figs. 4.43, 4.39 and 4.35, the movement of the 0°C isotherm looks almost identical for all graphs as if the thermal analysis of thaw deepening has just occurred in the gravel layer alone without accounting for the type and properties of the soil underlying it. This could be visualized also by comparing data from Tables 4.9, 4.8 and 4.7. Therefore, the heat transfer numerical analysis dealing with material with no phase change (i.e. $L = 0$) and zero moisture content ($w = 0\%$), has produced identical results for thawing in time (maximum depth $\approx 2.00\text{ m}$) regardless of the geometry of the finite element mesh considered, whether it was mesh 1 or mesh 2, and consequently has

demonstrated the accuracy of the proposed algorithm to solve also pure heat transfer problems.

4.8.2 Neumann Problem for Peat with Gravel on Top

$$\text{From Fig. 4.42, and Eq. (4.2), } T_g = -2.742^\circ \text{ C} \quad (4.22)$$

The Equivalent Parameters Approach will also be used to determine the thawing depth, function of the square root of time for this case. The equivalent uniform medium has the following thermal properties:

$$K_f = 0.498 \text{ W/mk}$$

$$K_u = 0.296 \text{ W/mK}$$

$$C_f = 14.036 \text{ W.day/m}^3\text{K}$$

$$C_u = 23.192 \text{ W.day/m}^3\text{K}$$

$$L = 1447.826 \text{ W.day/m}^3.$$

Following the same concept of problem # 1 (section 4.3.2), the thawing depth using the Equivalent Parameters Approach is estimated as follows:

$$X(m) = 0.059 \sqrt{t-110.38} \text{ for } 110.38 \leq t \leq 280.00 \text{ days} \quad (4.23)$$

The comparative results of both numerical and Neumann problems are summarized in Table 4.9.

Figure 4.44 displays graphically the comparative analysis between the two solution and Fig. 4.45 represents the relative error with respect to the Neumann problem. Figure 4.45 shows that the Neumann solution overestimated the depth of thaw for the first thirty

days only and underestimated it later with an error reaching maximum over 200 % at one time. Therefore, the Neumann solution, using the Equivalent Parameters Approach, has underpredicted the thawing depth in time for the case of peat with gravel on top with an error difference of 175 % compared to that produced by a uniform peat soil as graphically shown in Fig. 4.33. The maximum error with uniform peat was under 25 % under.

Now that the Equivalent Parameters Approach associated to the Neumann problem has produced bigger error for peat than for sand and clay, we will try to examine the case where the gravel is considered as a semi-infinite uniform medium and estimate the depth of thawing , function of the square root of time.

The following assumptions are useful to make the solution possible.

1- The depth of thaw propagates only in the gravel layer without reaching the underlain soil.

2- The unit weight of gravel is 1800 kg/m^3 and the water content is taken as

$$w = 0.5 \% \quad (4.24)$$

3- The thermal conductivities and the volumetric heat capacities for both frozen and unfrozen states remain unchanged as defined by section 4.6 with:

$$K_f = 0.130 \text{ W/mK}$$

$$K_u = 0.100 \text{ W/mK}$$

$$C_f = C_u = 10.42 \text{ W.day/m}^3\text{K}$$

4- Substituting Eq. (4.24) into Eq. (2.15), the volumetric latent heat is calculated as,

$$L = 34.69 \text{ W.day/m}^3 \quad (4.25)$$

5- Substituting Eq. 2.15 into Eq. 2.32, the Stefan number which is the ratio of the

sensible heat to the latent heat is, $Ste = 3.36$ (4.26)

With the uniform ground temperature $T_g = -2.814^\circ \text{C}$ and following the same concept of Problem # 1 (section 4.3.2), the thawing depth is estimated as:

$$X(m) = 0.137 \sqrt{t-110.38} \text{ for } 110.38 \leq t \leq 280.00 \text{ days} \quad (4.27)$$

Figure 4.46 illustrates graphically Eq. (4.27) in comparison with Eq. (4.23) and the numerical solution. It can be concluded then that the solution obtained by Eq. (4.27) is more satisfactory than that obtained by Eq. (4.23) and therefore could be used as a better estimate for the model of gravel overlying peat.

Employing Eq. (4.27) in a comparative analysis for both models of sand and clay, neglecting the difference in T_g which is in the order of 0.07°C , it can be concluded that the Neumann solution with gravel considered as a semi-infinite medium enhances the solution for the clay model and underestimates it for sand model as shown in Fig. 4.47 and Fig. 4.48 respectively.

In conclusion, for almost the same depth of gravel, the Neumann solution with the Equivalent Parameters Approach could be employed for the sand model and with the gravel considered as semi-infinite medium, for clay and peat with a determined factor of safety for each model.

CHAPTER V

FROST ACTION AND FOUNDATIONS

5.1 Introduction

Frost action in soils is a term used to describe:

- 1- the detrimental process of frost heaving resulting mainly from the accumulation of moisture in the form of ice lenses at the freezing planes in the soil during the winter period, and also,
- 2- the thaw-weakening or decrease in the bearing strength when the frozen soil thaws in the summer period.

Soils that display one or both of these aspects are referred to as being frost susceptible.

Significant damage and costly maintenance result from frost heaving and thaw weakening of soils and therefore the effects of frost action constitute a major consideration in the design and construction of various structures and facilities (Johnston, 1981).

For instance, frost heaving results in distortion of structures due to expansion and

lifting of the soil and therefore seriously affects the riding quality and use of traffic surfaces.

Serious effects also occur during the thaw period to structures founded on the ground surface or in the active layer. The active layer is defined as the top layer of the soil which depth correspond to the maximum thawing depth in the summer. Thaw-weakening is particular concern to highways, railways and airports. Thawing of ice lenses at a rate faster than the released moisture can escape, accompanied by loading of the soil causes a larger decrease in bearing capacity. Differential thaw, of course, will result in irregular settlement of the previously heaved foundations and further complicate internal drainage.

5.2 Frost Action Process

The frost action process is extremely complex and many studies of it and related problems have been carried out (Johnson, 1952 and Jessberger, 1970). The three basic conditions that must exist for frost action to occur are a frost-susceptible soil, moisture or water content and sufficiently low temperatures to cause some of the soil water to freeze. The physics of the interaction of these factors is generally referred to as the mechanism of frost action.

The frost heave that occurs in a frost-susceptible soil as the freezing plane penetrates is partly caused by the volume change resulting from freezing of the in-situ pore water. Freezing of pore water in soils will cause a volume expansion or heave of 9 % in coarse sands (McRoberts and Morgenstern, 1975), the larger part of the total

heave which is of major concerns to the engineer, is mainly due to the growth of ice lenses at the freezing front caused by the ice segregation process.

It is also possible that additional and perhaps significant heaving can be generated in already frozen soil, particularly when freezing conditions persist over long periods of time (Hoekstra, 1966, Miller 1970, Miller et al., 1975 and Williams, 1977).

The thaw-weakening process is also complex and may occur in soils, particularly clays, whether or not ice lenses have formed during the freezing period. The number of freeze-thaw cycles, closed system versus open system freezing, swelling and shrinkage of unsaturated soils and moisture movement are some factors that influence the thaw-weakening process. For instance, consolidation of clayey soil during the thawing period results in a negative skin friction, a downdrag force acting on the pile in the active layer.

5.3 Frost-Heaving Forces on Foundations

Frost action in the active layer can subject foundations and structures to large uplift forces and destruction movements. It is an important consideration in the design of foundations for unheated buildings, bridges, power transmission and communication towers and structures supported by ventilated foundations such as piles. The frost-action process and associated mechanism have been discussed in section 5.2.

The maximum depth and rate of freeze and thaw penetration may be determined with reasonable accuracy using the method outlined in Chapter III. The numerical algorithm used for the thermal analysis determined the depth of the active layer for three types of soil: sand, peat and clay with different water contents, $w \neq 0$ and the detailed

computations and results were shown in Chapter IV. These results constitutes basic information to determine analytically the heaving forces acting in the active layer of pile embedded in frozen soil as will be developed in Chapter VII.

5.4 Frost Heave and Adfreezing Forces

Heaving forces developed in frost-susceptible soils are transmitted to foundations by adfreezing of the soil to the sides of a foundation unit. Because of the many variables involved, it is difficult to predict the magnitude of the heave forces mobilized when the growth of ice lenses in a frost-susceptible soil is influenced by overburden pressure, foundation loads or other factors. These variables include soil type and arbitrary variation of soil temperature with depth and time, rate of freezing, water content, type of foundations surface (smooth or rough, coated or uncoated, steel, concrete or other material), methods to place foundations and rate and duration of loading.

The adfreeze strength of frozen ground is defined as the resistance to the force that is required to separate the frozen ground from the object (e.g. pile) to which it is frozen. The tangential adfreeze strength is the resistance to the force that is required to shear off an object (e.g. pile) that is frozen to the ground and to overcome the friction along the plane of its contact with ground (Johnston, 1981). It varies with:

- a- the moisture content, w ,
- b- temperature, T ,
- c- texture and porosity of the ground (sand, or clay, or peat)
- d- nature of the surface of the foundation (smooth or rough)

In most cases, the maximum adfreeze strength occurs when the ground is completely saturated with ice.

5.5 Experimental Studies Using Sand, Peat and Clay

Samples will be conducted in Chapter VI to determine the adfreeze bond strength at the sides of steel piles tested with both smooth and rough surfaces. The tangential adfreeze bond strength will be computed as a function of the sample temperature and water content. The freezing temperature of the sample is achieved by keeping the sample inside the freezer and monitored by the use of accurate thermocouple wires. At selected freezing temperature, the adfreeze bond strength will be determined graphically. First, the sample will be loaded using a calibrated flat load cell and the displacement will be measured using three linear DC-potentiometers until rupture occurs. Then, the shear stress, calculated as the load divided by the surface area of the cylindrical pile, will be plotted against the displacement. The adfreeze bond strength of each sample will correspond to the maximum value of the shear stress on the graph when load starts to decrease as the displacement increases. The detailed laboratory work will be presented and discussed in Chapter VI and the results shown in Tables 6.1 and 6.2.

The total uplift force on a foundation is a function of the unit tangential adfreeze bond stress and the area of the foundation in contact with the frozen soil.

Crory and Reed (1965) have reported on the frost-heaving forces on piles. The heave force increased to a maximum value when the 0° C isotherm had penetrated 80 to 100 % of the seasonally thawed layer. The thawing depth varies with the thermal

properties and is highly influenced by the α , γ density and water content of the soil. Fine grained soils (i.e. clay) with higher moisture contents and associated latent heat, experience less frost or thaw penetration than do sands under the same freezing conditions (as discussed in Chapter IV). For instance, clay with $\gamma_d = 1200 \text{ kg/m}^3$ and $w = 15 \%$, had generated a thawing depth of 1.86 m, a value less than that for sand with $\gamma_d = 1400 \text{ kg/m}^3$ and $w = 15 \%$ equals to 1.95 m.

Because frost penetration into the ground and frost heaving occur in direction parallel to the direction of heat flow, the direction of heave for the design is considered to occur vertically parallel to the frost propagation. The foundation designers must include frost heaving considerations before deciding on the type of deep foundation to be used. The considerations for heaving forces acting on pile foundations will be detailed in Chapter VII in an attempt to determine the governing condition for design of the bearing capacity.

5.7 Control of Frost Heave

When evaluation of frost uplift forces indicates potential problems, these forces must be taken fully into design as must be necessary measures required to avoid detrimental effects from the structural stresses developed by the frost action.

Some of the active and passive methods of frost heave force remedial measures are (Phukan, 1985):

- 1- Replace existing ground material by excavating and backfilling with non-frost susceptible (NFS) granular soil (gravel).

- 2- Eliminate total bond contact area between foundation and soil (isolation)
- 3- Reduce frost penetration (or thawing).
- 4- Use thermal heat tubes to eliminate the formation of ice segregation.
- 5- Provide sufficient loading on the foundation to counterbalance heaving forces, which is referred to as suppression of heave.
- 6- Trade off between a basic non-heaving design and a heaving design with monitoring and heave correction during operations.

The design of foundations against frost-heave forces may consist of : designing of maximum anticipated heave force, modifying or improving soil conditions by excavation and backfill, and eliminating frost-heave force, by employing singly or in combination, any of the various design measures indicated above. Design of foundations against frost heave is discussed further in Chapter VII.

CHAPTER VI

PILE FOUNDATION AND ADFREEZE SHEAR STRENGTH

6.1 Introduction

Pile foundations are most commonly used in permafrost to support and transfer both vertical and lateral loads to a depth where volume changes as well as loss of shear strength, are minimal due to change of temperature.

The load carrying capacity of the piles in permafrost is attained by the adfreeze bond developed between the soil and the pile interface. The adfreeze bond and corresponding load capacity of piles in permafrost are temperature-dependent. The cooler the permafrost temperature is, the higher the adfreeze strength between the pile surface and the surrounding soil is. The end bearing capacity of piles is counted only where the supporting materials consist of either hard bedrock or dense sands and gravels.

6.2 Pile Types

Pile material consists of timber, steel, concrete and composite material of concrete and steel. The selection of a particular pile depends on several factors, such as soil type and composition, temperature profile, loads to be carried, length of embedment, availability of construction material and construction equipment, initial installation cost and construction schedule (Phukan, 1985).

6.2.1 Timber Piles

Timber piles are generally the least expensive pile type, easy to bundle and readily available in length from 10 to 20 m. Spruce, Douglas fir, or western pine is commonly used. Timber piles 6 to 15 m long are usually 0.15 m to 0.25 m in diameter at the top and 0.3 m to 0.35 m at the butt. They must be protected in the active layer against deterioration and decay (Linell and Johnston, 1973).

Either pressure treating with various wood preservatives, creosoting, or brushed-on preservative applications may be used to protect timber piles from deterioration. Since the creosote coating reduces the adfreeze bonds below that which can develop for bare wood, in design, the tangential adfreeze working stresses, τ_a , must be reduced. Furthermore, they cannot be driven mechanically into the ground. Thus, the limited installation procedures with the reduction in the adfreeze bond between the pile and the soil have narrowed their use for frozen-ground application (Johnston, 1981). Some field applications are shown in Figs. 6.1, 6.2 and 6.3.

6.2.2 Steel Piles

Pipe piles and H-piles are the most common types of steel piles, although other types like box sections and angles have been used. Oxidation and corrosion of steel must be protected in the active layer. Laboratory tests should be made on the soils and water in which steel piles will be exposed to determine whether the corrosion will be a problem.

Pipe piles filled with concrete or sand may be used to provide high load capacity. Due to uniform cross section, pipe piles are superior to H-sections piles when designing against lateral loads. Heat tubes may readily be placed inside the pipe pile if required to maintain existing thermal regime. Open-ended steel pipe and H-piles can be driven in relatively warm permafrost to great lengths and can carry high loads. The average compressive strength on steel pipe and H-piles under the design load should not exceed 62 MN/m^2 (Andersland, O.B., 1978).

6.2.3 Concrete Piles

Precast reinforced concrete piles are expensive and seldom used in northern Canada (N.W.T.). Transportation of cement and precast piles from the south is costly. Local gravels, if available, usually require washing, screening and crushing to obtain suitable aggregates. On-site fabrication is only economical if large number of piles are required. They may be cast in round, square, H or multi-sided shapes. Precast concrete piles must be handled with care to prevent damage during transport and installation and field design changes in length are difficult. High tensile stress may be induced by frost heave, and will cause the concrete to crack if insufficient reinforcing steel is provided.

Careful analysis is required to ensure that reinforcing steel is sufficient for the structural loading (Myska and How, 1978).

Cast-in-place concrete piles have been used occasionally in frozen ground due to problems of thermal degradation strength and freezing of concrete. The use of concrete piles is controlled by:

- a- The appropriate estimation of the maximum depth of thaw or the active layer.
- b- The depth of the permafrost layer below which the lower part of the pile should be embedded.

Therefore the pile is embedded in unfrozen ground below the bottom of the permafrost layer resulting in additional loads imposed by downdrag (negative skin friction) as the thawing soil settles and consolidates. This situation is encountered when the pile is driven in clayey soil. During the thawing season, the soil gradually consolidates under the effect of rise in temperature. The consolidation process will provide a downward drag force on the pile during the period of thawing.

6.3 Installation of Piles

The following methods are used to place piles in frozen ground

- 1- Placement in a bored hole of diameter greater than the pile diameter
- 2- Placement in a prethawed hole of diameter greater than the pile diameter.
- 3- Direct driving into natural frozen ground.
- 4- Driving into undersized holes or steamed holes of diameter less than the pile diameter.

- 5- Vibratory pile driving.
- 6- Various combinations or modifications of techniques 1 to 5.

6.4 Design for Vertical Loads

6.4.1 Adfreeze Strength and Pile Capacity

Pile foundations in permafrost areas must be designed to support sustained loads without exceeding allowable total or differential settlement and resist heave forces due to frost action in the active layer, short-term loads such as those imposed by wind or dynamic loading and downdrag loads caused by settlement of the soil in a degrading permafrost situation.

Typical forces acting on a pile in permafrost are shown in Figs. 6.4 to 6.6 they depend on:

- 1- The type of soil the pile is embedded in (sand, clay or peat)
- 2- The conditions of loading divided into:
 - a- summer conditions
 - b- winter conditions.

Figures 6.4 to 6.6 show the development of the active layer in the summer and winter for the three types of soil (sand, clay and peat) and the forces acting on them.

The usual design approach is to predict the loads to be carried and determine the depth to which a pile of suitable type and size should be embedded in the frozen ground to resist them by the adfreeze strength and end bearing. Vertical pile loading should not exceed the allowable compressive stress of the pile material.

End bearing is normally taken into account when a dense competent stratum is encountered below the pile. For most piles, where the soil below the tip is the same as that along the pile shaft, adfreeze bond will take most of the load. The contribution of end bearing to the total pile capacity will usually be relatively small and it is conservative to ignore it (Crory, 1966).

The adfreezing strength of frozen soil to timber, steel or concrete is both temperature-and-time dependent.

The adfreeze strength used for design is also dependent on a number of other factors including method of pile placement, properties of the soil, ground temperature, type of pile material and nature of its surface, loading rate and duration. Some early Soviet data on the short-term tangential adfreeze strength between various soils and wood and concrete are given by Kaplar (1971) but the reliability of the data is not known because the conditions were not given. Adfreeze bond strength relationship for short-term and sustained loadings, proposed by Johnston (1981), are shown in Fig. 6.7, some of the load test data on which the relationships are based are also known. These indicate the pile shaft stresses that will prevent rupture of the adfreeze bond over short and relatively long periods, and must be used with caution.

Where the temperature varies with the depth, the total pile capacity is obtained by integrating the adfreeze strength $\tau(z)$ with depth:

$$P = \pi d \int_0^L \tau(z) dz \quad (6.1)$$

where: P = the total capacity of the pile in kN

d = diameter of circular pile in m

L = length of the embedment of pile in m.

This can be carried out graphically and the embedment depth determined for a specified load and safety factor. The comparison with Johnston's proposal for the graphical solution will be carried out in the experimental study detailed in the following section. However, the determination of the bearing capacity of piles, resulting from adfreeze shear stresses, will be carried out in Chapter VII of the present thesis.

6.4.2 Experimental Procedure

The purpose of the experimental study is to evaluate the adfreeze bond strength around the pile shaft as a function of soil temperature and water content without the simulation of the behaviour of the pile embedded in frozen ground, (Stelzer, D.L. and Andersland, O.B., 1991) and later to determine the ultimate bearing capacity of the pile.

In an attempt to better define the effects of temperature, soil water content and pile surface on the pile adfreeze strength, a model pile testing program was conducted. The experimental work reviews the factors pertinent to the adfreeze strength testing and design in frozen soils and describes the results of adfreeze bond strength between soil and pile material.

6.4.2.1 Pertinent Factors Affecting Pile Capacity

A- Effect of Soil Temperature

It is well documented that decreases in the temperature of a frozen soil result in an increase in the strength and a decrease in the time-dependent deformation owing to the reduction of unfrozen water and the increased cohesion of the ice (Parameswaran, 1980).

The determination of the pile capacity is significantly affected by the surrounding soil. At temperature near the freezing point of the pore water, adfreeze bonds are weak and the soil is highly susceptible to time-dependent deformation. A summary of the variation of the adfreeze bond strength with changes in temperature in frozen materials is reported in Weaver and Morgenstern (1981).

Phukan (1985) presented data on the adfreeze strength of soils and soil-pile interface at various temperatures as shown in Fig. 6.8. His recommended relationship is modified from Johnston (1981) approach and also shows all the related experimental data without the specification whether it is a short-term or a long-term relationship.

Sanger (1969) presented average values for the ultimate adfreeze bond strength for saturated fine sands, saturated silts with ice lenses, and ice as shown in Fig. 6.9. But he cautioned that these values should be checked by field tests for final design. Thus the adfreeze bond strength between soil and pile interface is highly affected by the temperature changes and should be studied for each type of soil in order to determine the appropriate relationship.

B- Effect of Pile Surface and Size

B.1 Pile Surface Effect

The effect of pile surface roughness on the strength of adfreeze bond has been studied by many authors. Generally, the rougher the surface, the greater the adfreeze bond strength is. Biggar and Sego (1989) pointed out that if the surface is sufficiently rough it may result in crushing or compressive failure of the frozen soil as the pile displaces. Hence, the pile capacity will be dependent on the shear strength of the soil rather than the adfreeze bond strength between the pile and the soil.

Weaver and Morgenstern (1981) suggested that for smooth surfaces, air is trapped between the pile material and the ice, reducing the effective contact area and inhibiting mobilization of shear strength of the ice.

Velli *et al.* (1973) suggested that the adfreeze bond strength specified in the Soviet (old notation) codes be maintained for rough concrete and wooden surfaces and reduced by 25 % for metal piles.

Thus in conditions where adfreeze bond strength governs the pile capacity design, roughening the surface between the pile and the soil (backfill) increases the pile capacity.

B.2 Size Effects

Vyalov (1959) examines conditions for similarity for piles of various dimensions by performing pull-out tests on wooden model piles with various length to diameter ratios (L/d). Experimental results show that as the pile diameter increases, failure stress decreased, even when the L/d ratios were maintained constant.

Nixon and McRoberts (1976) developed an expression for pile displacement velocity based upon work by Johnston and Ladanyi (1972). The formulation assumes that the constitutive behaviour of soil may be expressed by a simple power law, that the pile displaces at a constant rate (secondary creep) and that the deformation of the frozen ground around the pile shaft is idealized by shearing of concentric cylinders. Their relationship supports Vyalov's (1959) observations, indicating that doubling the pile diameter reduces allowable shaft stresses by approximately 30 %.

Saeki *et al.* (1986) also reports a reduction in adfreeze bond strength with increasing pile diameter in tests of piles frozen into ice sheets. Therefore, a mathematical expression must be made to extrapolate model pile test results to field conditions.

C- Effect of Soil Water Content

Water and soil are not only the most important materials in the world but also the most complex ones, each in its own category, water as a liquid and soil as a multi-phase dispersed system (Farouki, 1981). Water in all its form has important and very complex effects on thermal properties of soil as it has been demonstrated in Chapter II of the present thesis.

Previous studies have shown that for saturated frozen soils, the higher the water content, the higher its resistance to rupture is (Phukan, 1985). Thus, it is conservative to say that sand, for example, has higher resistance to rupture for water content, $w = 20\%$ than $w = 15\%$, the same applies to clay with water contents $w = 30\%$ and $w = 15\%$ and for peat with $w = 120\%$ and $w = 80\%$.

Therefore the adfreeze strength of the soil-pile interface increases with the total water content of the frozen soil and it is important to consider it as a characteristic factor for design.

6.4.2.2 Testing Procedure

In order to simulate the failure strength rupture between the pile surface and different types of soils with different water contents and variable temperature, the special setup was developed and shown in Fig. 6.10.

Two model steel pile sections (Fig. 6.11 and 6.47) are shown embedded in frozen soil. No point bearing forces are developed by these model pile arrangements. The first model is a pile of diameter 1" (25.4 mm) and total length of 6" (152.4 mm) with a rough surface. The second model is a pile of diameter 1" (25.4 mm) and a total length of 5" (127.0 mm) with a smooth surface. The surface roughness of model 1 was determined by the uniform distribution of threads along the perimeter of the pile. Unfrozen samples were prepared by filling a cylinder model of length 12" (304.8 mm) and diameter of 6" (152.4 mm) with soil including sand, clay and peat. Freezing of samples was achieved inside the cooler, where temperature is monitored using thermocouple wires placed at three different locations inside a groove and along the pile length. The thermocouple wires are T-type, can measure temperature ranging between -200°C and $+350^{\circ}\text{C}$, calibrated with three point calibration using environmental chamber set at 0°C , 15°C and -15°C , accurate to $\pm 0.001^{\circ}\text{C}$.

After preparation, the frozen soil sample with the corresponding model pile was

mounted within the frame loading system shown in Fig. 6.10. The top of the pile was connected to the flat load cell of 5000 lbs. total capacity calibrated on a TINIUS Olsen Universal Testing Machine, measuring loads to an accuracy close to ± 0.1 % FS. Three displacement DC-potentiometers, Pot 0, Pot 1 and Pot 2, connected to the top of the pile and soil in the vicinity of the pile surface from the left (L) and right (R) side, respectively, measured average displacements to an accuracy close to ± 0.05 % FS.

In order to improve the accuracy of execution, the load cell, DC-potentiometers and thermocouple wires were connected to the interfaces of the Data Acquisition System includes the Megadac and PC system. The performance of storage and execution of data were done by using the Test Control Software (TCS). TCS provides data acquisition software package, accessible to all MEGADAC functions and features. During the acquisition and post-test processing, all data were automatically available to be monitored and reviewed numerically and graphically. The static load was applied by the lever arm of the high power hydraulic pump having a maximum pressure of 10000 psi (700 bars), Fig. 6.48. Load monitored by the load cell was transferred to the top of pile through stiff connection. The Data Acquisition System is shown in Fig. 6.49.

6.4.2.3 Soil Description and Classification

The soil used in these experiments is divided into three types:

1- Sand: The sand grain size distribution is shown in Fig. 6.12 for a sample weighing 500 g according to Unified Soil Classification system, the coefficient of uniformity, C_u , and the coefficient of curvature, C_c , determined whether the sand is well graded or not.

These coefficients are defined as:

$$C_u = \frac{D_{60}}{D_{10}} \quad (6.2 a)$$

$$C_c = \frac{(D_{30})^2}{D_{60} \times D_{10}} \quad (6.2 b)$$

where D_{60} = grain diameter, in mm, corresponding to 60 % passing by weight

D_{10} = grain diameter, in mm, corresponding to 10 % passing by weight.

D_{30} = grain diameter, in mm, corresponding to 30 % passing by weight.

And if $1 \leq C_c \leq 3$ and $C_u \geq 6$, the sand is considered well graded .

From the above requirements, and using the graph of Fig. 6.12, it follows that: $C_c = 1.24$ and $C_u = 3.5$. Thus, the sand is medium to fine grained and poorly graded (PS).

2- Clay: Clayey soil corresponds to fine grained soil having 50 % or more material passing No 200 sieve (0.0075 mm diameter). The clay soil used for experimental procedure is a white bentonite clay having more than 80 % passing No. 200 sieve.

3- Peat: (Pt) is a highly organic soil, classified based on visual description and identification. The peat moss used for the experimental procedure, sphagnum, is fibrous, dark brown in colour, very light in weight (γ (pt) varies between 200 and 250 kg/m³) and have an unpleasant odour when moist. The peat unit weight is less than that of water and possesses a high degree of absorption. It was observed that peat may reach more than 400 % in water content before saturation occurs. The difference between wet and dry

peat is shown in Fig. 6.50. The nomenclature for the experimental procedure with 19 successful samples is presented in Table 6.1.

6.4.3 Experimental Results

6.4.3.1 General

The test results were analyzed in terms of the shear stress at the pile surface versus the measured relative displacement δ in mm. Twenty seven test samples, each with pile of diameter 1" (25.4 mm) and total length of 5" (127 mm) for a smooth surface and 6" (152.4 mm) for a rough surface, were used to examine the effects of temperature, soil moisture content and pile performance on the adfreeze strength between the soil and the pile surface. The test results are summarized in Table 6.2.

The analysis of the data are plotted for each sample separately from Fig. 6.13 to Fig. 6.37. Reference to L-curve and R-curve, refer to the plot of τ or load versus δ from the left side (Pot 1) and the right side (Pot 2) in the direct vicinity of the pile, respectively. For most specimens, the plots of τ versus δ generally show an initial linear portion, which is believed to describe the behaviour of the frozen soil in the elastic range, followed by a curvilinear line (almost flat in some cases) which describes the behaviour after the soil matrix ruptured and the resistance of the soil became mobilized until failure. In few tests, the adfreeze bond between the pile and soil failed, resulting in a dramatic reduction in pile capacity to a residual value due to a bulk motion of both pile and soil upon loading. In the remaining tests, the τ versus δ behaviour was strengthening until the termination of the test after the soil failure in shear releasing the bonds at the soil-pile

interface and the pile displacement did not exceed 25 mm (Seltzer, D. and Andersland, O., 1991) the limit for pile design criteria.

The performance of the loading frame was examined during the plot of the $\tau - \delta$ curves for each sample. When two specimens of the same soil had the same water content and temperature, the $\tau - \delta$ responses of the tests were similar, for instance, the response of samples 16, (Fig. 6.51) and 17, (Fig. 6.52) for sand, samples 26 (Fig. 6.53) and 27 (Fig. 6.54), for peat were practically similar (refer to Table 6.2). The mode of failure for peat samples are also shown in Fig. 6.55 where concentric rupture circle appeared around the pile surface.

6.4.3.2 Effect of Temperature and Water Content on Adfreeze Strength

The main factor affecting adfreeze strength is temperature. Each sample test was conducted with a specified temperature taken as the mean value measured in time, during the loading process. The effect of the temperature on the adfreeze shear strength for sand and peat soil is also shown in Table 6.2.

Observation of the resulting data shows, an increase in τ of approximately 94 % between tests 10 and 11 when the temperature dropped from -1.89 to -6.07° C for sand with a water content, $w = 7.9$ %, an increase of 58 % between tests 15 and 17 when the temperature dropped from -2.61 to -4.86° C for sand with water content, $w = 14.2$ %, 67% between tests 22 and 24 when the temperature dropped from -1.35 to -4.40° C for peat with average water content $w = 412.5$ %.

The responses of piles in soils with similar water contents was best-fitted into a

linear variation of the adfreeze shear stress with temperature until the temperature drops below - 5° C when the adfreeze shear stress stabilizes, keeping an approximately constant value, reaching its ultimate strength (Biggar, K and Segoo, D. 1993). These responses are plotted in Figs. 6.38 to 6.42. The load test data on which the relationships are bases are also shown. The observation of the experimental results show that between tests 8 and 11 for sand samples, τ , has increased only by approximately 2 % when the temperature dropped by - 1.57 °C from - 4.5° C to - 6.07° C. Thus, it is conservative to assume it to be constant for this range of temperature. This conclusion will constitute the basic assumption to plot τ versus T for a specified water content of the soil considered in the design of piles (sand, clay, peat).

Figure 6.44 shows the illustration of τ versus T for sand filled soil with water contents, $w = 7.9 \%$, 14.2% , 15% , 20% , respectively. These diagrams represent best-fit straight lines, a linear regression between lab data of samples having approximately similar water contents. The curves of water content, $w = 15 \%$ and $w = 20 \%$ were linearly extrapolated from the data of $w = 7.9 \%$ and 14.2% . They are interpreted as:

$$\text{For } w = 15 \% \quad \tau = 334.46 - 97.47 \times T \quad (6.3)$$

and

$$\text{For } w = 30 \% \quad \tau = 611.61 - 126.81 \times T \quad (6.4)$$

where τ = adfreeze shear strength in kPa, and

T = temperature in °C.

They provide information to calculate the pile bearing capacity for both summer and winter conditions and determine its ultimate carrying strength.

Figure 6.44 show the illustration of τ versus T for peat filled soil with water content, $w = 80 \%$, 120% , 275% , and 412% , respectively. The curves of $w = 80 \%$ and $w = 120 \%$ were linearly extrapolated from the data of $w = 275 \%$ and $w = 412 \%$ and interpreted as:

$$\text{For } w = 80 \% \quad \tau = 25.5 - 13.30 \times T \quad (6.5)$$

and

$$\text{For } w = 120 \% \quad \tau = 43.11 - 51.40 \times T \quad (6.6)$$

Figure 6.45 shows the illustration of τ versus T for clay filled pile with water content $w = 15 \%$, 20% and 30% , as well as the approximated approach proposed by Johnston in 1981 for short-term loads for silty clay (independent of water content). Because the tests conducted with clay soil have failed due to equipment difficulties, an assumption was made to carry out these diagrams. Using the average approximation between Johnston approach and the graphical results of sand for $w = 15 \%$ and 20% , the diagrams for both $w = 15 \%$ and $w = 20 \%$, were derived respectively. The diagram for $w = 30 \%$ was linearly extrapolated from the diagrams of $w = 15 \%$ and $w = 20 \%$.

They are interpreted as:

$$\text{For } w = 15 \% \quad \tau = 179.73 - 73.73 \times T \quad (6.7)$$

and

$$\text{For } w = 30 \% \quad \tau = 559.45 - 117.75 \times T \quad (6.8)$$

To justify the extrapolation assumption, the results with sand were compared to the laboratory results found by K Biggar, and D. Seg0 (1993) on the strength and

deformation of model adfreeze and grouted piles in saline frozen soil, considering only data pertaining to non-saline frozen soil. For roughened surface pile, K. Biggar and D. Sego found that the adfreeze strength of dense sand backfill tested at $T = -5.3^{\circ} \text{C}$ was approximately 935 kPa with pile diameter, $d = 33 \text{ mm}$ ($1 \frac{5}{16} \text{ ''}$) and an average water content, $w = 17.5 \%$ which corresponded to an average value between diagrams of $w = 15 \%$ and $w = 20 \%$ at $T = -5^{\circ} \text{C}$, as illustrated in Fig. 6.46. Therefore the linear relationship between the adfreeze shear strength and temperature of frozen soil surrounding pile foundation could be determined, once the soil water content is known.

6.4.3.3 Pile Performance and Adfreeze Strength

As discussed earlier in this chapter, two models of pile were considered for laboratory experiments. Model 1 with rough surface having a total length of 6" (152.4 mm) and a diameter of 1" (25.4 mm), and Model 2 with smooth surface having a total length of 5" (127.0 mm) and a diameter of 1" (25.4 mm). 16 successful tests were conducted with model 1 and only 2 successful tests with model 2.

To avoid the pile to resist by end bearing when embedded in frozen sand and frozen peat with high water content (over 270 %) special arrangements were considered. For sandy soils, the testing cylinder was first filled with dry peat to the tip of the pile level than with sand to the top.

For peat soils, with high water content, a solid circular piece of foam having a centred hole of diameter $1 \frac{1}{16} \text{ ''}$ (27 mm) and a variable depth of 1" (25.4 mm) to 1.25" (31.8 mm) was introduced to separate the moist and dry peat, as shown in Figs. 6.10 and

6.57. The setup of peat samples is also shown in Fig. 6.57.

The effective embedment length of pile was measured during the preparation of sample and was reported in Table 6.1.

The performance of pile using the above mentioned arrangements has improved after the examination of sampling tests run with sand filling the whole cylinder and peat without the insulation surface. Tests with sand showed that the applied load reached its maximum capacity (22 kN) before failure has occurred and the pile settled more than 25 mm, and tests with peat showed that failure occurred by compression rather than shear for high water content. However, with the above mentioned arrangements, lab results showed that failure has occurred by rupture of the shear bonds between the soil and the pile surface rather than crushing by compression.

CHAPTER VII

BEARING CAPACITY OF PILES EMBEDDED IN FROZEN SOIL

7.1 Introduction

The bearing capacity of piles in cold climates is determined by the adfreeze bond strength developed between surface of the pile and the adjacent soil. (Andersland, O.B. and Anderson D.M., 1978 and Phukan, 1985). The end bearing capacity of piles is taken into account only if the end of the pile penetrates firm and strong soil. For the determination of the bearing capacity of the piles requires the estimation of the active layer which defines the maximum depth of thaw in the summer and the maximum depth of heave in the winter for each type of soil. August 20 is selected as the date location for summer condition. Thermal analyses conducted in Chapter IV have shown that to this date corresponded, 80 % to 100 % of the total depth of thaw, L_A . December 22 is selected as the date location for winter conditions. It provided the completion of the freezing cycle in the active layer where heave forces are developed. Also, it is assumed that the bed rock layer lays deep enough below the tip of the piles to neglect end bearing

forces in soil. The adfreeze strength acting on the interface between the pile and the soil is strongly temperature-dependent as demonstrated in Chapter VI. The ultimate adfreeze strength was found to occur at practically -5°C for all types of soil. To determine the pile load capacity, summer and winter conditions should be calculated separately and then decide on the governing load to be used for the design. Three types of soil were investigated, peat, sand and clay with water content, $w \neq 0$ for the analysis.

7.2 Summer Conditions

The temperature profiles within soil medium on the pile-soil interface are the results of the thermal analysis defined graphically in Chapter IV of the present thesis. The crucial point of transient heat transfer problem with phase change is the determination of the maximum location of the 0°C isotherm as the result of the applied external temperature changes. It defines the depth of active layer and the time instant for warmest profile within the soil medium. Then, the associated adfreeze strength as a function of temperature should be found. Experimental studies were performed to find the adfreeze shear strength for the temperature distribution allocated for each type of soil individually.

The determination of the bearing capacity of piles, P_{ult} , is based on equilibrium equation. The imposed system of forces depends on the type of soil surrounding the pile and the adfreeze strength profile over its embedment length. The analysis involves three types of soil to be investigated: sand, clay and peat. The system of forces acting on the pile for summer conditions are shown in Fig. 7.1.

The profiles for adfreeze strength distribution along the pile shaft are shown in Figs. 7.2 to 7.7 for sand, clay and peat soil, respectively.

7.3 Pile Embedded in Sand

For coarse grained soil (sand), it is recommended to place fill such to promote the drainage away from the foundation (McFadden, T.T. and Bennett, F.L., 1991). This implies that in the active layer of sand, the angle of internal friction, ϕ , can be effectively involved in transfer of the load and consequently must be taken into account in analysis of the bearing capacity (Coduto, D.P., 1994, and Das, B.M., 1990). Writing the equation of equilibrium for the system of forces acting on Fig. 7.1 a, we get:

$$P_{ult} = \pi \int_0^{L_e} \tau_p dl + \pi d L_A \tau_f \quad (7.1)$$

where P_{ult} = ultimate structural load on pile, in kN.

d = diameter of pile = 0.4 m for both mesh 1 and mesh 2)

L_A = active later thickness, in m.

L_e = effective pile embedment length, in m.

= total length of the pile minus $L_A = 5.0 - L_A$.

τ_p = shaft adfreeze strength in the permafrost zone, in kPa.

τ_f = average frictional resistance for the active layer, in kPa.

given by Coyle and Castello (1981) as:

$$\tau_f = k \sigma'_v \tan \delta \quad (7.2)$$

where k = lateral earth pressure coefficient

$$= 1 - \sin \phi$$

δ = soil-pile friction angle = 0.8ϕ .

σ'_v = average effective overburden pressure in the active layer, in kPa

$$= \gamma_{\text{moist}} \times L_A$$

where γ_{moist} = wet unit weight of soil in kN/m³.

Hence, combining equations (7.1) and (7.2),

$$P_{ult} = \pi d \int_0^{L_u} \tau_p dL + \pi d L_A K \bar{\sigma}'_v \tan \delta \quad (7.3 \text{ a})$$

$$P_{ult} = P_{1 \text{ ult}} + P_{2 \text{ ult}} \quad (7.3 \text{ b})$$

For design purposes, the weight of the pile and the end bearing force were neglected. In equation (7.3), the temperature profiles as well as L_A were allocated to the medium using the thermal analysis discussed in chapters III and IV of the present thesis. The mathematical algorithm used on 8-noded rectangular finite element model described in Mesh 1 for sand.

7.3.1 Problem 1 a

Determination of P_{ult} for a pile embedded in sand with unit weight $\gamma_d = 1400 \text{ kg/m}^3$ and water content, $w = 15 \%$.

From Fig. 4.6, the depth of thaw which defines the active layer, was found, $L_A = 1.95 \text{ m}$, $L_e = 5 - 1.95 = 3.05 \text{ m}$

$$k = 1 - \sin 32 = 0.47$$

$$\gamma_{moist} = \gamma_{dry} = (1 + w_t) g \quad (\text{Phukan, 1985}) \quad (7.4)$$

where $\gamma_d = \text{dry unit weight of sand} = 1400 \text{ kg/m}^3$.

$$w_t = w = \text{total water content} = 15 \% \quad (0.15)$$

$$g = \text{gravitational acceleration} = 9.81 \text{ m/sec}^2.$$

$$\gamma_{moist} = \text{wet unit weight of soil} = 1.4 (1 + 0.15) 9.81 = 15.79 \text{ kN/m}^3.$$

$$\bar{\sigma}'_v = 15.79 \times 1.95 = 30.75 \text{ kPa.}$$

$$\delta = 0.8 \times 32 = 25.6^\circ$$

Using Eq. (7.2). $\tau_f = 0.47 \times 30.75 \tan (25.6) = 6.93 \text{ kPa}$

The second part of the right hand side of Eq. (7.3 b) is,

$$P_{2ult} = \pi d L_A k \bar{\sigma}'_v \tan \delta = \pi d L_A \tau_f = 16.95 \text{ kN} \quad (7.5)$$

Using August 20th as the time condition for summer loads, the temperature distribution plotted against the soil elevation for the model of mesh 1 is shown in Fig. 4.4 (August 20). Only values corresponding to the pile embedment in the soil will be used.

Then the associated adfreeze strength is calculated based on Eq. 6.3 , where,

$$\text{for } w = 15 \%, \tau = 334.46 - 97.47 \times T$$

where T = temperature value at the corresponding length of the pile in, ° C.

The distribution of the adfreeze shear strength in the permafrost zone plotted versus the pile elevation is shown in Fig. 7.2. To determine the first term of the right hand side of Eq. (7.3 b), P_{ult} , the trapezoidal integration method was used to calculate the integrand.

$$\int_0^{L_e=3.05} \tau_p dL = 1437.54 \text{ kN/m} \quad (7.6)$$

Hence,

$$P_{ult} = 1437.54 \times \pi \times 0.4 = 1806.47 \text{ kN} \quad (7.7)$$

Substituting equations (7.6) and (7.7) into (7.1) gives:

$$P_{ult} = 1806.47 + 16.95 = 1823.41 \text{ kN} \quad (7.8)$$

7.3.2 Problem 2a

Determination of P_{ult} for a pile embedded in sand with dry unit weight $\gamma_d = 1400 \text{ kg/m}^3$ and water content $w = 20 \%$. From Fig. 4. , $L_A = 1.77 \text{ m}$, $L_e = 5.0 - 1.77 = 3.23$

m.

Using Eq. (7.4),

$$\gamma_{moist} = \frac{1400}{1000} (1 + 0.2) \times g = 16.48 \text{ kN/m}^3$$

$$\bar{\sigma}'_v = 16.48 \times 1.77 = 29.17 \text{ kPa}$$

$$\delta = 25.6^\circ$$

Using Eq. (7.2), $\tau_f = 0.47 \times 29.17 \times \tan(25.6) = 7.23 \text{ kPa}$.

From Eq.(7.3),

$$P_{2ult} = \pi d L_A \tau_f = 14.61 \text{ kN} \quad (7.9)$$

From Eq. (6.4), for $w = 20 \%$, $\tau = 611.6084 - 126.811 \times T$

The adfreeze strength τ_f versus the soil elevation along the pile in the permafrost zone is shown in Fig. 7.3.

$$\int_0^{L_p=3.23m} \tau_p dL = 2491.88 \text{ kN/m.}$$

$$P_{1ult} = \pi \times 0.4 \times 2491.88 = 3131.39 \text{ kN} \quad (7.10)$$

Substituting Eqs. (7.9) and (7.10) into Eq. (7.1) gives,

$$P_{ult} = 2467.12 + 17.68 = 2484.81 \text{ kN} \quad (7.11)$$

7.4 Pile Embedded in Clay

For clayey soil, the equilibrium equation should take into account the developed negative skin friction τ_D in the active layer due to consolidation, as shown in Fig. 7.1 b. Consolidation is likely to occur during the thawing period providing a downward drag force acting on the pile (Phukan, A, 1985).

Writing the equation of static equilibrium for the system of forces acting on Fig. 7.1 b, we get:

$$P_{ult} = \pi d \int_0^{L_e} \tau_p dL - \pi d \int_0^{L_A} \tau_D dz \quad (7.12)$$

where: d , τ_p , L_e , L_A are as defined in Eq. (7.1)

τ_D = downdrag shear stress, in kPa.

$$= k' \sigma'_v \tan \delta \quad (7.13)$$

where $k' =$ earth pressure coefficient $= k_0 = 1 - \sin \phi$

$\sigma'_v =$ vertical effective stress at any depth $z = \gamma'_f z$ in kPa

γ'_f = effective unit weight of clay

= γ_{moist} in the absence of water table in the active layer, in kN/m³ (Eq. 7.4)

ϕ = internal angle of friction, $\phi = 16^\circ$.

δ = soil-pile friction angle $\approx 0.6 \phi = 9.6^\circ$

Hence, combining Eqs. (7.12) and (7.13),

$$P_{ult} = \pi d \int_0^{L_e} \tau_p dL - \pi d \int_0^{L_A} k' \sigma'_v \tan \delta dz \quad (7.14 a)$$

$$P_{ult} = P_{1\text{ ult}} - P_{2\text{ ult}} \quad (7.14 b)$$

where

$$P_{1\text{ ult}} = \pi d \int_0^{L_e} \tau_p dL, \text{ in kN} \quad (7.14 c)$$

$$P_{2\text{ ult}} = \pi d \int_0^{L_A} k' \sigma'_v \tan \delta dz$$

= negative skin friction force after Das, B.M., 1990.

$$= \pi d \int_0^{L_A} k' \gamma_{moist} \tan \delta z dz = \frac{\pi d k' \gamma_{moist} \tan \delta (L_A)^2}{2}, \text{ in kN} \quad (7.14 \text{ d})$$

In Eqs. (7.14), τ_p profile, as well as, L_A values were determined using the results of the thermal analysis discussed in Chapter III of the present thesis. An 8-noded rectangular finite element was used to define the geometry of the model, called mesh 2, for clay. The distribution of $\tau_p = \tau_p (T)$ are shown in Fig. 7.4 for $w = 15 \%$ and Fig. 7.5 for $w=30\%$. Values were determined after Eqs. (6.7) and (6.8), respectively.

7.4.1 Problem 3.a

Determination of P_{ult} for pile embedded in clay with dry unit weight, $\gamma_d = 1200 \text{ kg/m}^3$ and water content, $w = 15 \%$. From Fig. 4.16 the depth of thaw which defines the active layer, was found as $L_A = 1.55 \text{ m}$. $L_e = 3.45 \text{ m}$.

$$k = 1 - \sin (16) = 0.72$$

From Eq. (7.4),

$$\gamma'_{moist} = \frac{1200}{1000}(1 + 0.15) \times g = 13.54 \text{ kN/m}^3$$

and

$$\sigma'_v = \gamma'_f z = 13.54 \times 1.55 = 20.97 \text{ kPa}$$

From Eq. (7.13), $\tau_d = 0.72 \times 20.97 \times \tan (9.6) = 2.57 \text{ kPa}$.

From Eq. (7.14 d) the downdrag force in the active layer is:

$$P_{2\text{ ult}} = \pi d \left(\frac{\tau_D \times L_A}{2} \right) = \pi \times 0.4 \frac{2.57 \times 1.55}{2} = 2.50 \text{ kN} \quad (7.15)$$

Using August 20 as the time condition for summer loads, the temperature distribution plotted versus the soil elevation considered for the finite element model of mesh 2 is shown in Fig. 4.14 d, and used to determine the adfreeze shear strength along the pile shaft. The adfreeze shear strength was found after laboratory studies, in Eq. (6.7) as follows:

$$w = 15 \% , \tau = 179.73 - 73.73 \times T$$

where T = temperature value at the corresponding length of the pile, in °C

The distribution of the adfreeze shear strength, τ_p , in the permafrost zone is shown in Fig.7.4

Therefore from Eq. (7.14):

$$P_{1\text{ ult}} = \pi d \int_0^{L_*} \tau_p dL = \pi \times 0.4 \int_0^{L_*=3.45} \tau_p dL$$

Using the trapezoidal method of integration, $P_{1\text{ ult}}$ is computed as:

$$P_{1\text{ ult}} = \pi \times 0.4 \times 1147.51 = 1442.37 \text{ kN} \quad (7.16)$$

Substituting Eqs. (7.15) and (7.16) into Eq. (7.12) and Eq. (7.14),

$$P_{ult} = 1442.37 - 2.50 = 1439.87 \text{ kN} \quad (7.17)$$

7.4.2 Problem 4.a

Determination of P_{ult} for pile embedded in clay with dry unit weight, $\gamma_d = 1400 \text{ kg/m}^3$ and water content, $w = 30 \%$.

From Fig. 4.17, $L_A = 1.32 \text{ m}$, $L_e = 5 - 1.32 = 3.68 \text{ m}$

$$k = 0.72$$

The downdrag force in the active layer calculated from Eq. (7.14 d) is

$$P_{2 \text{ ult}} = \pi d \left(\tau_D \times \frac{L_A}{2} \right) = \pi \times 0.4 \times \left(2.47 \times \frac{1.32}{2} \right) = 2.04 \text{ kN} \quad (7.18)$$

The adfreeze shear strength in the permafrost zone, τ_p , derived in Eq. (6.8), is plotted versus the soil elevation and is shown in Fig. 7.5, such that for $w = 30 \%$,

$$\tau_p = 559.45 - 117.75 \times T$$

Therefore, using Eq. (7.14), the ultimate force in the permafrost zone is:

$$P_{1 \text{ ult}} = \pi d \int_0^{L_e=3.68} \tau_p \, dL = 3617.95 \text{ kN} \quad (7.19)$$

Substituting Eqs. (7.18) and (7.19) in Eqs. (7.14), the ultimate load capacity of the

pile is:

$$P_{ult} = 3617.95 - 2.04 = 3615.91 \text{ kN} \quad (7.20)$$

7.5 Pile in Peat Soil

The unfrozen peat in active layer does not constitute any support to transfer the load, therefore it is neglected in the determination of the bearing capacity for summer conditions. The equilibrium equation will consider only the reaction in the permafrost zone and, the equilibrium of the system of forces acting on Fig. 7.1.c gives:

$$P_{ult} = \pi d \int_0^{L_a} \tau_p dL \quad (7.21)$$

which is the same as the first term in the right hand side of Eqs. (7.1) and (7.2).

The temperature profiles and L_A values were determined using the thermal analysis developed in Chapter III. An 8-noded rectangular finite element was used to define the geometry of the medium called mesh 2, for peat. The geometry defined for peat is similar to that for clay.

7.5.1 Problem 5.a

Determination of P_{ult} for a pile embedded in peat with dry unit weight, $\gamma_d = 400 \text{ kg/m}^3$ and water content $w = 80 \%$, (from Fig. 4.26).

$$L_A = 0.82 \text{ m}$$

$$L_e = 5.0 - 0.82 = 4.18 \text{ m}$$

The temperature distribution was plotted in Fig.4.24 d and the allocated adfreeze strength were determined in Eq. (6.9) such that for $w = 80 \%$, $\tau_p = 25.5 - 13.3 \times T$.

The adfreeze shear strength in the permafrost zone, τ_d , is plotted versus the soil elevation and shown in Fig. 7.6.

Where T = temperature distribution along the pile, in the permafrost zone, in ° C. Therefore, from Eq. (7.21), and using the trapezoidal integration method to find the area enclosing the adfreeze shear strength in depth in the permafrost zone of the pile,

$$P_{ult} = \pi \times 0.4 \int_0^{L_e=4.18} \tau_p dL = 317.29 \text{ kN} \quad (7.22)$$

7.5.2 Problem 6.a

Determination of P_{ult} for a pile embedded in peat with dry unit weight $\gamma_d = 400 \text{ kg/m}^3$ and water content $w = 120 \%$.

$$L_A = 0.80 \text{ m (from Fig. 4.27)}$$

$$L_e = 5.0 - 0.8 = 4.20 \text{ m}$$

The adfreeze shear strength in the permafrost zone, τ_d , is plotted versus the soil elevation and shown in Fig. 7.7.

From Eq. (6.10), the equation of adfreeze shear strength, τ_p , as a function of the temperature is:

For $w = 120\%$, $\tau_p = 43.1 - 21.2 \times T$

Therefore Eq. (7.21) gives:

$$P_{ult} = \pi \times 0.4 \int_0^{L_e=4.2} \tau_p dL = 512.61 \text{ kN} \quad (7.23)$$

The summary for the calculations for the ultimate bearing capacity of pile in the summer, for three types of soil: sand, clay and peat are shown in Table 7.1, 7.2, and 7.3, respectively.

The detailed calculations of the bearing capacity of the pile calculations for summer condition (August 20) for all analyzed soils are shown in Table 7.4.

7.6 Determination of the Bearing Capacity of the Pile for Winter Condition

In the active layer, during winter time, because of closer location to the cold changes of temperature, the top soil is much colder than in lower parts where the permafrost zone is. The colder temperature of the active layer results in development of strong adfreeze bonds and resulting in heaving forces acting at the pile-soil interface. The developed upward heaving stresses, τ_H , are restrained by opposite directed shear stresses, τ_p , in permafrost. This implies that at a cross section of the pile, the internal force of the pile must be sufficient to resist the tensile stress resulting from heave in the active layer and adfreeze resisting forces in the permafrost zone. The ultimate force, P_{ult} , determined for winter conditions is such that equilibrium condition should be satisfied.

The systems of forces imposed on the pile for December 22 (winter condition) are

shown in Fig. 7.8.

In order to mitigate the effect of heave on bearing capacity of deep foundations, soil improvement can be obtained by the application of grease mixed with sand or wax with sand slurry around the pile in the active layer (Johnston, 1981). It is obvious that for this improved situation, the developed direction of shear stress in permafrost, τ_p , is the same as for summer conditions, that is directed upward.

The same problems solving P_{ult} for summer condition, will be developed to determine the winter conditions for three types of soil: sand, clay and peat. All the time the static equilibrium of vertical forces acting on the pile should be maintained.

7.6.1 Ultimate Capacity with Heave Considered in the Active Layer

For static equilibrium, the sum of forces acting on the pile given in Fig. 7.8 a should be equal to zero (Andersland or Phukan).

$$\sum F_y = 0$$

and

$$P_{ult} - P_H + P_p = 0 \quad (7.23)$$

Hence,

$$P_{ult} - \pi d \int_0^{L_A} \tau_H dL + \pi d \int_0^{L_s} \tau_p dL = 0 \quad (7.24)$$

and

$$P_{ult} = \pi d \left[\int_0^{L_A} \tau_H dL - \int_0^{L_s} \tau_p dL \right] \quad (7.25)$$

where, P_{ult} = ultimate bearing capacity of the pile for winter conditions, in kN.

d = diameter of the pile in m.

τ_H = tensile heave stress distributed along the shaft of the pile in the active layer, in kPa.

τ_p = compressive adfreeze strength in the permafrost zone, in kPa

L_A = depth of the active layer, in m, and

L_e = depth of the permafrost zone = $5.0 - L_A$, in m.

In Eq. (7.25), because colder temperature are expected in the active layer and warmer temperature in the permafrost zone, then, τ_H will have larger values than τ_p , and consequently;

$$\tau_H \geq \tau_p \rightarrow P_H \geq P_p \quad (7.26)$$

Applying the property of Eq. (7.26) to Eq. (7.25), hence, the integral difference of Eq. (7.25) will have a positive value and, therefore, P_{ult} will be positive on the compressive side. However, this case is ideal if we neglect the following two major factors:

- 1) Variation of the temperature along the pile length, since the shear strength is strongly dependent of temperature.
- 2) Variation in the permafrost zone moving up and down, decreasing or increasing the permafrost adfreeze strength.

In the following problems, we will examine the importance of these factors in the computation of the ultimate bearing capacity neglecting the end bearing, and the pile own

weight.

7.6.2 Ultimate Bearing Capacity Without Heave Considered in the Active Layer

Writing the equation of equilibrium for the system forces shown in Fig. 7.8 c with τ_H , the ultimate bearing capacity without heave is

and

$$P_{ult} = \pi d \int_0^{L_e} \tau_p dL \quad (7.27)$$
$$P_{ult} - \pi d \int_0^{L_e} \tau_p dL = 0$$

where d and L_e are as defined in Eq. (7.25).

τ_p = adfreeze strength developed in the permafrost zone, in kPa. Equation (7.27) looks similar to the equation of the ultimate bearing capacity of peat soil during the summer, where only tensile forces acting in the permafrost zone are considered. This is true because the active layer, being insulated, becomes ineffective and the permafrost table interface separating the active layer and the permafrost zone will become the soil surface when loads are applied.

7.7 Problem 1. b

Determination of P_{ult} in winter, of a pile embedded in sand with water content, $w=15\%$ and dry unit weight of $\gamma_d = 1400 \text{ kg/m}^3$

Using the data from problem 1.a:

$$L_A = 1.95 \text{ m}, \quad L_e = 5 - 1.77 = 3.05 \text{ m}, \quad d = 0.4 \text{ m}$$

$$\tau = 334.46 - 97.47 \times T \text{ kPa} \quad T \geq -4.5^\circ \text{ C}$$

$$\tau = 993.1 \text{ kPa} \quad T < -4.5^\circ \text{ C}$$

The distribution of the adfreeze shear stress versus the soil elevation where heave is considered is shown in Fig. 7.9 and heave is neglected in Fig. 7.12.

7.7.1 Case 1: Heave is considered in the analysis

Using trapezoidal integration method to calculate the right hand side terms of Eq. (7.25) and the diagram of Fig. 7.9, it follows:

$$P_H = \pi \times 0.4 \int_0^{L_A=1.95} \tau_H dL = 2179.09 \text{ kN} \quad (7.28 \text{ a})$$

and

$$P_p = \pi \times 0.4 \int_0^{L_s=3.05} \tau_p dL = 1591.85 \text{ kN} \quad (7.28 \text{ b})$$

therefore, the property of Eq. (7.26) is satisfied and $P_H > P_p$, and

$$P_{ult} = 2179.09 - 1591.85 = 587.24 \text{ kN} \quad (7.29)$$

7.7.2 Case 2: Neglect Heave in the Analysis

Using the trapezoidal integration method to calculate the right hand side of Eq.

(7.27) and Fig. 7.10, it follows:

$$P_{ult} = \pi \times 0.4 \int_0^{L_e=3.05} \tau_p dL = 1591.85 \text{ kN} \quad (7.30)$$

The pile should be designed to carry the load determined for the worst condition when comparing summer and winter results. This discussion will be carried out for each type of soil at the end of calculations for winter conditions.

7.8 Problem 2.b

Determination of P_{ult} , in winter, for a pile embedded in sand with water content, $w = 20\%$ and dry unit weight, $\gamma_d = 1400 \text{ kg/m}^3$.

Using the data from Problem 2.a,

$$L_A = 1.77 \text{ m}, \quad L_e = 5 - 1.77 = 3.23 \text{ m}$$

$$\tau = 611.61 - 126.81 \times T \text{ kPa} \quad T \geq -4.5^\circ \text{ C}$$

$$\tau = 1245.66 \text{ kPa}, \quad \text{kPa} \quad T < -5^\circ \text{ C}$$

The distribution of the adfreeze strength versus the soil elevation where heave is considered is shown in Fig. 7.11 and heave neglected in Fig. 7.12.

7.8.1 Case 1: Heave is Considered in the Analysis

Using the trapezoidal integral method to calculate the right hand side terms of Eq. (7.25), and the diagram of Fig. 7.11, it follows:

$$P_H = \pi \times 0.4 \int_0^{L_A=1.77} \tau_H dL = 2591.42 \text{ kN} \quad (7.31 \text{ a})$$

and

$$P_P = \pi \times 0.4 \int_0^{L_e=3.23} \tau_p dL = 2714.42 \text{ kN} \quad (7.31 \text{ b})$$

From Eqs. (7.31), the property of Eq. (7.26) is not satisfied and $P_H < P_P$, and the resulting P_{ult} is negative (- 123.46 kN) meaning that heave cannot develop for this particular problem in order to balance the overburden compressive force acting in the permafrost zone. Johnston approach (Fig. 7.8 b) with stresses acting upward will be used as an alternative solution for this case.

7.8.2 Case 2: Heave is Neglected in the Analysis

Using the trapezoidal method of integration to calculate the enclosed area shown in Fig. 7.12. Only shear values corresponding to elevation in the permafrost zone are considered and Eq. 7.27 gives:

$$P_{ult} = \int_0^{L_e=3.23} \tau_p dL = 2714.88 \text{ kN} \quad (7.32)$$

7.9 Problem 3.b

Determination of P_{ult} in winter, for a pile embedded in clay with water content, $w = 15\%$ and dry unit weight, $\gamma_d = 1200 \text{ kg/m}^3$.

Using the data from problem 3.a,

$$L_A = 1.55 \text{ m}, \quad L_e = 3.45 \text{ m}$$

$$\tau = 179.73 - 73.73 \times T \text{ (kPa)} \quad T \geq -5^\circ \text{ C.}$$

$$\tau = 547.63 \text{ (kPa)} \quad T < -5^\circ \text{ C.}$$

The distribution of the adfreeze strength versus the soil elevation where heave is considered is shown in Fig. 7.13 and heave neglected in Fig. 7.14.

7.9.1 Case 1: Heave is Considered in the Analysis

Using the same procedure of Problem 2.b (Case 1)

$$P_H = \pi \times 0.4 \int_0^{L_A=1.55} \tau_H dL = 1065.71 \text{ kN} \quad (7.33)$$

$$P_p = \pi \times 0.4 \int_0^{L_e=3.45} \tau_p dL = 2594.55 \text{ kN} \quad (7.34)$$

In this case, the property of equation (7.26) is not satisfied; having $\tau_H \geq \tau_p$ did not consequently lead to $P_H \geq P_p$, and therefore P_{ult} is negative in tension meaning that : the heave cannot develop for this particular problem in order to balance the overburden

compressive force acting in the permafrost zone.

7.9.2 Case 2: Heave is Neglected in the Analysis

Using the procedure of Problem 2.b, (Case 2),

$$P_{ult} = \int_0^{3.45} \tau_p dL = 2594.55 \text{ kN} \quad (7.35)$$

7.10 Problem 4.b

Determination of P_{ult} in, winter, for a pile embedded in clay with water content, $w = 30 \%$ and dry unit weight, $\gamma_d = 1200 \text{ kg/m}^3$.

Using the data from Problem 4.a,

$$L_A = 1.32 \text{ m}, \quad L_e = 3.68 \text{ m}$$

$$\tau = 559.45 - 117.75 \times T \text{ (kPa)} \quad T \geq -5^\circ \text{ C.}$$

$$\tau = 1147.90 \quad \text{(kPa)} \quad T < -5^\circ \text{ C.}$$

The distribution of the adfreeze strength versus the soil elevation, where heave is considered, is shown in Fig. 7.14 and heave neglected in Fig. 7.15.

7.10.1 Case 1: Heave is Considered in the Analysis

Using the same procedure of Problem 2.6 (Case 1);

$$P_H = \pi \times 0.4 \int_0^{L_A=1.32} \tau_H dL = 1904.09 \text{ kN}$$

and

$$P_p = \pi \times 0.4 \int_0^{L_e=3.68} \tau_p dL = 4164.95 \text{ kN} \quad (7.36)$$

In this case, too, the property of Eq. (7.26) is not satisfied and $\tau_H \geq \tau_p$ did not consequently lead to $P_H \geq P_p$.

Comparing this result to that of problem 3.b (Case 1), it shows that the increase of the adfreeze shear strength in the soil with water content and temperature as it has been demonstrated experimentally in Chapter VI, lead to an increase of the compressive force, P_p in the permafrost zone in an amount of 2335.68 kN from 1334.20 kN ($w = 15\%$) to 3669.88 kN ($w = 30\%$).

7.10.2 Case 2: Heave is Neglected in the Analysis

Using the same procedure of Problem 2.6 (Case 2);

$$P_{ult} = \pi \times 0.4 \int_0^{3.0} \tau_p dL = 4164.95 \text{ kN} \quad (7.37)$$

7.11 Problem 5.b

Determination of P_{ult} , in winter, for a pile embedded in peat with water content, $w = 80\%$, and a dry unit weight, $\gamma_d = 400 \text{ kg/m}^3$.

Using the data from Problem 5.a;

$$L_A = 0.82 \text{ m}, \quad L_e = 4.18 \text{ m}$$

$$\tau = 25.5 - 13.3 \times T \text{ (kPa)} \quad T \geq -4.5^\circ \text{ C.}$$

$$\tau = 85.35 \text{ (kPa)} \quad T < -4.5^\circ \text{ C.}$$

The distribution of the adfreeze shear strength versus soil elevation where heave is considered is shown in Fig. 7.16, and heave neglected in Fig. 7.17.

7.11.1 Case 1: Heave is Considered in the Analysis

Using the same procedure of Problem 2.6 (Case 1);

$$P_H = \pi \times 0.4 \int_0^{L_A=0.82} \tau_H dL = 89.00 \text{ kN}$$

and

$$P_p = \pi \times 0.4 \int_0^{L_e=4.18} \tau_p dL = 356.56 \text{ kN} \quad (7.38)$$

Hence the property of Eq. (7.26) is not satisfied and $P_p > P_H$ resulting in a negative force acting on the pile by considering the equilibrium of Eq. (7.24).

Therefore, heave cannot develop for the peat soil with $w = 80\%$, leading to

unrealistic results.

7.11.2 Case 2: Heave is Neglected in The Analysis

Using same procedure for Problem 2.b (Case 2);

$$P_{ult} = \pi \times 0.4 \int_0^{4.18} \tau_p dL = 356.56 \text{ kN} \quad (7.39)$$

7.12 Problem 6.b

Determination of P_{ult} , in winter, for a pile embedded in peat with water content, $w = 120 \%$ and dry unit weight, $\gamma_d = 400 \text{ kg/m}^3$.

Using the data from Problem 6.a

$$L_A = 0.80 \text{ m}, \quad L_e = 4.20 \text{ m}$$

$$\tau = 43.1 - 21.2 \times T \text{ (kPa)} \quad T \geq -5^\circ \text{ C.}$$

$$\tau = 149.1 \quad \text{(kPa)} \quad T < -5^\circ \text{ C.}$$

The distribution of the adfreeze shear strength versus the soil elevation where heave is considered is shown in Fig. 7.18 and heave neglected in Fig. 7.19.

7.12.1 Case 1: Heave is Considered in the Analysis

Using the same procedure for Problem 2.6 (Case 1);

$$P_H = \pi \times 0.4 \int_0^{L_A=0.8} \tau_H dL = 149.64 \text{ kN}$$

and

$$P_p = \pi \times 0.4 \int_0^{L_s=4.2} \tau_p dL = 624.26 \text{ kN} \quad (7.40)$$

The property of (Eq. 7.26) is not satisfied and $P_p > P_H$ resulting in a negative ultimate force acting on the pile to satisfy the equilibrium of equation (7.24).

Therefore, heave cannot develop for those conditions and Johnston approach is required to regain the static equilibrium of Eq. (7.24).

Comparing the results of Problem 5.b (Case 1) and Problem 6.b (Case 1), we have;

$$\frac{P_H (120)}{P_H (80)} = \frac{149.64}{89.00} = 1.68$$

$$\frac{P_p (120)}{P_p (80)} = \frac{624.66}{356.56} = 1.75 \quad (7.41)$$

Considering Eq. (7.41) and the predominance of permafrost forces over the heave forces, it follows that the heave and the permafrost forces increases with approximately the same ratio when the water content increases by 1.5 times, from 80 % to 120 %. This implies that, for peat soil, as the water content increases, the balance is such that Johnston approach of stress distribution is always required to maintain the static equilibrium of the

vertical forces acting on the pile, no matter how the ratio of increase of water content is.

7.12.2 Case 2: Heave is Neglected in the Analysis

Using the same procedure of Problem 2.b (Case 2);

$$P_{ult} = \pi \times 0.4 \int_0^{L_a=4.20} \tau_p dL = 624.66 \text{ kN} \quad (7.42)$$

The summary of the calculations for the ultimate load carrying capacity of pile in winter, for three types of soil ; sand, clay and peat are shown in Tables 7.5, 7.6 and 7.7, respectively.

The results for the comparative analysis for the determination of P_{ult} for winter conditions in the presence and absence of heave in the active layer are also shown in Table 7.8, considering December 22 as the worst time location for load applications.

7.13 Determination of the Design Load Capacity of Pile Embedded in Soil

7.13.1 Definitions and Assumptions

The purpose of the determination of the ultimate bearing capacities for different conditions; summer and winters, and mediums is to find the governing load capacity for the design of pile. So far, the numerical problems, solved in this chapter, have determined the ultimate bearing capacity for three separate conditions:

1- Summer,

2- Winter in the presence of heave in the active layer.

3- Winter in the absence of heave in the active layer, without making the comparative analysis to choose the best conditions to be used for the design. This is a very complex and delicate problem which requires a special approach to select the governing condition.

In winter, frost heave is a particularly serious problem and can result in a severe distortion of the structures. In addition, heaved soils may not return to their original position at the end of the thaw season because the underlying voids have been filled with ice (Pewe and Paige, 1963). Therefore, where frost heave appears to be eccentric, consideration should be made to account for during the design of the ultimate bearing capacity.

A- Heave Force

It is the maximum required force to maintain static equilibrium for the most unfavorable stress distribution which induced tensile stresses along the pile shaft in the determined active layer.

B- Suppression of Heave

Suppression of heave force is the maximum compressive force which prevents heave to develop by applying a dead load, double and in opposite direction to the load to be carried in the permafrost zone, P_p .

This definition was made to confine with the proposed theory by Johnston (1981).

He assumed the permafrost stress to be acting upward, then, wrote the equation of static equilibrium in compression for the system of forces to be resisted by the pile.

$$\sum F_y = 0 \downarrow \rightarrow P_{ult} - P_H - P_P = 0$$

and

$$P_{ult} = P_H + P_P \quad (7.43)$$

Now, the equation of equilibrium according to the definition of "suppression of heave" could be written as:

$$\sum F_y = 0 \downarrow \rightarrow P_{ult} - P_H + P_P - 2P_P = 0$$

and

$$P_{ult} = P_H + P_P \quad (7.44)$$

where P_{ult} , P_H , and P_P are defined by the winter conditions in section 7.6.

Therefore, Eqs. (7.43) and (7.44), are identical and Johnston proposal coincides with the suppression of heave definition.

To determine the most unfavorable condition that control the design, we should compare results from summer and winter conditions for each type of soil individually.

Assumptions are made and a method of solution is proposed as follows:

Step 1: If summer condition provided the least value for the ultimate capacity as recommended by many authors (Johnston, 1981, Anderson and Andersland, 1978 and Phukan, 1985), it will govern the design.

Step 2: If winter conditions with the absence of heave dominated, it will be considered

for design only if the active layer can be properly insulated. Some requirements are presented below:

2-a proper drainage is essential to prevent ice lens growth,

2-b control of or reduction in the depth of the active layer should be attempted,

2-c layers of insulation placed around the pile can be effective in reducing the depth of frost penetration or thawing (Robinsky and Bespflug, 1975).

2-d surcharge loading of the ground surface with a gravel pad, together with improved drainage, can reduce but may not eliminate seasoned heaving, however, these methods are generally not practical, expensive and may afford only temporary relief (Johnston, 1981). Therefore using the winter conditions with heave should be carefully considered for design because it induces a high factor of safety each time the method of insulation used to prevent heave propagation is not accurate and safe and does not yield a 100 % protection of the soil.

Step 3- If winter condition with the presence of heave dominated the design with the ultimate load in the permafrost zone, P_p , directed downward, the internal pile strength must be sufficient to resist the tensile stresses resulting from the opposing forces acting on it (upward heaving force and restraining permafrost force) (McFadden, 1991). In addition, the application of summer conditions must be supported during winter time, following the proposed procedure:

$$3-a \tau = \tau (T) \text{ as demonstrated in Chapter VI} \quad (7.45)$$

where: τ = adfreeze shear strength, in kPa

T = temperature, in ° C.

$$3-b \tau \text{ (compression)} \equiv \tau \text{ (Tension)} \text{ at } T = \text{constant} \quad (7.46)$$

The maximum adfreeze strength caused by a compressive force acting on the pile has the same magnitude but in opposite direction to that caused by a pulling out force (tension) for the same constant temperature.

3-c For the same temperature distribution in the permafrost zone, the adfreeze shear strength, τ , varies linearly with P_p , from τ_p maximum directed downward (tension) to τ_p maximum directed upward (compression), as shown in Fig. 7.19.

3-d The developed heave force, P_H , in the active layer is kept constant through out the analysis because it represents the maximum calculated force for the worst winter time (December 22)

For the procedure and assumptions stated above, the design load capacity for piles embedded in sand, clay and peat, each soil considered separately will be presented below and a discussion of results will be carried out.

7.13.2 Problem 7

Determination of Design Load Capacity for Pile Embedded in Sand.

Using the output dates from Problems 1-a and 1-b for $w = 15 \%$ and Problems 2-a and 2-b for $w = 20 \%$, and Table 7.8, we had:

condition	w = 15 % (Case A)	w = 20 % (Case B)
Summer Condition, noted as (S)	$P_p = 1806.47 \text{ kN}$ $P_{ult} = 1806.47 \text{ kN}$	$P_p = 3131.39 \text{ kN}$ $P_{ult} = 3146.00 \text{ kN}$
Winter Condition with Heave, noted as (WH)	$P_p = 1591.85 \text{ kN}$ $P_H = 2179.09 \text{ kN}$ $P_{ult} = 587.24 \text{ kN}$	$P_p = 2714.88 \text{ kN}$ $P_H = 2591.42 \text{ kN}$ $P_{ult} = -123.46 \text{ kN}$
Winter Condition Without Heave, Noted as (WWH)	$P_p = 1591.85 \text{ kN}$ $P_{ult} = 1591.85 \text{ kN}$	$P_p = 714.88 \text{ kN}$ $P_{ult} = 2714.88 \text{ kN}$

A- Sand with Water Content, w = 15 %

These results indicate that the winter condition with heave govern the design of pile embedded in sand with moisture content, w = 15 %. However, we should verify that summer condition could be supported by the winter loading condition according to step 3 of the proposed solution procedure.

The discussion will be carried out using the information of the schematic representation of the system of forces shown in Fig. 7.20. Figure 7.20 b shows that applying Johnston (1981) theory ,where stresses were defined to act upward in the

permafrost zone and definition of the suppression of heave, Eq. (7.43) or Eq. (7.44) gives:

$$P_{ult} = 2179.09 + 1591.85 = 3770.94 \text{ kN}$$

This force cannot be supported in the summer where

$$P_{ult} = 1806.47 < 3770.94 \text{ kN}$$

Therefore, according to the assumptions and definitions proposed for the solution, the winter condition with suppression of heave cannot govern the design. According to Step 3-c of the proposed solution method and Fig. 7.20 c, a force, $P_p = 372.62 \text{ kN}$ is required to support the summer loading condition in the winter. This force is less than the permafrost force as shown in Fig. 7.20 a, which equals to 1591.85 kN .

Therefore, the summer condition provides a smaller driving force in the permafrost zone of the frozen soil.

Now the results from winter without heave and summer imply that:

$$P_{ult,WWH} = 1591.85 \text{ kN} < P_{ult,S} = 1806.47 \text{ kN}$$

This property shows that winter without heave control the design at this stage. However, this result can be adopted as a design value only if step 2 of the proposed method can be accurately assumed, and the insulation of the active layer could be totally insured.

B- Sand with Water Content, $w = 20 \%$

The results indicate that heave frost cannot develop producing a pullout force acting on top of the pile (-123.46) kN). That is due to two important factors:

- i- Reduction in the active layer depth by 9.23 % (18 cm) when the water content increases from 15 to 20 %.
- ii- Increase in the adfreeze shear strength in the permafrost zone when water content increases from 15 % to 20 % for the same constant temperature (refer to Chapter VI).

These factors had acted upon increasing the tensile force at the permafrost table by increasing the driving force in the permafrost zone, and hence, producing a negative tensile force to be resisted by the pile.

Applying Johnston theory (Eq. 7.43), or Eq. 7.44 to calculate the force required to suppress heave in the active layer,

$$P_{ult} = 2714.88kN + 2591.42 kN = 5306.30 kN$$

Therefore, the winter condition with heave cannot govern the design of the pile because it produces the highest value for the ultimate capacity.

The comparison between summer condition (S) and winter condition without heave (WWH) implies:

$$P_{ult}(WH) = 2714.88 kN < P_{ult}(S) = 3131.39 kN \quad (7.47)$$

Equation (7.47) shows that if step 2 of the proposed method can be accurately performed, the winter condition without heave governs, otherwise, the summer will govern the design. Comparing results between Case A ($w = 15\%$) and Case B ($w = 20\%$), an increase of 13% in the permafrost force was observed in the summer and 70% in the winter when the water content increases by approximately 33%. That is, the force resulting from adfreeze bond strength between the sand and the pile interface, which is temperature-dependent is strongly affected by the variation of the sand water content.

7.13.3 Problem 8: Determination of Design Load Capacity for Pile Embedded in

Clay

Using the output data from problems 3a and 3b for $w = 15\%$ and Problems 4 a and 4 b for $w = 30\%$ and Table 7.8, we had:

condition	w = 15 % (Case A)	w = 30 % (Case B)
Summer Condition Noted as (S)	$P_p = 1442.37 \text{ kN}$ $P_{ult} = 1439.87 \text{ kN}$	$P_p = 3617.75 \text{ kN}$ $P_{ult} = 3615.91 \text{ kN}$
Winter Condition with Heave Noted as (WH)	$P_p = 1528.84 \text{ kN}$ $P_H = 1065.71 \text{ kN}$ $P_{ult} = -463.13 \text{ kN}$	$P_p = 4164.95 \text{ kN}$ $P_H = 1904.09 \text{ kN}$ $P_{ult} = -2260.86 \text{ kN}$
Winter Condition Without Heave Noted as (WWH)	$P_p = 1528.84 \text{ kN}$ $P_{ult} = 1528.84 \text{ kN}$	$P_p = 4164.95 \text{ kN}$ $P_{ult} = 4164.95 \text{ kN}$

These results indicate that, for clay with water contents, $w = 15 \%$ and $w = 30 \%$, heave forces cannot develop because they produce a pull out force acting on the top of the pile. However applying either Johnson (1981) theory, Eq. (7.43), where uplift stresses mobilized between the pile shaft and the frozen soil were assumed to develop in the permafrost zone, or Eq. (7.44), the winter condition with heave (WH) static equilibrium implicates:

$$\text{for } w = 15 \%, P_{ult} = 1065.71 + 1528.84 = 2594.55 \text{ kN} \quad (7.48)$$

$$\text{for } w = 30 \%, P_{ult} = 1904.09 + 4164.95 = 6069.04 \text{ kN} \quad (7.49)$$

To determine the design load capacity of piles embedded in clay, for different

water contents ($w = 15\%$ and 30%), a comparison between results from summer(S), winter without heave (WWH), and Eqs. (7.48) and (7.49) should be attempted for each water content, respectively.

For $w = 15\%$ $P_{ult}(S) = 1439.87 \text{ kN} < P_{ult}(WWH) = 1528.84 < P_{ult}(WH) = 2594.55 \text{ kN}$.
and;

For $w = 30\%$ $P_{ult}(S) = 3615.91 \text{ kN} < P_{ult}(WWH) = 4164.95 < P_{ult}(WH) = 6069.04 \text{ kN}$.

Therefore, for pile embedded in clayey soil, the summer conditions always governs over the other conditions and,

$$P_{ult}(w = 15\%) = 1439.87 \text{ kN} = \tag{7.50}$$

$$P_{ult}(w = 30\%) = 3615.91 \text{ kN} \tag{7.51}$$

Comparing Eqs. 7.51 (case A) and 7.52 (case B), 151% increase in the ultimate bearing capacity of the pile was observed when the water content doubled from $w = 15\%$ to 30% .

Therefore, the capacity of the pile resulting from the adfreeze bond strength between the clay and the pile interface is strongly affected by the variation of the water content.

7.13.4 Problem 9: Determination of the Load Capacity for Pile Embedded in Peat

Using output data from Problem 5 A and 5 B for $w = 80\%$ and Problems 6 A and 6 B for $w = 120\%$ and Table 7.8, we had:

condition	w = 15 % (Case A)	w = 30 % (Case B)
Summer Condition Noted as (S)	$P_p = 317.29 \text{ kN}$ $P_{ult} = 317.29 \text{ kN}$	$P_p = 351.61 \text{ kN}$ $P_{ult} = 512.61 \text{ kN}$
Winter Condition with Heave Noted as (WH)	$P_p = 356.56 \text{ kN}$ $P_H = 88.96 \text{ kN}$ $P_{ult} = -267.60 \text{ kN}$	$P_p = 624.66 \text{ kN}$ $P_H = 149.64 \text{ kN}$ $P_{ult} = -475.02 \text{ kN}$
Winter Condition Without Heave Noted as (WWH)	$P_p = 356.56 \text{ kN}$ $P_{ult} = 356.56 \text{ kN}$	$P_p = 624.66 \text{ kN}$ $P_{ult} = 624.66 \text{ kN}$

These results indicate that for peat with water content, $w = 80 \%$ and $w = 120 \%$, heave forces cannot develop because they produce a pull out force acting on top of the pile.

Using Eqs. (7.43) and (7.44), the required force to suppress the heave in the active layer of peat is:

$$\text{For } w = 80 \%, P_{ult} = 88.96 + 356.56 = 445.53 \text{ kN} \quad (7.52)$$

$$\text{For } w = 120 \%, P_{ult} = 149.64 + 624.66 = 774.31 \text{ kN} \quad (7.53)$$

The results from summer, winter conditions without heave, and Eqns (7.52) and (7.53), respectively for $w = 80 \%$ and $w = 120 \%$ implicate that:

For $w = 80 \%$, $P_{ult}(S) = 317.29 \text{ kN} < P_{ult}(WWH) = 356.56 \text{ kN} < P_{ult}(WH) = 445.53 \text{ kN}$.

and;

For $w = 120 \%$, $P_{ult}(S) = 512.61 \text{ kN} < P_{ult}(WWH) = 624.66 \text{ kN} < P_{ult}(WH) = 774.31 \text{ kN}$.

Therefore, summer conditions always govern the design of pile embedded in peat,

and,

$$P_{ult} = 317.29 \text{ kN for } w = 80 \% \quad (7.54)$$

$$P_{ult} = 512.61 \text{ kN for } w = 120 \% \quad (7.55)$$

Eqs (7.55) and (7.56) indicate that the design capacity of the pile embedded in peat soil increases by approximately 62 % when the water content increases by 50 %. The proportional rate of increase between P_{ult} and w could be explained by the fact that the depth of the active layer, has decreased only by 2.5 % when the water content increased from 80 % to 120 %. Therefore the resulting capacity of the pile depends in a great amount on the water content variation in the peat soil.

7.14 Summary

In this chapter, the analysis of bearing capacity of deep foundations embedded in frozen homogeneous soils is presented. The concrete pile of diameter $d = 0.4 \text{ m}$ and total length, $L = 5.0 \text{ m}$ is surrounded by sand with $\gamma_a = 1400 \text{ kg/m}^3$, clay with $\gamma_a = 1200 \text{ kg/m}^3$ and peat with $\gamma_a = 400 \text{ kg/m}^3$ with water contents $w \neq 0$. The determination of the active layer which develops the maximum thaw in the summer (August 20) and maximum heave

in the winter (December 22) was based on transient thermal analysis discussed in Chapters III and IV. The bearing capacity was determined for both summer and winter conditions. The system of forces imposed for each case was presented and discussed. A special approach based on assumptions was developed to determine the governing condition of the design.

The analytical results for clay and peat soils agreed with the recommended condition for design which is summer condition, where for sandy soil the choice was to be made between summer and winter without heave. An analysis was attempted to show the safety factor assumed by considering the winter without heave for the design, specially when the method of insulation of the active layer where heave forces had developed could not be properly insulated and most of the time expensive.

Finally , the comparison of the results between Problems 7 (sand), 8 (clay) and 9 (peat), in this order lead to: first, the capacity of the pile resulting from the adfreeze bond strength at the soil-pile interface increases with water content within the same soil in the summer and decreases with the texture of soil, (sand > clay > peat). Second, the heave force developed in the active layer increases with water content within the same soil and decrease with the texture of soil. This is obvious because the depth of the active layer had decreased from sand to clay to peat, independently of the water content for each type of soil.

CHAPTER VIII

SUMMARY, CONCLUSIONS AND RECOMMENDATIONS

8.1 Summary

In the first phase of the thesis, the integral formulation of the heat transfer problem with phase change is presented. It is based on the law of conservation of energy for continuum with discontinuities. The discrete form is obtained by application of the Galerkin-Bubnov approach for representation of the weighting functions connected with piece-wise approximation of temperature functions. It resulted in application of the finite element method with respect to spatial variables.

The integration with respect to temporal variables employs the Euler backward finite difference method. The sequential dependence of the current time instant with respect to the previous time instant is obtained by the implementation of the incremental decomposition procedure with respect to all temperature dependent quantities. The application of the FEM to solve the heat transfer problem with phase change required special treatment for the moving phase-change interface and its evolution with respect to

depth. In discrete form, the phase-change moving front was simulated by means of curvilinear finite element in an arbitrary fashion. This concept required modification of the original discrete equations of the problems.

The proposed numerical algorithm was employed in thermal analysis of some geotechnical problems of practical importance. Nine modelling problems, representing a concrete pile embedded in initially frozen media, were investigated. Six models examined uniform media (sand, clay and peat) and three models examined two-layered media with a height of gravel overlaying the same uniform soils. Then, a comparative analysis with the Neumann problem was conducted for each model and observations were drawn to show the difference and relative errors between the parametric analysis and the theoretical formulation. Having gained confidence in the proposed finite element modelling and the results of the numerical analysis, the second phase of this research was attempted. It was divided into the following two steps:

- 1- Laboratory determination of the adfreeze shear strength for different types of frozen soil surrounding a steel pile model.
- 2- Numerical determination of the ultimate bearing capacity of the concrete pile used for the thermal analysis for both winter and summer conditions.

The laboratory procedure consisted of testing 27 samples of different soil types with various water contents surrounding steel model piles with smooth or rough surfaces. The results were analyzed in terms of loads and shear stresses which have produced bond rupture at the soil-pile interface. The effects of water contents temperatures and pile surfaces on the adfreeze shear stress have been examined for each soil separately.

For a fixed water content and soil type, the relationship between adfreeze bond strength and freezing temperatures were best-fitted into an-easy-to-use expressions using linear regression techniques. The developed formulas are recommended to determine adfreeze bond strength as a function of temperature.

The determination of the ultimate bearing capacity of the concrete pile embedded in uniform soil (sand, clay and peat) used the combined results from both thermal analysis and experimental study. Consequently, the adfreeze bond distribution around the pile for both summer (August 20) and winter (December 22) conditions were determined for each type of soil. A proposed method, based on vertical static equilibrium and stability of the structure, has been developed and employed to determine analytically the ultimate bearing capacity of the pile for both conditions.

The effect of heave forces, developed in the active layer of each soil, on the bearing capacity have been examined. A proposed method based on assumptions has been employed to judge on the governing condition for design.

The developed analytical method is recommended to predict the ultimate bearing capacity of a deep foundation embedded in uniform soil as a function of the adfreeze bond strength at the soil-pile interface.

8.2 Conclusions

- 1- Thermal analysis for each type of soil (sand, clay and peat) should be treated separately, defining different ranges of thermal properties.
- 2- The thermal properties of the soil material are formulated and plotted in terms of

its dry unit weight and water content for each type of soil.

- 3- Within each type of soil, the obtained distribution temperature fields are not strongly affected by the variable water content. The thaw front appears on the top boundary of each soil at the same time instant independently of the variation in water content.
- 4- The presented results from the thermal analysis indicate that under arbitrary temperature distribution, they induce:
 - a- The appearance and propagation of the first phase change interface representing the thawing front.
 - b- The appearance and propagation of the second phase change interface representing the freezing front.
 - c- The merge and disappearance of the multi-phase-change interface in the medium.
- 5- The rate of thaw propagation varies with water content of the soil medium. The higher the water content, the slower the process of thaw deepening is.
- 6- Comparing homogeneous and non-homogeneous media, the following conclusions can be drawn:
 - a- For the two media with given thermal properties, the onset of thaw for the homogeneous soil (sand with $w = 20\%$, clay with $w = 30\%$ and peat with $w = 120\%$) is initiated in cooler medium than in non-homogeneous soil.
 - b- For the analyzed two media with the same geometry, thermal boundary conditions and subjected to the same changes of temperature, the rate of thaw is

slower in homogeneous than in non-homogeneous medium.

c- The onset of winter period in non-homogeneous soil with dry gravel on top is initiated in warmer medium. After complete freeze back of the thawed zone or active layer, the non-homogeneous medium slower propagate the winter temperature changes.

7- The comparative thermal analysis employing Neumann modified solution indicate considerable differences in the rate of propagation of the phase-change front within both homogeneous and non-homogeneous media:

a- The thermal properties of both media are intrinsic and invariant with temperature and time. The volumetric latent heat, L , is calculated and lumped at 0° C. Ignoring temperature-dependent latent heat effects introduces significant errors and furthermore a conservative assumption for the thaw depth in soil.

b- The movement of the 0° C isotherm for both media was plotted against the square root of time instead of being plotted point by point resulting in an overestimated depth in the beginning and an underestimated depth at the later stage when the thawing process is deepening with time. (The equivalent parameters approach for non-homogeneous medium is considered for the comparison).

c- For both media, the Neumann problem is confined to one-dimensional solution which estimates the thaw depth under an infinitely wide area. Consequently, the thermal properties of the concrete piles embedded in the soil are completely ignored.

- d- the results of the comparative analysis to Neumann problem for homogeneous medium are closer to the non-homogeneous when employing the equivalent parameters approach.
- 8- The Ontario Building Code (1990) specified a depth of 42 inches (1.067 m) of thawing for deck foundation based on 30 years forecast. However, this specification disagrees with the analytical results for sand and clay when the maximum depth of thaw was at least 24 % bigger (1.32 m) for clay with 30 % moisture content, and 66 % bigger (1.77 m) for sand with 20 % moisture content.
 - 9- For homogeneous medium with fixed water content, the adfreeze shear strength of soil surrounding deep foundation varies linearly with temperature for values greater than -5°C , then constantly afterwards.
 - 10- Within each type of unsaturated soil, the adfreeze shear strength increases with water content for a fixed temperature. At -2.5°C , the adfreeze strength has increased 61 % for a 33 % increase in the water content for sand and 135 % for 100 % increase in water content for clay.
 - 11- The determination of the ultimate bearing capacity of pile embedded in homogeneous medium was attempted for each type of soil (sand, clay and peat) separately. It was based on static equilibrium of vertical forces acting along the pile length and neglecting the pile own weight and end bearing force.
 - 12- The temperature distributions in depth for August 20 and December 22, resulting from the thermal analysis in time were essential to determine the adfreeze bond strength at the pile-soil interface for summer and winter conditions, respectively.

August 20 determined the active layer depth when the thaw deepening reached the permafrost table in summer and December 22 determined the heave layer, also called active layer, depth where complete merge of the thawing fronts have occurred in the winter.

- 13- In the active thawed layer, when calculating the bearing capacity of the pile for summer condition, the contribution of the friction force in sand or the downdrag force in clay is very small compared to the force resulting from adfreeze shear stress distribution along the pile length in the permafrost zone, and could be omitted. Therefore, the angle of internal friction, ϕ , does not consist a design characteristic for bearing capacity of pile embedded in frozen soil.
- 14- When calculating the bearing capacity of the pile for winter condition with the assumption that the force in the permafrost zone is acting downward, the heave effect resulted in a pull-out force to be carried by the pile for all types of soil embedment using Phukan and Andersland approach. On the other hand, when the permafrost force is acting upward, also referred to as suppression of heave forces or Johnston approach, the static equilibrium resulted in very large forces to be supported by the pile.
- 15- The design of the bearing capacity of the pile was always governed by the summer condition for both peat and clayey soils. For sandy soils, a comparison between summer and winter without heave conditions is necessary, specially for low water content.

8.3 Recommendations for Further Research

The following points related to the current investigation are recommended for further research:

- 1- Studying the effect of different pile material and size including timber and steel sections on the thermal analysis of heat transfer in homogeneous medium.
- 2- Studying the effect of variable dry densities on the heat transfer analysis for sandy, clayey and peat soils each treated separately.
- 3- Extending the laboratory research for the determination of the adfreeze shear strength at the soil-pile interface which takes into account :
 - a- The effect of length-to-depth ratio, L/d , for each sample which results in a constant adfreeze strength.
 - b- The effect of the pile surface roughness.
 - c- The effect of the pile material (timber, steel or concrete sections)
 - d- The effect of sand slurry in contact with different native material. For example, sand slurry + sand, sand slurry + clay and sand slurry + peat.
- 4- Studying the combined effect of points 1, 2, and 3 on the determination of the bearing capacity of piles and selecting the most economical section for design for the same homogeneous medium.
- 5- Studying the effect of frozen layered soil on the determination of the bearing capacity of piles.

Table 2.1 : Thermal Conductivity for Sand

a - FROZEN		$k_f (W/m \text{ } ^\circ K)$			
Water Content		$\gamma_{dry} (kg/m^3)$			
w (%)		1200	1400	1600	1800
0		0.13	0.16	0.24	0.38
5		0.40	0.57	0.88	1.34
10		0.69	1.02	1.56	2.38
15		1.00	1.52	2.31	3.58
20		1.31	1.97	2.97	--
30		1.92	2.86	--	--

b - UNFROZEN		$k_u (W/m \text{ } ^\circ K)$			
Water Content		$\gamma_{dry} (kg/m^3)$			
w (%)		1200	1400	1600	1800
0		--	--	--	--
5		0.69	0.94	1.25	1.65
10		0.91	1.19	1.62	2.13
15		1.00	1.33	1.79	2.38
20		1.06	1.43	1.91	--
30		1.19	1.59	--	--

Table 2.2 : Thermal Conductivity for Clay

a - FROZEN		$k_f (W/m \text{ } ^\circ K)$			
Water Content		$\gamma_{dry} (kg/m^3)$			
w (%)		1000	1200	1400	1600
0		0.04	0.08	0.13	0.25
5		0.24	0.33	0.42	0.62
10		0.40	0.57	0.74	1.00
15		0.61	0.80	1.03	1.38
20		0.80	1.03	1.33	1.75
30		1.17	1.50	1.98	--

b - UNFROZEN		$k_u (W/m \text{ } ^\circ K)$			
Water Content		$\gamma_{dry} (kg/m^3)$			
w (%)		1000	1200	1400	1600
0		--	--	--	--
5		0.24	0.32	0.45	0.58
10		0.43	0.56	0.73	1.00
15		0.53	0.69	0.88	1.23
20		0.58	0.79	1.01	1.38
30		0.70	0.93	1.20	--

Table 2.3 : Thermal Conductivity for Peat

a - FROZEN		$k_f (W/m \text{ } ^\circ K)$			
Water Content		$\gamma_{dry} (kg/m^3)$			
w (%)		150	200	300	400
40		0.05	0.06	0.09	0.14
80		0.08	0.11	0.19	0.32
120		0.13	0.18	0.33	0.60
160		0.24	0.31	1.56	1.05
200		0.37	0.48	0.78	--

b - UNFROZEN		$k_u (W/m \text{ } ^\circ K)$			
Water Content		$\gamma_{dry} (kg/m^3)$			
w (%)		150	200	300	400
40		0.05	0.06	0.07	0.09
80		0.07	0.08	0.13	0.22
120		0.11	0.14	0.22	0.35
160		0.17	0.21	0.31	0.44
200		0.23	0.28	0.39	--

Table 2.4 : Volumetric Heat Capacity for Sand

a - FROZEN

c_v (Wday/m ³ °K)				
Water Content	γ_{dry} (kg/m ³)			
w (%)	1200	1400	1600	1800
0	10.42	12.15	13.89	15.62
5	11.92	13.89	15.86	17.82
10	13.31	15.62	17.82	20.02
15	14.81	17.24	19.68	22.22
20	16.20	18.98	21.64	24.42
30	19.21	24.42	25.58	28.70

b - UNFROZEN

c_u (Wday/m ³ °K)				
Water Content	γ_{dry} (kg/m ³)			
w (%)	1200	1400	1600	1800
0	10.42	12.15	13.89	15.62
5	11.11	15.56	17.82	20.02
10	16.20	18.98	21.64	24.42
15	19.21	24.42	25.58	28.70
20	22.11	25.69	29.40	33.10
30	27.89	32.52	37.15	41.78

Table 2.5 : Volumetric Heat Capacity for Clay

a - FROZEN		$c_f (Wday/m^3 \text{ } ^\circ K)$			
Water Content		$\gamma_{dry} (kg/m^3)$			
w (%)		1000	1200	1400	1600
0		8.68	10.42	12.15	13.89
5		9.95	11.92	13.89	15.86
10		11.11	13.31	15.62	17.82
15		12.15	14.81	17.24	19.68
20		13.54	16.20	18.98	21.64
30		15.86	19.21	24.42	25.58

b - UNFROZEN		$c_u (Wday/m^3 \text{ } ^\circ K)$			
Water Content		$\gamma_{dry} (kg/m^3)$			
w (%)		1000	1200	1400	1600
0		8.68	10.42	12.15	13.89
5		11.11	13.31	15.62	17.82
10		15.86	19.21	24.42	25.58
15		18.40	22.11	25.69	29.40
20		23.15	27.89	32.52	37.15
30		28.01	33.68	39.24	44.91

Table 2.6 : Volumetric Heat Capacity for Peat

a - FROZEN

$c_f (Wday/m^3 \text{ } ^\circ K)$				
Water Content	$\gamma_{dry} (kg/m^3)$			
w (%)	150	200	300	400
40	2.75	3.68	5.51	7.35
80	4.21	5.61	8.41	11.22
120	5.66	7.55	11.32	15.09
160	7.11	9.48	14.22	18.96
200	8.56	11.41	17.12	22.82

b - UNFROZEN

$c_u (Wday/m^3 \text{ } ^\circ K)$				
Water Content	$\gamma_{dry} (kg/m^3)$			
w (%)	150	200	300	400
40	4.21	5.61	5.51	7.35
80	7.11	9.48	14.22	18.96
120	10.07	13.31	20.02	26.74
160	12.96	17.24	25.81	34.49
200	15.86	21.06	31.60	42.13

Table 2.7 : Thermal Properties of Common Materials

(After Andersland and Anderson, 1978)

Description	Thermal conductivity W/m K	Volumetric heat capacity MJ/m ³ K
Water	0.602	4.18
Ice	2.22	1.93
Air	0.024	0.00126
Snow, fresh	0.105	0.209
drifted and compacted	0.335	0.419–0.628
Granite	2.51–2.93	2.30–2.68
Limestone	1.674–2.93	2.39–4.18
Dolomite	5.02	2.51
Sandstone	2.51	2.51
Shale	1.46	1.84
Asphalt paving	1.51	2.05
Glass	0.879	1.76
Concrete with sand and gravel or stone aggregate	0.920	2.18
Steel	46.0	3.89
Wood (softwood)	0.126–0.230	0.502–0.544
Synthetic insulations e.g., polystyrene	0.029–0.063	0.0586
Sawdust	0.084	†

† Calculated from heat capacity of wood reduced by the ratio of the density of sawdust to the density of wood.

Table 2.8 : Volumetric Latent Heat in Soil

A - For SAND and CLAY

		$L (Wday/m^3)$				
w (%)	$\gamma_{dry} (kg/m^3)$					
	1000	1200	1400	1600	1800	
0	0.00	0.00	0.00	0.00	0.00	
5	192.71	231.25	269.79	308.33	346.88	
15	385.42	462.50	539.58	616.67	693.75	
20	578.13	693.75	809.38	925.00	1040.63	
30	1156.25	1387.50	1618.75	1850.00	2081.25	

B - For PEAT

		$L (Wday/m^3)$			
w (%)	$\gamma_{dry} (kg/m^3)$				
	150	200	300	400	
40	231.25	308.33	462.50	616.67	
80	462.50	616.67	925.00	1233.33	
120	693.75	925.00	1387.50	1850.00	
160	925.00	1233.33	1850.00	2466.67	
200	1156.25	1541.67	2312.50	3083.33	

Where: $L = 0.03854 \times \gamma_{dry} \times w$ (2.15)

Pile In Sand Soil, w= 15 %, Mesh -1- Comparative Analysis of Thawing Depth

Time,t,in Days	Curve (S1)* Meters	Curve (S2)** Meters	Difference (S3)***	Percentage (S3)/(S2)x100
1	2	3	4	5!
110	0.00000	0.00000	0.00000	0.00
114	0.00750	0.30632	0.29882	97.55
116	0.04267	0.38168	0.33901	88.82
125	0.22456	0.61560	0.39104	63.52
132	0.38714	0.74861	0.36147	48.29
135	0.47225	0.79886	0.32661	40.88
140	0.57140	0.87623	0.30483	34.79
145	0.66612	0.94730	0.28118	29.68
152	0.79834	1.03867	0.24033	23.14
154	0.86284	1.06333	0.20049	18.86
160	0.97104	1.13411	0.16307	14.38
161	0.98666	1.14548	0.15882	13.86
170	1.13276	1.24315	0.11039	8.88
175	1.21700	1.29422	0.07722	5.97
180	1.28979	1.34336	0.05357	3.99
184	1.35464	1.38141	0.02677	1.94
190	1.44742	1.43660	-0.01082	-0.75
195	1.50991	1.48102	-0.02889	-1.95
200	1.57252	1.52415	-0.04837	-3.17
210	1.70123	1.60694	-0.09429	-5.87
221	1.81337	1.69333	-0.12004	-7.09
223	1.83994	1.70857	-0.13137	-7.69
230	1.92814	1.76087	-0.16727	-9.50
240	2.01404	1.83300	-0.18104	-9.88
250	2.08923	1.90239	-0.18684	-9.82
260	2.15534	1.96934	-0.18600	-9.44
270	2.20782	2.03409	-0.17373	-8.54
273	2.22024	2.05311	-0.16713	-8.14
280	2.24240	2.09684	-0.14556	-6.94

* (S1): The Analytical Solution Based on F.E.M. with 8-Nodes Rectangular Elements

** (S2): The Neumann Solution Based on Eq: **$\text{SQRT}(t-110.38) \times 0.161$**

***(S3): The Difference Curve = (S2) - (S1), in Meters

! Col. 5 represents the percentage of error made with respect to Neumann solution

The " 0.00" in the first line of col. 5 represents a complete match between the analytical solution and the Neumann Problem, i.e. , the percentage of error = 0.00

Table 4.1 : Comparative Analysis for Sand with w = 15 %

Pile in Sand Soil, w= 20%, Mesh -1- Comparative Analysis of Thawing Depth

Time, t, in Days	Curve (S1)* Meters	Curve (S2)** Meters	Difference (S3)***	Percentage (S3)/(S2)x100
1	2	3	4	5!
110	0.00000	0.00000	0.00000	0.00
112	0.00000	0.20892	0.20892	100.00
116	0.02381	0.34016	0.31635	93.00
116	0.02541	0.34620	0.32079	92.66
120	0.09287	0.44103	0.34816	78.94
124	0.16899	0.52673	0.35774	67.92
129	0.26904	0.61736	0.34832	56.42
135	0.40437	0.71247	0.30810	43.24
141	0.53608	0.80137	0.26529	33.10
145	0.60129	0.85155	0.25026	29.39
150	0.68789	0.91039	0.22250	24.44
156	0.79158	0.97634	0.18476	18.92
160	0.86423	1.01691	0.15268	15.01
164	0.93735	1.05691	0.11956	11.31
169	1.00964	1.10487	0.09523	8.62
179	1.15326	1.19503	0.04177	3.50
180	1.16807	1.20367	0.03560	2.96
189	1.28889	1.27885	-0.01004	-0.79
194	1.35255	1.31561	-0.03694	-2.81
204	1.48044	1.39219	-0.08825	-6.34
214	1.58427	1.46477	-0.11950	-8.16
223	1.67833	1.52715	-0.15118	-9.90
233	1.76977	1.59359	-0.17618	-11.06
237	1.79896	1.61941	-0.17955	-11.09
246	1.87875	1.67418	-0.20457	-12.22
251	1.91799	1.70487	-0.21312	-12.50
261	1.97366	1.76463	-0.20903	-11.85
266	1.99476	1.79377	-0.20099	-11.20
271	2.01188	1.82244	-0.18944	-10.39
281	2.03457	1.87847	-0.15610	-8.31

* (S1): The Analytical Solution based on F.E.M. with 8-nodes rectangular elements

** (S2): The Neumann Solution based on Eq: $\text{SQRT}(t-110.38) \times 0.114$

*** (S3): The difference: (S2) - (S1), In Meters

! Col.5 represents the percentage of error made with respect to the Neumann solution

The " 0.00" in the first line of col. 5 represents a complete match between the analytical solution and the Neumann Problem, i.e. , the percentage of error = 0.00

Table 4.2 : Comparative Analysis for Sand with w = 20 %

Pile In Clay Soil, w= 15 %, Mesh - 2 - Comparative Analysis of Thawing Depth

Time,t,In Days 1	Curve (S1)* Meters 2	Curve(S1)** Meters 3	Difference (S1)*** 4	Percentage (S3)/(S2)x100 5!
110	0.00000	0.00000	0.00000	0.00
112	0.00021	0.14855	0.14834	99.86
114	0.01030	0.24051	0.23021	95.72
115	0.02772	0.27292	0.24520	89.84
123	0.16218	0.45565	0.29347	64.41
131	0.30608	0.58373	0.27765	47.56
134	0.36678	0.62503	0.25825	41.32
139	0.47527	0.69476	0.21949	31.59
140	0.49895	0.70663	0.20768	29.39
147	0.61055	0.78474	0.17419	22.20
155	0.71735	0.86542	0.14807	17.11
158	0.75808	0.89379	0.13571	15.18
164	0.84235	0.94801	0.10566	11.15
168	0.90045	0.98249	0.08204	8.35
173	0.97052	1.02395	0.05343	5.22
178	1.03238	1.06381	0.03143	2.95
183	1.08513	1.10222	0.01709	1.55
188	1.13292	1.13934	0.00642	0.56
190	1.15968	1.15191	-0.00777	-0.67
199	1.27446	1.21518	-0.05928	-4.88
209	1.36152	1.28182	-0.07970	-6.22
210	1.36995	1.28830	-0.08165	-6.34
220	1.45346	1.35134	-0.10212	-7.56
230	1.53371	1.41157	-0.12214	-8.65
240	1.60786	1.46933	-0.13853	-9.43
250	1.67142	1.52491	-0.14651	-9.61
260	1.71980	1.57853	-0.14127	-8.95
270	1.75239	1.63039	-0.12200	-7.48
279	1.76917	1.67569	-0.09348	-5.58
280	1.77027	1.68065	-0.08962	-5.33

* (S1): The Analytical Solution Based on F.E.M. with 8-Nodes Rectangular Elements

** (S2): The Neumann Solution Based on Eq: $\text{SQRT}(t-110.38) \times 0.129$

*** (S3): The Difference: (S2) -(S1), In Meters

!Col. 5 represents the percentage of error made with respect to the Neumann Solution

The " 0.00" in the first line of col. 5 represents a complete match between the analytical

solution and the Neumann Problem, i.e., the percentage of error = 0.00

Table 4.3 : Comparative Analysis for Clay with w = 15 %

**Pile in Clay Soil, w= 30 %, Mesh - 2 -
Comparative Analysis of Thawing Depth**

Time,t,in Days 1	Curve (S1)* Meters 2	Curve(S1)** Meters 3	Difference (S1)*** 4	Percentage (S3)/(S2)x100 5
110.38	0.00000	0.00000	0.00000	0.00
113.40	0.00344	0.18490	0.18146	98.14
114.50	0.00637	0.21597	0.20960	97.05
116.50	0.03423	0.26322	0.22899	87.00
120.50	0.09353	0.33848	0.24495	72.37
127.50	0.19270	0.44024	0.24754	56.23
133.50	0.28423	0.51161	0.22738	44.44
141.50	0.40525	0.59356	0.18831	31.73
147.60	0.51377	0.64913	0.13536	20.85
160.60	0.66936	0.75401	0.08465	11.23
170.60	0.77681	0.82568	0.04887	5.92
185.60	0.93699	0.92280	-0.01419	-1.54
198.60	1.05689	0.99937	-0.05752	-5.76
208.60	1.12341	1.05449	-0.06892	-6.54
214.46	1.19040	1.08549	-0.10491	-9.66
225.46	1.27730	1.14141	-0.13589	-11.91
235.46	1.33098	1.18997	-0.14101	-11.85
250.46	1.39900	1.25930	-0.13970	-11.09
260.46	1.43504	1.30348	-0.13156	-10.09
270.46	1.46073	1.34620	-0.11453	-8.51
280.46	1.48642	1.38761	-0.09881	-7.12

* (S1): The Analytical Solution Based on F.E.M. with 8-Nodes Rectangular Elements

** (S2): The Neumann Solution Based on Eq:

$$SQRT (t-110.38) \times 0.1064$$

*** (S3): The Difference: (S2) - (S1), in Meters

!Col. 5 represents the percentage of error made with respect to the Neumann Solution

The " 0.00" in the first line of col. 5 represents a complete match between the analytical solution and the Neumann Problem, i.e., the percentage of error = 0.00

Table 4.4 : Comparative Analysis for Clay with w = 30 %

**Pile in Peat Soil, w = 80%, Mesh -2-
Comparative Analysis of Thawing Depth**

Time, t, in Days	Curve (S1)* Meters	Curve (S2)** Meters	Difference (S3)***	Percentage (S3)/(S2)x100
1	2	3	4	5!
110.38	0.00000	0.00000	0.00000	0.00
114	0.00806	0.10769	0.09963	92.52
120	0.07254	0.17555	0.10301	58.68
128	0.14702	0.23759	0.09057	38.12
137	0.23202	0.29203	0.06001	20.55
143	0.29334	0.32326	0.02992	9.26
154	0.39563	0.37382	-0.02181	-5.84
158	0.45531	0.39058	-0.06473	-16.57
163	0.49278	0.41057	-0.08221	-20.02
168	0.52329	0.42964	-0.09365	-21.80
174	0.58812	0.45145	-0.13667	-30.27
187	0.66132	0.49544	-0.16588	-33.48
196	0.69353	0.52373	-0.16980	-32.42
208	0.73679	0.55922	-0.17757	-31.75
219	0.77766	0.58989	-0.18777	-31.83
230	0.81693	0.61904	-0.19789	-31.97
241	0.85295	0.64688	-0.20607	-31.86
250	0.87891	0.66879	-0.21012	-31.42
258	0.89706	0.68768	-0.20938	-30.45
268	0.91172	0.71059	-0.20113	-28.30
280	0.91553	0.73715	-0.17838	-24.20

* (S1): The Analytical Solution Based on F.E.M. with 8 nodes Rectangular elements

** (S2): The Neumann Solution Based on Eq: $SQRT(t-110.38) \times 0.0566$

*** (S3): The Difference: (S2) - (S1), In Meters

! Col. 5 represents the percentage of error made with respect to the Neumann Solution

The "0.00" in the first line of col. 5 represents a complete match between the analytical solution and the Neumann Problem, i.e., the percentage of error = 0.00

Table 4.5 : Comparative Analysis for Peat with w = 80 %

**Pile in Peat Soil, w= 120%, Mesh -2-
Comparative Analysis of Thawing Depth**

Time,t, in Days	Curve (S1)* Meters	Curve (S2)** Meters	Difference (S3)***	Percentage (S3)/(S2)x100
1	2	3	4	5!
110.38	0.00000	0.00000	0.00000	0.00
113.21	0.00035	0.09707	0.09672	99.64
113.91	0.00210	0.10841	0.10631	98.06
114.51	0.00588	0.11726	0.11138	94.99
115.51	0.01426	0.13069	0.11643	89.09
116.61	0.02553	0.14402	0.11849	82.27
117.61	0.03804	0.15515	0.11711	75.48
120.61	0.06987	0.18455	0.11468	62.14
130.61	0.16224	0.25952	0.09728	37.49
145.61	0.29734	0.34248	0.04514	13.18
155.61	0.38468	0.38805	0.00337	0.87
166.61	0.46919	0.43267	-0.03652	-8.44
170.15	0.51566	0.44608	-0.06958	-15.60
180.15	0.59863	0.48196	-0.11667	-24.21
195.15	0.66234	0.53125	-0.13109	-24.68
210.15	0.71865	0.57634	-0.14231	-24.69
222.15	0.76275	0.61001	-0.15274	-25.04
239.15	0.81933	0.65476	-0.16457	-25.13
249.15	0.84806	0.67971	-0.16835	-24.77
260.15	0.87241	0.70614	-0.16627	-23.55
270.15	0.88606	0.72933	-0.15673	-21.49
280.15	0.89011	0.75181	-0.13830	-18.40

* (S1): The Numerical Solution Based on F.E.M.with 8 nodes Rectangular elements

** (S2): The Neumann Solution Based on Eq: $\text{SQRT}(t-110.38) \times 0.0577$

*** (S3): The Difference: (S2) - (S1), in Meters

! Col. 5 represents the percentage of error made with respect to the Neumann Solution

The " 0.00" in the first line of col. 5 represents a complete match between the analytical solution and the Neumann Problem,i.e., the percentage of error = 0.00

Table 4.6: Comparative Analysis for Peat with w = 120 %

Pile in Sand Soil with Gravel on top
Comparative Analysis of Thawing Depth
 Depth of Gravel, d = 2.4 m, MESH - 1 -

Time,t, in Days 1	Curve (S1)* Meters 2	Curve (S2)** Meters 3	Difference (S3)*** 4	Percentage (S3)/(S2)x100 5!
110	0.00000	0.00000	0.00000	0.00
112	0.00000	0.20738	0.20738	100.00
114	0.03847	0.31001	0.27154	87.59
121	0.17534	0.53098	0.35564	66.98
125	0.27176	0.62300	0.35124	56.38
130	0.40440	0.72171	0.31731	43.97
135	0.53198	0.80846	0.27648	34.20
140	0.64358	0.88676	0.24318	27.42
150	0.85699	1.02559	0.16860	16.44
160	1.05284	1.14774	0.09490	8.27
170	1.24137	1.25809	0.01672	1.33
180	1.41933	1.35951	-0.05982	-4.40
190	1.56453	1.45387	-0.11066	-7.61
200	1.69109	1.54247	-0.14862	-9.64
210	1.79187	1.62625	-0.16562	-10.18
220	1.87603	1.70592	-0.17011	-9.97
230	1.93938	1.78204	-0.15734	-8.83
240	1.98863	1.85503	-0.13360	-7.20
250	2.02248	1.92526	-0.09722	-5.05
260	2.04618	1.99301	-0.05317	-2.67
270	2.05906	2.05854	-0.00052	-0.03
275	2.06109	2.09053	0.02944	1.41
277	2.06100	2.10319	0.04219	2.01
280	2.05981	2.12204	0.06223	2.93

* (S1): The Analytical Solution based on F.E.M. with 8-nodes rectangular elements

** (S2): The Neumann Solution based on Eq: $\text{SQRT}(t-110.38) \times 0.163$

*** (S3): The difference: (S2) - (S1), In Meters

! Col.5 represents the percentage of error made with respect to the Neumann solution

The " 0.00" in the first line of col. 5 represents a complete match between the analytical solution and the Neumann Problem, i.e. , the percentage of error = 0.00

Table 4.7 : Comparative Analysis for Sand with Gravel on Top, Sand Water Content, w = 20 %

Pile in Clay Soil with Gravel on top, w= 30%
Comparative Analysis of Thawing Depth
 Depth of Gravel, d = 2.5 m, MESH - 2 -

Time, t, in Days	Curve (S1)* Meters	Curve (S2)** Meters	Difference (S3)***	Percentage (S3)/(S2)x100
1	2	3	4	5 ^l
110	0.00000	0.00000	0.00000	0.00
111	0.00000	0.08992	0.08992	100.00
113	0.01775	0.18486	0.16711	90.40
114	0.03802	0.21729	0.17927	82.50
120	0.15259	0.35422	0.20163	56.92
125	0.26837	0.43667	0.16830	38.54
130	0.40194	0.50586	0.10392	20.54
140	0.64006	0.62155	-0.01851	-2.98
147	0.77623	0.69110	-0.08513	-12.32
157	0.97270	0.77978	-0.19292	-24.74
163	1.08747	0.82844	-0.25903	-31.27
170	1.22251	0.88182	-0.34069	-38.63
180	1.39364	0.95291	-0.44073	-46.25
190	1.54464	1.01905	-0.52559	-51.58
200	1.67993	1.08115	-0.59878	-55.38
210	1.79185	1.13988	-0.65197	-57.20
220	1.88789	1.19572	-0.69217	-57.89
230	1.96294	1.24907	-0.71387	-57.15
240	2.02180	1.30023	-0.72157	-55.50
250	2.06312	1.34945	-0.71367	-52.89
263	2.10005	1.41088	-0.68917	-48.85
273	2.11482	1.45637	-0.65845	-45.21
277	2.11710	1.47417	-0.64293	-43.61
280	2.11741	1.48738	-0.63003	-42.36

* (S1): The Analytical Solution based on F.E.M. with 8-nodes rectangular elements

** (S2): The Neumann Solution based on Eq: $\text{SQRT}(t-110.38) \times 0.1142$

*** (S3): The difference: (S2) - (S1), In Meters

^l Col.5 represents the percentage of error made with respect to the Neumann solution

The " 0.00" in the first line of col. 5 represents a complete match between the analytical solution and the Neumann Problem, i.e. , the percentage of error = 0.00

**Table 4.8 : Comparative Analysis for Clay with Gravel
 on Top, Clay Water Content, w = 30 %**

Pile in Peat Soil with Gravel on top, w= 120 %
Comparative Analysis of Thawing Depth
 Depth of Gravel, d = 2.5 m, MESH - 2 -

Time, t, in Days	Curve (S1)* Meters	Curve (S2)** Meters	Difference (S3)***	Percentage (S3)/(S2)x100
1	2	3	4	5!
110	0.00000	0.00000	0.00000	0.00
113	0.01747	0.09550	0.07803	81.71
120	0.15123	0.18300	0.03177	17.36
128	0.34542	0.24766	-0.09776	-39.47
132	0.45203	0.27433	-0.17770	-64.77
135	0.52757	0.29275	-0.23482	-80.21
140	0.63243	0.32110	-0.31133	-96.96
150	0.82145	0.37137	-0.45008	-121.19
155	0.91500	0.39411	-0.52089	-132.17
160	1.00866	0.41560	-0.59306	-142.70
165	1.10076	0.43604	-0.66472	-152.44
170	1.19100	0.45556	-0.73544	-161.44
175	1.27949	0.47428	-0.80521	-169.77
180	1.35452	0.49229	-0.86223	-175.15
190	1.49781	0.52646	-0.97135	-184.51
200	1.63031	0.55854	-1.07177	-191.89
210	1.75053	0.58888	-1.16165	-197.27
220	1.85186	0.61773	-1.23413	-199.79
230	1.94463	0.64529	-1.29934	-201.36
240	2.01129	0.67172	-1.33957	-199.42
250	2.06775	0.69715	-1.37060	-196.60
260	2.11197	0.72168	-1.39029	-192.64
270	2.14423	0.74541	-1.39882	-187.66
280	2.16369	0.76841	-1.39528	-181.58

* (S1): The Analytical Solution based on F.E.M. with 8-nodes rectangular elements

** (S2): The Neumann Solution based on Eq: $\text{SQRT}(t-110.38) \times 0.059$

*** (S3): The difference: (S2) - (S1), in Meters

! Col.5 represents the percentage of error made with respect to the Neumann solution

The " 0.00" in the first line of col. 5 represents a complete match between the analytical solution and the Neumann Problem, i.e., the percentage of error = 0.00

Table 4.9 : Comparative Analysis for Peat with Gravel on Top, Peat Water Content, w = 120 %

Table 6-1 : Nomenclature for experimental procedure

1	2	3	4	5	6	7	8
SAMPLE #	SOIL TYPE	SOIL TEMP. C	WATER CONTENT %	PILE L (in)	PILE d (in)	L/d RATIO	PILE SURFACE TYPE
6	Clay	-5.69	24.0	4.00	1.00	4.00	Rough
8	Sand	-4.50	8.0	3.50	1.00	3.50	Rough
9	Sand	-3.84	8.2	4.20	1.00	4.20	Rough
10	Sand	-1.89	7.4	3.90	1.00	3.90	Rough
11	Sand	-6.07	8.0	4.20	1.00	4.20	Rough
12	Sand	-5.22	11.5	3.50	1.00	3.50	Rough
13	Sand	-3.67	11.5	4.00	1.00	4.00	Rough
14	Sand	-2.54	11.0	3.50	1.00	3.50	Smooth
15	Sand	-2.61	14.2	5.00	1.00	5.00	Rough
16	Sand	-4.52	14.2	5.10	1.00	5.10	Rough
17	Sand	-4.86	14.0	5.50	1.00	5.50	Rough
19	Peat	-2.51	278.0	2.50	1.00	2.50	Rough
20	Peat	-1.78	278.0	2.50	1.00	2.50	Rough
21	Peat	-2.54	370.0	4.20	1.00	4.20	Rough
22	Peat	-1.35	418.0	2.50	1.00	2.50	Rough
24	Peat	-4.40	407.0	2.50	1.00	2.50	Rough
25	Peat	-4.25	407.0	1.50	1.00	1.50	Smooth
26	Peat	-4.26	272.0	2.50	1.00	2.50	Rough
27	Peat	-4.39	273.0	3.00	1.00	3.00	Rough

Col 3 : Average Temperature during loading procedure

Col 4 : Soil moisture content based on amount of water added to the dry weight of the sample

Col 5 : L = Effective embedment length measured during the preparation of the sample

L-total of the pile = 6" for rough surface, 5" for smooth surface

Col 6 : d = Diameter of the pile, constant during the whole procedure

Col 7 : Effective length to depth ratio for loading purpose

Col 8 : Type of the pile surface in contact with the soil where Rough means threads spreaded uniformly along the pile shaft, Smooth means, simply, a steel rod

Table 6-2 : Summary of experimental results

1	2	3	4	5	6	7	8
SAMPLE #	SOIL TYPE	SOIL TEMP. C	WATER CONTENT w %	PILE L (mm)	MAX LOAD P (kN)	MAX DISPL (mm)	MAX STRESS (kPa)
6	Clay	-5.69	24.0	101.60	-----	-----	-----
8	Sand	-4.50	8.0	88.90	2.41	0.27	340
9	Sand	-3.84	8.2	106.68	2.38	0.24	280
10	Sand	-1.89	7.4	99.06	1.26	0.15	160
11	Sand	-6.07	8.0	106.68	2.95	0.23	347
12	Sand	-5.22	11.5	88.90	2.50	0.14	352
13	Sand	-3.67	11.5	101.60	2.84	0.14	350
14	Sand	-2.54	11.0	88.90	1.74	0.15	245
15	Sand	-2.61	14.2	127.00	5.98	0.33	590
16	Sand	-4.52	14.2	129.54	8.06	0.42	780
17	Sand	-4.86	14.0	139.70	9.13	0.43	819
19	Peat	-2.51	278.0	63.50	1.32	2.50	260
20	Peat	-1.78	278.0	63.50	0.96	1.60	190
21	Peat	-2.54	370.0	106.68	3.32	1.10	390
22	Peat	-1.35	418.0	63.50	1.82	0.51	360
24	Peat	-4.40	407.0	63.50	3.04	0.80	600
25	Peat	-4.25	407.0	38.10	1.75	0.66	575
26	Peat	-4.26	272.0	63.50	1.52	1.17	300
27	Peat	-4.39	273.0	76.20	2.19	1.25	360

Col 5 : L = Effective embedment length measured during the preparation of the sample

L-total of the pile = 152.4 mm for rough surface, 127 mm for smooth surface

Col 6 : Maximum load to produce failure between the pile surface and the surrounding soil

Col 7 : Measured displacement at maximum load, producing shear failure

Col 8 : Maximum adfreeze shear stress at the soil - Maximum load over pile surface area

Table 7.1 : Pile Capacity in Sand for Summer Condition

Pile in Sandy Soil, w = 15 %							
T	L	dL	Shear Stress	Integral area	Coyle and Castello	Output datas	
C	m	m	kPa	kPa/m		Unit	
-2.00	0.00		529.39		K =	0.47	
-2.20	0.71		548.89			sigma =	30.75 kPa
-2.50	2.10		578.13			L =	1.95 m
-2.56	2.95		584.17			*fl =	6.93 kPa
-2.56	3.05		584.17			P2 ult.=	16.95 kN
-2.50	3.76		578.13			Graphical solution Based on Equation : ** f = 334.46 - 97.47 x T in kPa	
-2.27	4.50		555.70				
-2.20	4.82	0.32	548.89	178.79			
-2.00	5.25	0.43	529.39	229.42			
-1.50	6.06	0.81	480.66	410.44			
-1.00	6.71	0.65	431.93	296.86			
0.00	7.55	0.84	334.46	322.03			
				1437.54	P1 ult.=	1806.47 kN	

P tot. = 1823.41 kN

Pile in Sandy Soil, w = 20 %							
T	L	dL	Shear Stress	Integral area	Coyle and Castello	Output data	
C	m	m	kPa	kPa/m		Unit	
-2.00	0.00		865.23		K =	0.47	
-2.20	1.00		890.59			Sigma =	29.17 kPa
-2.35	2.05		909.61			L =	1.77 m
-2.38	2.51		913.04			*fl =	6.57 kPa
-2.20	4.27		890.59			P2 ult.=	14.61 kN
-2.00	4.50		864.60			Graphical solution Based on Equation : ** f = 611.61 - 126.81 x T in kPa	
-1.50	5.95	1.45	801.82	1208.52			
-1.00	6.73	0.78	738.42	602.30			
-0.50	7.35	0.62	675.01	437.15			
0.00	7.73	0.38	611.61	243.90			
				2491.88	P1 ult.=	3131.39 kN	

P tot. = 3146.00 kN

* fl = Tangential shear stress in the unfrozen soil calculated after Coyle and Castello

** f = Adfreeze shear stress found after laboratory experimental studies

Table 7.2 : Pile Capacity in Clay for Summer Condition

Pile in Clayey Soil, w = 15 %					
T	L	dL	Shear Stress*	Integral area	Output
C	m	m	kPa	kPa/m	Das datas Unit
-3.0	6.50		403.26		K= 0.72
-3.0	7.08	0.58	400.80	231.74	sigma = 20.97 kPa
-2.7	7.68	0.61	378.69	236.65	L= 1.55 m
-2.5	7.99	0.30	363.95	112.36	**f= 2.57 kPa
-2.2	8.37	0.38	341.84	134.48	P2 ult. = 2.50 kN
-2.0	8.59	0.22	327.10	74.63	
-1.0	9.45	0.86	253.40	249.44	
0.0	9.95	0.50	179.70	108.50	
				1147.80	P1 ult. = 1442.37 kN

Ptot. = 1439.87 kN

Pile in Clayey Soil, w = 30 %					
T	L	dL	Shear Stress*	Integral area	Output
C	m	m	kPa	kPa/m	Das data Unit
-2.9	6.50		900.73		
-2.8	7.00	0.50	884.57	446.33	K = 0.72 kPa
-2.5	7.67	0.67	853.65	585.17	sigma= 20.14 kPa
-2.2	8.16	0.48	818.34	403.18	L = 1.32 m
-2.0	8.44	0.29	794.80	230.14	**f = 2.47 kPa
-1.0	9.60	1.16	677.10	853.43	P2 ult. = 2.04 kN
0.0	10.18	0.58	559.40	360.83	
				2879.07	P1 ult. = 3617.95 kN

P tot. = 3615.91 kN

* Adfreeze shear stress calculated after laboratory studies as follows :

for w = 15 %, $f = 179.73 - 73.73 \times T$, and,

for w = 30 %, $f = 559.45 - 117.75 \times T$

** f1 = downward drag stress in the unfrozen soil calculated after Das, B. M.

Table 7.3 : Pile Capacity in Peat for Summer Condition

Pile in Peat Soil, w = 80 %							
T	L	dL	Shear Stress*	Integral area	Output data		
C	m	m	kPa	kPa/m	Force	Unit	
-3.1	6.50		67.36				
-3.3	7.00	0.50	68.86	34.05			
-3.2	8.51	1.51	68.06	103.31			
-3.0	8.87	0.37	65.40	24.38	Graphical Solution Based on Equation : *f = 25.5 - 13.3 x T		
-2.0	9.86	0.98	52.10	57.86			
-1.0	10.36	0.50	38.80	22.64			
0.0	10.68	0.32	25.50	10.25		in	kPa
				252.50		P ult. =	317.29 kN

Pile in Peat Soil, w = 120 %						
T	L	dL	Shear Stress*	Integral area	Output data	
C	m	m	kPa	kPa/m	Force	Unit
-3.4	6.5		115.39			
-3.4	7.00	0.50	115.29	57.67		
-3.4	7.21	0.21	115.18	24.67		
-3.2	8.07	0.85	110.94	96.51		
-3.0	8.50	0.43	106.70	47.13	Graphical Solution Based on Equation : *f = 43.1 - 21.2 x T	
-2.7	8.96	0.46	100.34	47.90		
-2.4	9.34	0.37	93.98	36.13		
-2.0	9.73	0.39	85.50	35.19		
0.0	10.70	0.98	43.10	62.72		in
				407.92	P ult. =	512.61 kN

* Adfreeze shear stress formula and data found after laboratory experimental studies

TABLE 7-4: The results of bearing capacity analysis for summer condition (August 20)

Length of pile.	(m)	5.50	5.50	5.50	5.50	5.50	5.50
Perimeter of pile.	(m)	1.26	1.26	1.26	1.26	1.26	1.26
Type of soil		Sand	Sand	Clay	Clay	Peat	Peat
Water content,	%	15	20	15	30	80	120
Angle of internal friction.	ϕ	32	32	16	16	na	na
Angle of internal friction between pile and soil.	d	25.60	25.60	9.60	9.60	na	na
Depth of active layer .	(m)	1.95	1.77	1.55	1.32	0.82	0.80
Friction Force.	(kN)	16.95	14.61	na	na	na	na
Downdrag Force.	(kN)	na	na	2.50	2.04	na	na
Range of adfreeze strength in permafrost		334.46	611.61	179.70	559.40	25.50	43.10
	(kN/m ²)	555.70	864.60	403.26	900.73	67.36	115.39
Mean adfreeze strength in permafrost.	(kN/m ²)	445.08	738.11	291.48	730.07	46.43	79.25
Pult.	(kN)	1823.41	3146.00	1439.87	3615.91	317.29	512.61

na : " not applicable " wherever it shows in the table

Table 7.5 : Pile Capacity in Sand for Winter Condition

Pile in Sandy Soil, w = 15 %						
T	L	dL	Shear Stress	Integral area	Output	
C	m	m	kPa	kPa/m	Condition datas Unit	
4.50	-1.0		430.11		Case 2 : WITHOUT HEAVE	
5.42	-0.7	0.92	402.69	384.58		
6.30	-0.5	0.88	383.20	344.19		
6.91	-0.7	0.61	402.69	241.28		
7.15	-1.0	0.23	431.93	96.99		
7.55	-2.3	0.40	556.68	199.70		P ult. = 1591.85 kN
7.71	-3.0	0.16	626.86	97.48	Case 1 : WITH HEAVE	
7.88	-4.0	0.16	724.32	108.94		
8.01	-5.0	0.14	821.79	105.77		
9.50	-21.4	1.49	821.79	1222.17		P ult. = 587.24 kN

Pile in Sandy Soil, w = 20 %					
T	L	dL	Shear Stress	Integral area	Output
C	m	m	kPa	kPa/m	Condition data Unit
-0.9	4.50		729.23		Case 2 : WITHOUT HEAVE
-0.2	6.92	2.42	636.97	1654.24	
0.1	7.55	0.63	611.61	392.55	
-0.3	7.73	0.18	654.35	113.65	
-1.0	7.81	0.08	738.42	54.35	Case 1 : WITH HEAVE
-2.0	7.91	0.10	865.23	81.94	
-3.0	8.01	0.10	992.04	90.85	
-5.0	8.19	0.18	1245.66	206.48	
-21.0	9.50	1.31	1245.66	1628.57	

Suppression of Heave Assumption : P ult. = 5306.30 kN

• The negative sign means that heave cannot develop and the assumption of "Heave Suppression" should be utilized

Table 7.6 : Pile Capacity in Clay for Winter Condition

Pile in Clayey Soil, w = 15 %						
T	L	dL	Shear Stress	Integral area	Output data	
C	m	m	kPa	kPa/m	Condition	Unit
-1.9	6.50		316.76		Case 2 : WITHOUT HEAVE	
-1.7	7.00	0.50	302.81	154.89		
-1.6	7.17	0.17	297.52	51.32		
-1.6	8.29	1.11	297.52	331.58		
-2.0	8.72	0.44	327.00	136.07		
-2.4	8.93	0.21	352.80	71.52		
-3.0	9.21	0.28	400.70	103.72		
-4.0	9.49	0.29	474.40	124.76		
-5.0	9.71	0.22	547.63	112.09		
-6.4	9.95	0.24	547.63	130.67	P ult. =	1528.84 kN
-21.0	11.43	1.55	547.63	848.06	Case 1 : WITH HEAVE	
					*P ult. =	-463.13 kN

Suppression of Heave Assumption : P ult. = 2594.55 kN

Pile in Clayey Soil, w = 30 %						
T	L	dL	Shear Stress	Integral area	Output data	
C	m	m	kPa	kPa/m	Condition	Unit
-1.9	6.50		787.71		Case 2 : WITHOUT HEAVE	
-1.9	7.00	0.50	788.16	393.97		
-2.0	8.37	1.37	794.80	1081.60		
-2.2	8.52	0.16	818.34	127.03		
-2.5	8.70	0.18	853.65	150.35		
-3.0	8.94	0.23	912.50	204.94		
-4.0	9.27	0.34	1030.20	325.87		
-5.0	9.48	0.21	1147.90	227.95		
-9.0	10.18	0.70	1147.90	802.67	P ult. =	4164.95 kN
-21.4	11.50	1.32	1147.90	1515.23	Case 1 : WITH HEAVE	
					*P ult. =	-2260.86 kN

Suppression of Heave Assumption : P ult. = 6069.05 kN

* The negative sign means that heave cannot develop and the assumption of " Heave Suppression " should be utilized

Table 7.7 : Pile Capacity in Peat for Winter Condition

Pile in Peat Soil, w = 80 %				Integral area kPa/m	Output data	
T C	L m	dL m	Shear Stress kPa		Condition	Unit
-2.5	6.50		58.75	29.38 143.87 25.33 27.14 58.04	Case 2 : WITHOUT HEAVE P ult. = 356.56 kN	
-2.5	7.00	0.50	58.75			
-3.0	9.32	2.32	65.40			
-4.0	9.67	0.35	78.70			
-4.5	10.00	0.33	85.35			
-11.2	10.68	0.68	85.35			
-22.0	11.51	0.83	85.35			70.80

Suppression of Heave Assumption : P ult. = 445.53 kN

Pile in Peat Soil, w = 120 %				Integral area kPa/m	Output data	
T C	L m	dL m	Shear Stress kPa		Condition	Unit
-2.5	6.50		96.10	48.05 23.31 35.72 33.87 33.58 29.08 60.58 33.12 199.79	Case 2 : WITHOUT HEAVE P ult. = 624.66 kN	
-2.5	7.00	0.50	96.10			
-2.4	7.25	0.25	93.98			
-2.4	7.63	0.38	93.98			
-2.5	7.98	0.36	96.10			
-2.7	8.32	0.34	100.34			
-3.0	8.60	0.28	106.70			
-4.0	9.12	0.52	127.90			
-5.0	9.36	0.24	149.10			
-13.6	10.70	1.34	149.10			
-22.0	11.50	0.80	149.10			119.08

Suppression of Heave Assumption : P ult. = 774.31 kN

* The negative sign means that heave cannot develop and the assumption of " Heave Suppression " should be utilized

TABLE 7-8: The results of bearing capacity analysis for winter condition (December 22)

Length of pile, (m)	5.50	5.50	5.50	5.50	5.50	5.50
Perimeter of pile, (m)	1.26	1.26	1.26	1.26	1.26	1.26
Type of soil	Sand	Sand	Clay	Clay	Peat	Peat
Water content, %	15	20	15	30	80	120
Depth of active layer, (m)	1.95	1.77	1.55	1.32	0.82	0.80
Range of temperature in active layer, C	-21.40 -3.00	-21.00 -0.30	-21.00 -6.40	-21.40 -9.00	-22.00 -11.20	-22.00 -13.60
Range of Adfreeze strength in heave layer (kN/m ²)	556.68 821.79	654.35 1245.66	547.63 547.63	1147.90 1147.90	85.35 85.35	149.10 149.10
Mean adfreeze strength in active layer, (kN/m ²)	689.24	950.01	547.63	1147.90	85.35	149.10
Heave force, (kN)	2179.09	2591.42	1065.71	1904.09	88.96	149.64
Depth of permafrost, (m)	3.05	3.23	3.45	3.68	4.18	4.20
Range of temperature in permafrost, C	-2.30 -1.00	-0.90 0.10	-6.40 -1.90	-9.00 -1.90	-11.20 -2.50	-13.60 -2.50
Range of adfreeze strength in permafrost (kN/m ²)	430.11 556.68	611.61 729.23	316.76 547.63	787.71 1147.90	58.75 85.35	96.10 149.10
Mean adfreeze strength in permafrost, (kN/m ²)	493.40	670.42	432.20	967.81	72.05	122.60
Pult with heave, (kN)	587.24	*****	*****	*****	*****	*****
Pult without heave, (kN)	1591.85	2174.88	2594.55	4164.95	356.56	624.66
Pult. calculated with suppression of Heave, (kN)	3770.94	5306.30	2594.55	6069.05	445.53	774.31

* : this table shows that heave can't develop for sand (20 %), Clay (15 & 30 %), and Peat (80 & 120 %)

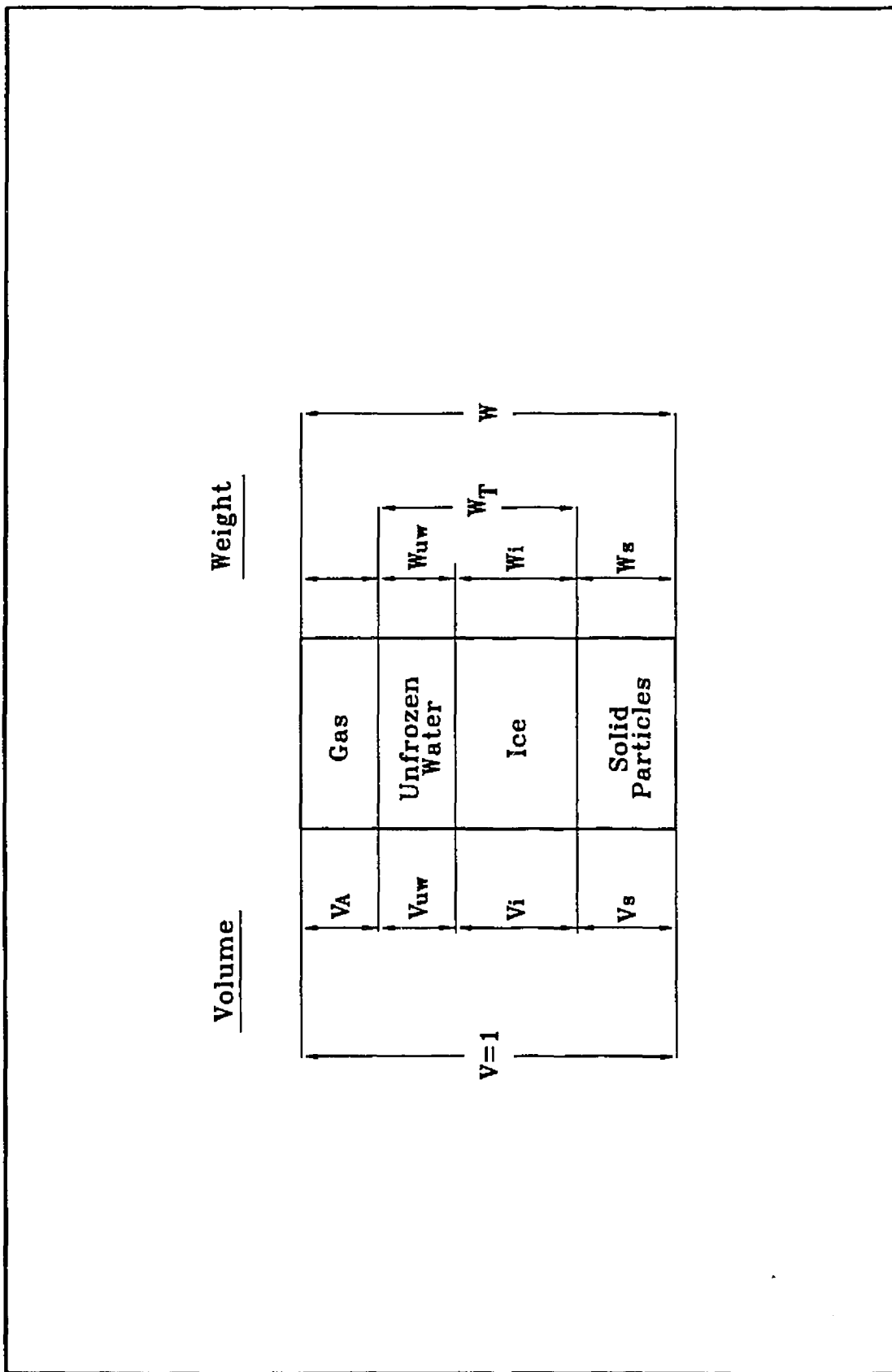


FIG. 2.1 Constitution of Frozen Soil

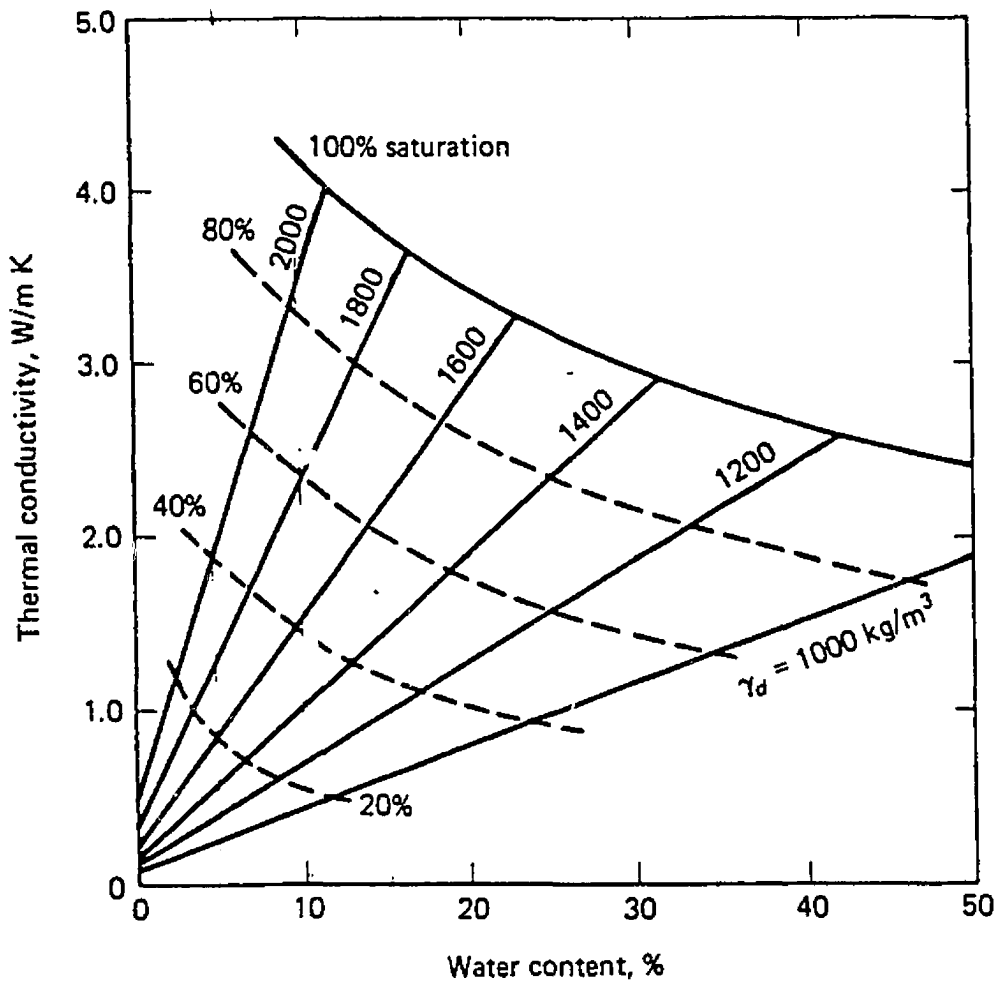


Fig 2.2 Average Thermal Conductivity for Sand as a Function of Water Content and Bulk Dry Density. **FROZEN.** (After Kersten, 1949)

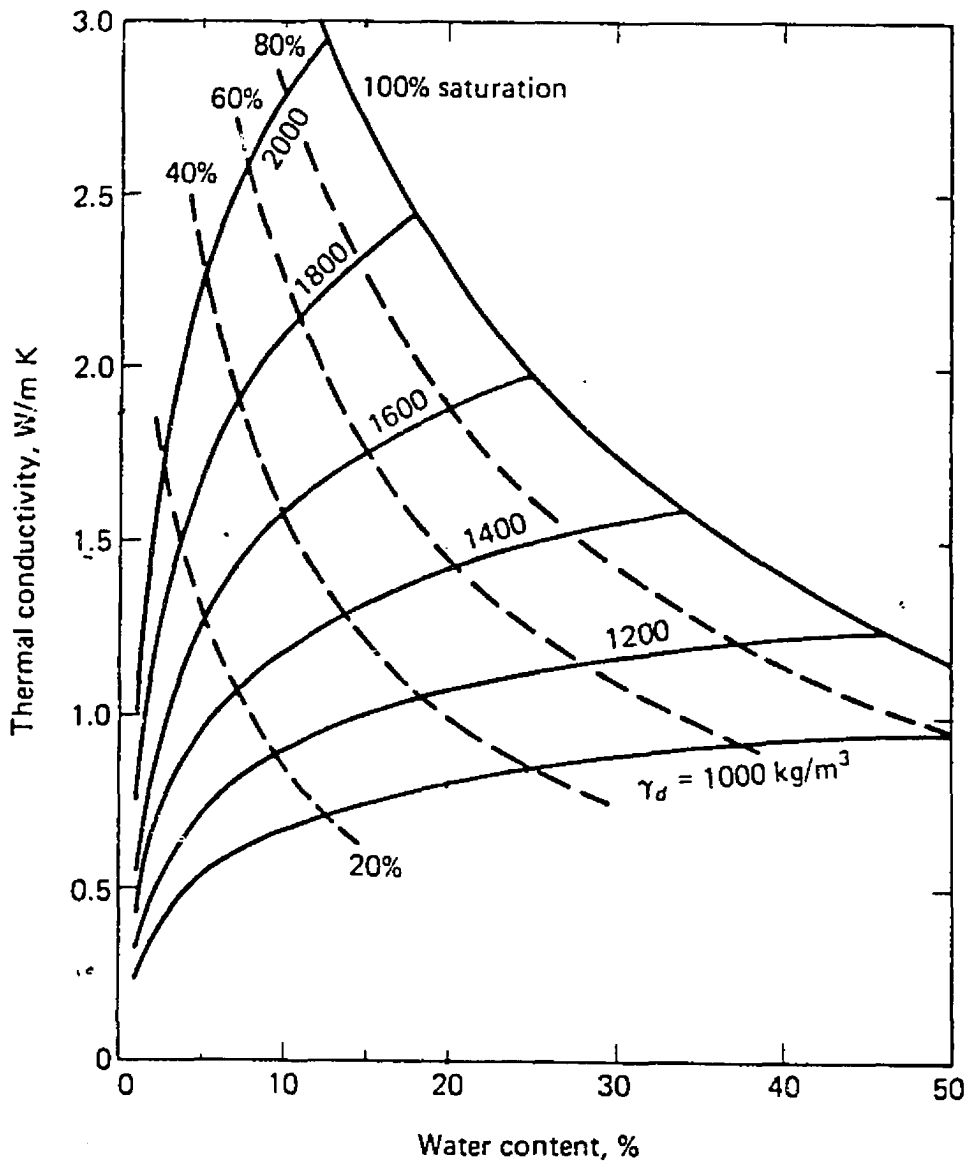


Fig 2.3 Average Thermal Conductivity for Sand as a Function of Water Content and Bulk Dry Density. UNFROZEN. (After Kersten, 1949)

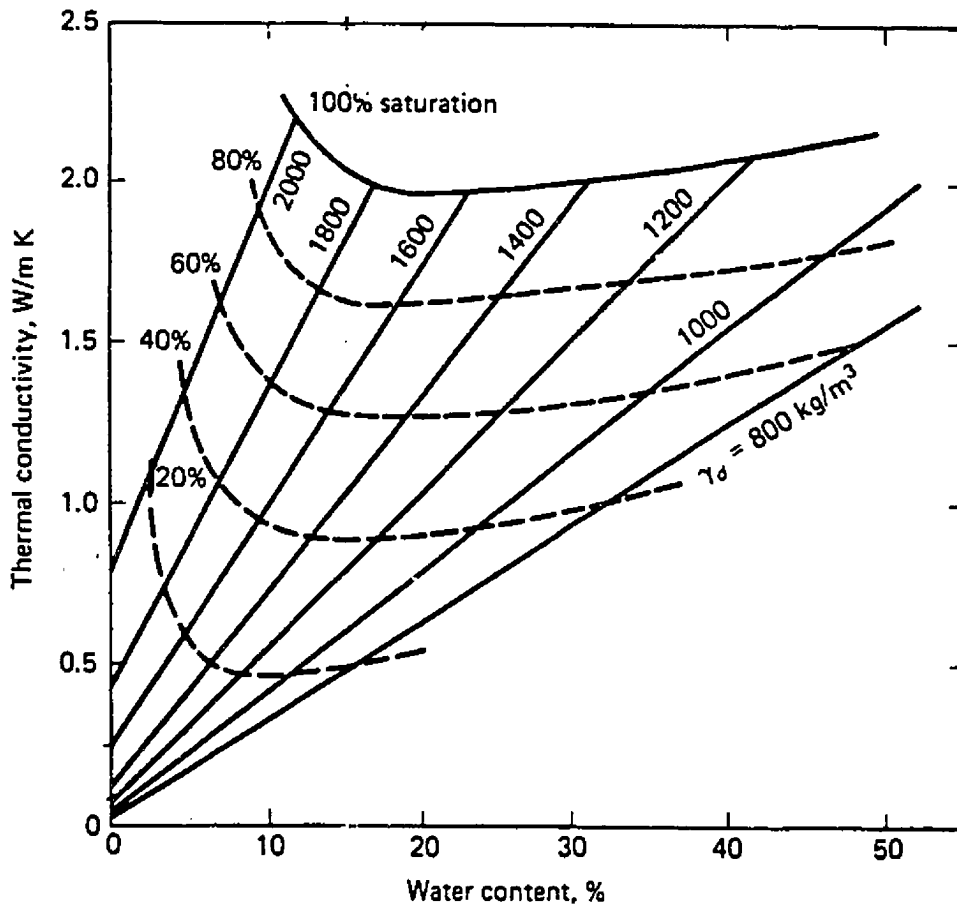


Fig 2.4 Average Thermal Conductivity for Clay as a Function of Water Content and Bulk Dry Density. *FROZEN.* (After Kersten, 1949)

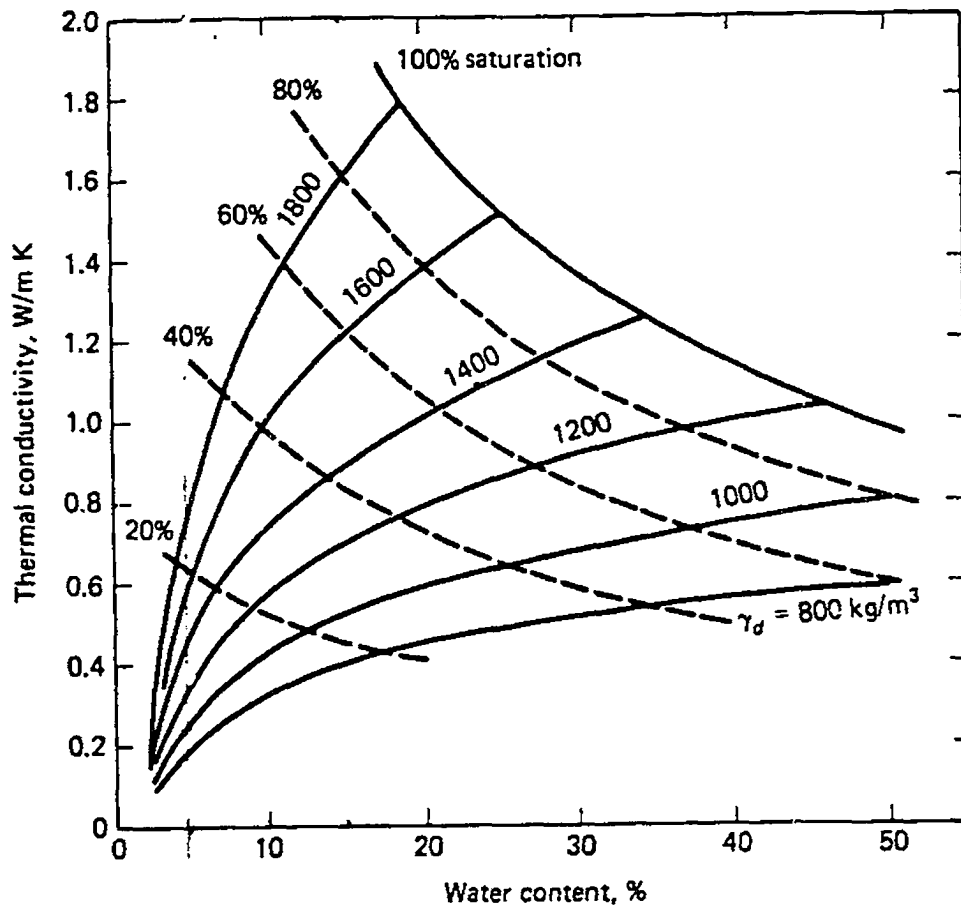


Fig 2.5 Average Thermal Conductivity for Clay as a Function of Water Content and Bulk Dry Density. UNFROZEN. (After Kersten, 1949)

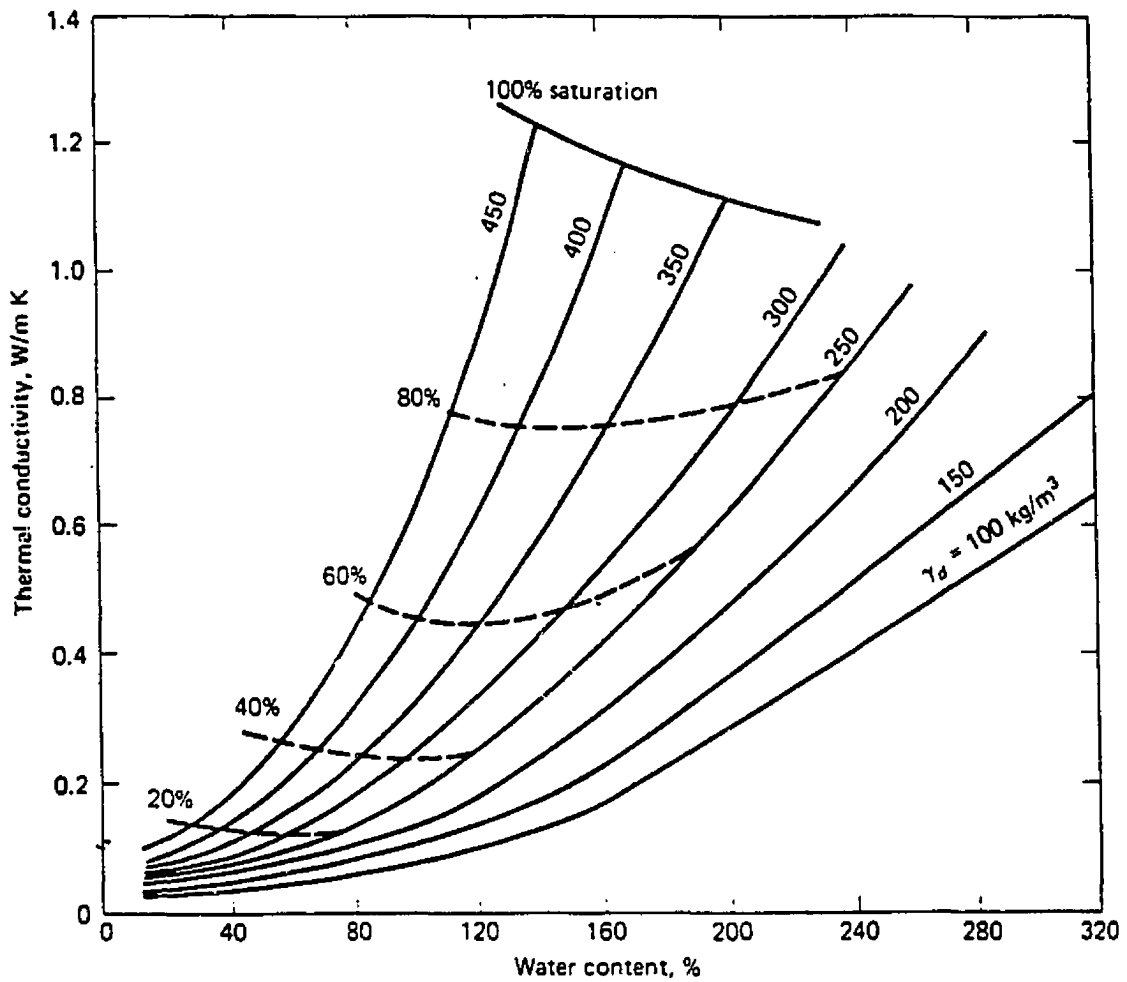


Fig 2.6 Average Thermal Conductivity for Peat as a Function of Water Content and Bulk Dry Density. FROZEN. (After Kersten, 1949)

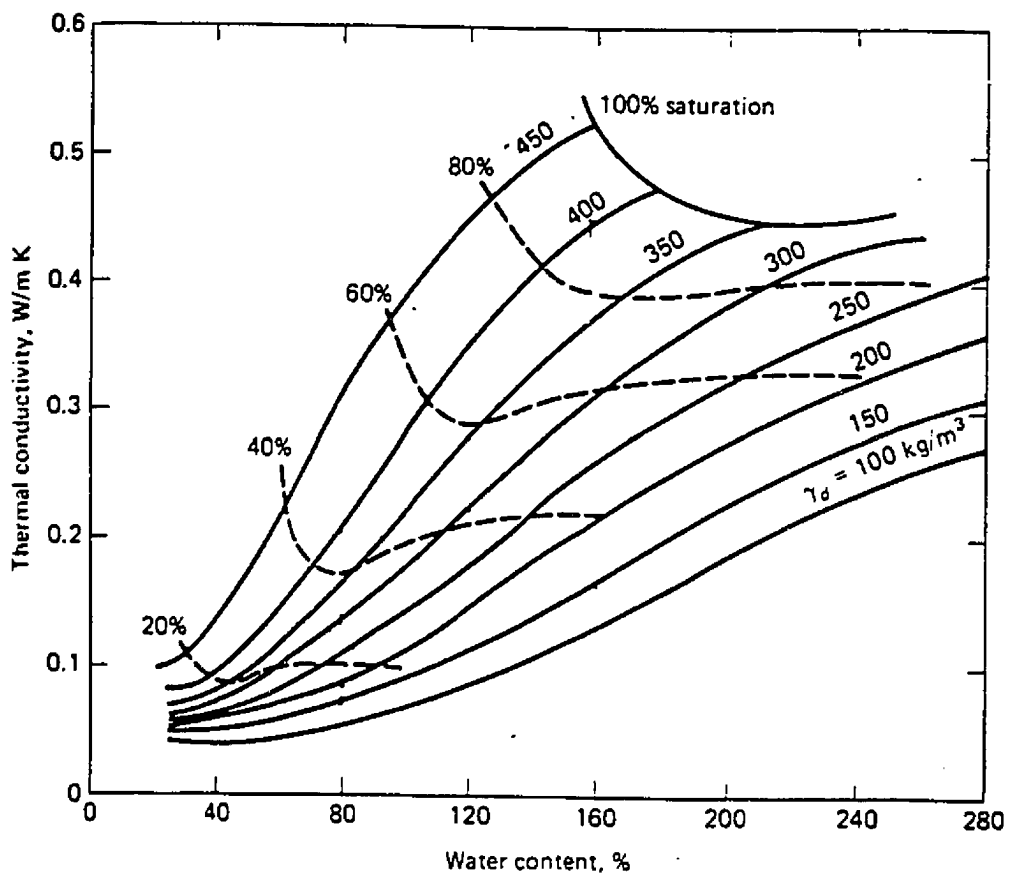


Fig 2.7 Average Thermal Conductivity for Peat as a Function of Water Content and Bulk Dry Density. UNFROZEN. (After Kersten, 1949)

Enthalpy Function of Temperature Material Without Phase Change

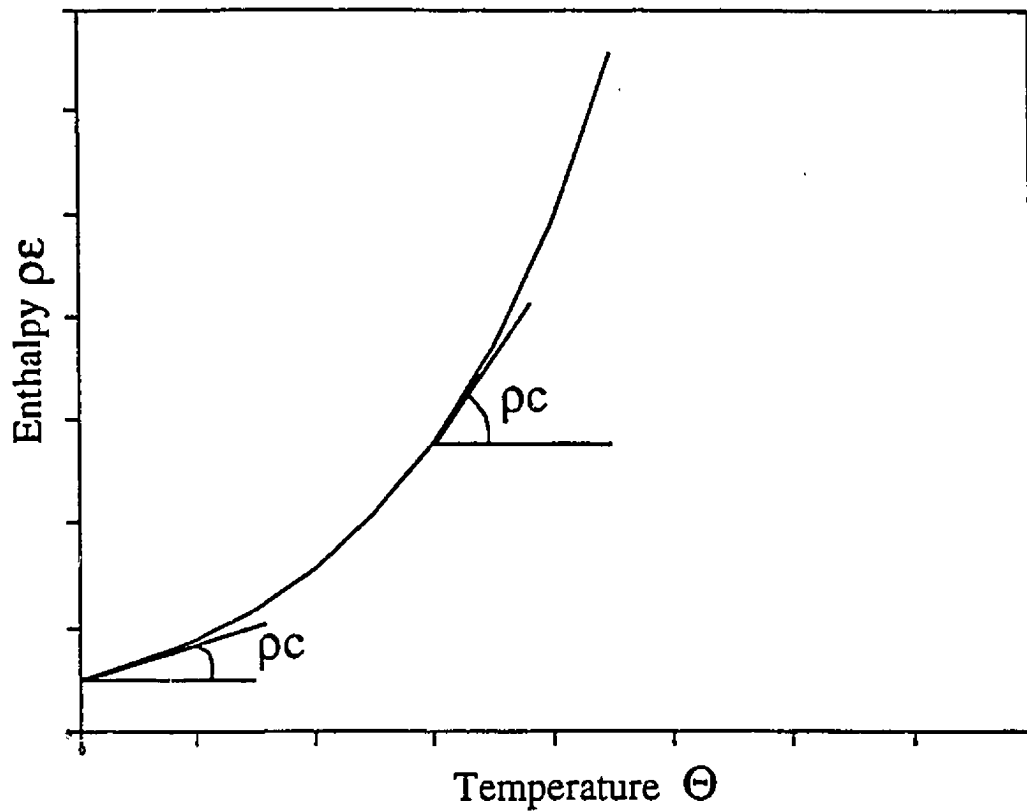


Fig. 2.8 Enthalpy versus Temperature for Continuum Medium

Enthalpy For Melting Procedure Medium With Phase Change

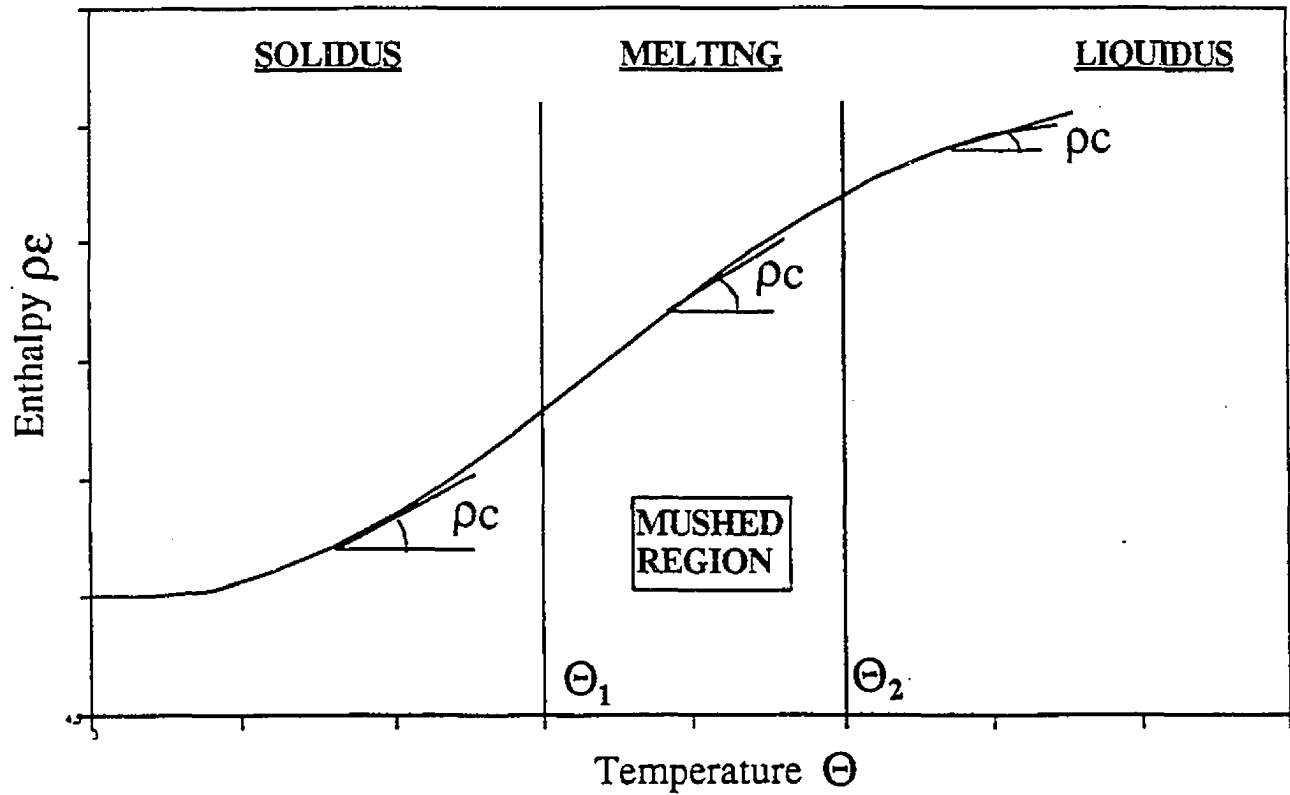


Fig. 2.9 Enthalpy for Melting Procedure of a Medium with Phase Change

Enthalpy For Melting Procedure Medium With Phase Change

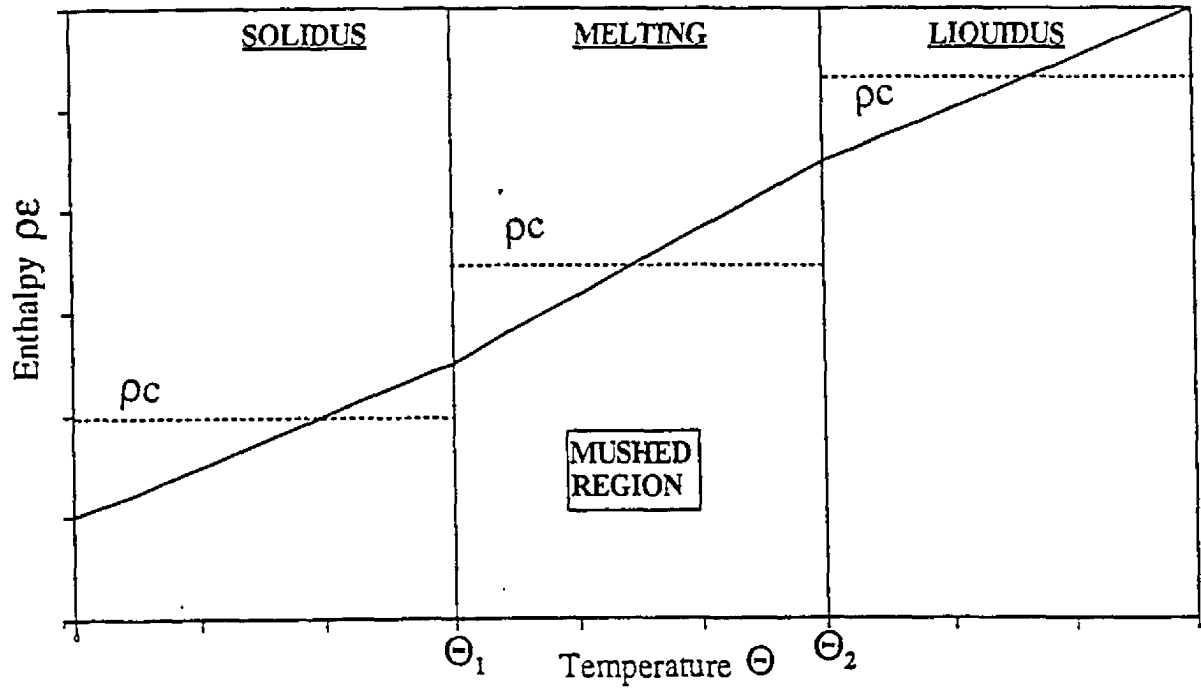


Fig. 2.10 Enthalpy for Melting Procedure of a Medium with Phase Change
Straight Line Approximation

Uniform Frozen Soil Subjected to Step Increase in Temperature

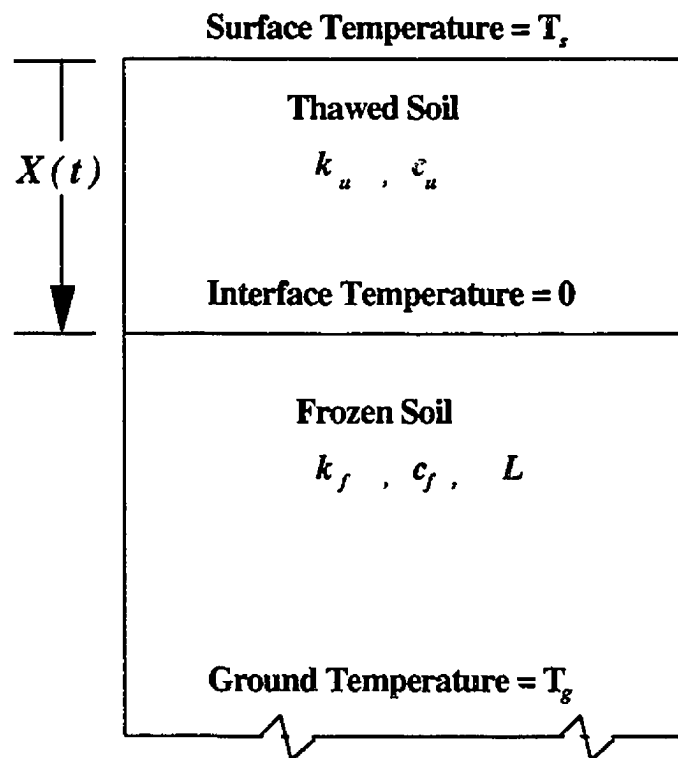


Fig. 2.11 The Neumann Problem. (After Nixon and Mc Roberts, 1973)

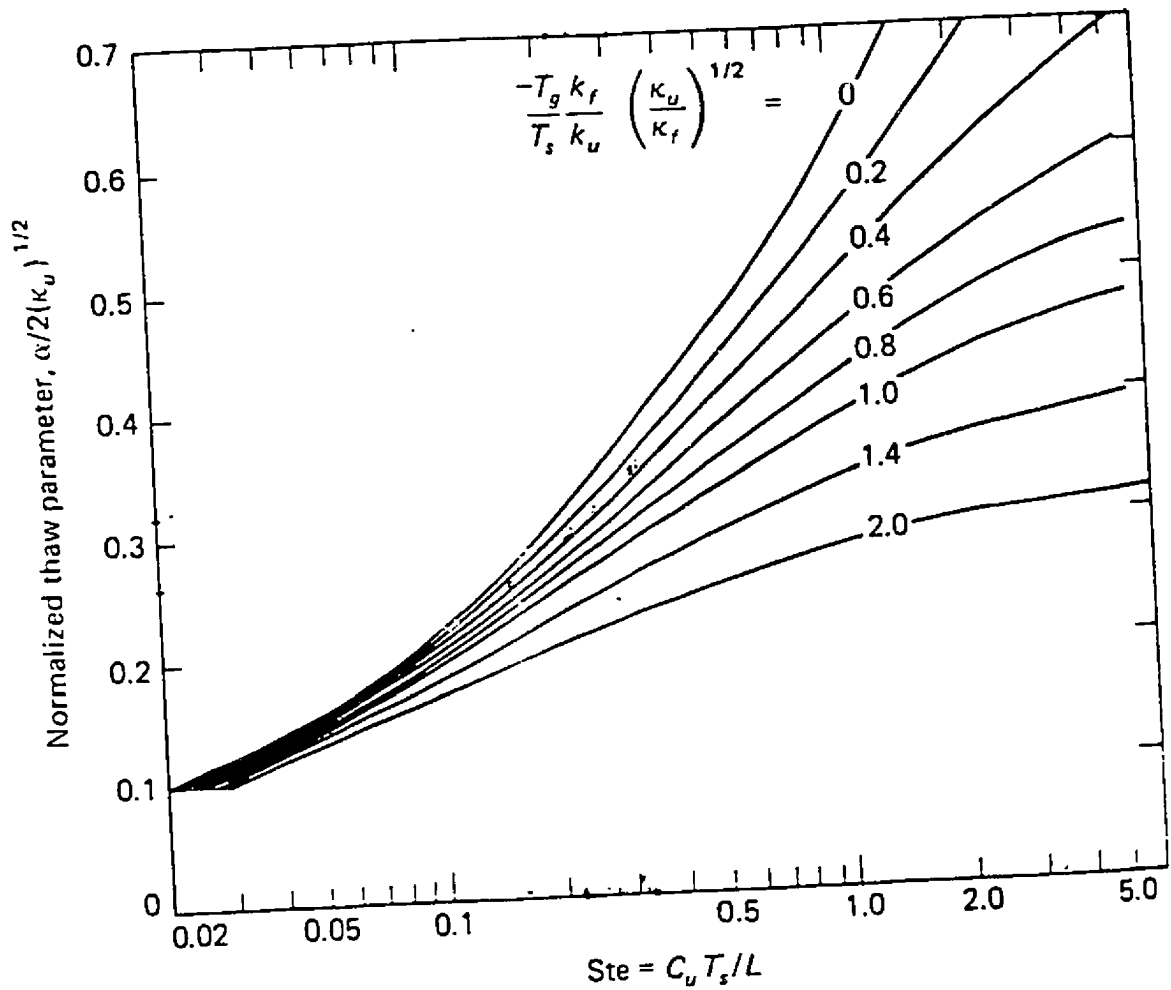


Fig 2.12 Graphical Solution of the Neumann Equation. (After Nixon and Mc Roberts, 1973)

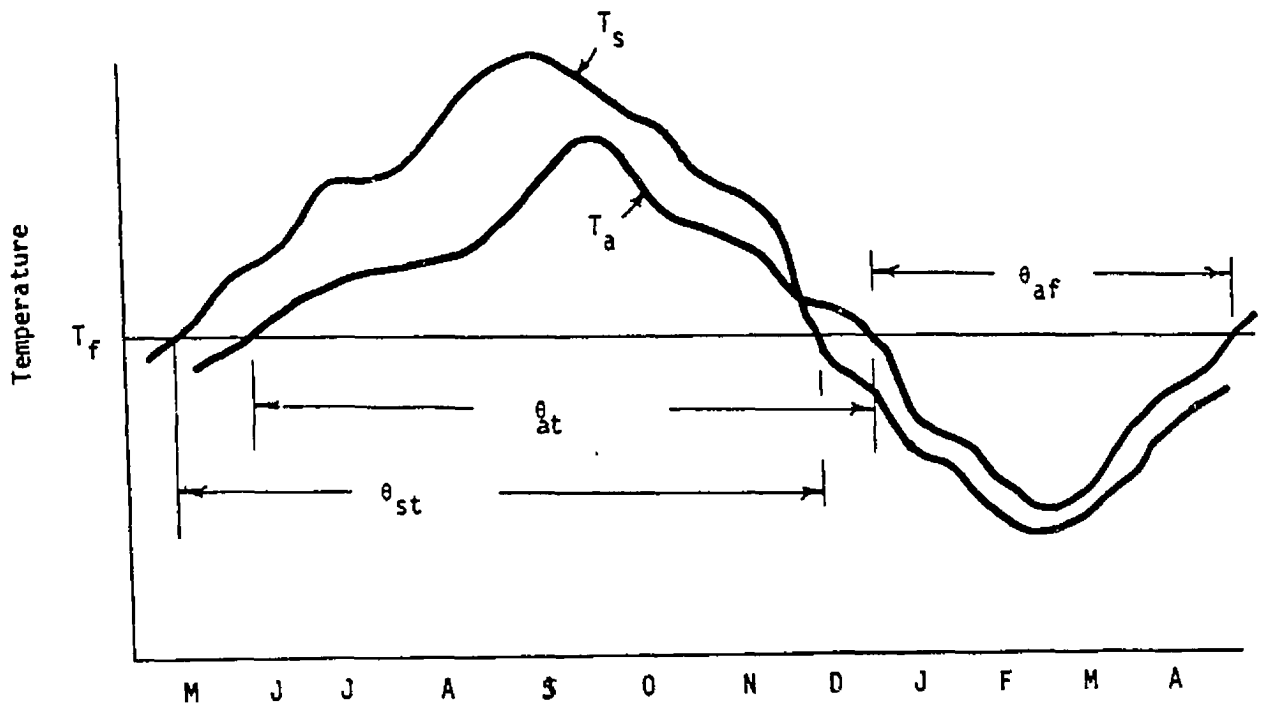


Fig 2.13 Phase Change Seasons for Air and Surface Temperatures. (After Lunardini , 1981)

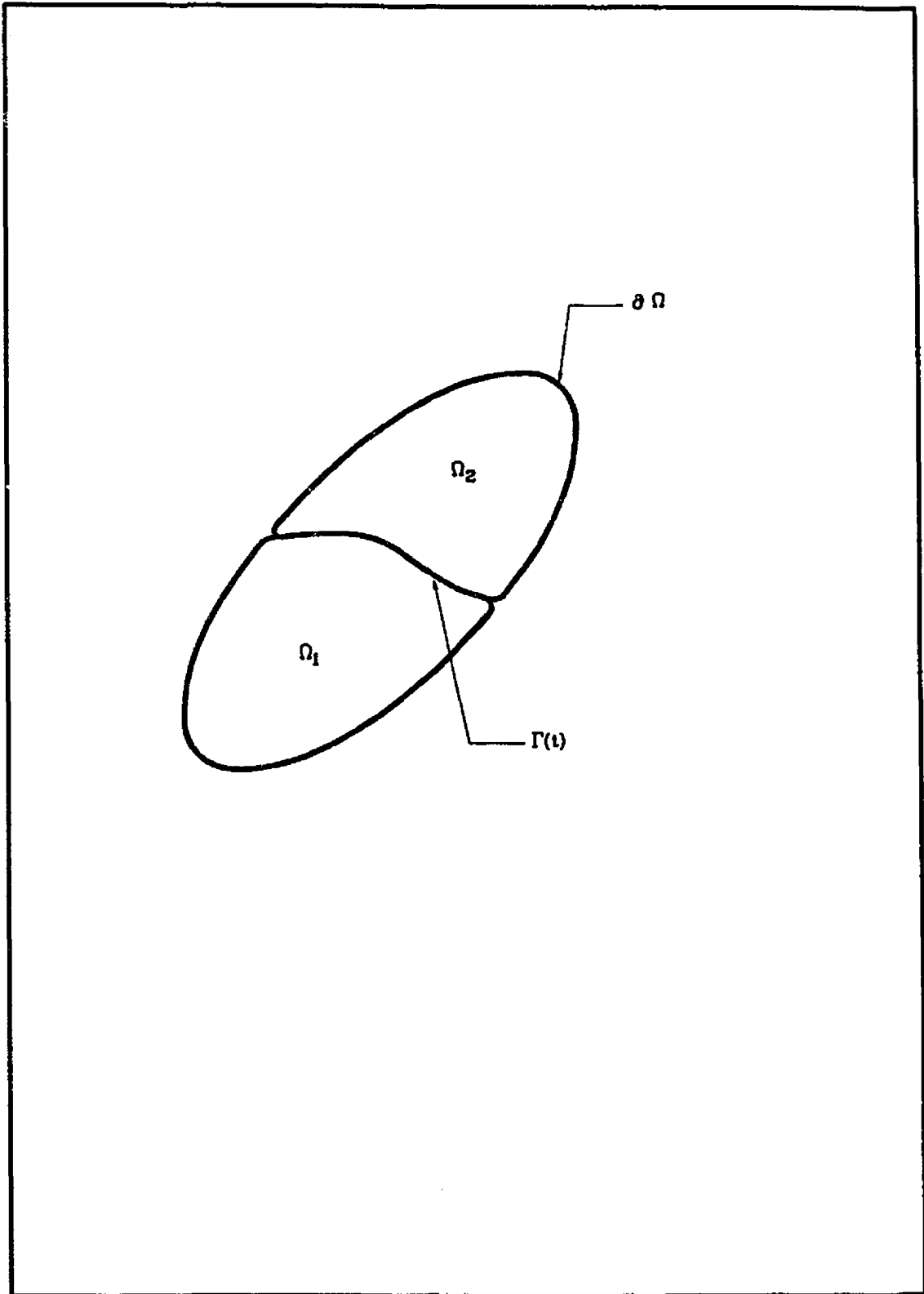


Fig. 3.1 Control Volume with Moving Interface Boundary

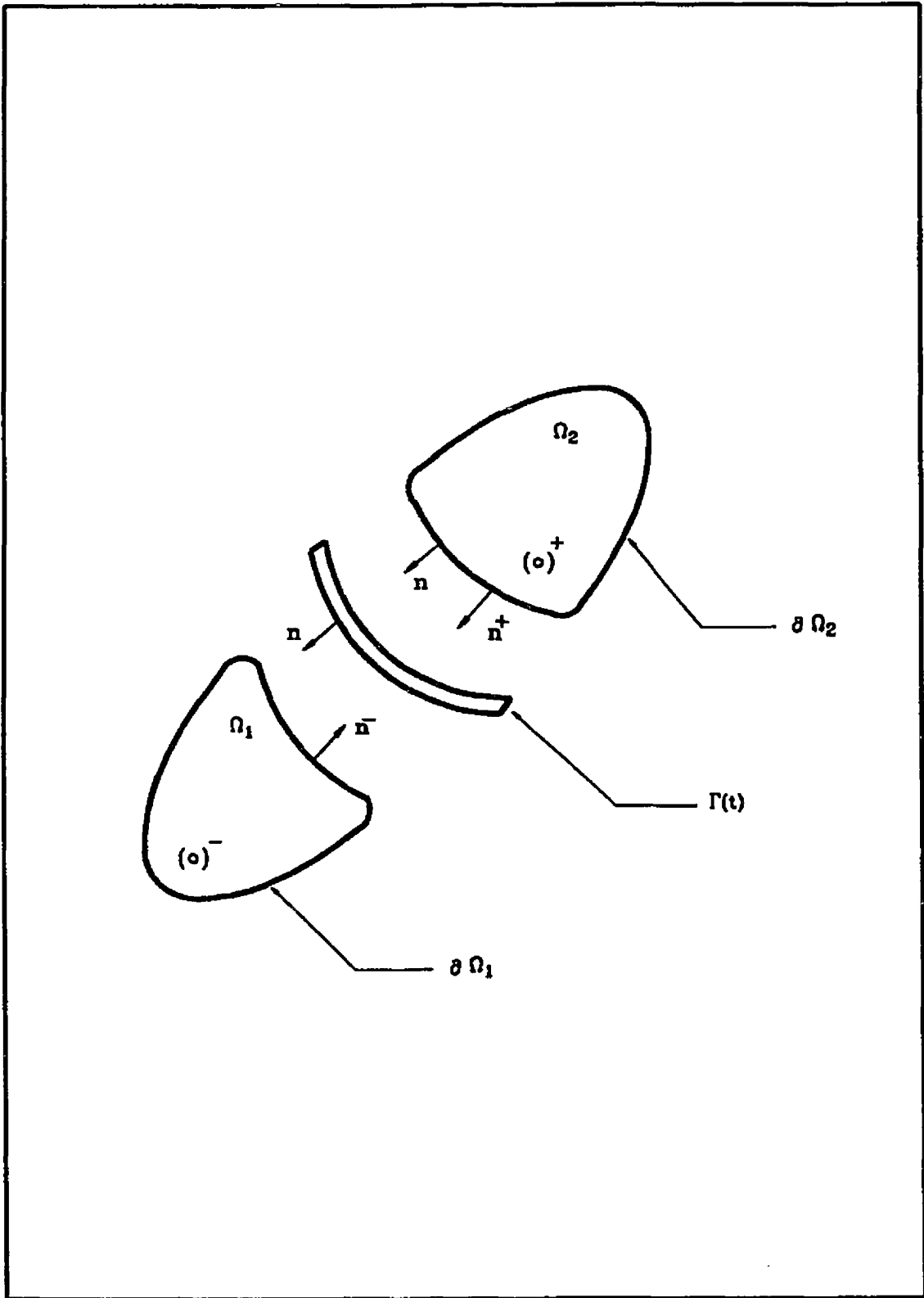


Fig. 3.2 Discontinuity Surface (after Eringen, 1967)

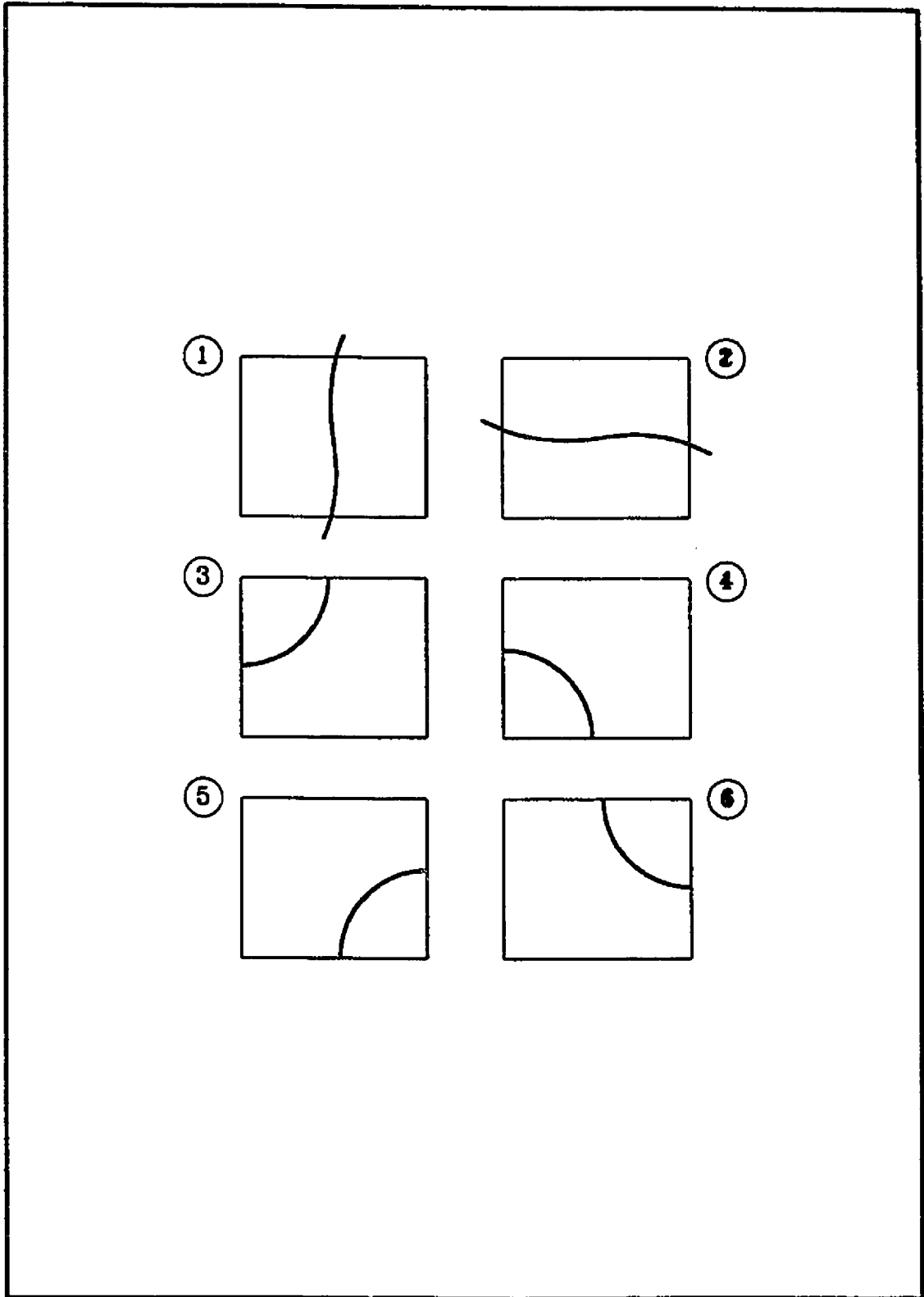
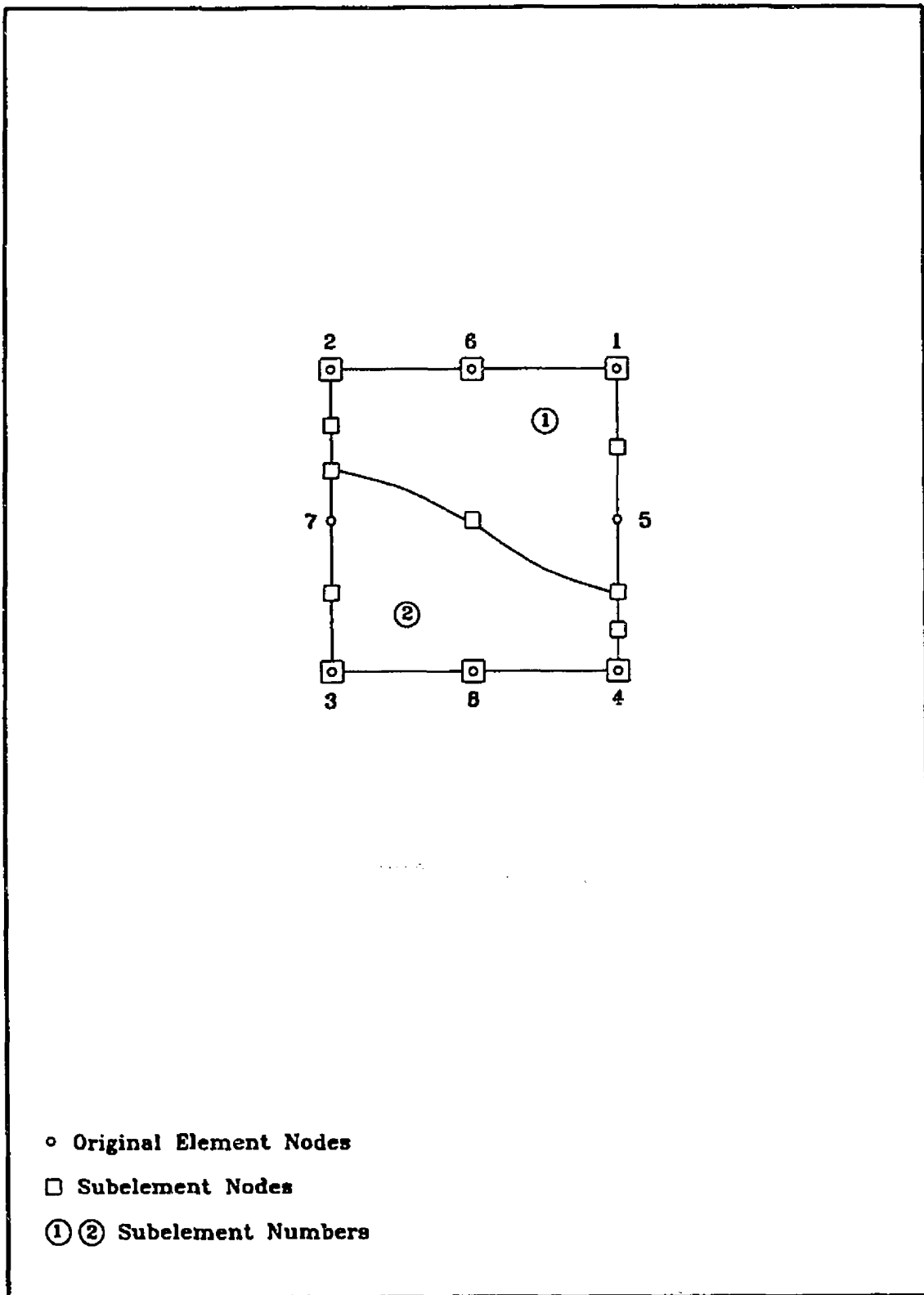


Fig. 3.3 Types of Intersection of the Interface Layer



- Original Element Nodes
- Subelement Nodes
- ① ② Subelement Numbers

Fig. 3.4 a First Group of Intersection for the Interface Position in the Finite Element

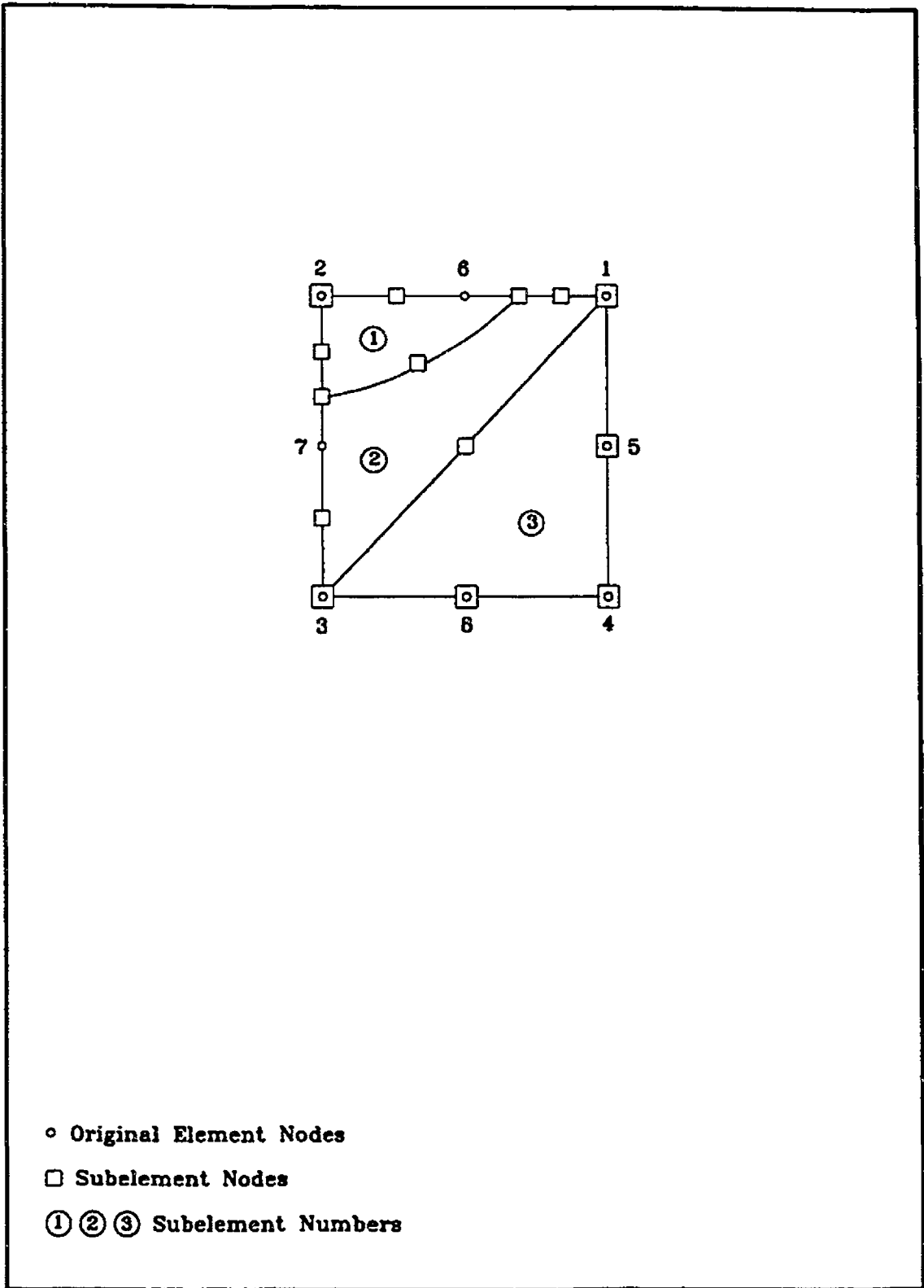


Fig. 3.4 b Second Group of Intersections for the Interface Position in the Finite Element

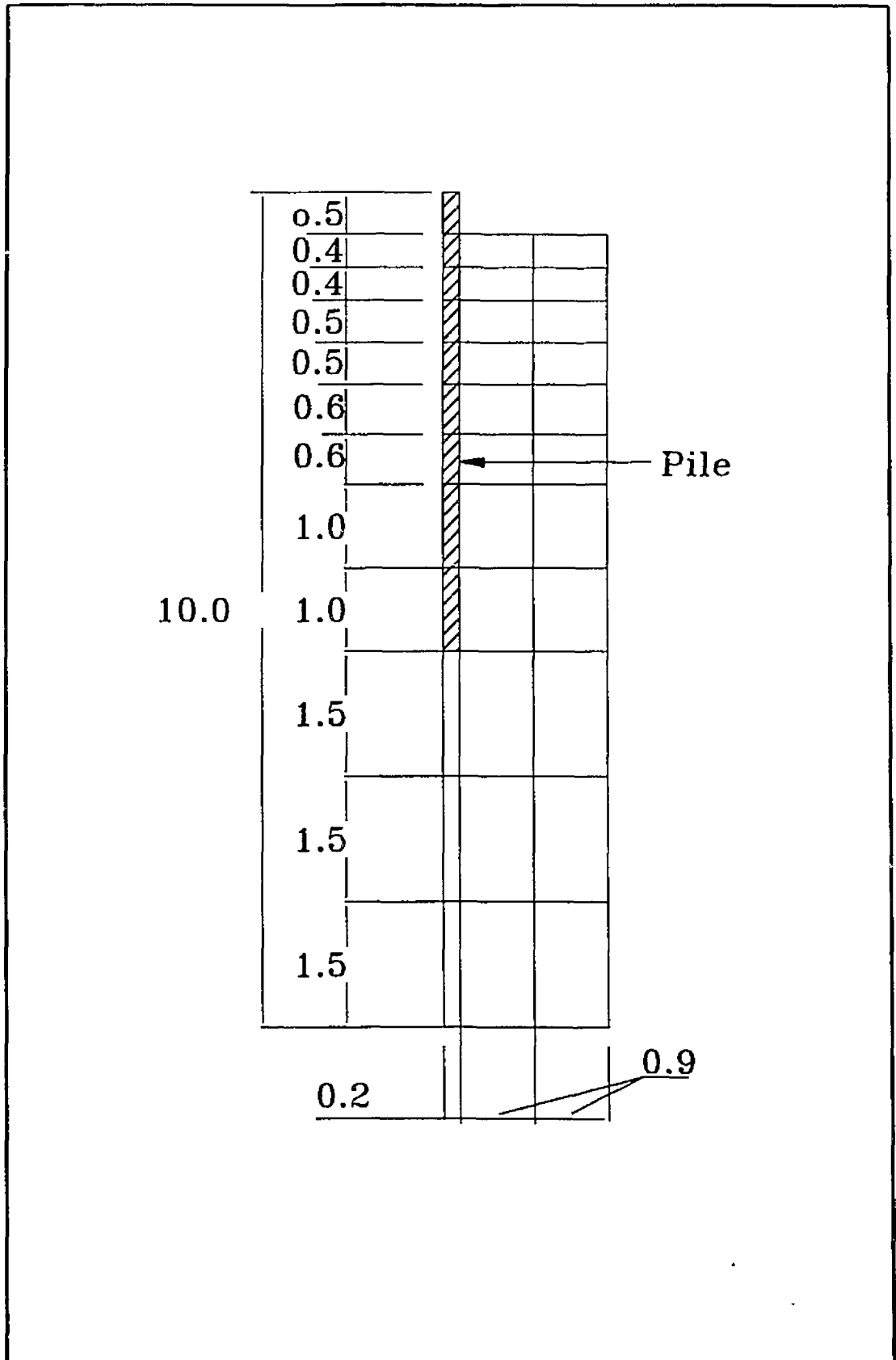


Fig. 4.1a Geometry of Mesh # 1

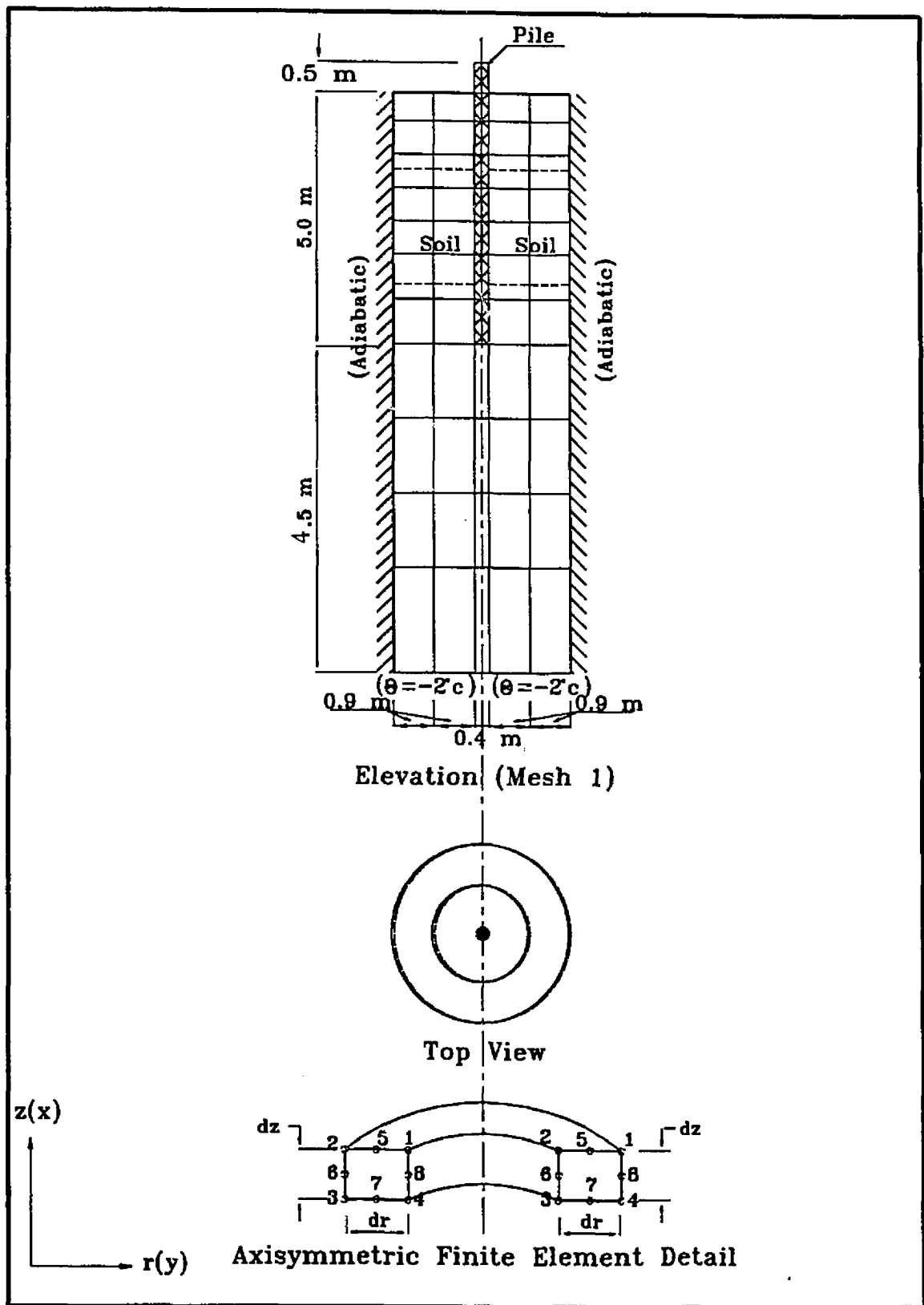


Fig. 4.1b Idealization of the Axisymmetrical Finite Elements for Mesh # 1

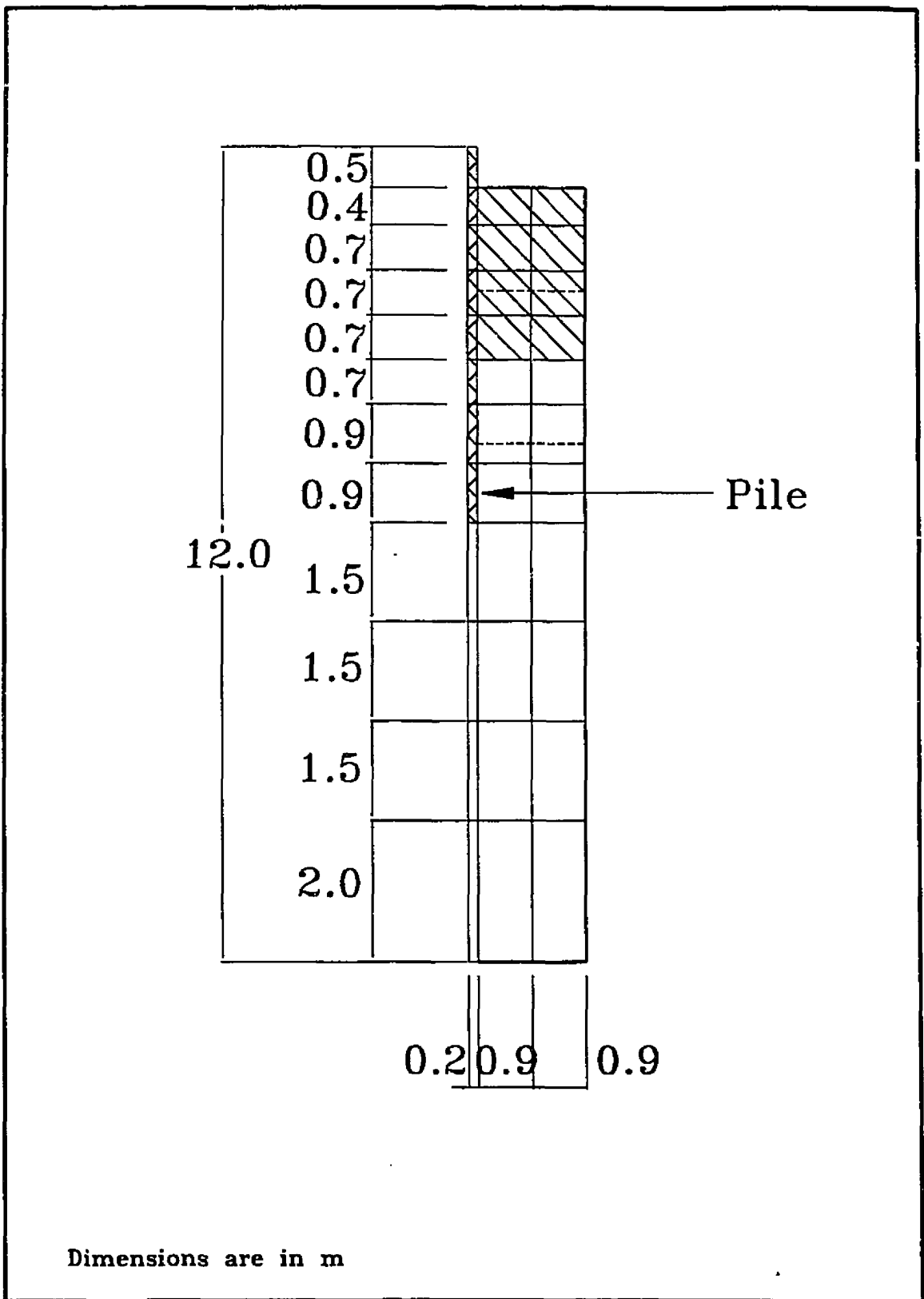


Fig. 4.2a Geometry of Mesh # 2

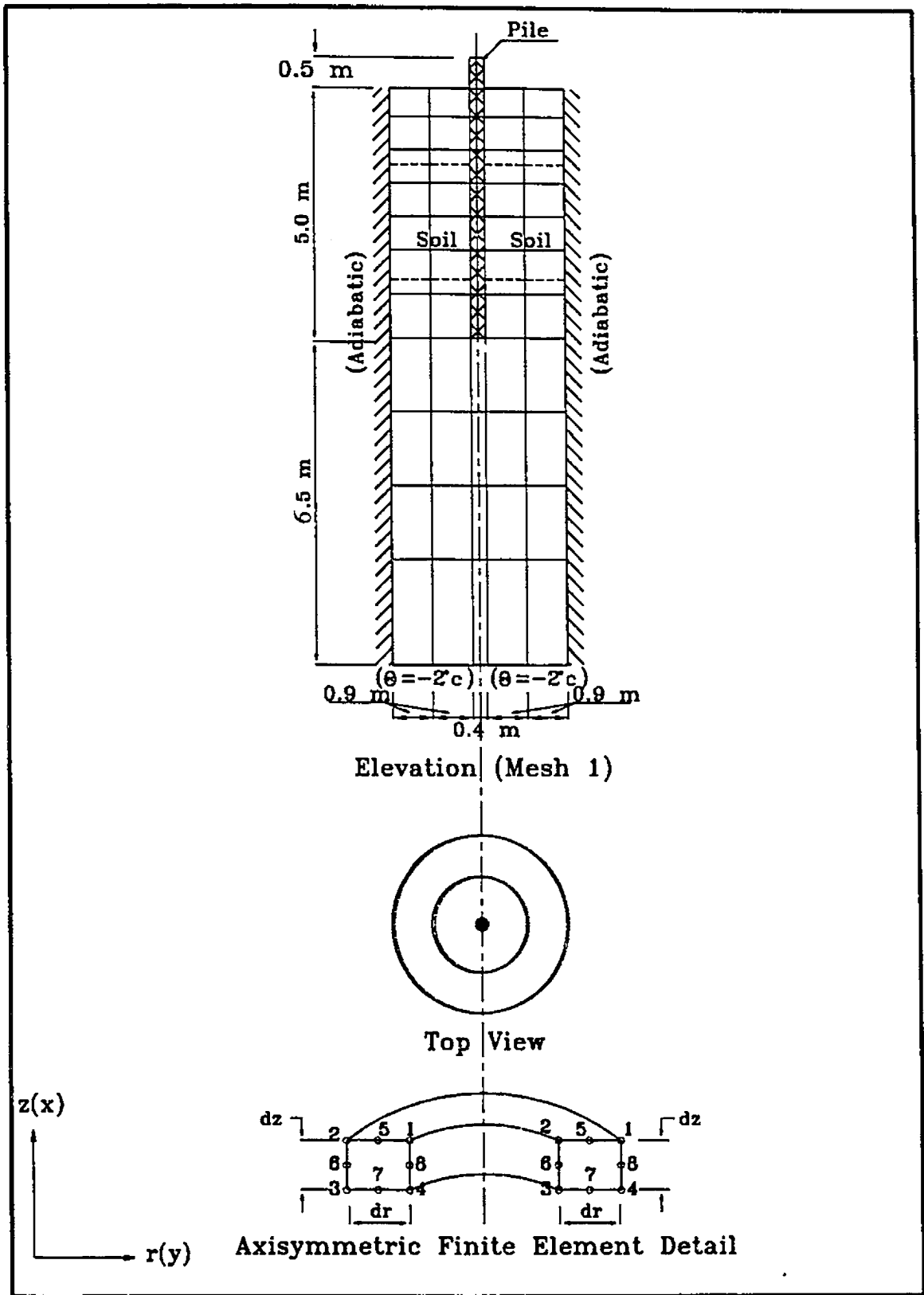


Fig. 4.2b Idealization of the Axisymmetrical Finite Elements for Mesh # 2

Mean Air Temperature Distribution

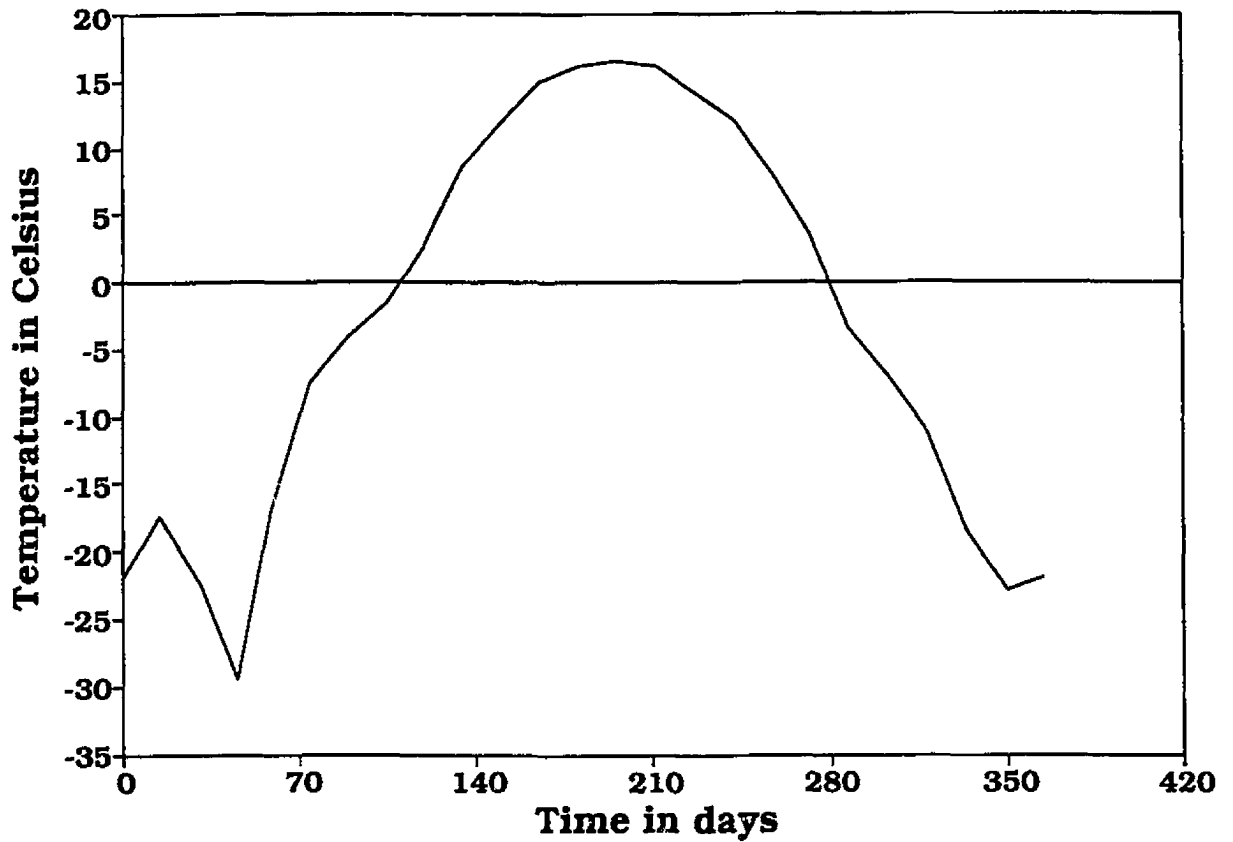


Fig. 4.3 Temperature Distribution at the Boundary of the soil for a period of one year (Based on the data by Jumikis for 1950)

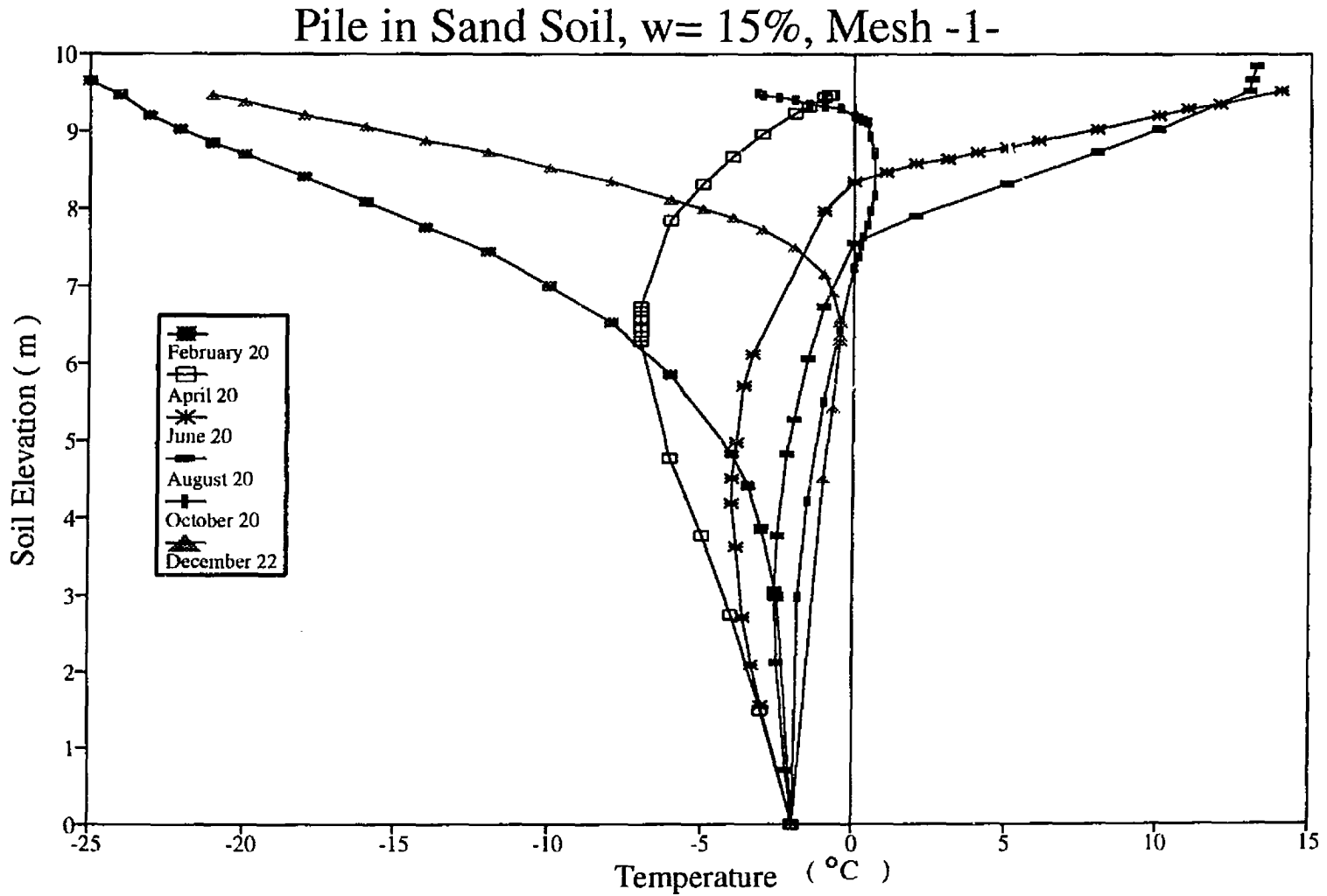


Fig. 4.4 Temperature Fields Distribution Around Pile Foundation in Sand with Water Content, $w = 15\%$

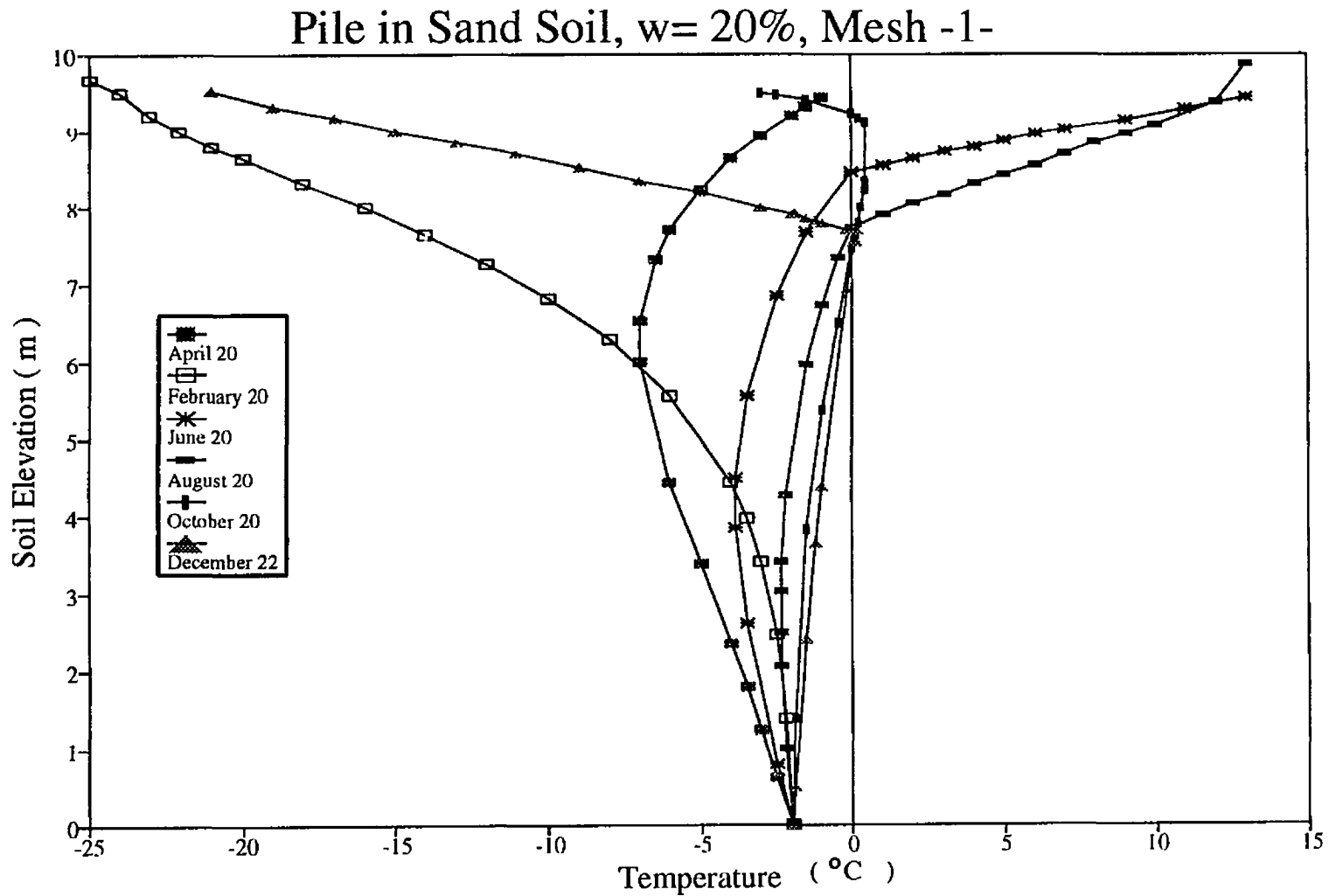


Fig. 4.5 Temperature Fields Distribution Around Pile Foundation in Sand with Water Content, $w = 20\%$

Pile in Sand Soil, $w = 15\%$, Mesh -1-zero Isotherm around the pile

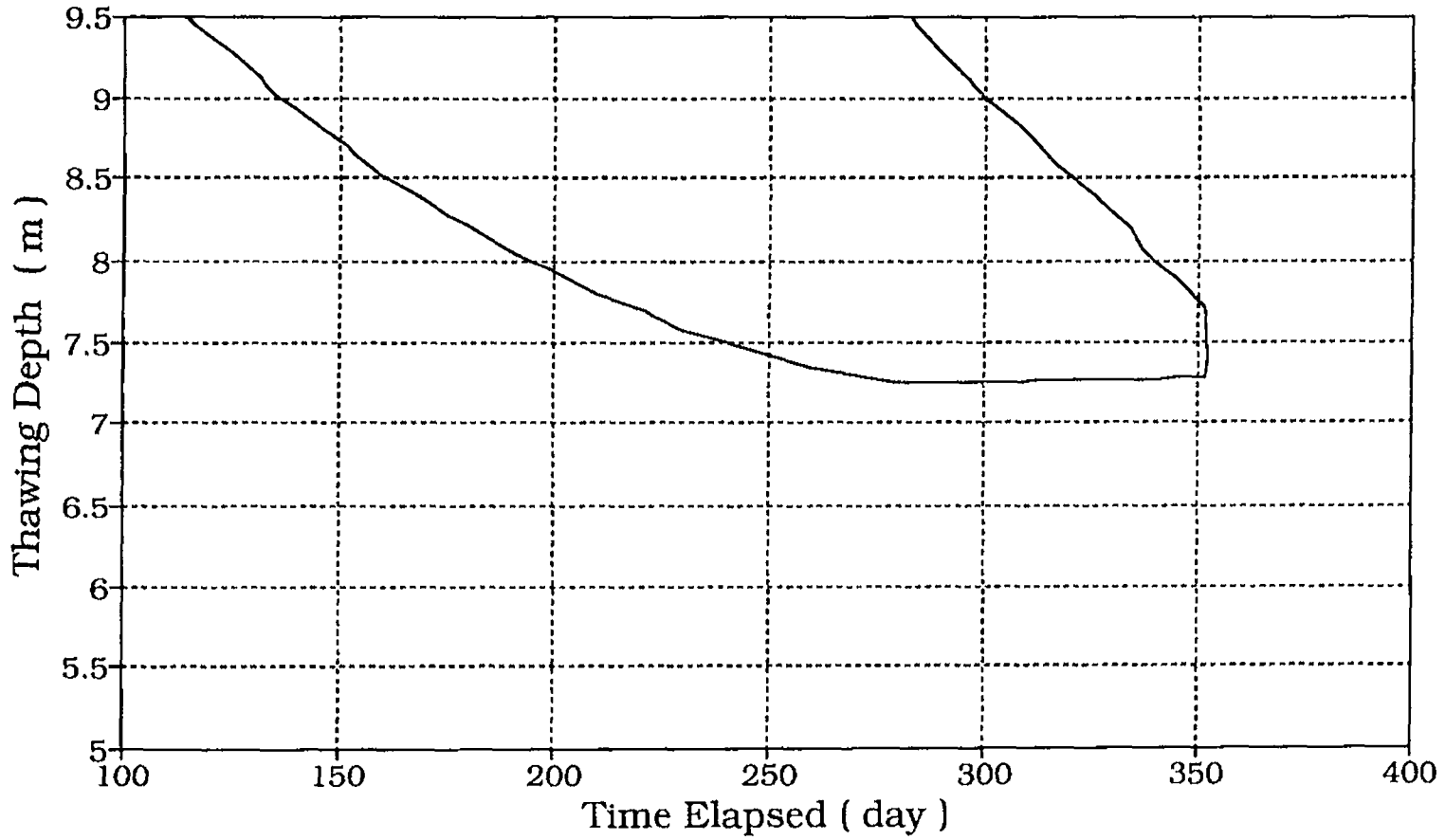


Fig. 4.6 Zero Isotherm Propagation Around Pile in Sand with water content, $w = 15\%$

Pile in Sand Soil, $w = 20\%$, Mesh - 1-zero Isotherm around the pile

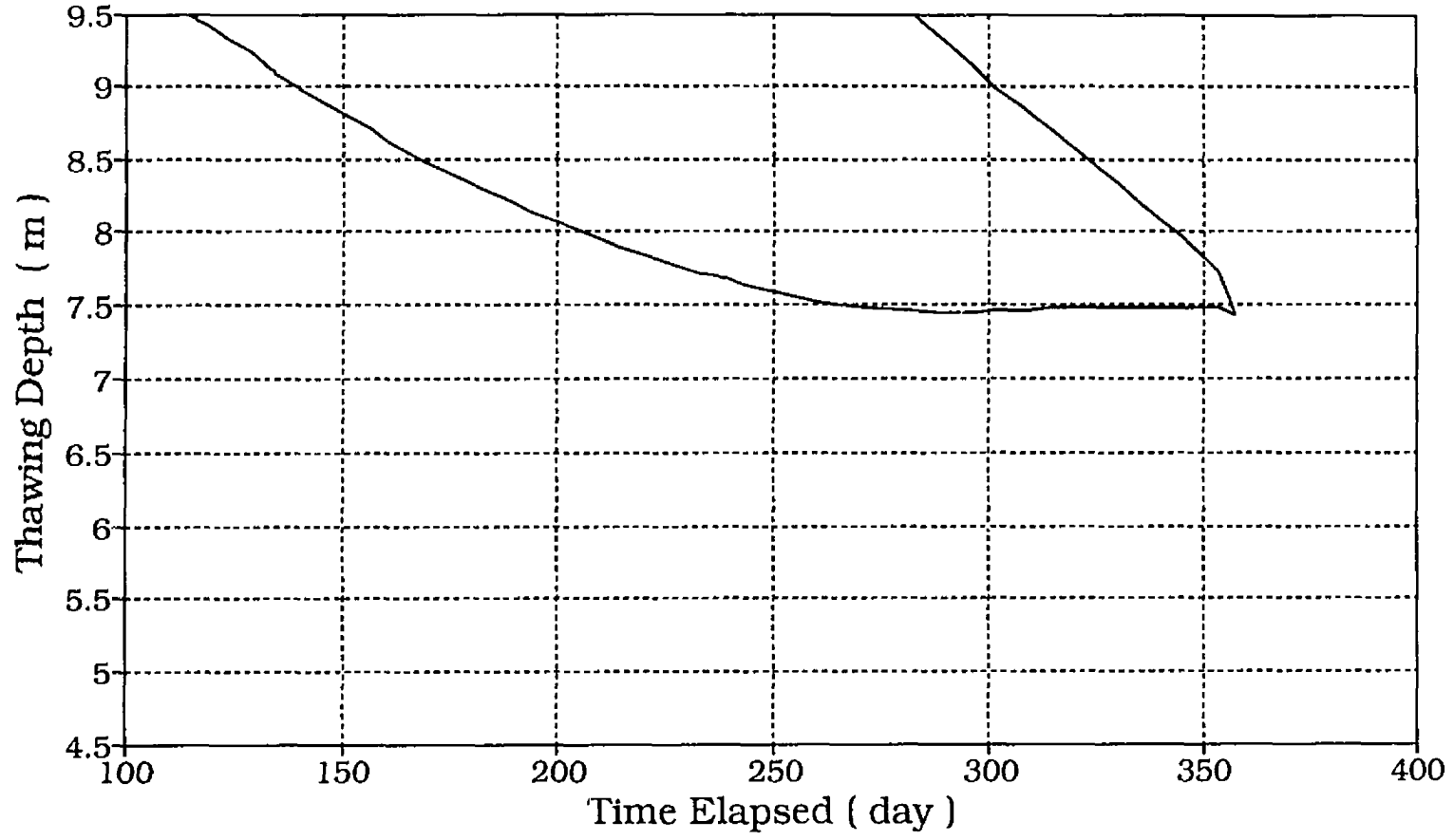


Fig. 4.7 Zero Isotherm Propagation Around Pile in Sand with water content, $w = 20\%$

Pile in Sand Soil, $w = 15\%$ - Mesh 1-
Isotherms Plot: -2, -1, +1, +2

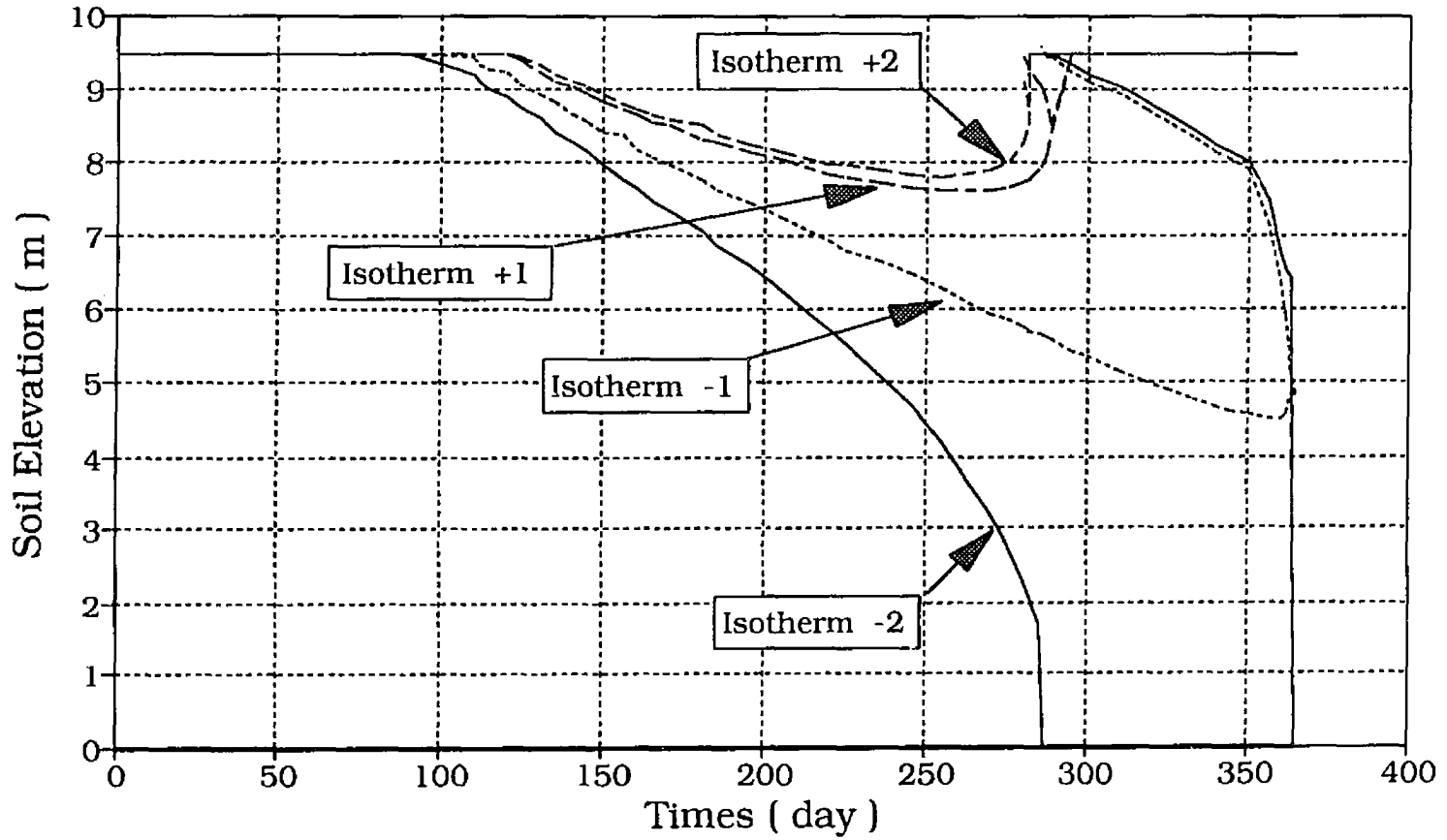


Fig. 4.8 Plots of Isotherms : -2, -1, +1, +2 for Sand with water content, $w = 15\%$

Pile in Sand Soil, $w = 20\%$ - Mesh 1- Isotherms Plot: -2, -1, +1, +2

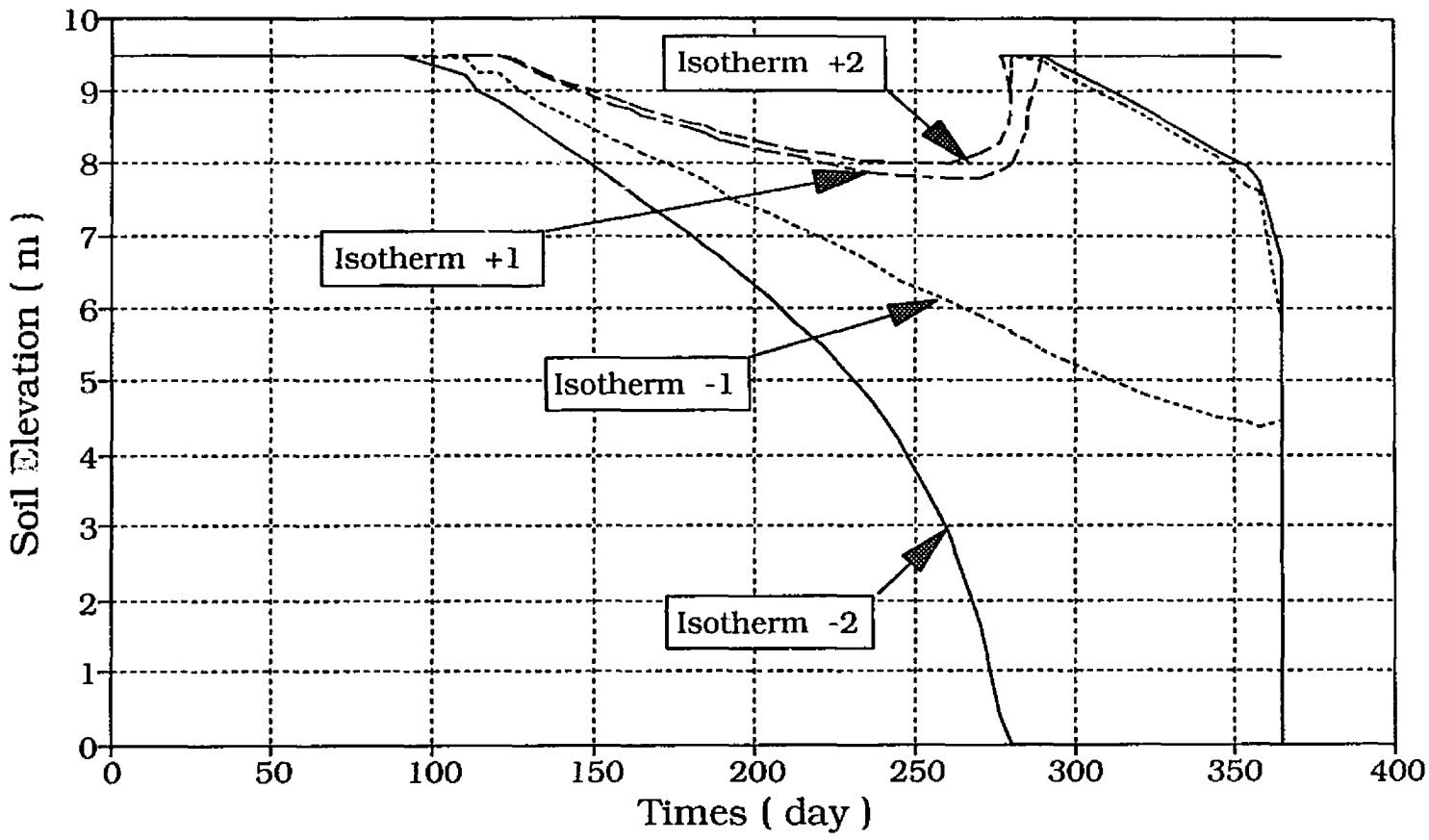


Fig. 4.9 Plots of Isotherms : -2, -1, +1, +2 for Sand with water content, $w = 20\%$

Pile in Sand Soil, $w=15\%$, Mesh -1- Thawing Depth around the Pile

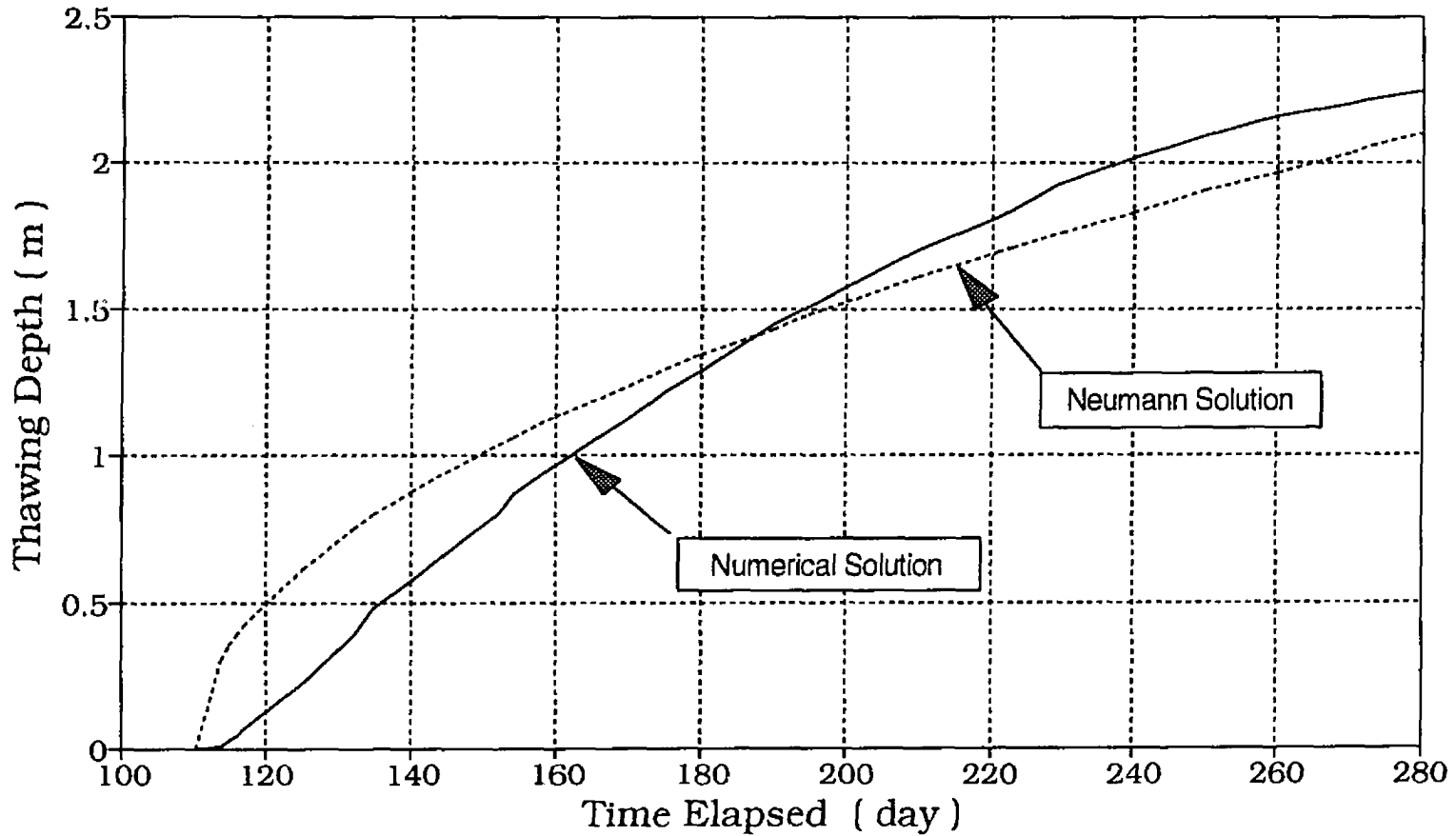


Fig. 4.10 The Comparative Analysis Between the Numerical and Neumann Solutions for Thawing Penetration in Sand with $w = 15\%$

Pile in Sand Soil, $w=15\%$, Mesh -1- Relative error to Neumann Solution

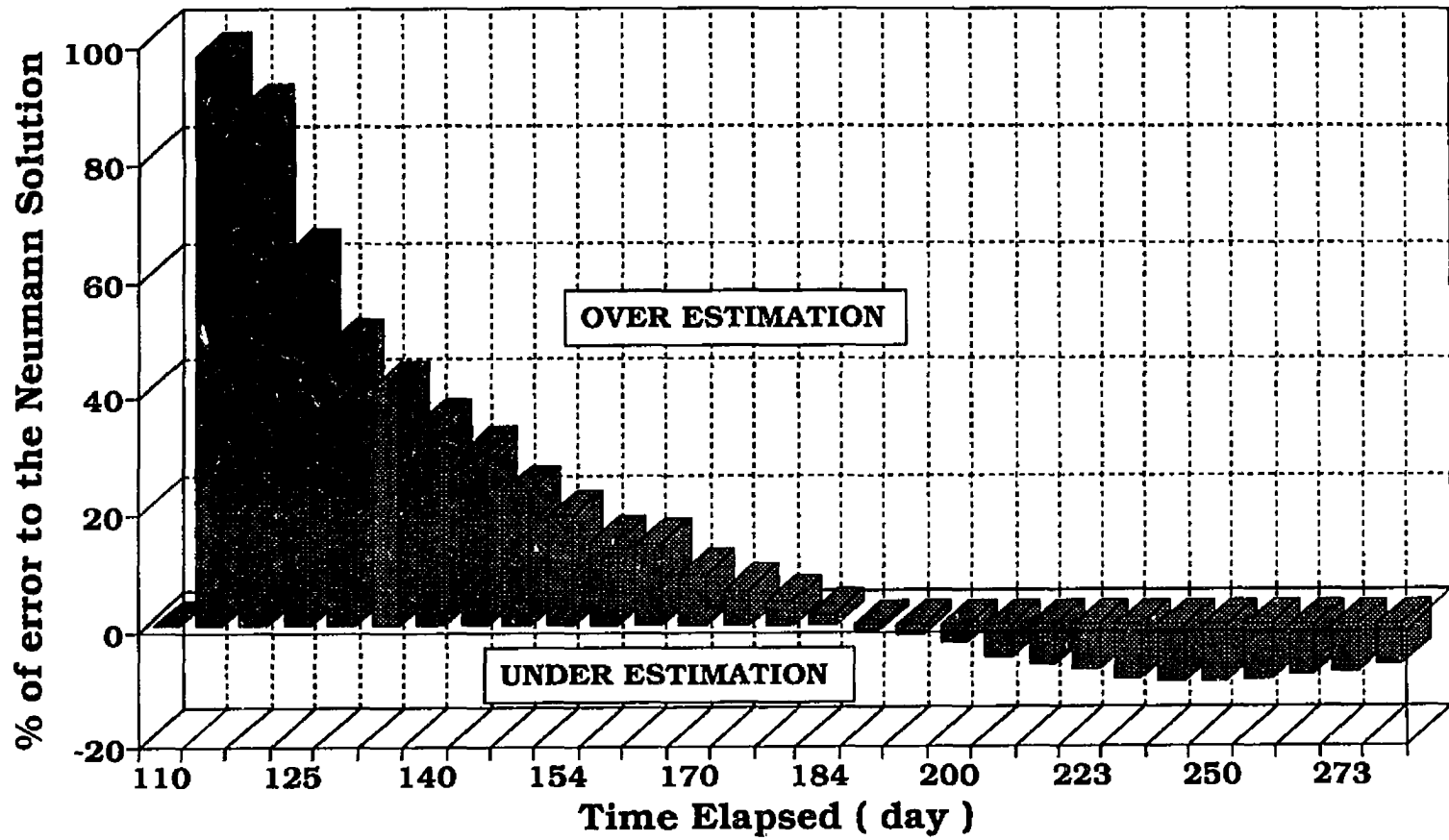


Fig. 4.11 Percentage of Error Between the Numerical and the Neumann Solutions for Sand with $w = 15\%$

Pile in Sand Soil, $w=20\%$, Mesh - 1 - Thawing Depth around the Pile

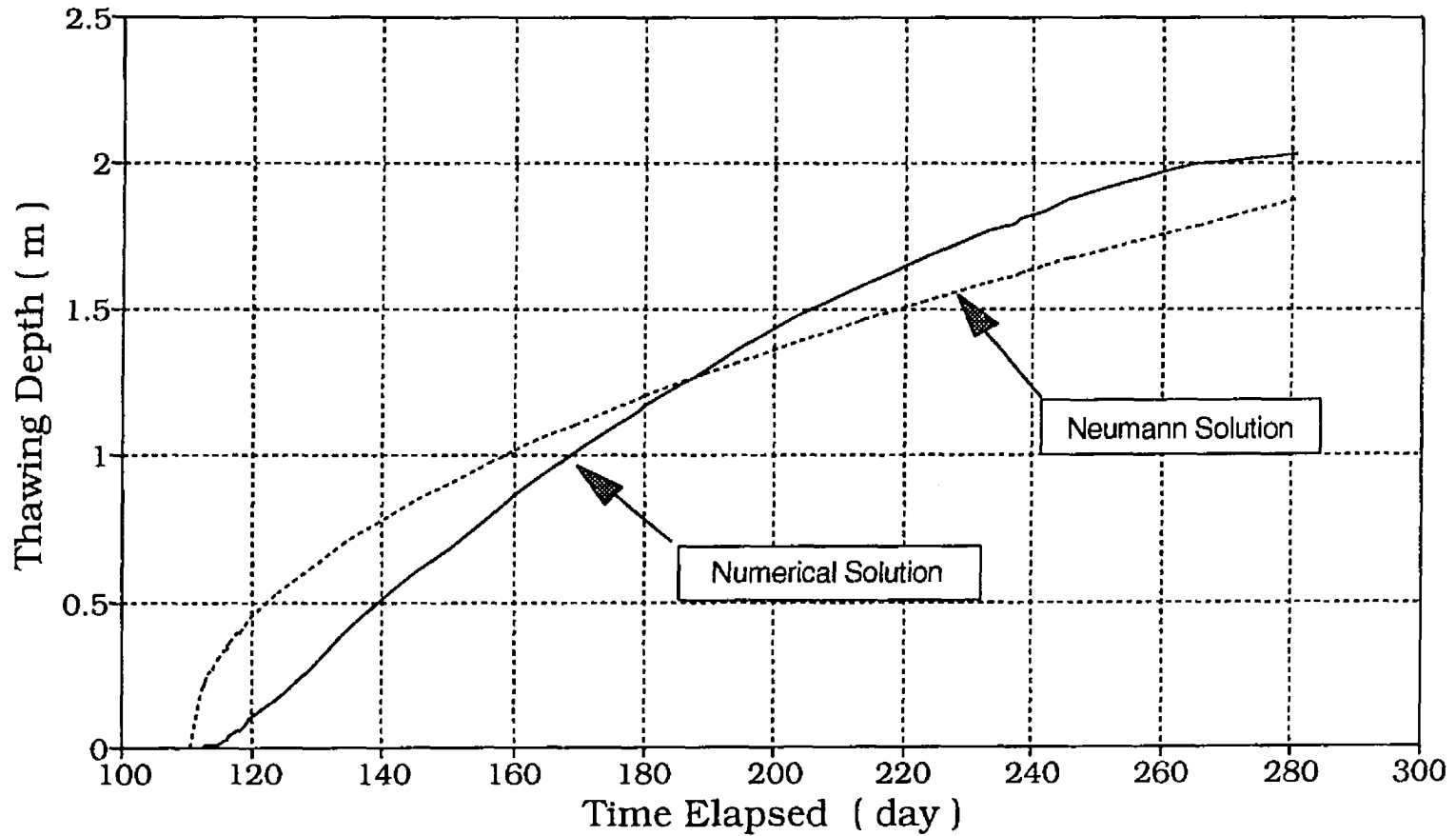


Fig. 4.12 The Comparative Analysis Between the Numerical and Neumann Solutions for Thawing Penetration in Sand with $w = 20 \%$

Pile in Sand Soil, $w=20\%$, Mesh -1- Relative error to Neumann Solution

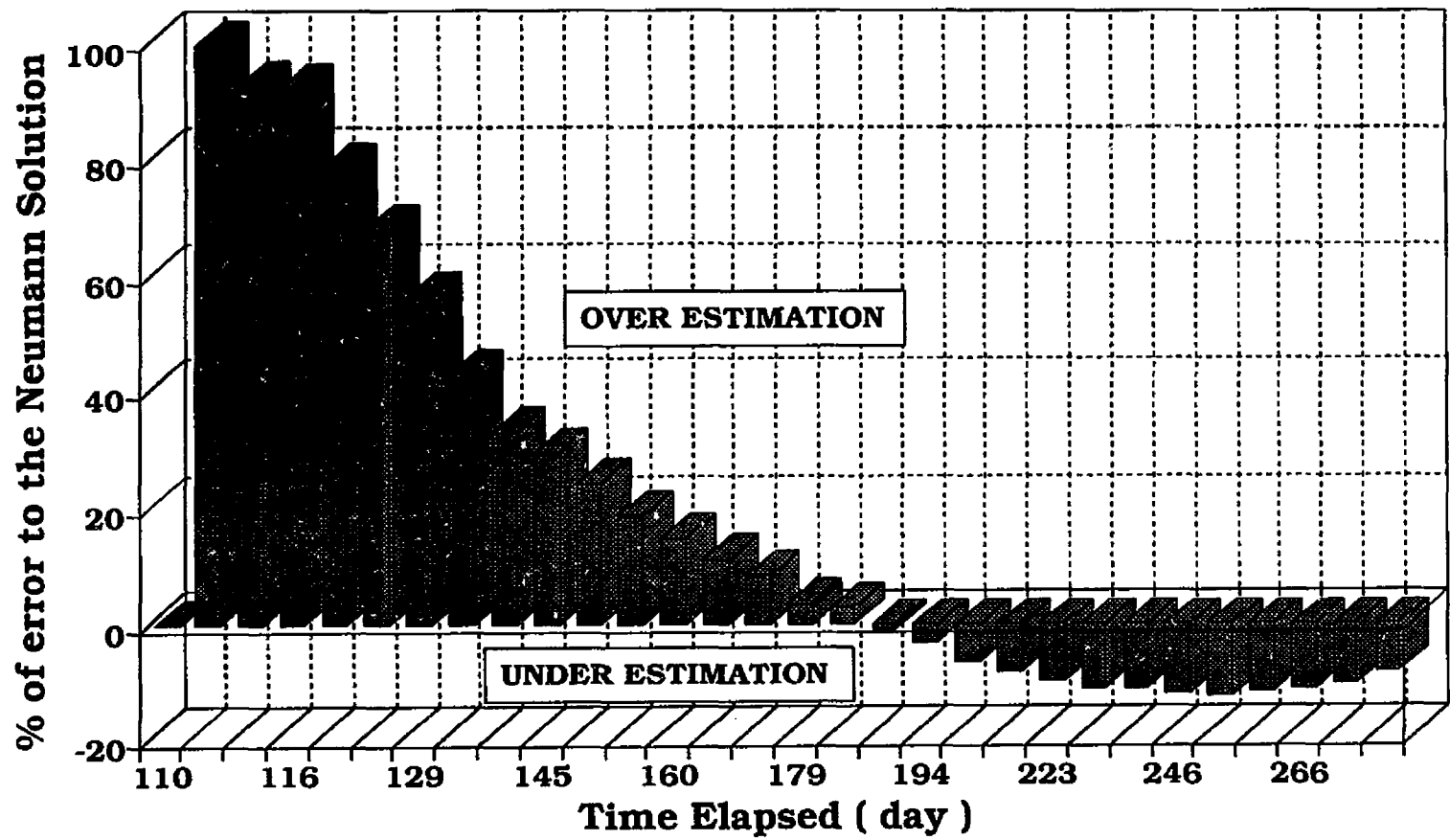


Fig. 4.13 Percentage of Error Between the Numerical and the Neumann Solutions for Sand with $w = 20\%$

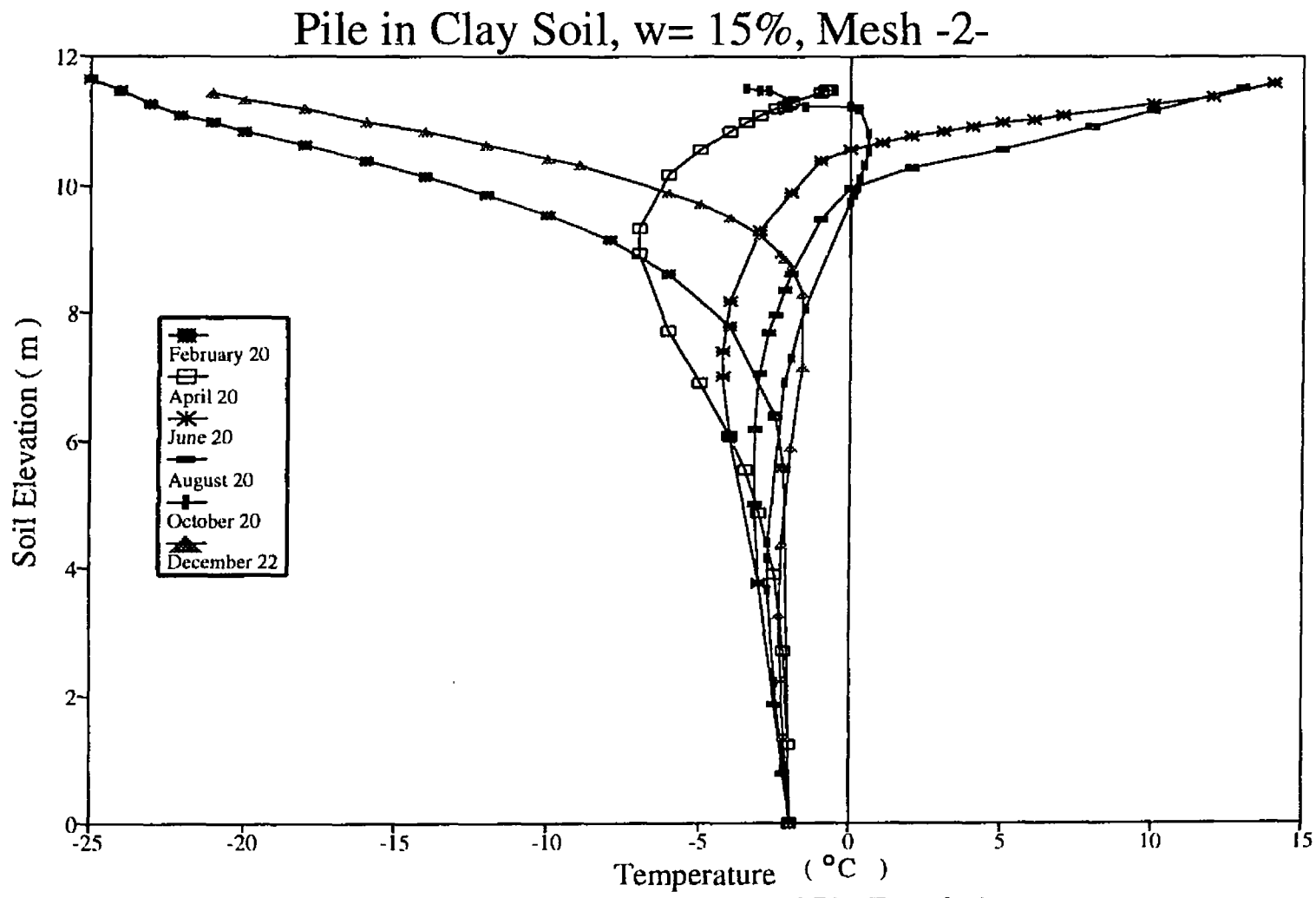


Fig. 4.14 Temperature Fields Distribution Around Pile Foundation in Clay with Water Content, $w = 15\%$

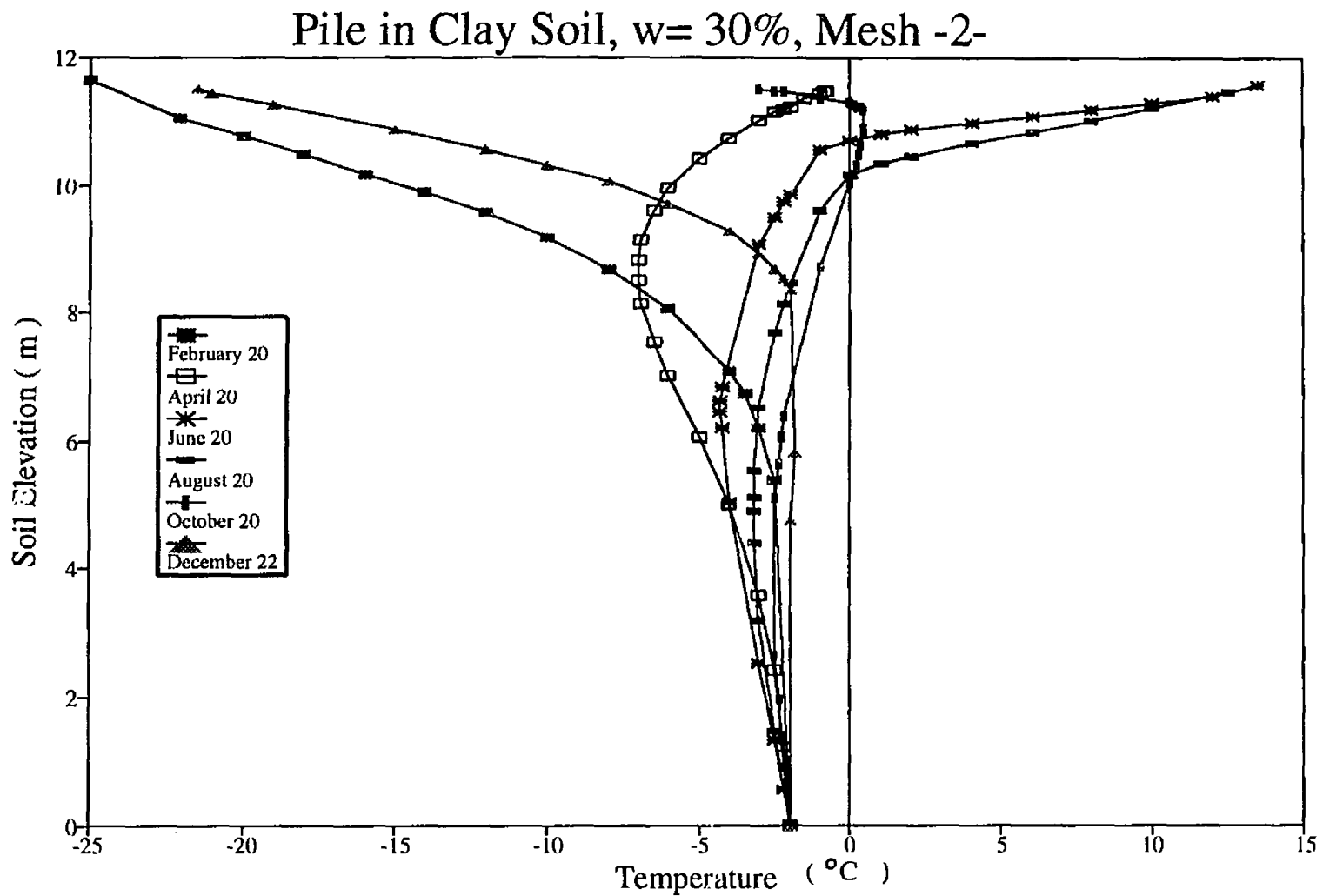


Fig. 4.15 Temperature Fields Distribution Around Pile Foundation in Clay with Water Content, $w = 30\%$

Pile in Clay Soil, $w = 15\%$, Mesh -2-
zero Isotherm around the pile

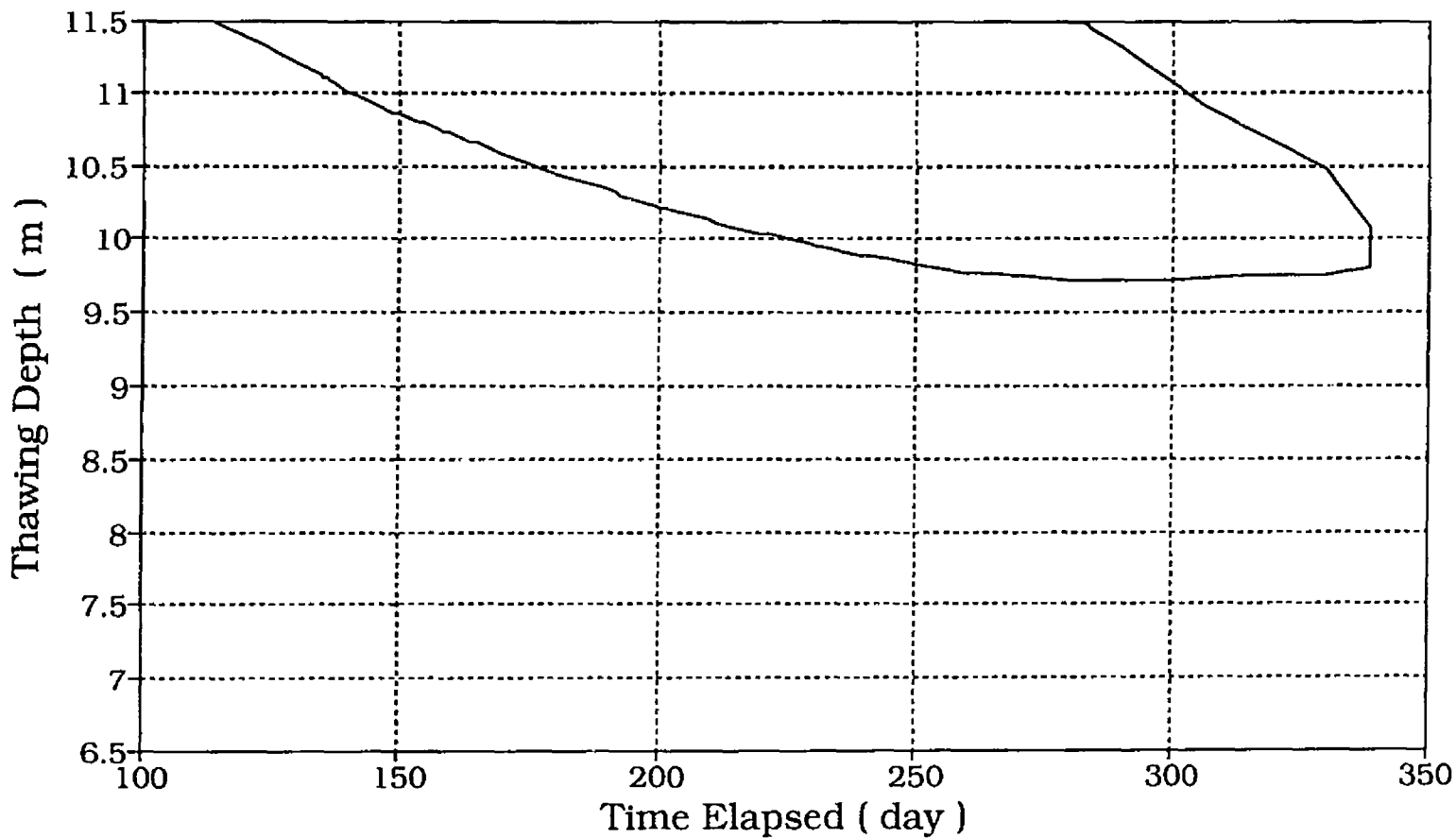


Fig. 4.16 Zero Isotherm Propagation Around Pile in Clay with water content, $w = 15\%$

Pile in Clay Soil, $w = 30\%$, Mesh -2-
zero Isotherm around the pile

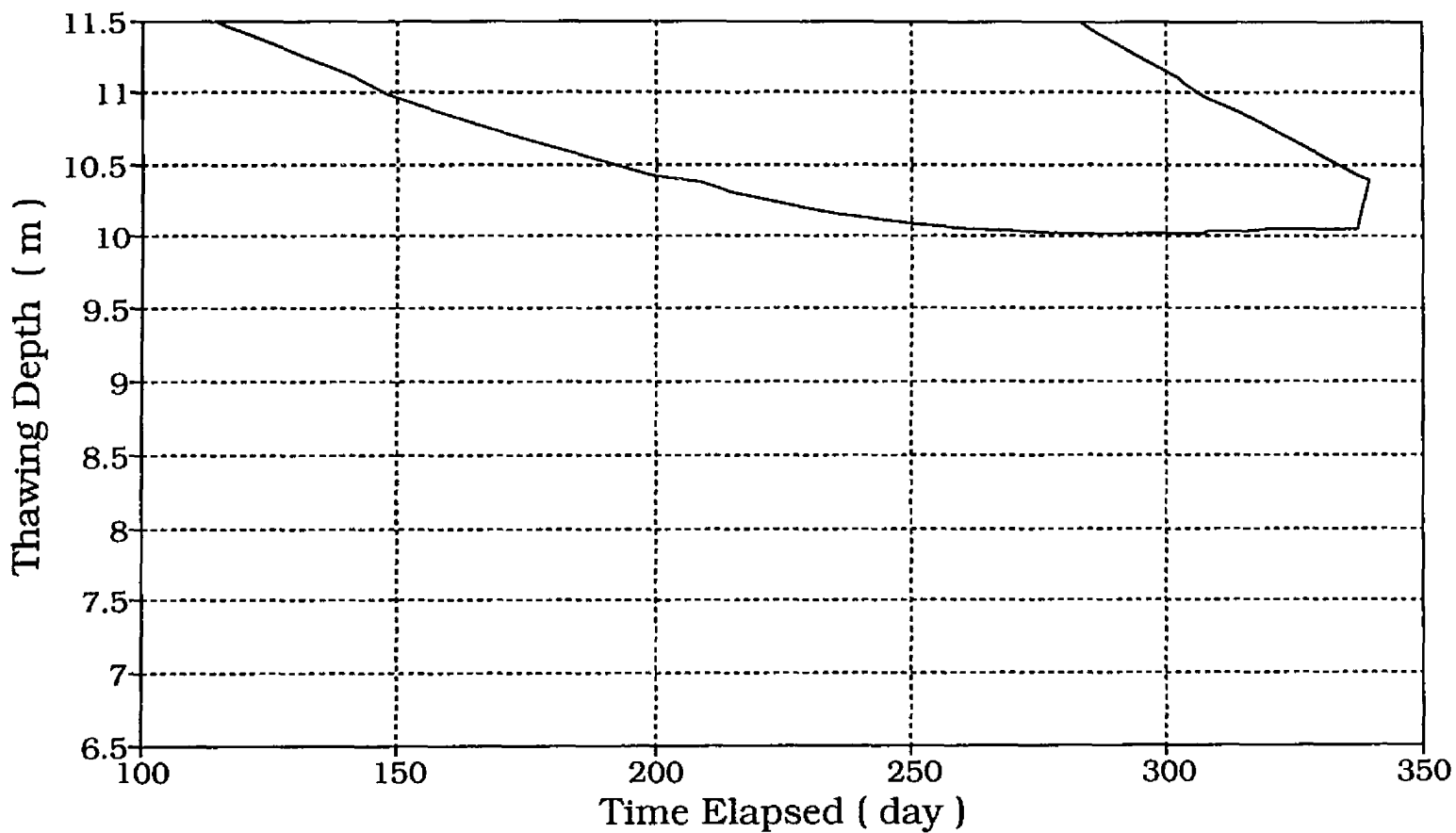


Fig. 4.17 Zero Isotherm Propagation Around Pile in Clay with water content, $w = 30\%$

Pile in Clay Soil, $w = 15\%$, Mesh -2-
Isotherm Plots: -2, -1, +1, +2

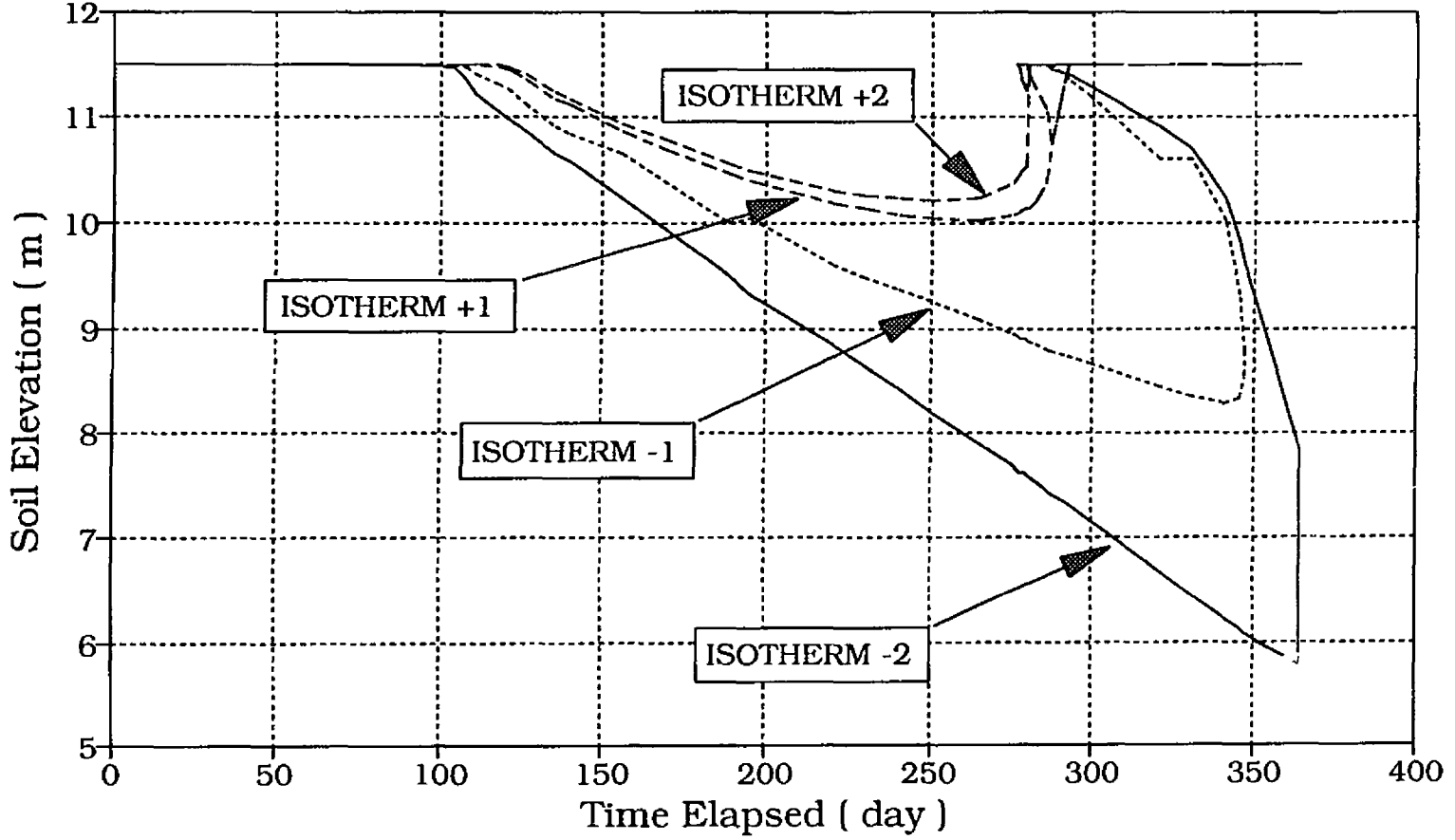


Fig. 4.18 Plots of Isotherms : -2, -1, +1, +2 for Clay with water content, $w = 15\%$

Pile in Clay Soil, $w = 30\%$, Mesh -2-
 Isotherm Plots: -2, -1, +1, +2

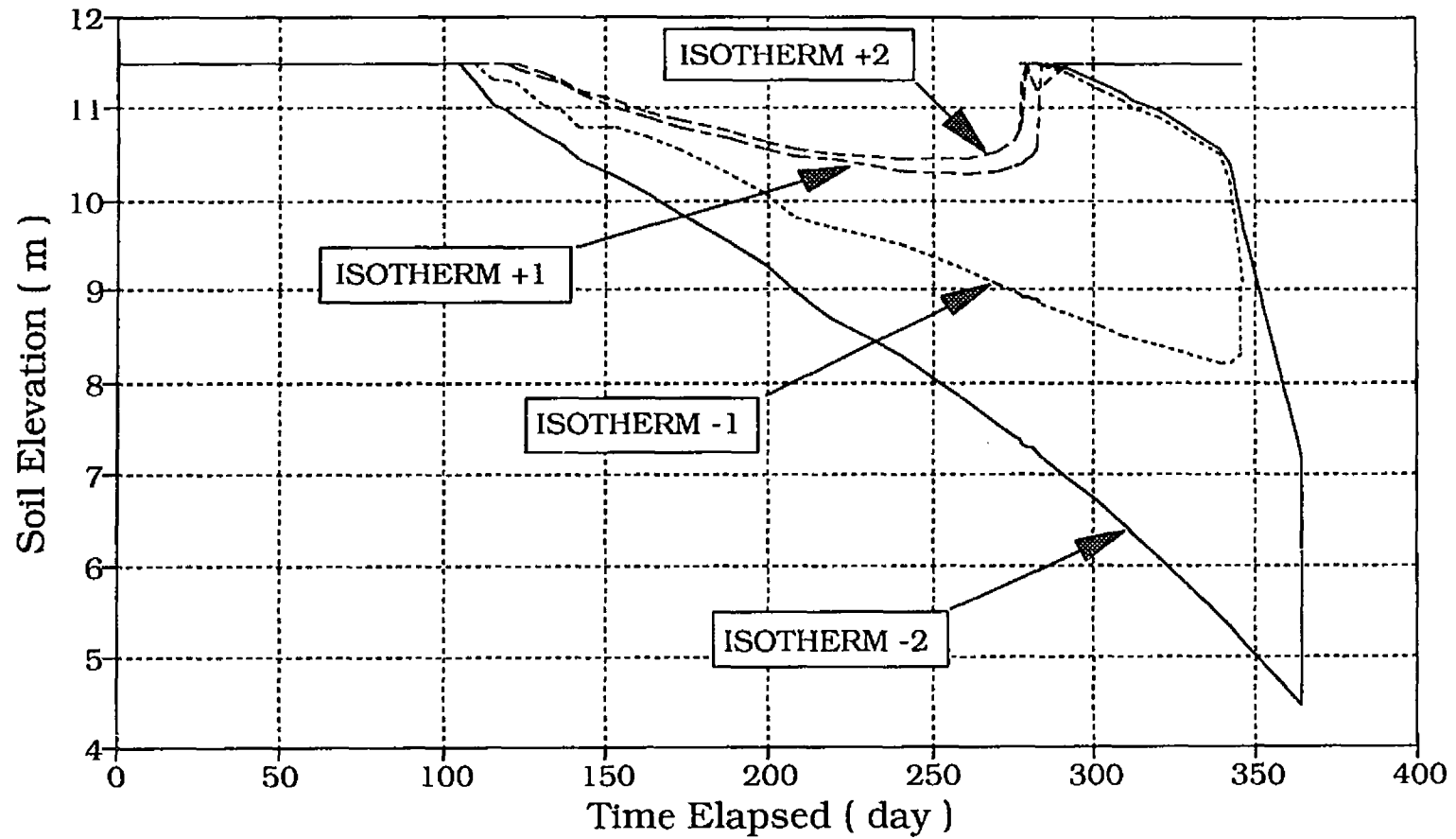


Fig. 4.19 Plots of Isotherms : -2, -1, +1, +2 for Clay with water content, $w = 30\%$

Pile in Clay Soil, $w=15\%$, Mesh -2- Thawing Depth around the Pile

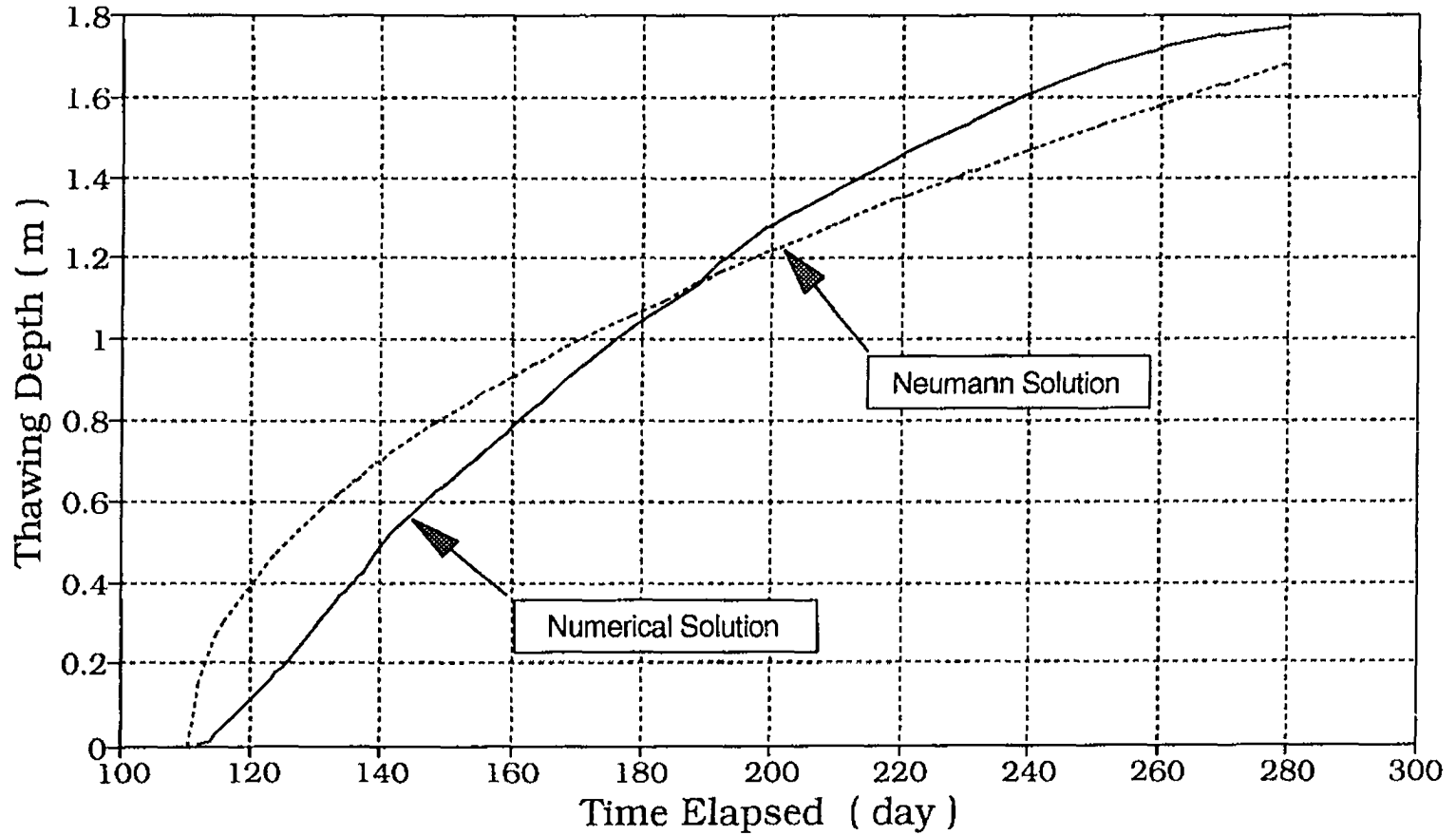


Fig. 4.20 The Comparative Analysis Between the Numerical and Neumann Solutions for Thawing Penetration in Clay with $w = 15\%$

Pile in Clay Soil, $w=15\%$, Mesh -2- Relative error to Neumann Solution

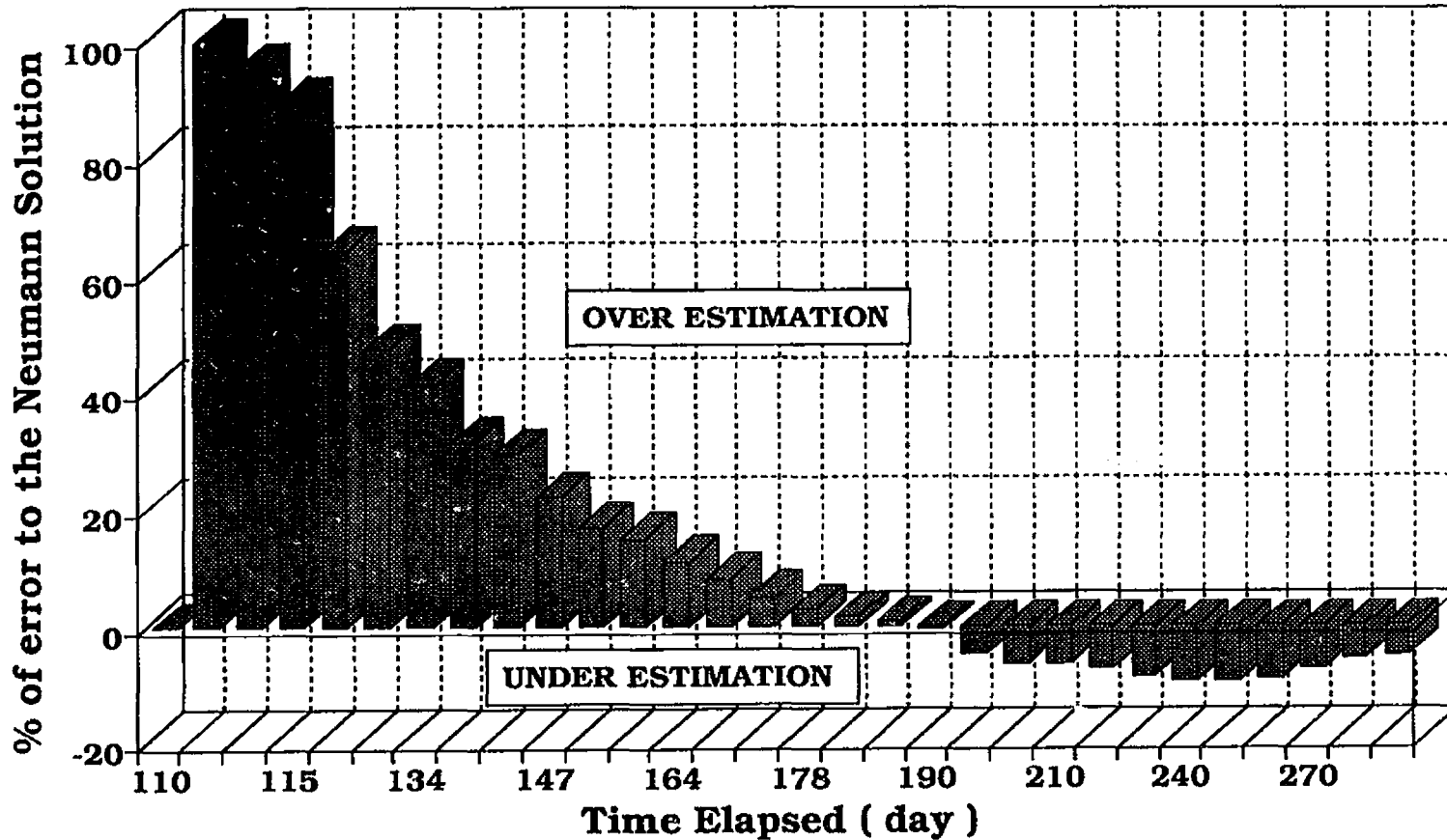


Fig. 4.21 Percentage of Error Between the Numerical and the Neumann Solutions for Clay with $w = 15\%$

Pile in Clay Soil, $w=30\%$, Mesh -2- Thawing Depth around the Pile

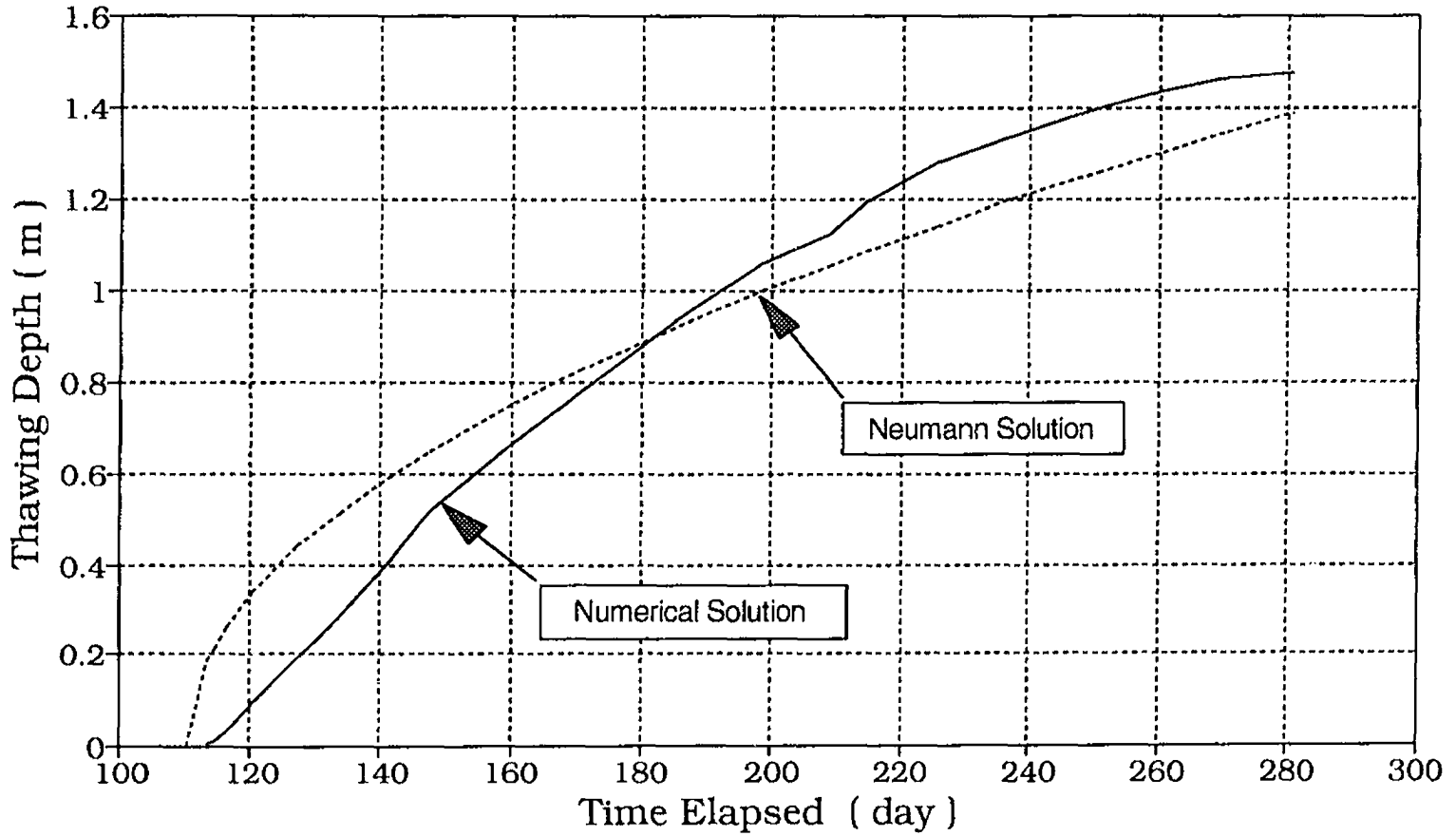


Fig. 4.22 The Comparative Analysis Between the Numerical and Neumann Solutions for Thawing Penetration in Clay with $w = 30\%$

Pile in Clay Soil, $w=30\%$, Mesh -2- Relative error to Neumann Solution

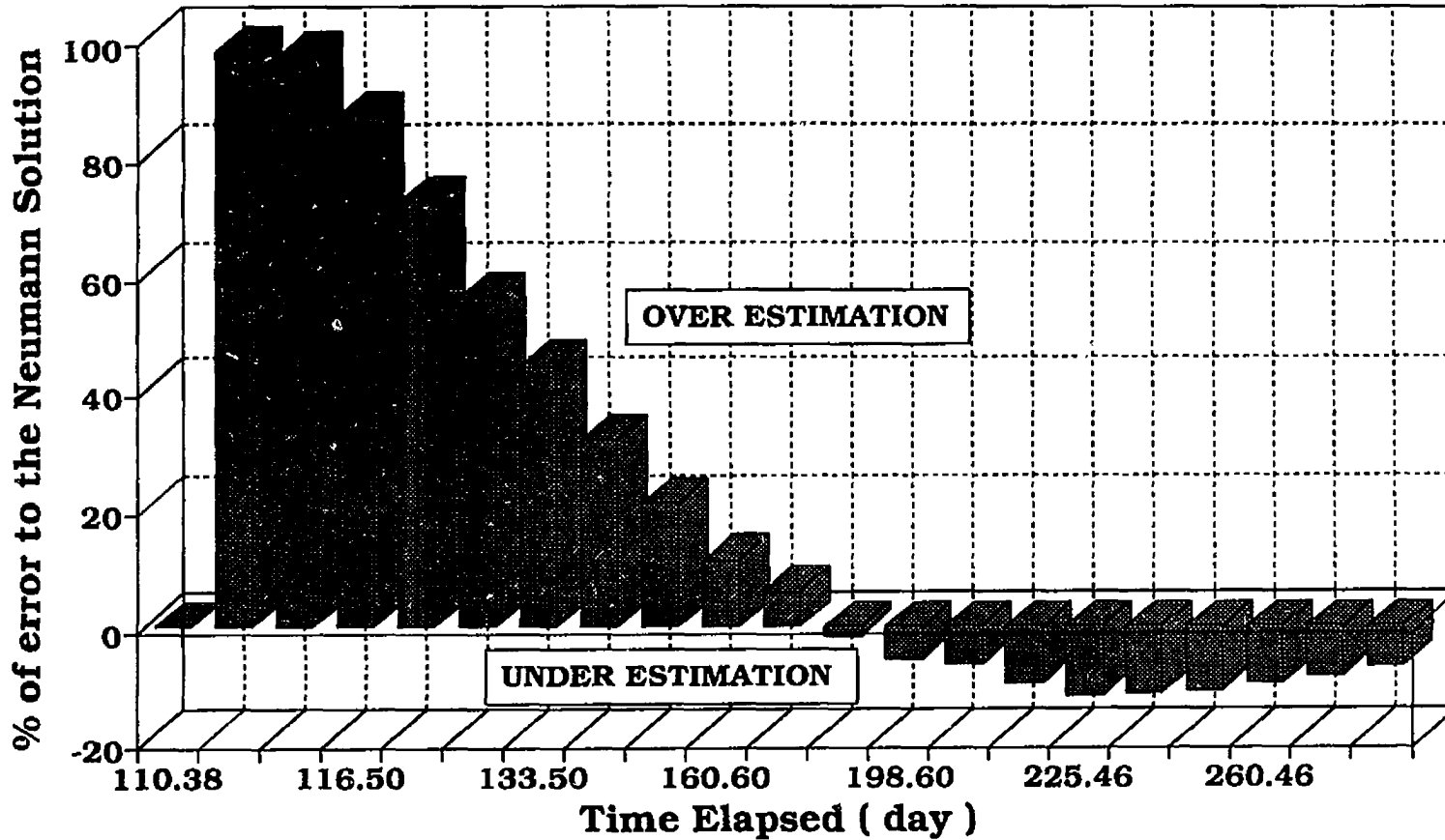


Fig. 4.23 Percentage of Error Between the Numerical and the Neumann Solutions for Clay with $w = 30\%$

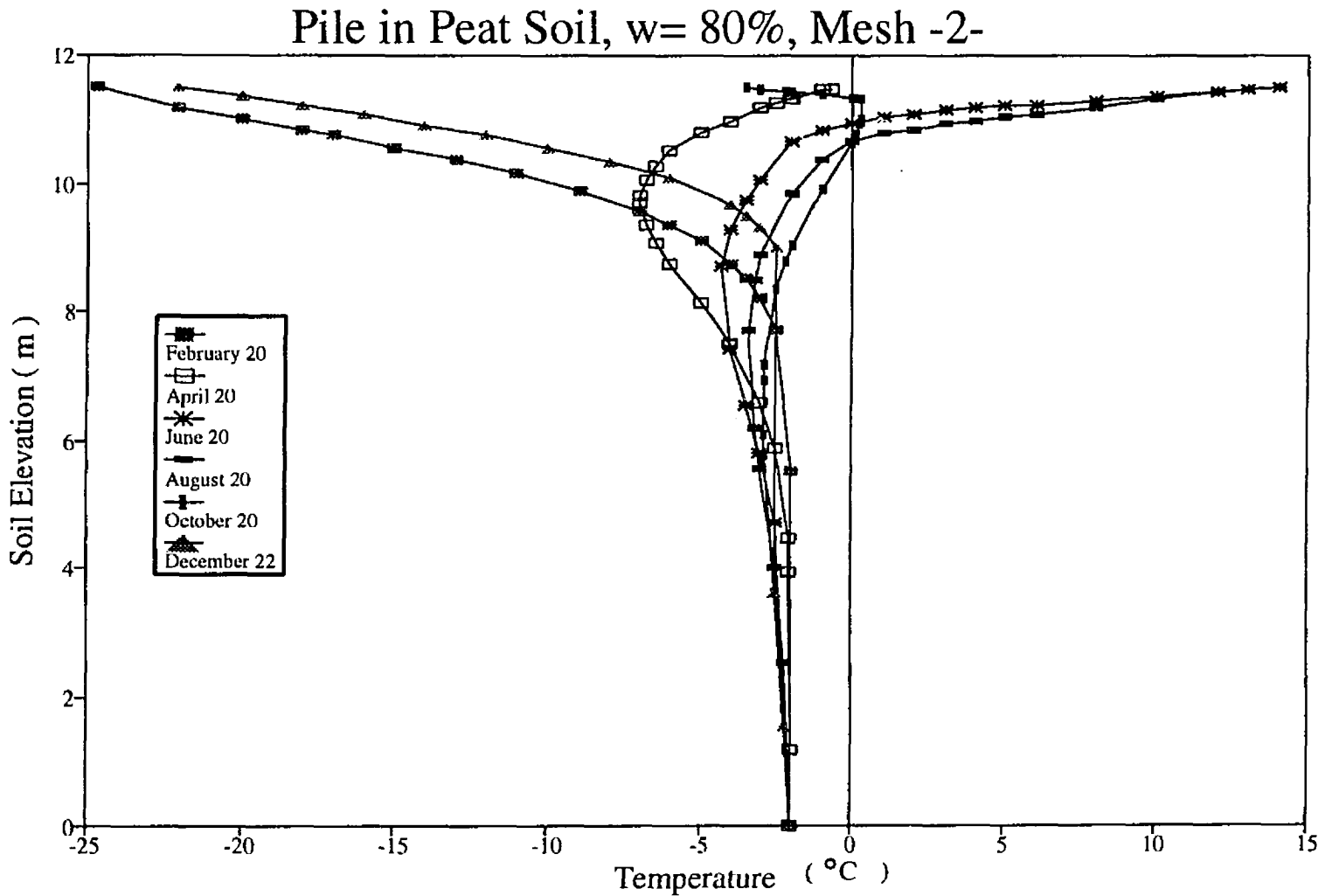


Fig. 4.24 Temperature Fields Distribution Around Pile Foundation in Peat with Water Content, $w = 80\%$

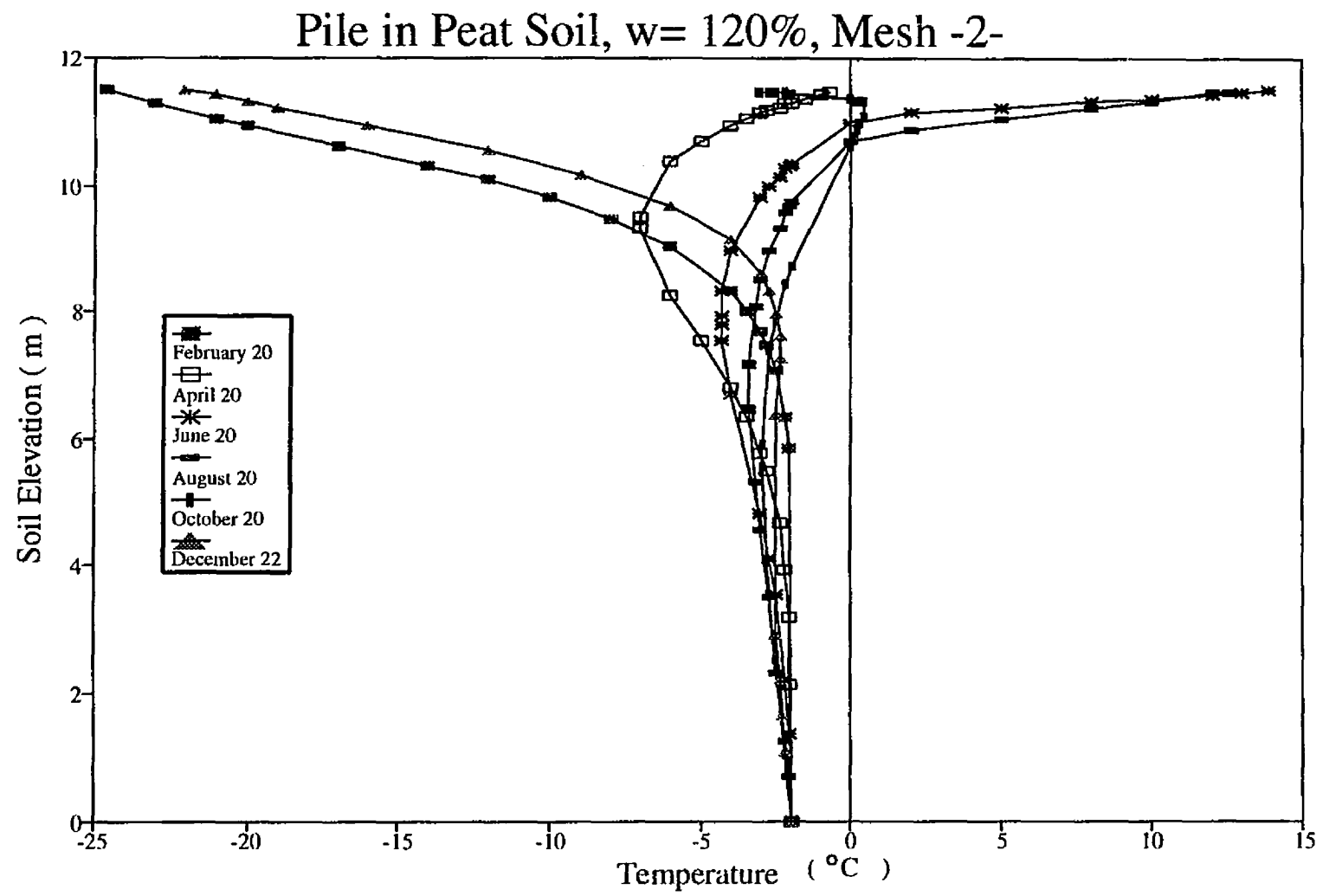


Fig. 4.25 Temperature Fields Distribution Around Pile Foundation in Peat with Water Content, $w = 120\%$

Pile in Peat Soil, $w = 80\%$, Mesh -2-
zero Isotherm around the pile

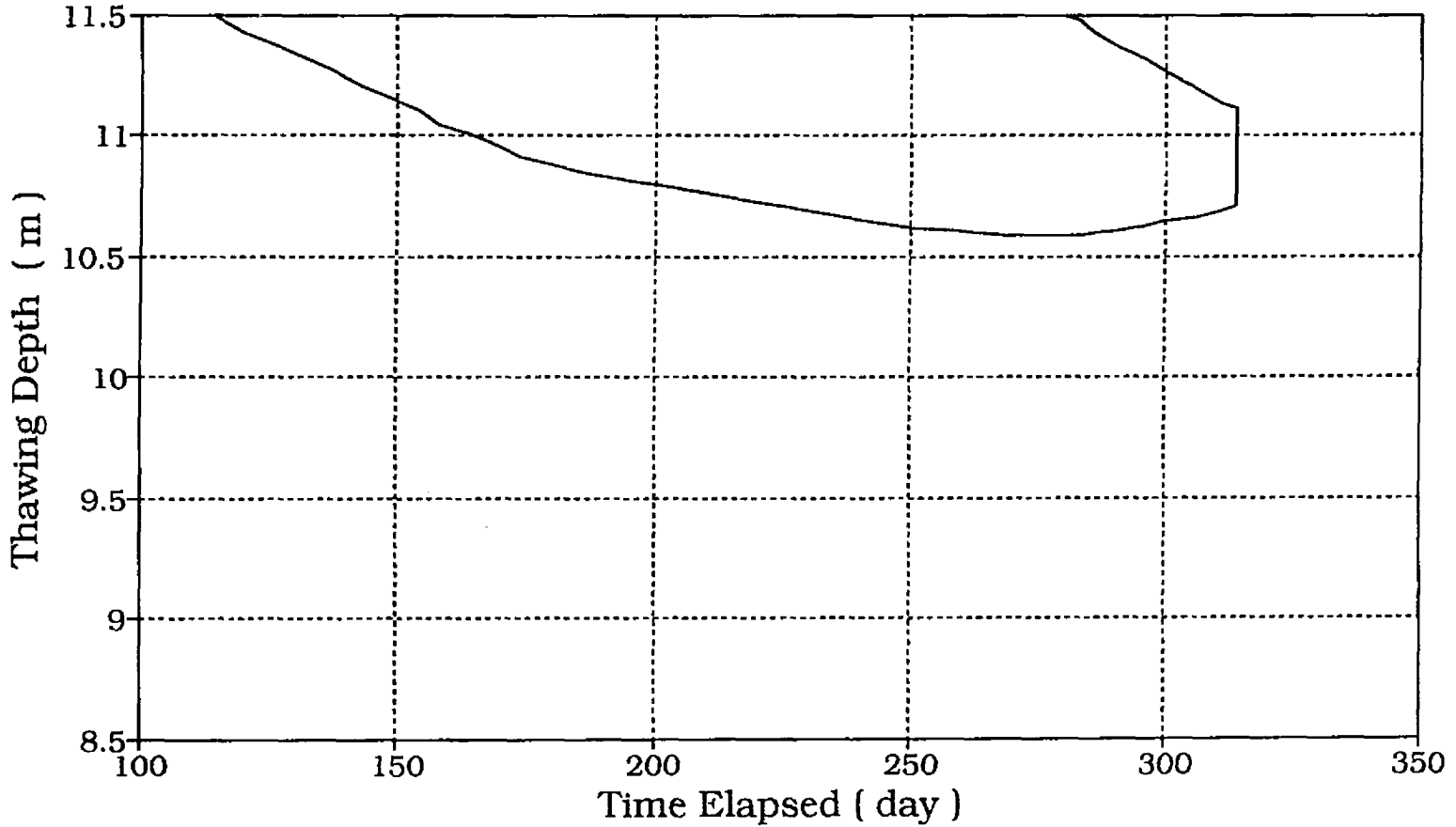


Fig. 4.26 Zero Isotherm Propagation Around Pile in Peat with water content, $w = 80\%$

Pile in Peat Soil, $w = 120\%$, Mesh -2-zero Isotherm around the pile

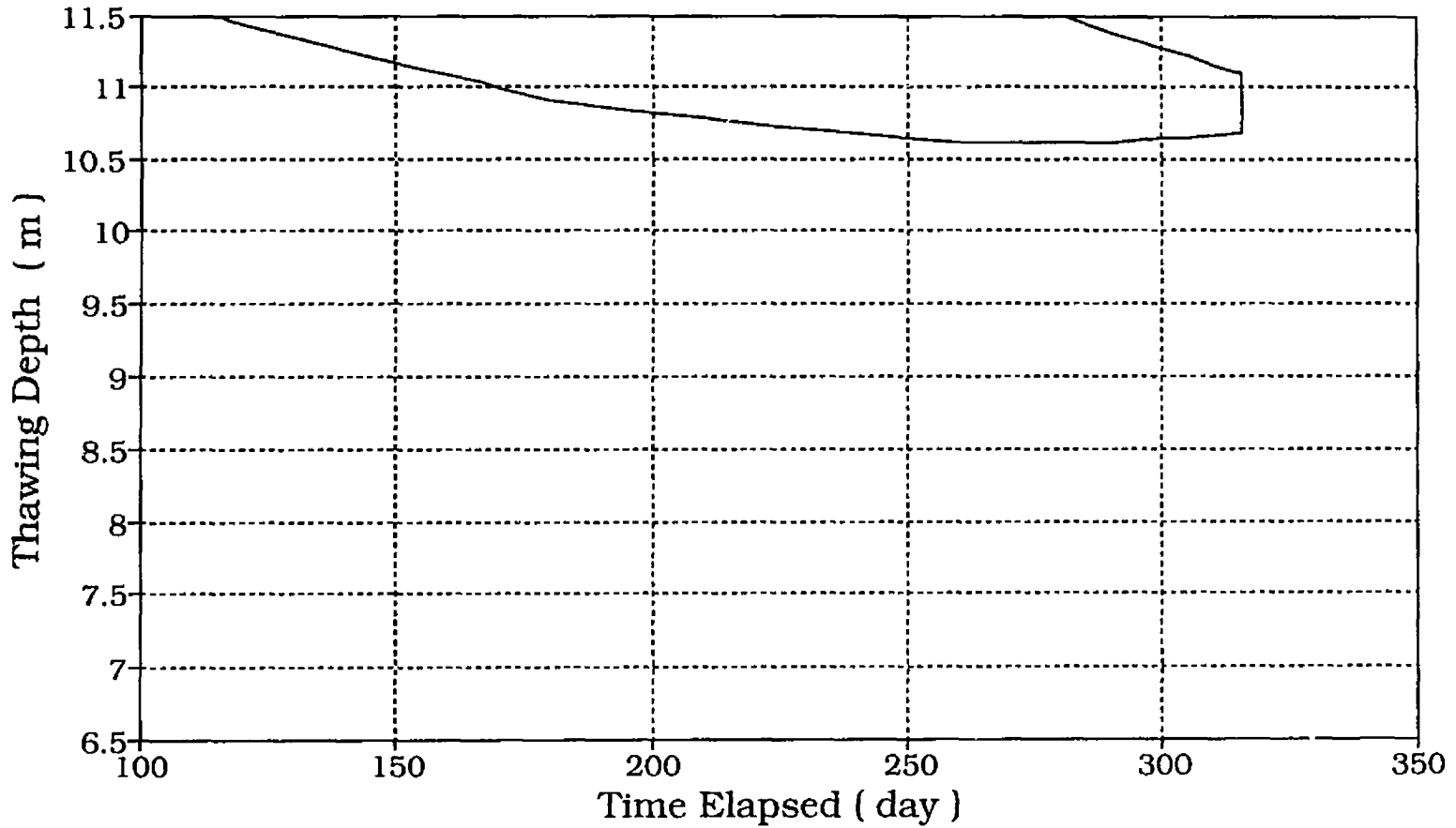


Fig. 4.27 Zero Isotherm Propagation Around Pile in Peat with water content, $w = 120\%$

Pile in Peat Soil, $w = 80\%$ - Mesh -2-
 Isotherms Plot: -2, -1, +1, +2

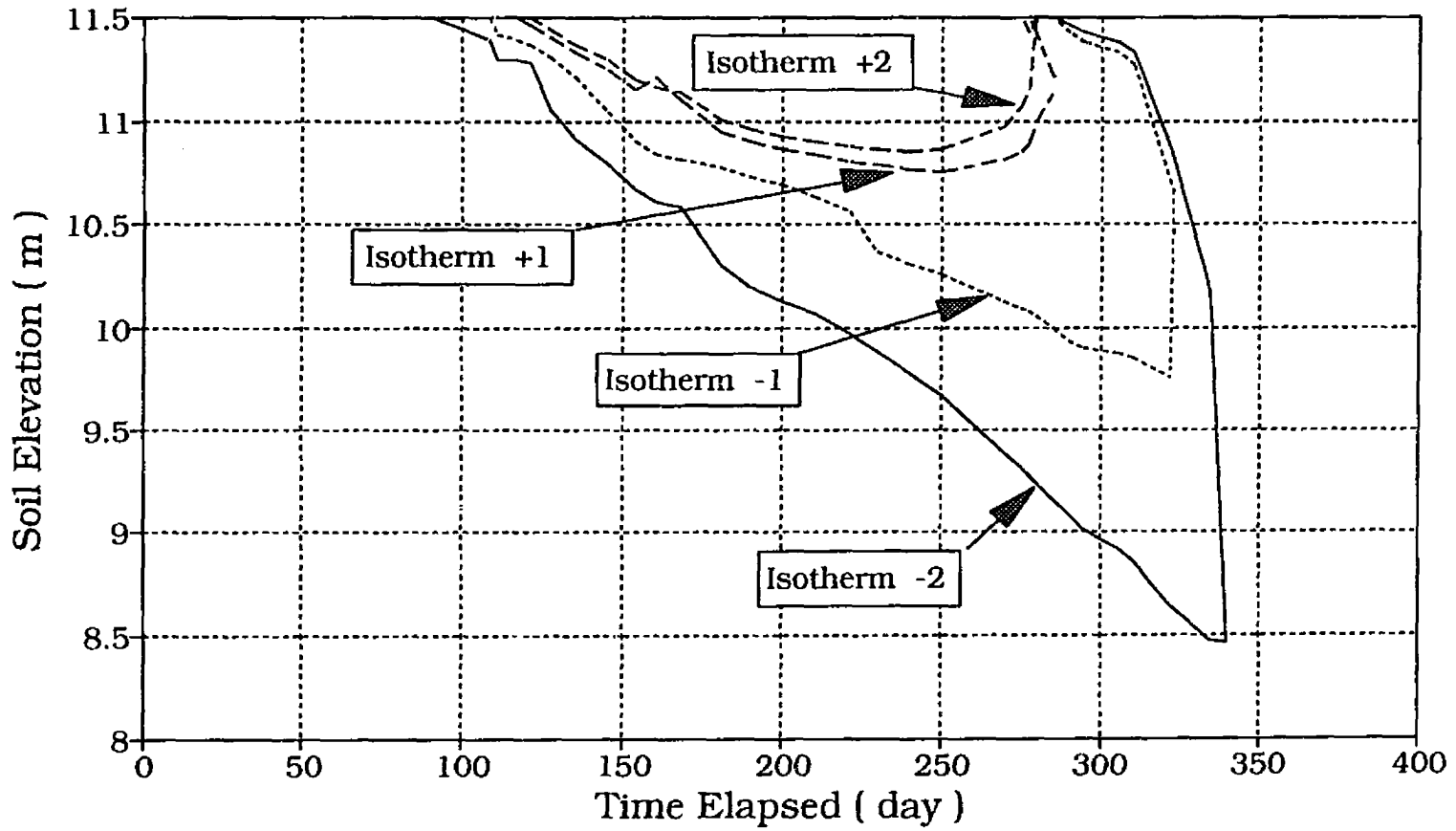


Fig. 4.28 Plots of Isotherms : -2, -1, +1, +2 for Peat with water content, $w = 80\%$

Pile in Peat Soil, $w = 120\%$ - Mesh -2-
Isotherms Plot: -2, -1, +1, +2

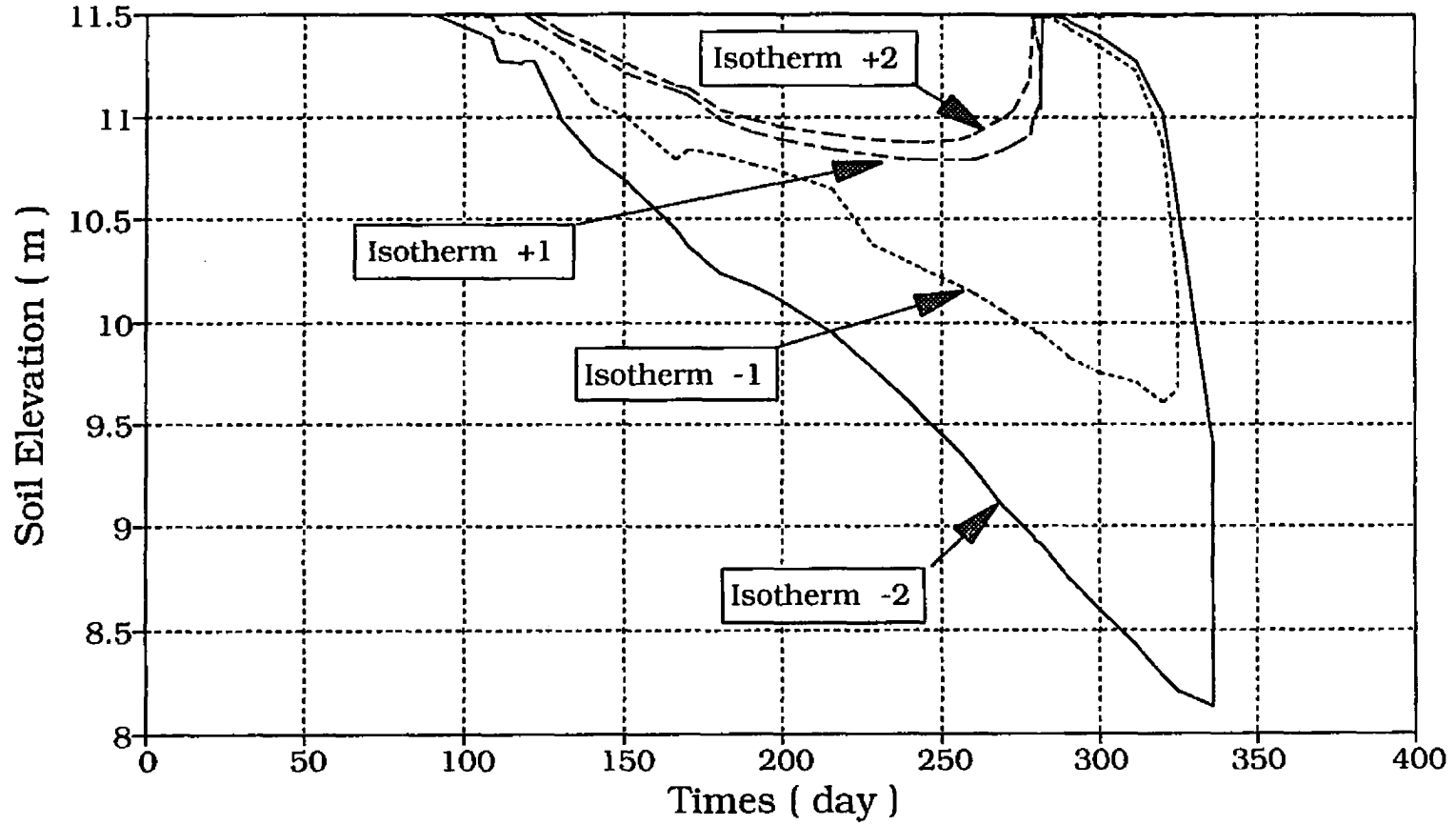


Fig. 4.29 Plots of Isotherms : -2, -1, +1, +2 for Peat with water content, $w = 120\%$

Pile in Peat Soil, $w=80\%$, Mesh -2-
Thawing Depth around the Pile

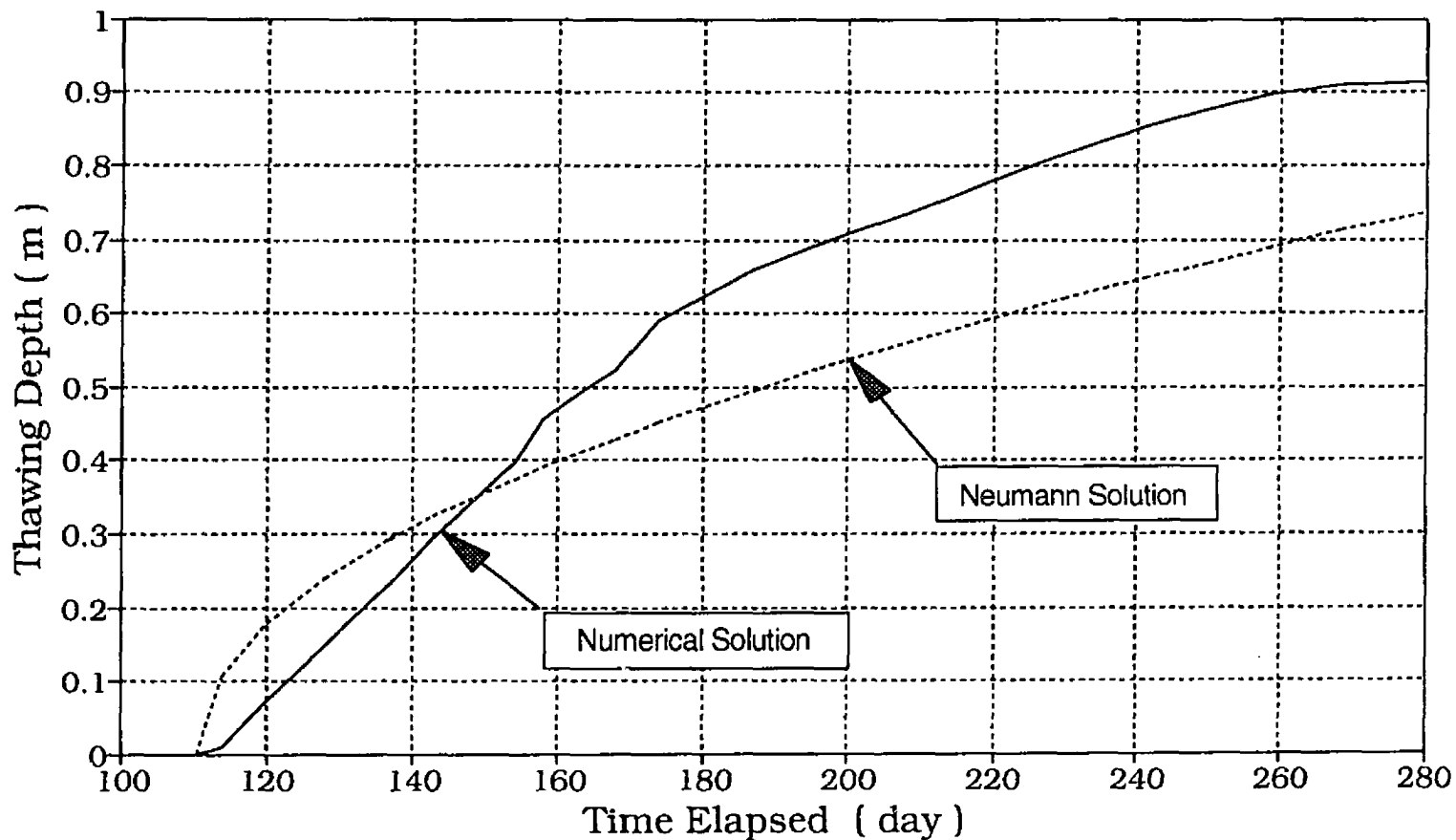


Fig. 4.30 The Comparative Analysis Between the Numerical and Neumann Solutions for Thawing Penetration in Peat with $w = 80\%$

Pile in Peat Soil, $w=80\%$, Mesh -2- Relative error to Neumann Solution

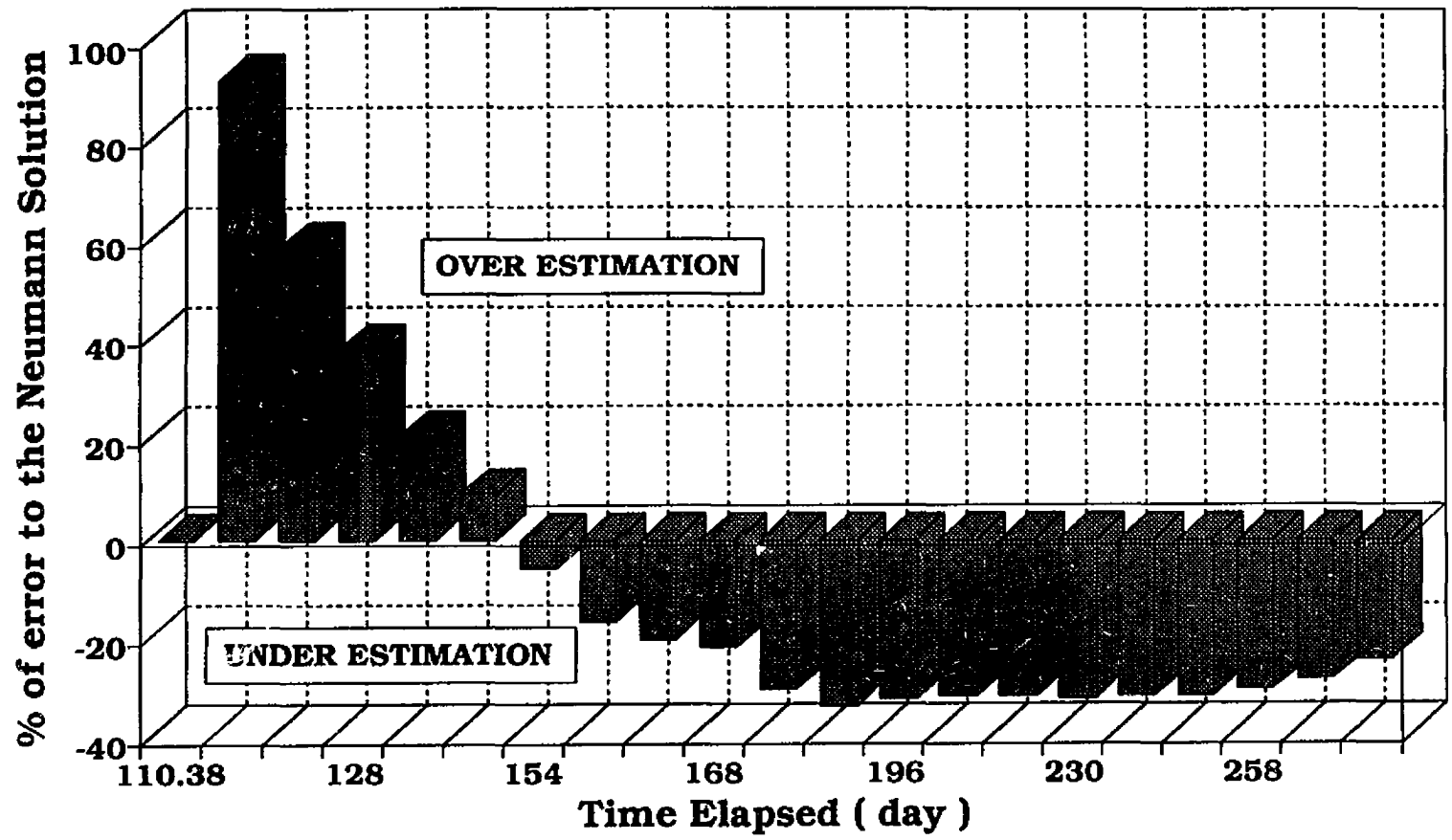


Fig. 4.31 Percentage of Error Between the Numerical and the Neumann Solutions for Peat with $w = 80\%$

Pile in Peat Soil, $w=120\%$, Mesh -2-
Thawing Depth around the Pile

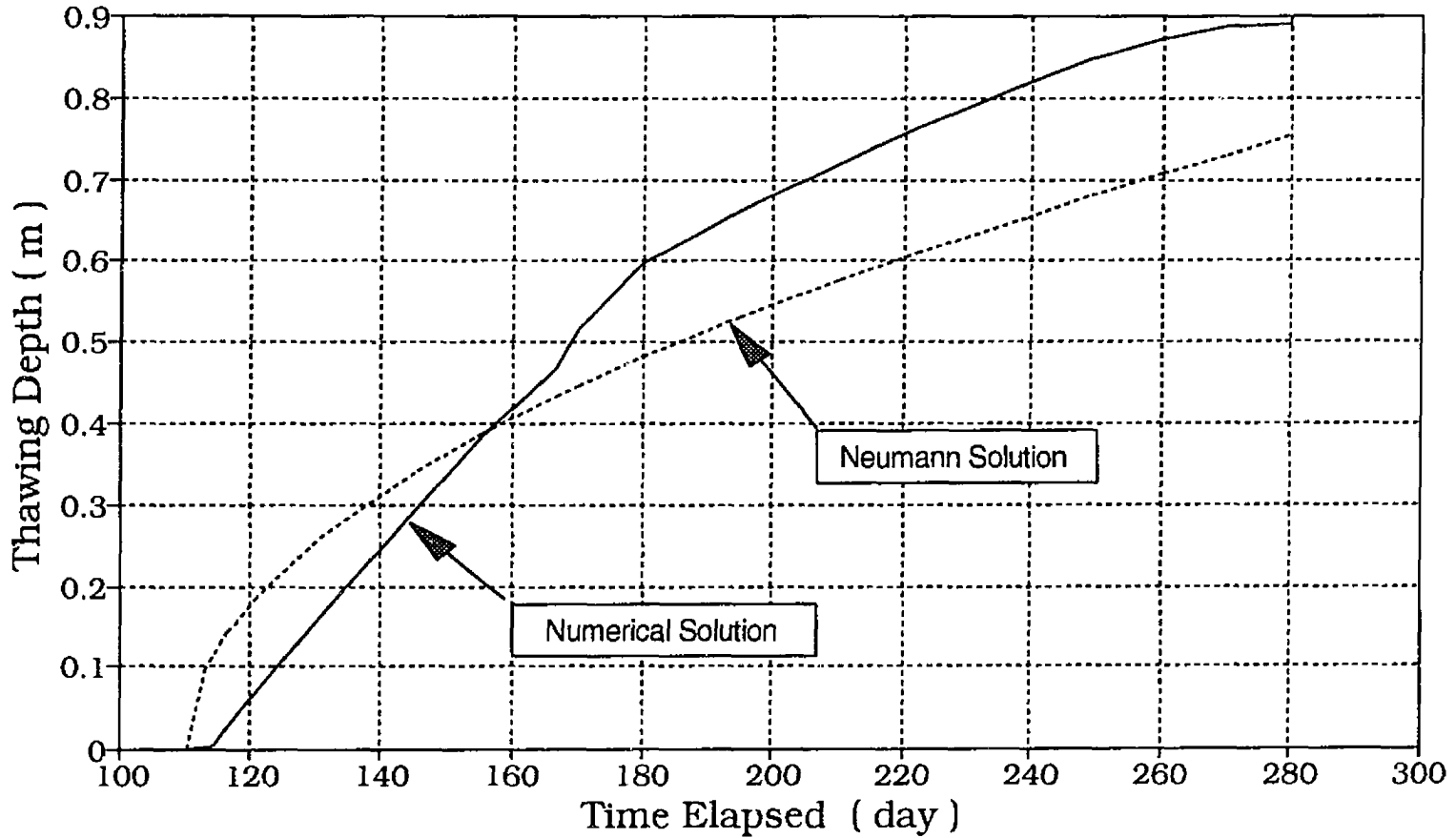


Fig. 4.32 The Comparative Analysis Between the Numerical and Neumann Solutions for Thawing Penetration in Peat with $w = 120\%$

Pile in Peat Soil, $w = 120\%$, Mesh -2- Relative Error w.r.t. Neumann Solution

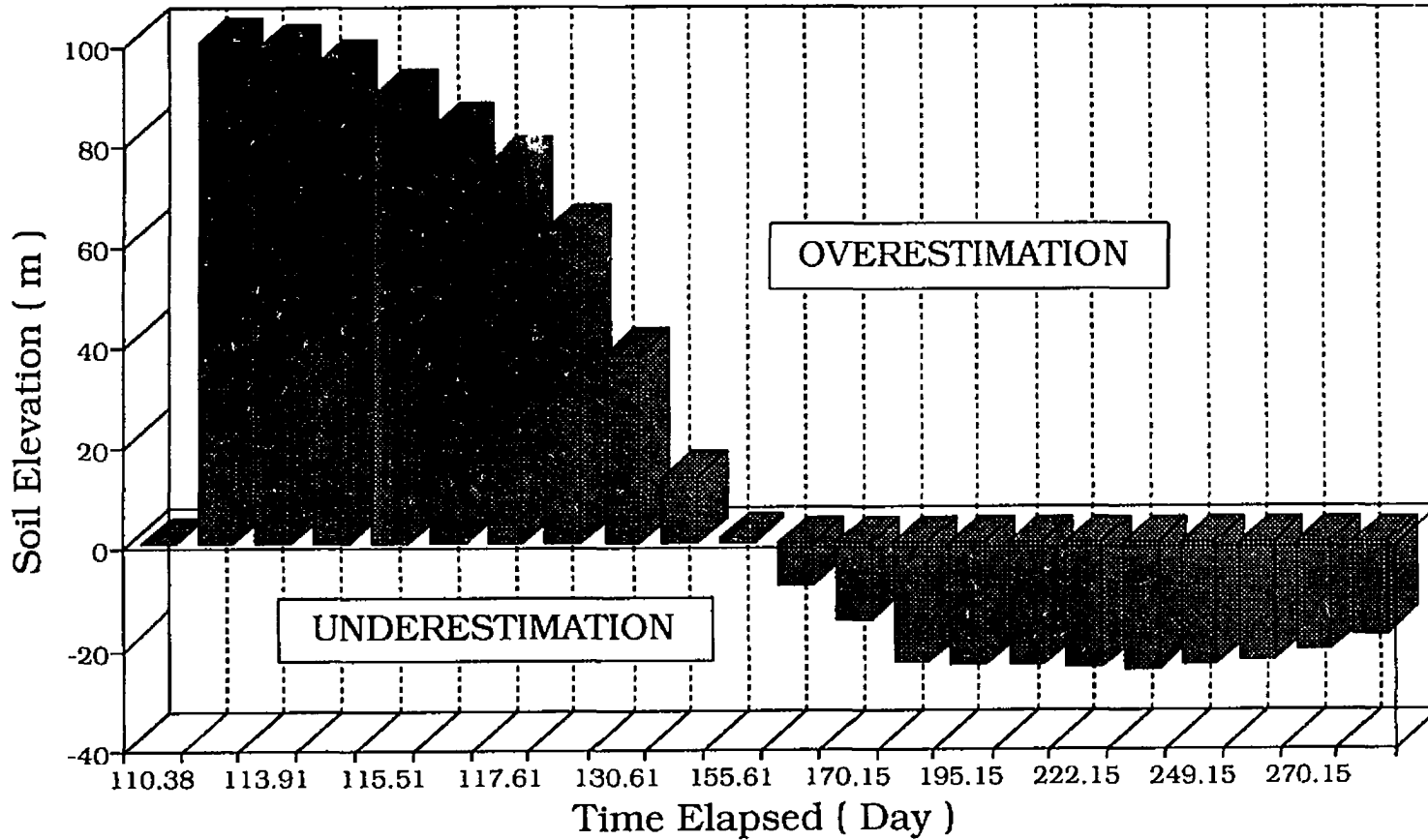


Fig.4.33 Percentage of Error Between the Numerical and Neumann Solutions for Thawing Penetration in Peat with $w = 120\%$

Pile in Sandy Soil with Gravel on top

April 20, Mesh - 1 -

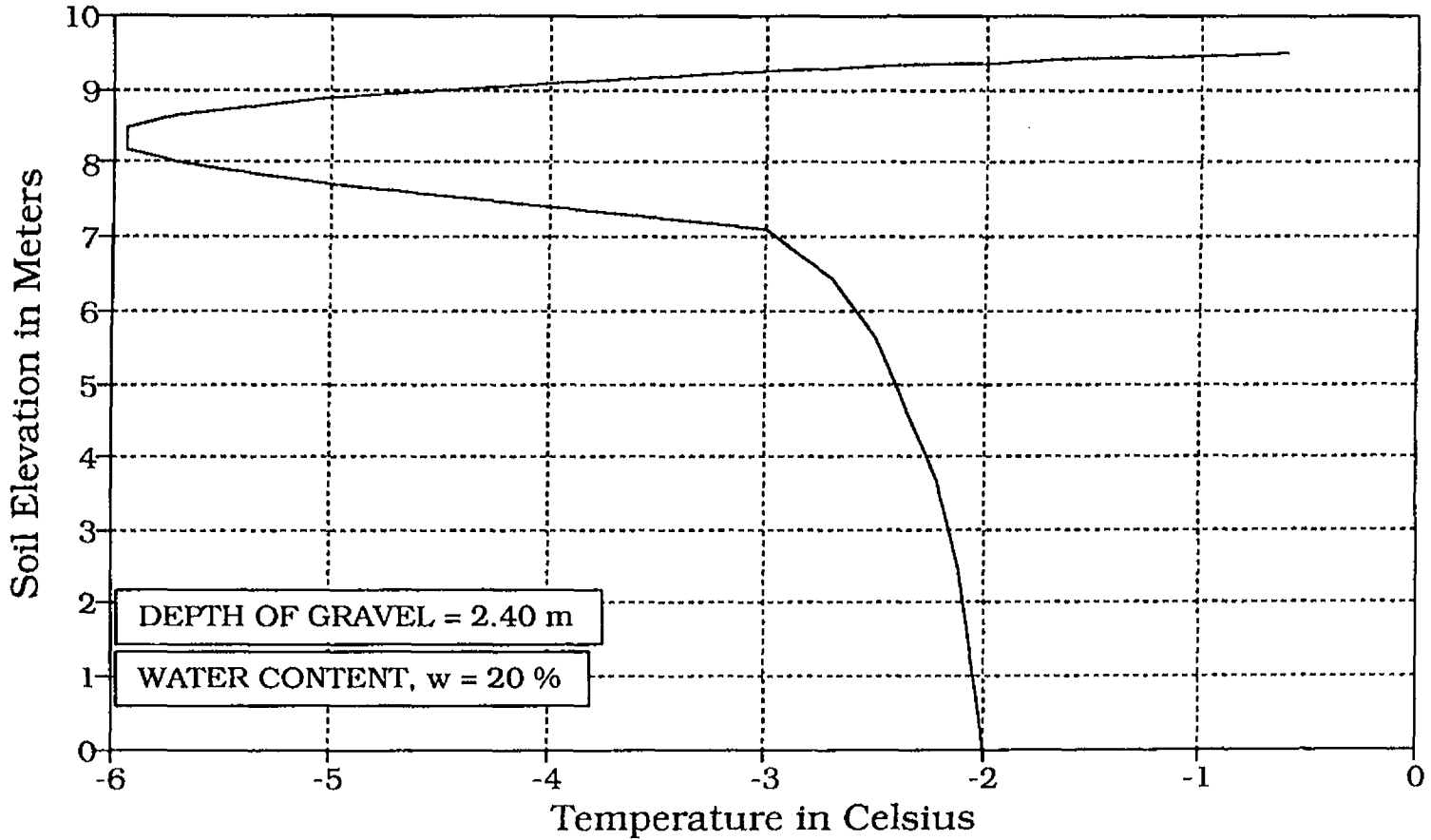


Fig. 4.34 Temperature Distribution for April 20 in Sand with Gravel on Top

Pile in Sandy Soil with Gravel on top

Zero Isotherm propagation around pile

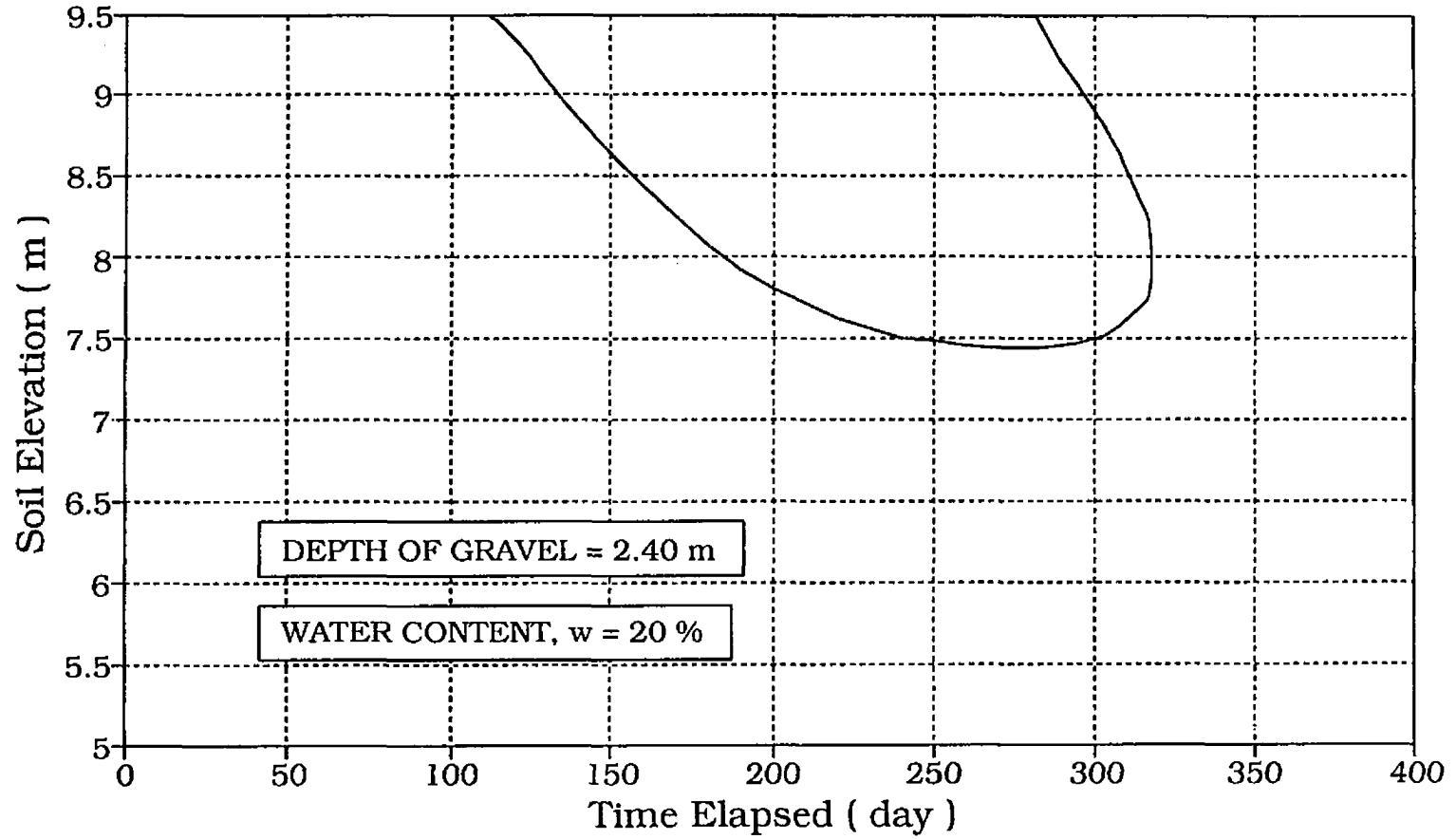


Fig. 4.35 0° C Isotherm Propagation in Sand with gravel on Top

Pile in Sandy Soil with Gravel on top

Comparative solution of thawing depth

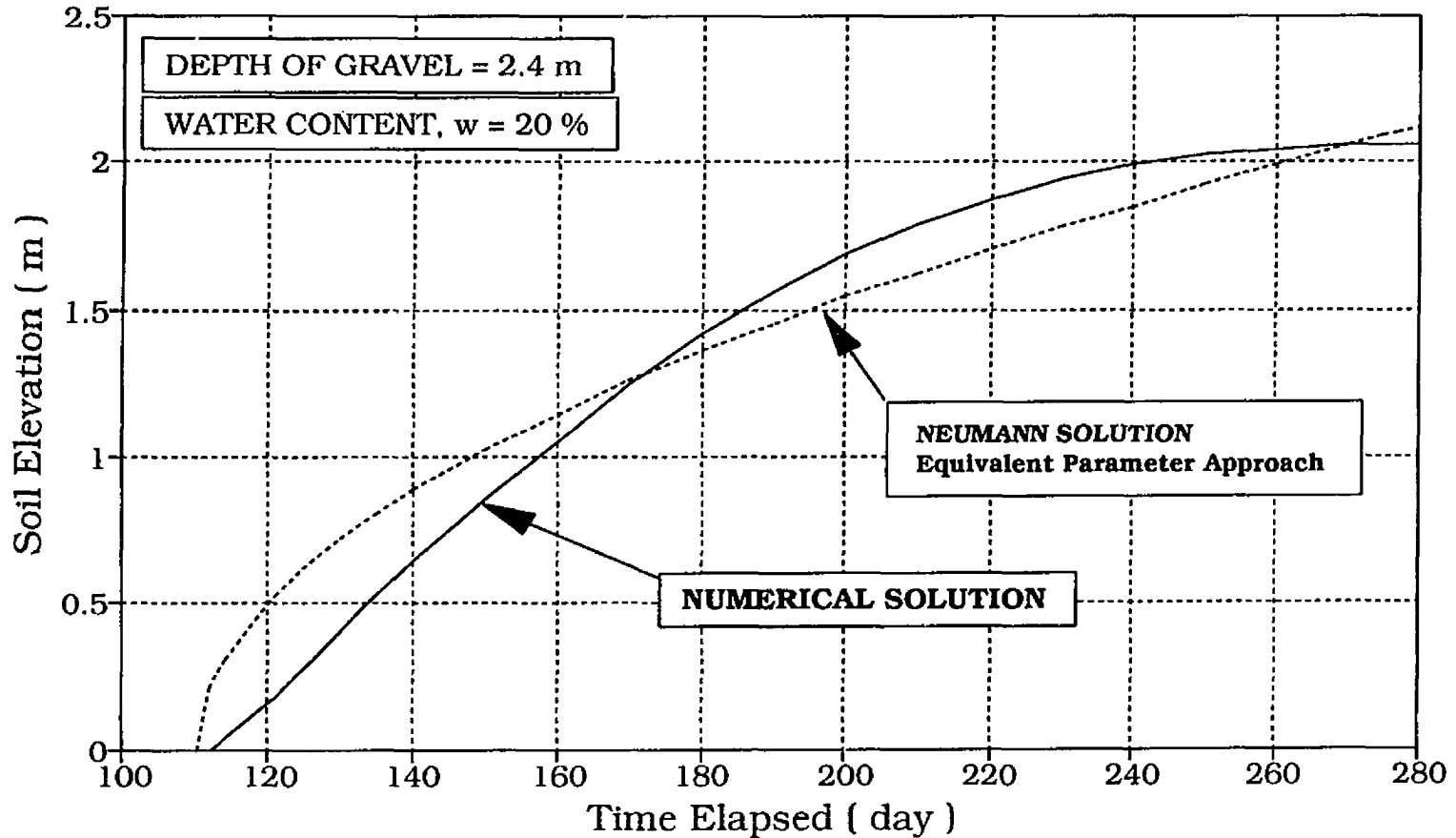


Fig. 4.36 Comparative Analysis Between the Numerical and Neumann Solutions for Pile Foundation in Sand with Gravel on top

Pile in Sandy Soil with Gravel on top

Relative error to Neumann Solution

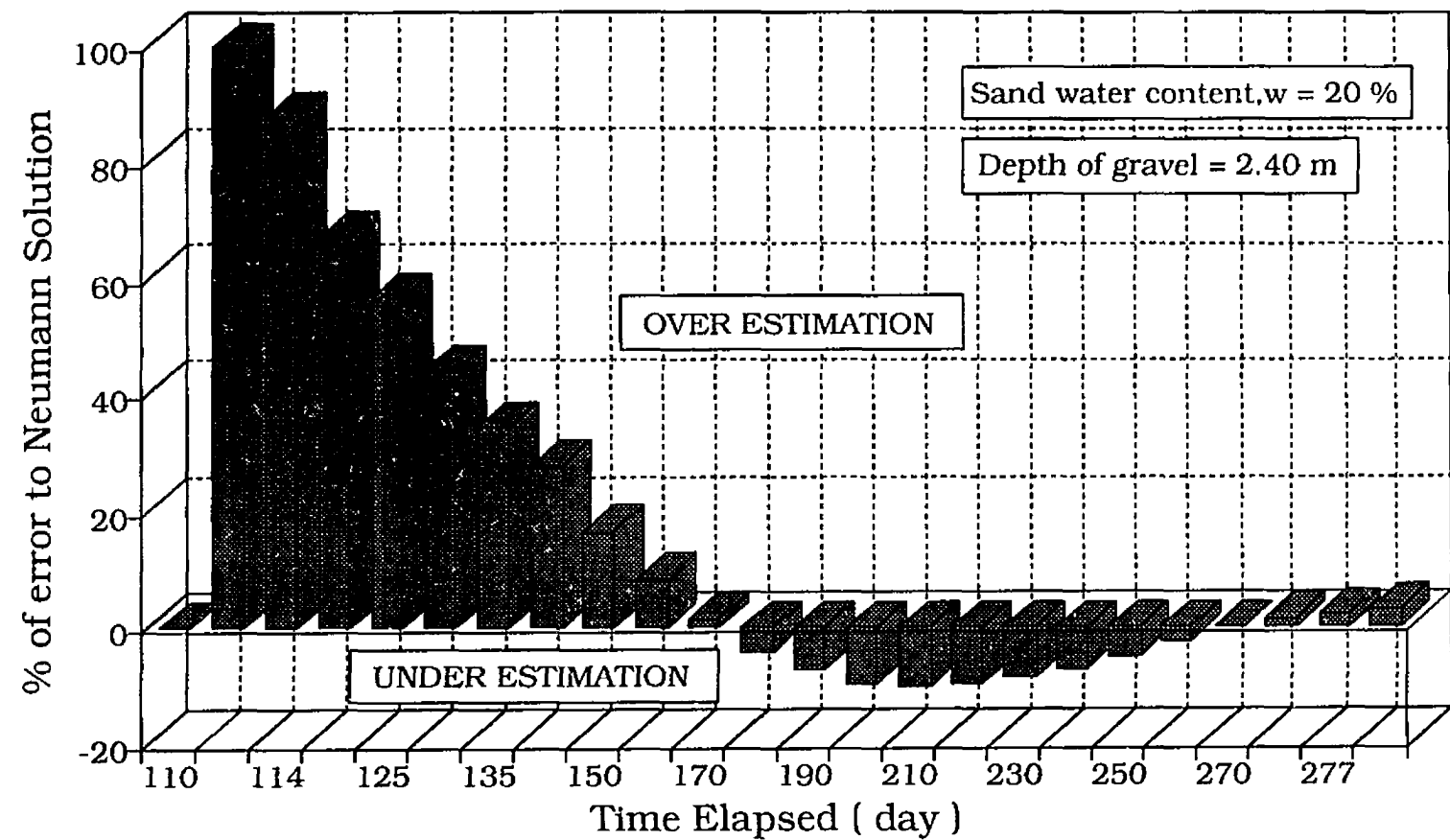


Fig. 4.37 Percentage of Error Between the Analytical and Neumann Solutions for Sand with Gravel on top

Pile in Clayey Soil with Gravel on top April 20, Mesh - 2 -

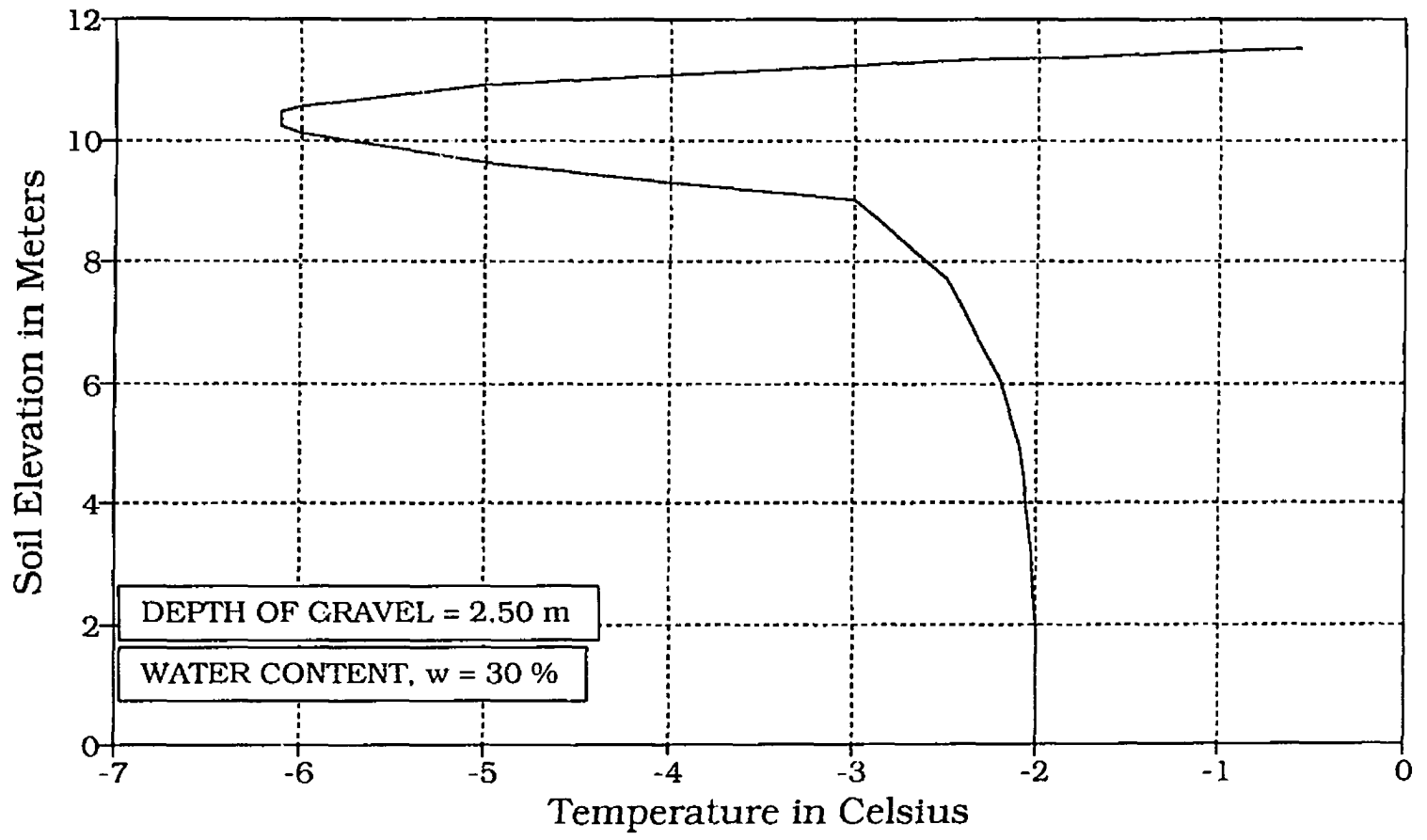


Fig. 4.38 Temperature Distribution for April 20 in Clay with Gravel on Top

Pile in Clayey Soil with Gravel on top

Zero Isotherm propagation around pile

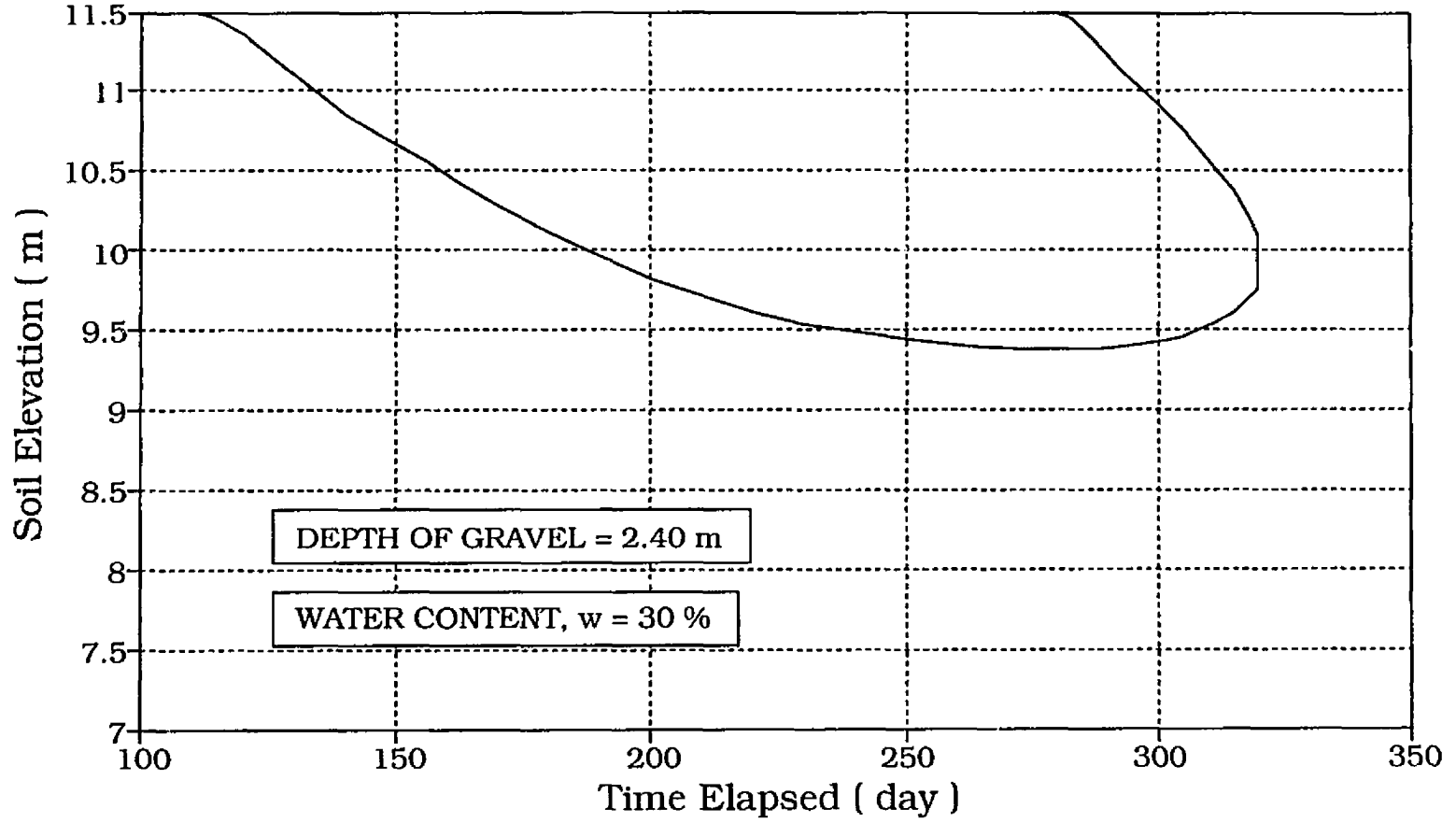


Fig. 4.39 0°C Isotherm Propagation in Clay with gravel on Top

Pile in Clayey Soil with Gravel on top

Comparative solution of thawing depth

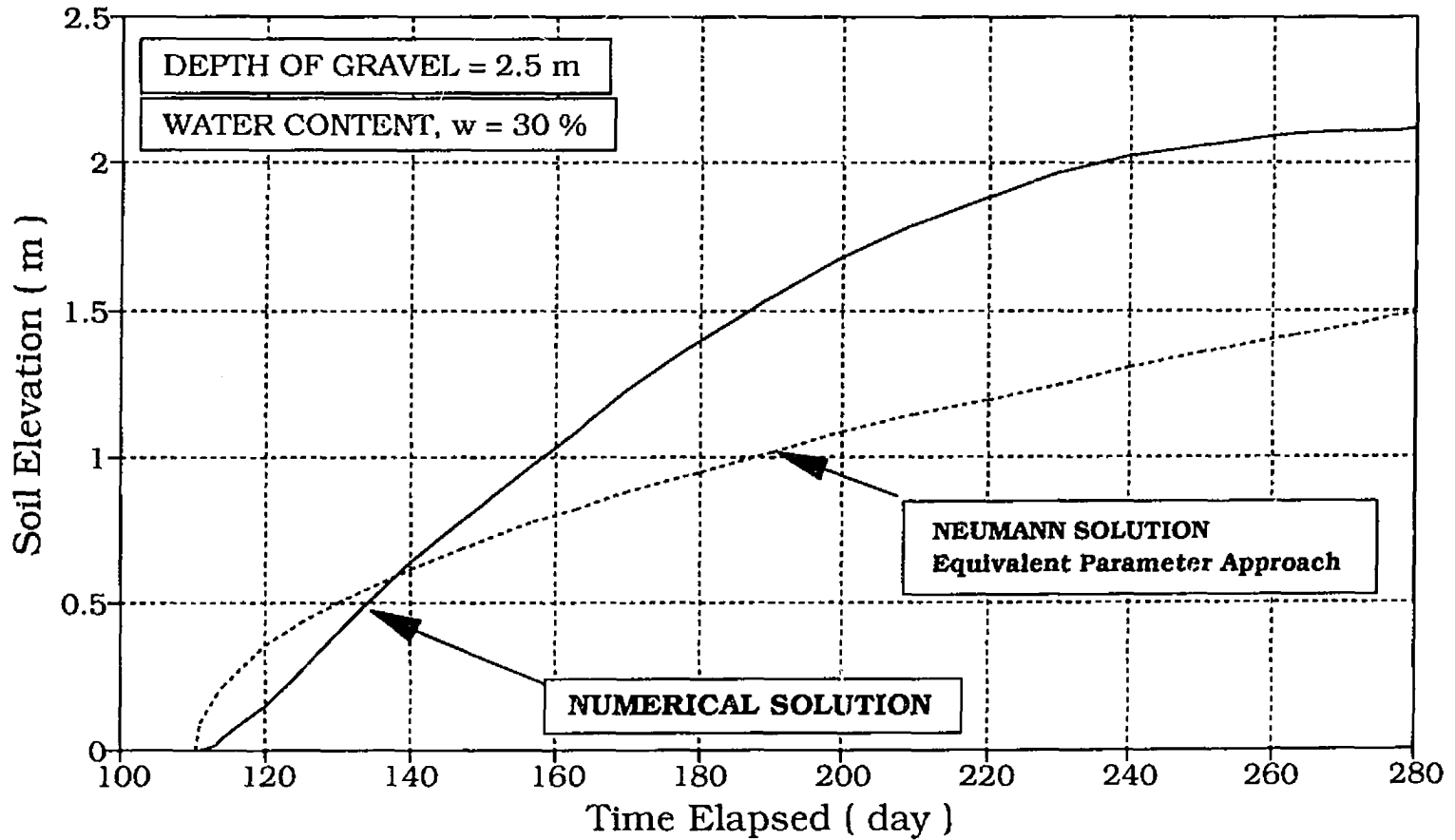


Fig. 4.40 Comparative Analysis Between the Numerical and Neumann Solutions for Pile Foundation in Clay with Gravel on top

Pile in Clayey Soil with Gravel on top

Relative error to Neumann Solution

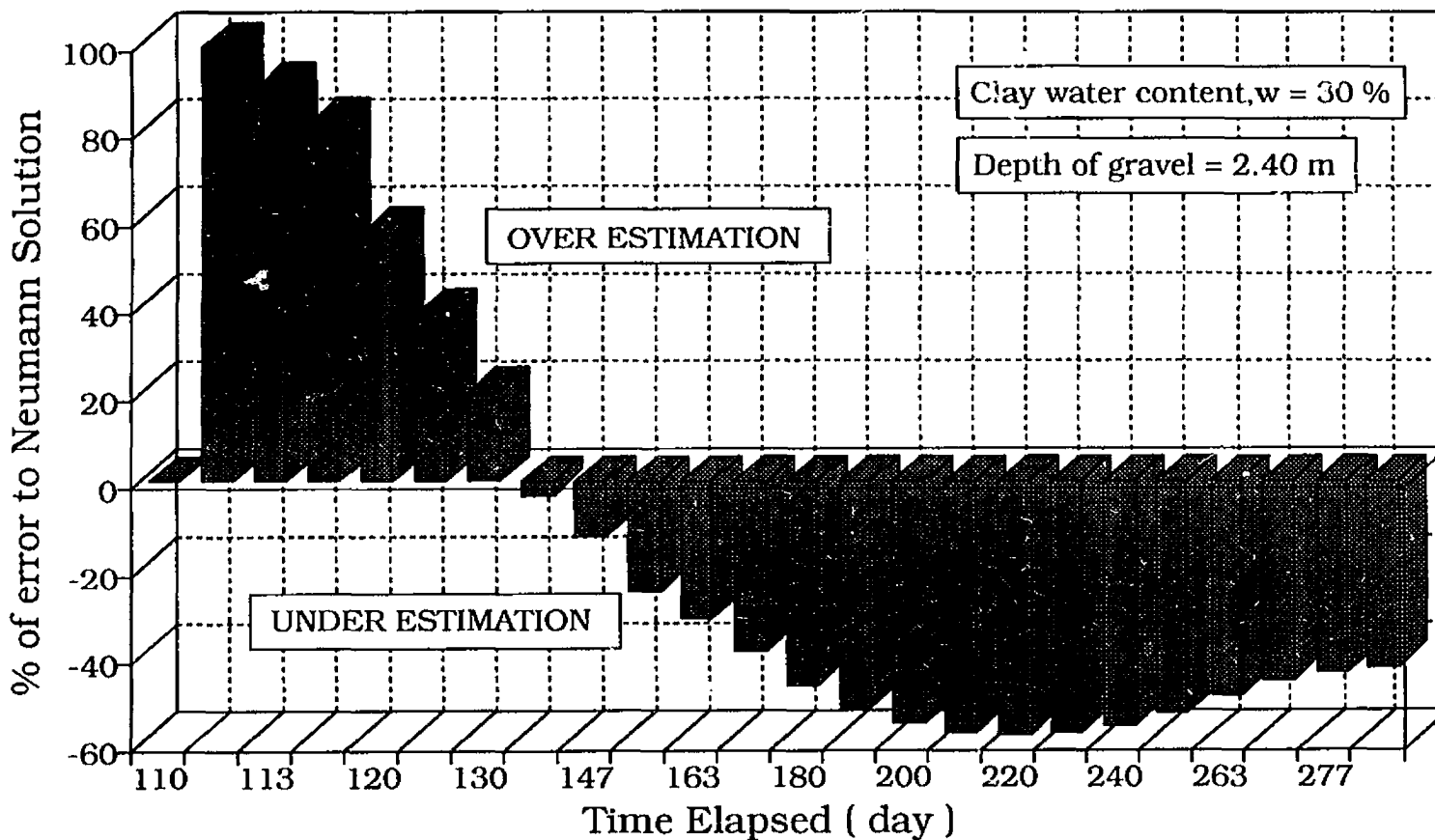


Fig. 4.41 Percentage of Error Between the Numerical and Neumann Solutions for Clay with Gravel on top

Pile in Peat Soil with Gravel on top

April 20, Mesh - 2 -

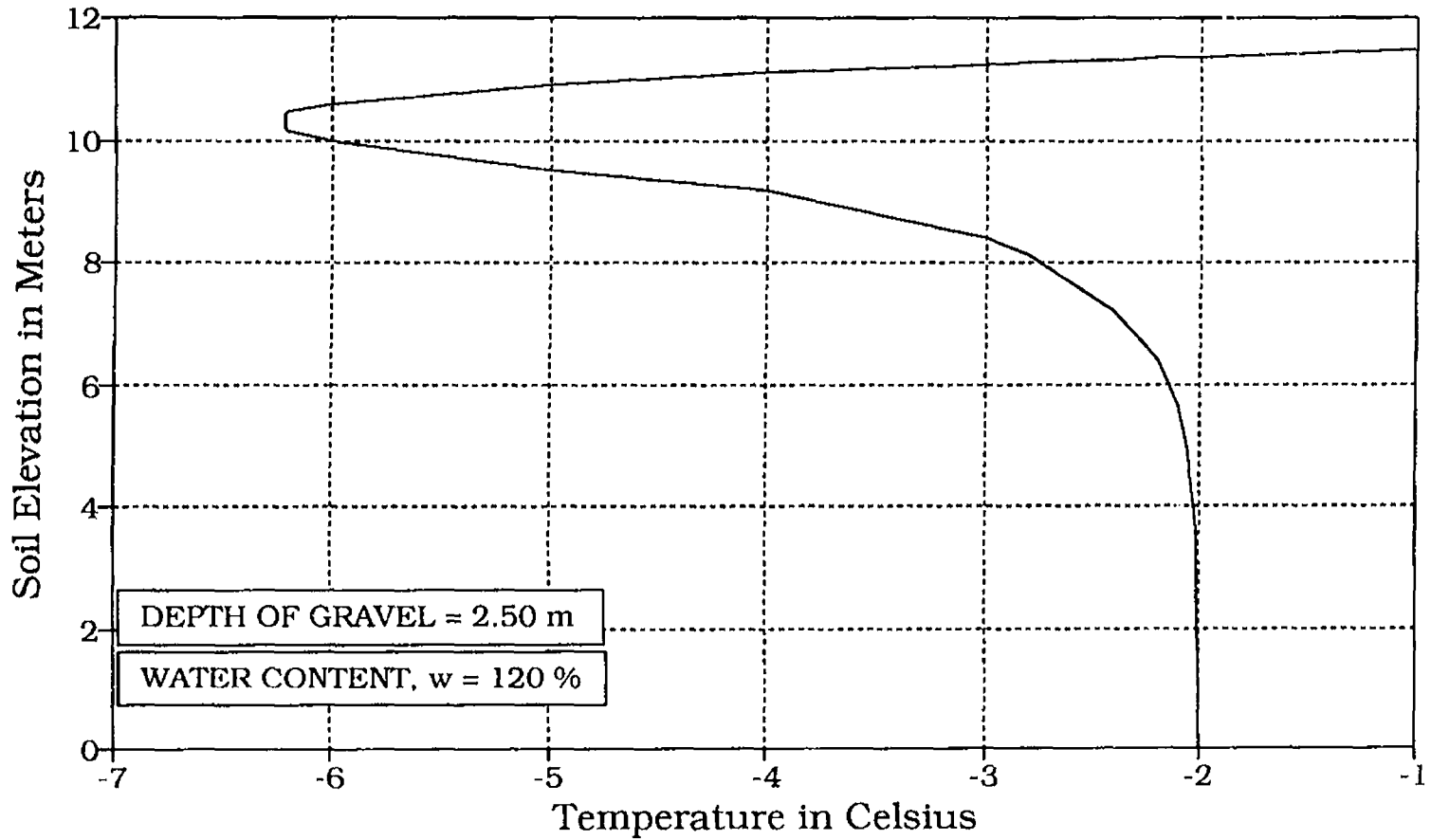


Fig. 4.42 Temperature Distribution for April 20 in Peat with Gravel on Top

Pile in Peat Soil with Gravel on top

Zero Isotherm propagation around pile

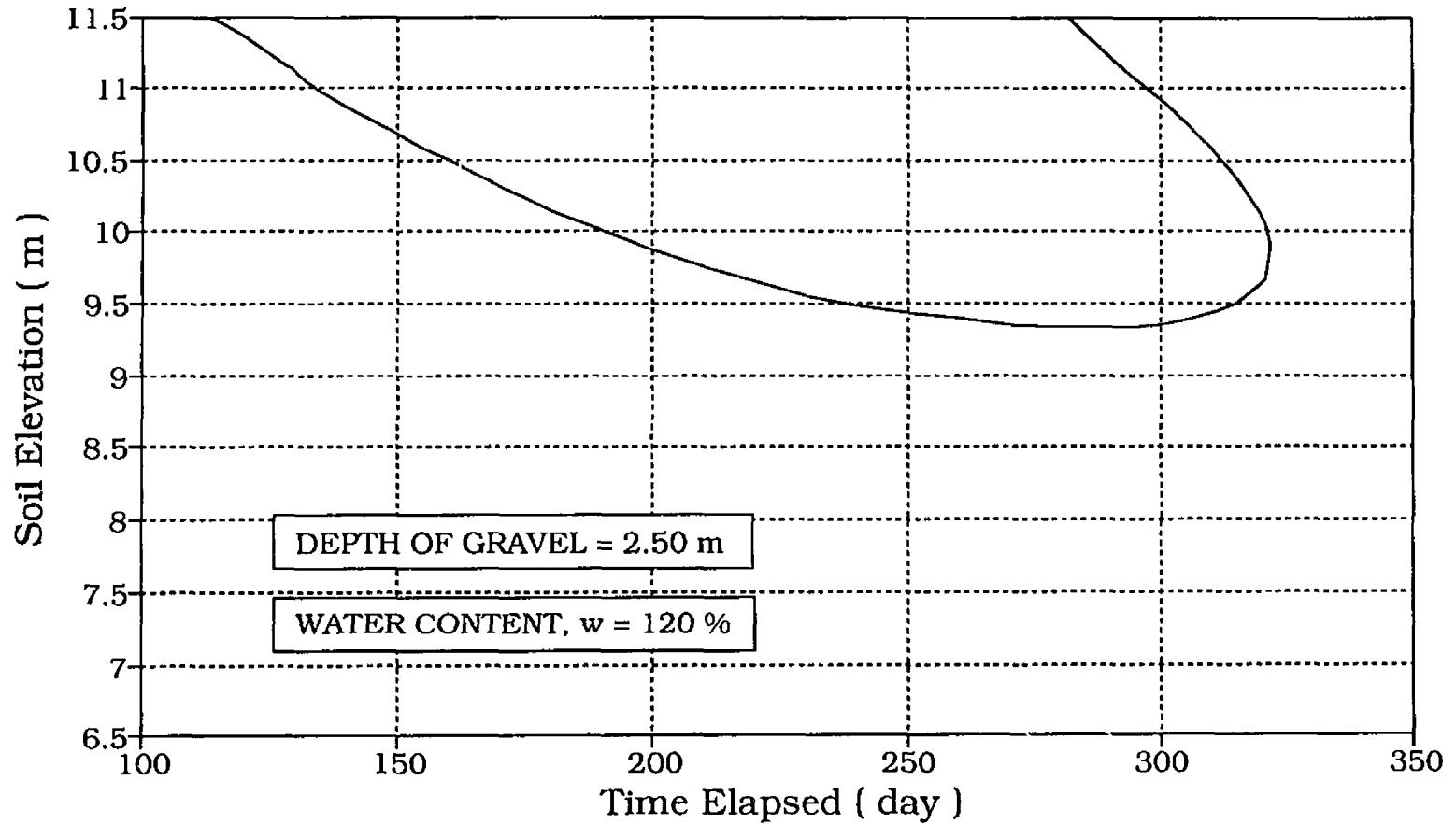


Fig. 4.43 0° C Isotherm Propagation in Peat with gravel on Top

Pile in Peat Soil with Gravel on top Comparative solution of thawing depth

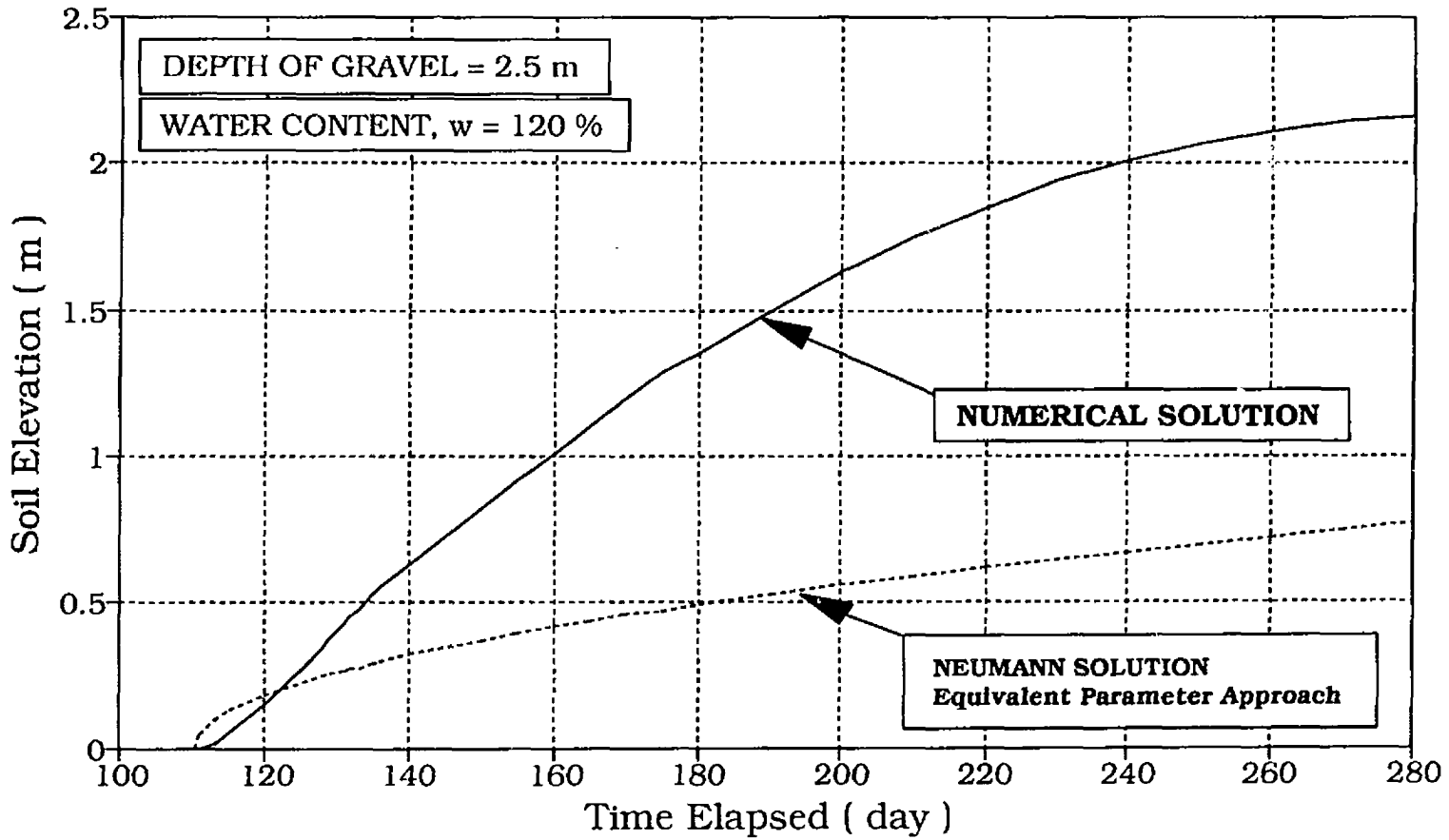


Fig. 4.44 Comparative Analysis Between the Numerical and Neumann Solutions for Pile Foundation in Peat with Gravel on top

Pile in Peat Soil with Gravel on top

Relative error to Neumann Solution

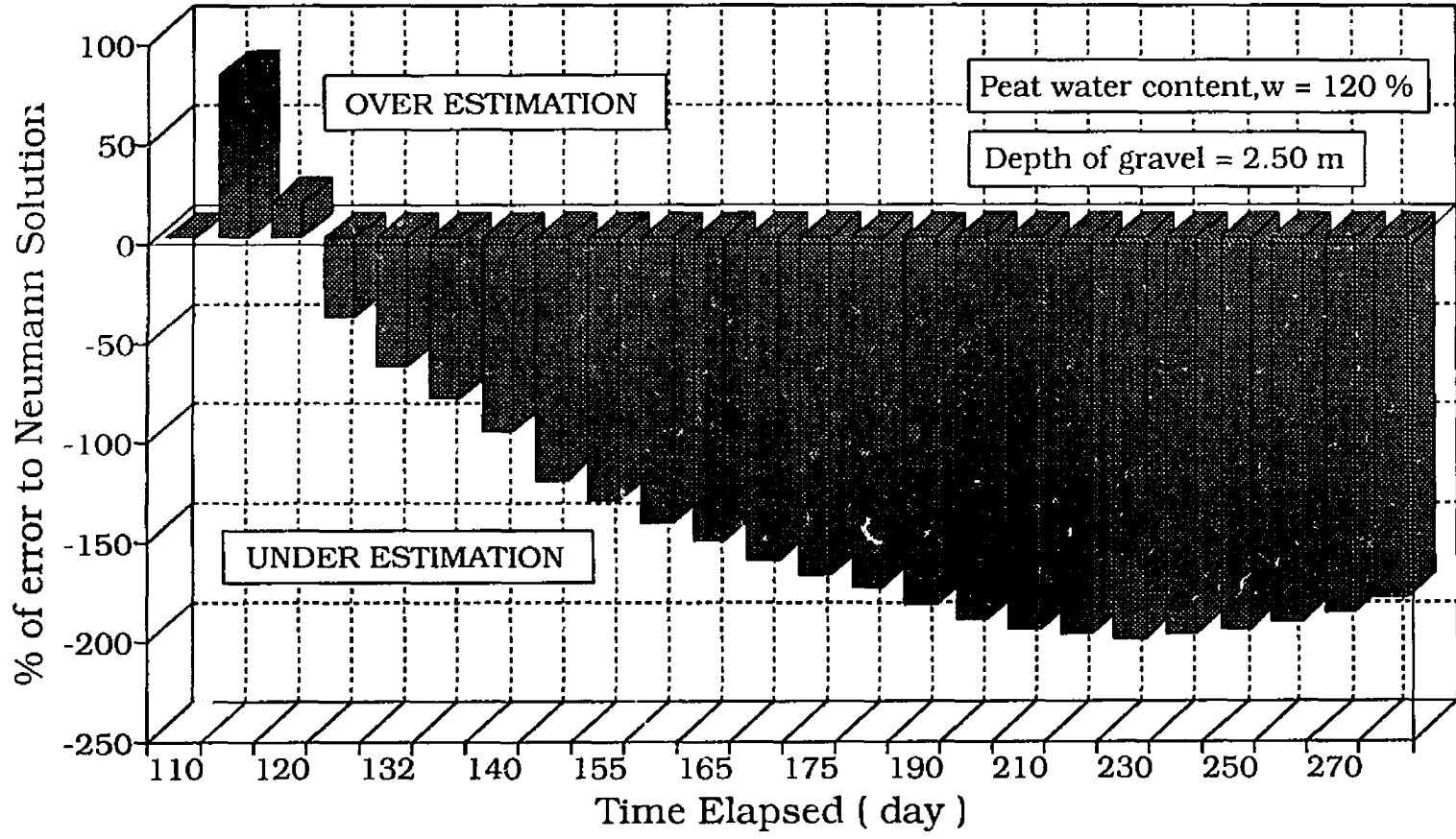


Fig. 4.45 Percentage of Error Between the Numerical and Neumann Solutions for Peat with Gravel on top

Pile in Sand with Gravel on Top, $w = 20\%$ Comparative solution of thawing depth

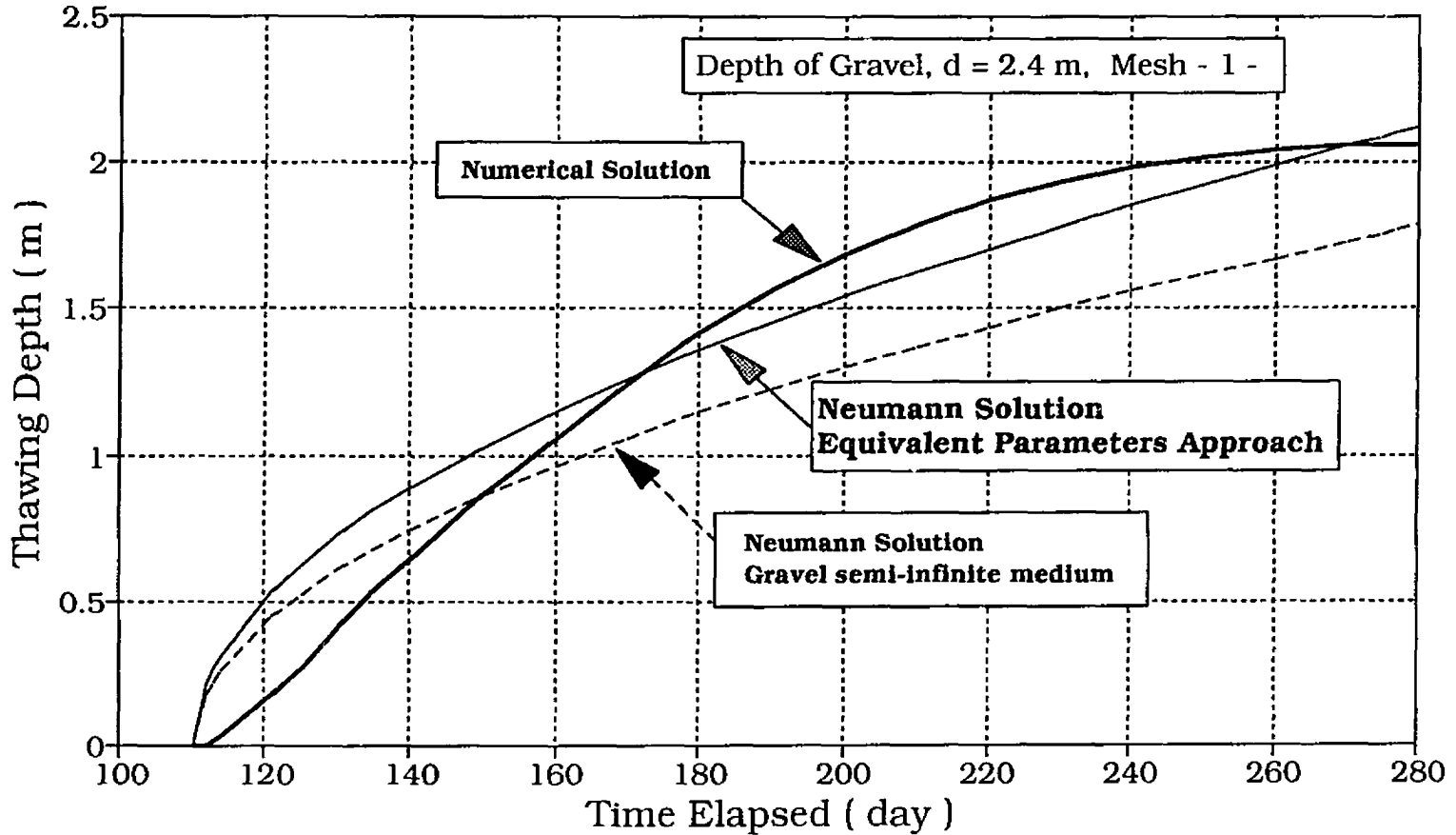


Fig. 4.46 Comparative Analysis Between the Numerical and Neumann Solutions for Pile Foundation in Sand with Gravel on top, as semi-infinite medium

Pile in Clay with Gravel on Top, $w = 30\%$

Comparative solution of thawing depth

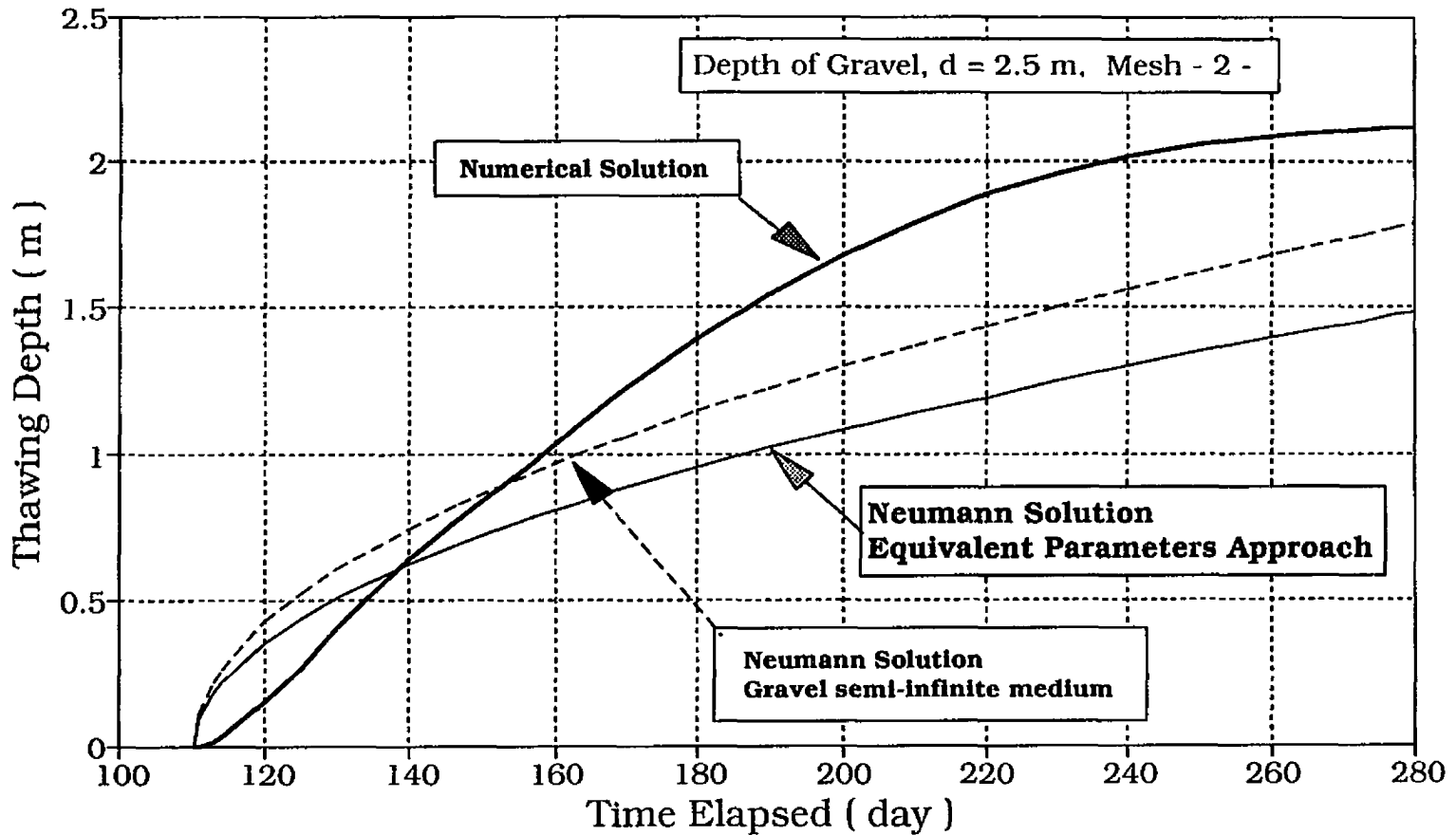


Fig. 4.47 Comparative Analysis Between the Numerical and Neumann Solutions for Pile Foundation in Clay with Gravel on top, as semi-infinite medium

Pile in Peat with Gravel on Top, $w = 120\%$ Comparative solution of thawing depth

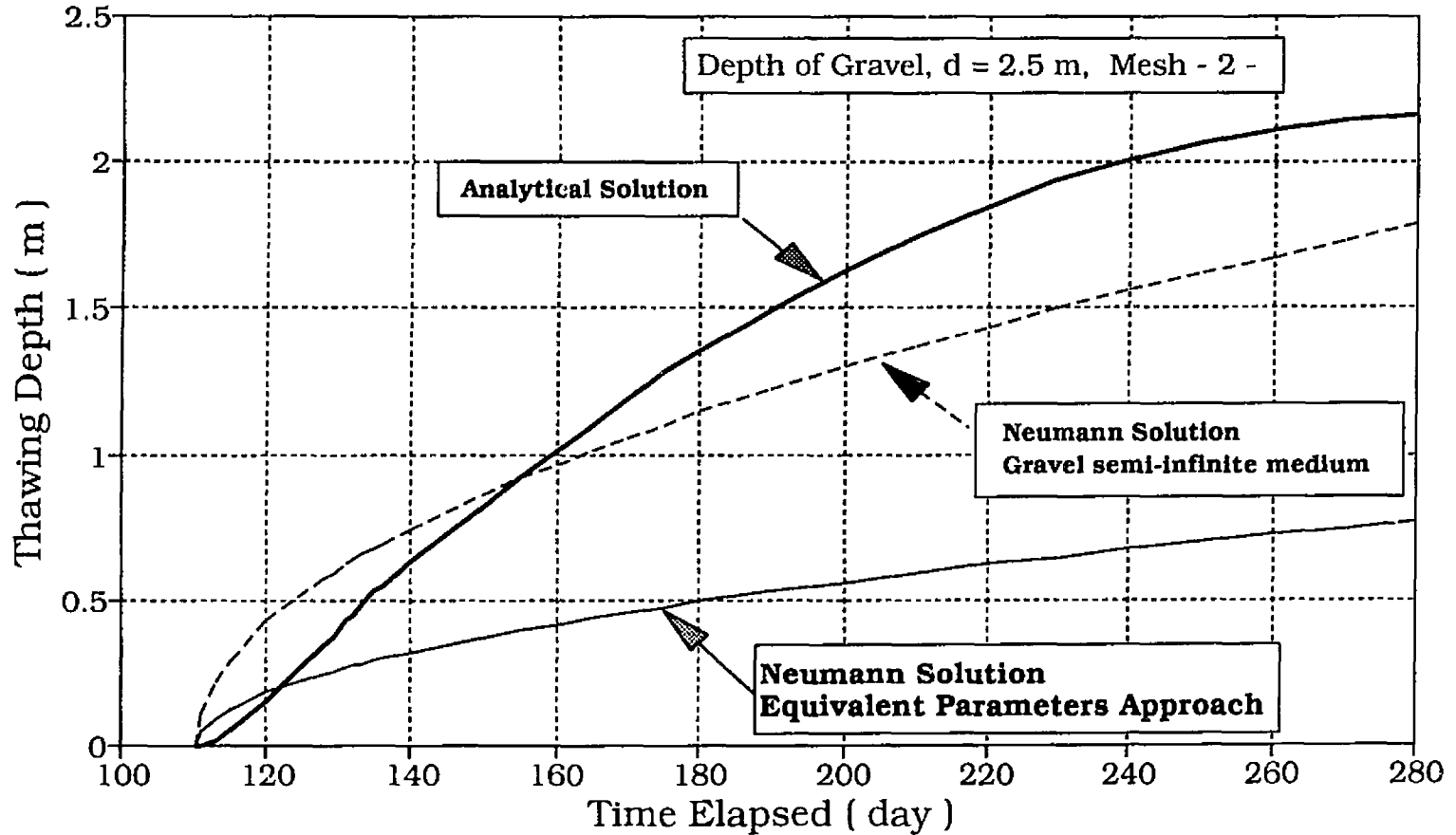


Fig. 4.48 Comparative Analysis Between the Analytical and Neumann Solutions for Pile Foundation in Peat with Gravel on top, as semi-infinite medium

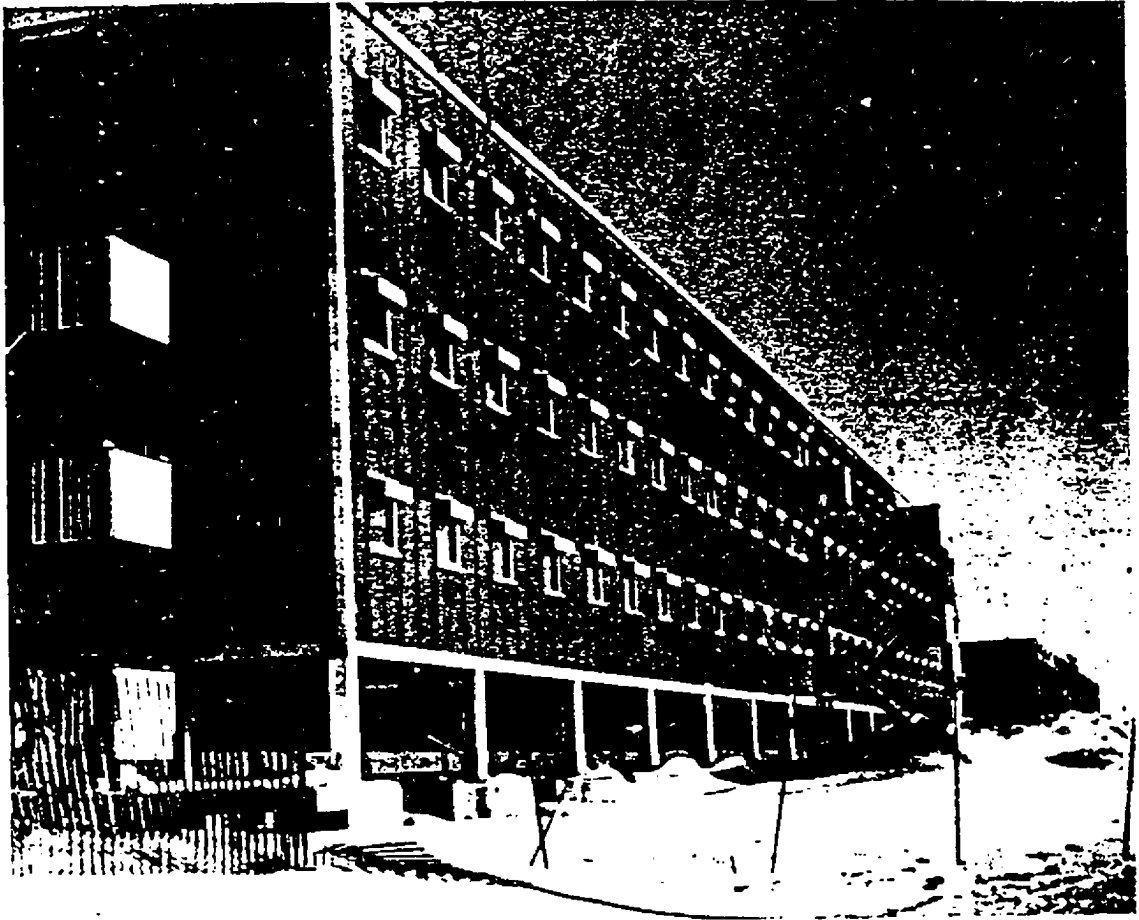


Fig. 6.1 Large Building on Pile Foundations. Timber piles Placed in 8 m Deep, Dry-Augered Holes backfilled with Compacted Saturated Sand (After Johnston, Edition 1981)

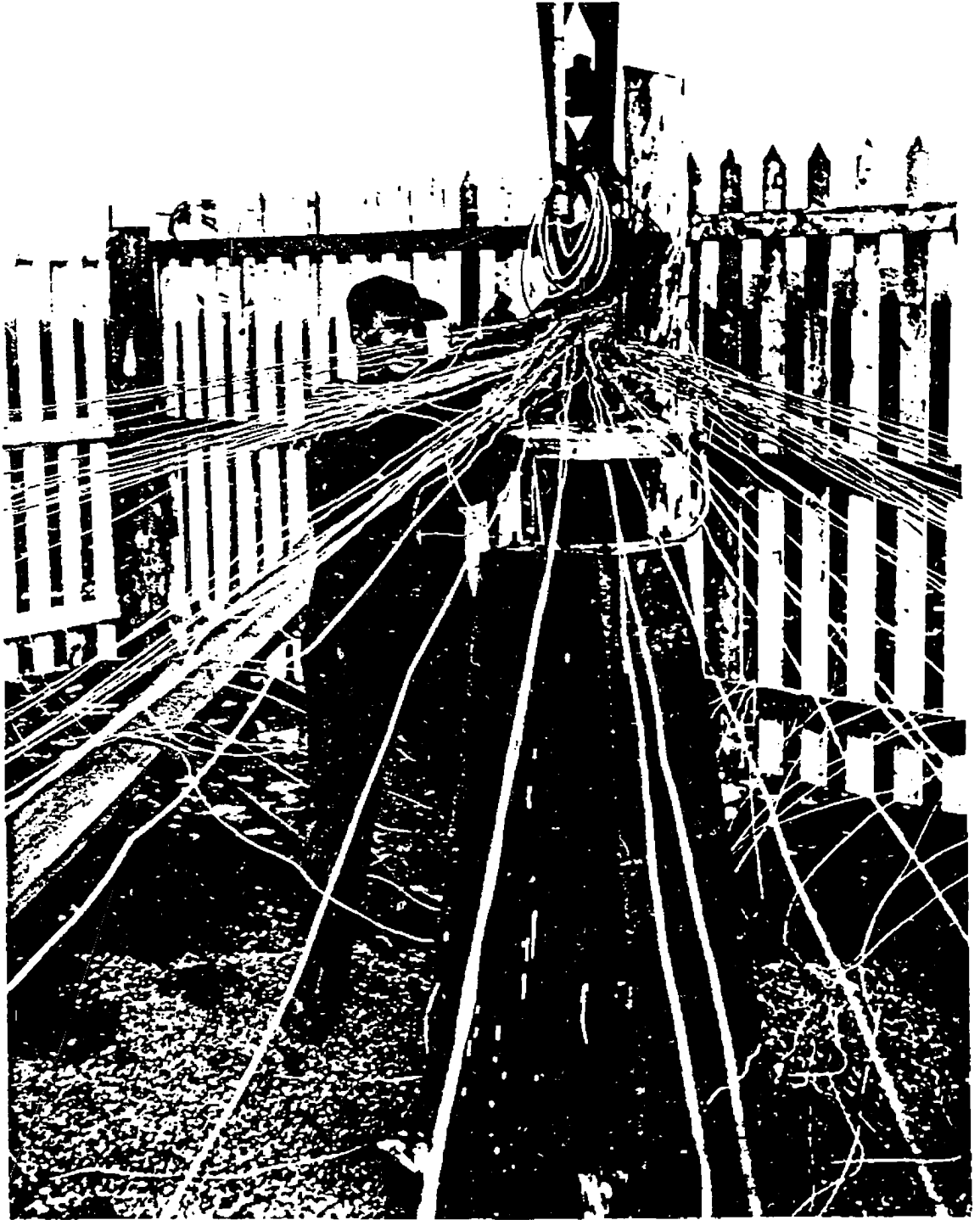


Fig. 6.2 Guyed Communication Tower, 50 m High, supported by a Single Timber Pile Placed to a depth of 8 m in Permafrost. Note Tapered Concrete Cap on top of Pile (*After Johnston, Edition 1981*)



Fig. 6.3 Unsuccessful Attempt to Drive 8 m Wood Piles. Note Treated Portion of Piles to be Placed in the Active Layer and Ground Temperature Cable Attached to Pile to monitor Freezeback (*After Johnston, Edition 1981*)

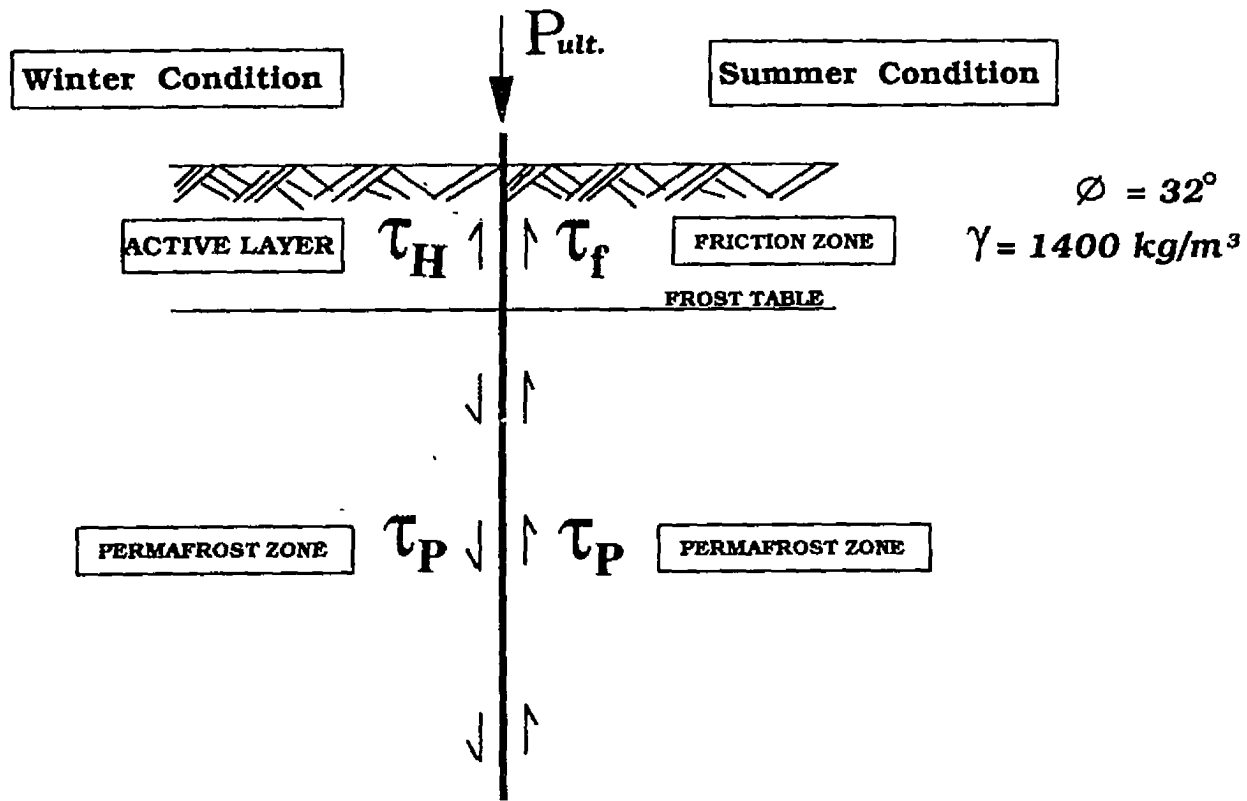


Fig. 6.4 Forces Acting on Pile Embedded in Sand for Summer and Winter Conditions.

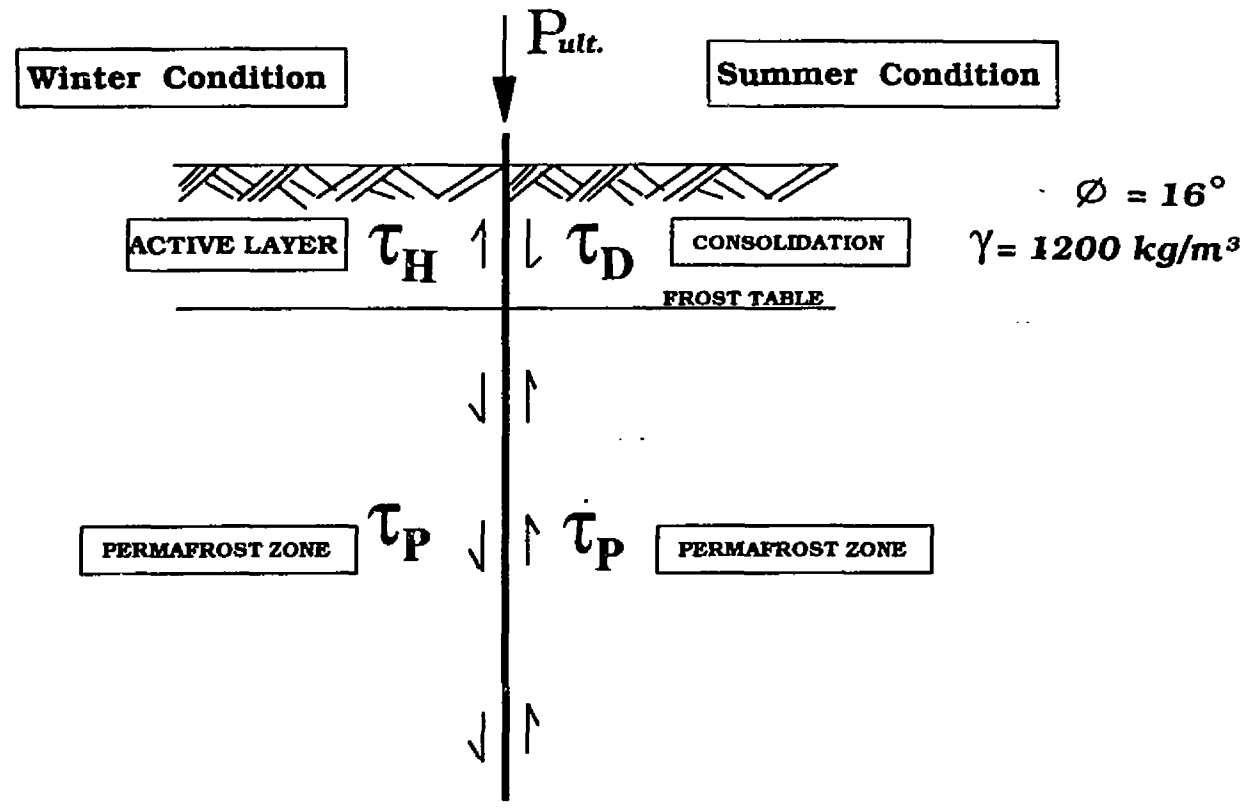


Fig. 6.5 Forces Acting on Pile Embedded in Clay for Summer and Winter Conditions.

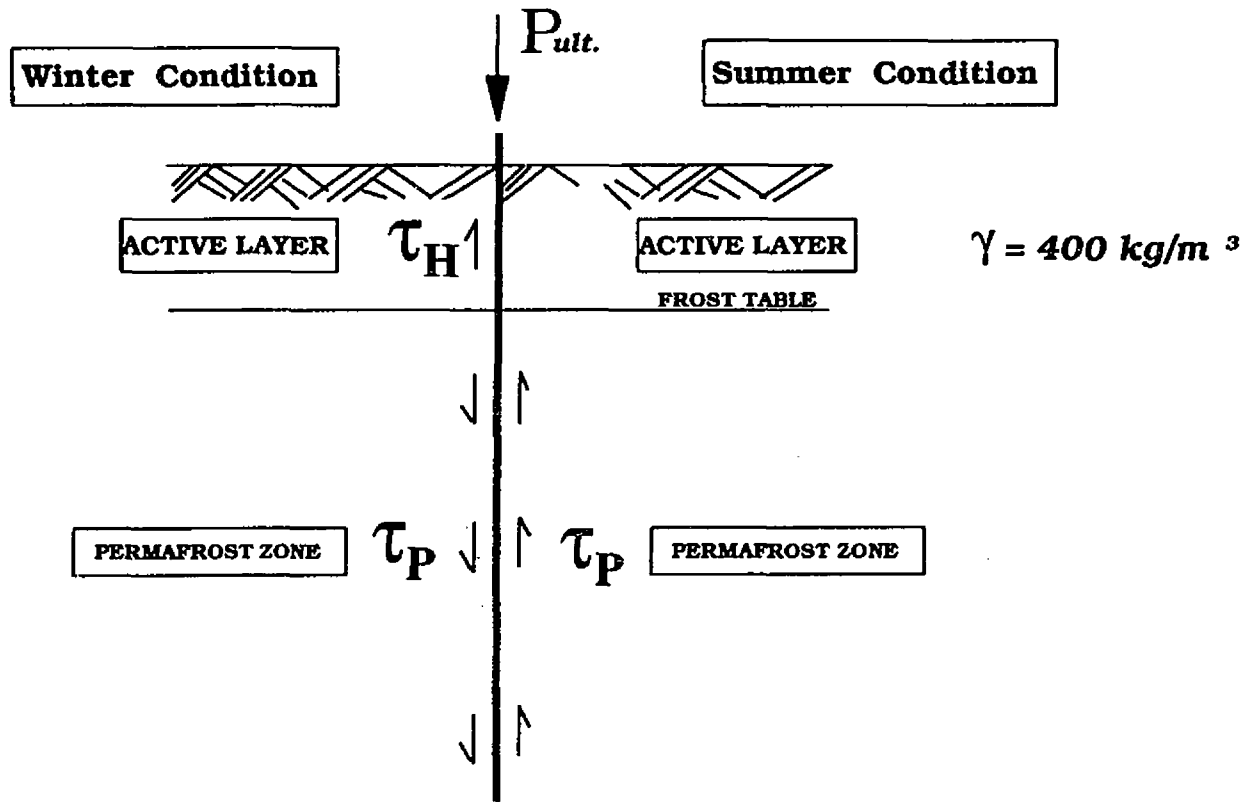


Fig. 6.6 Forces Acting on Pile Embedded in Peat for Summer and Winter Conditions.

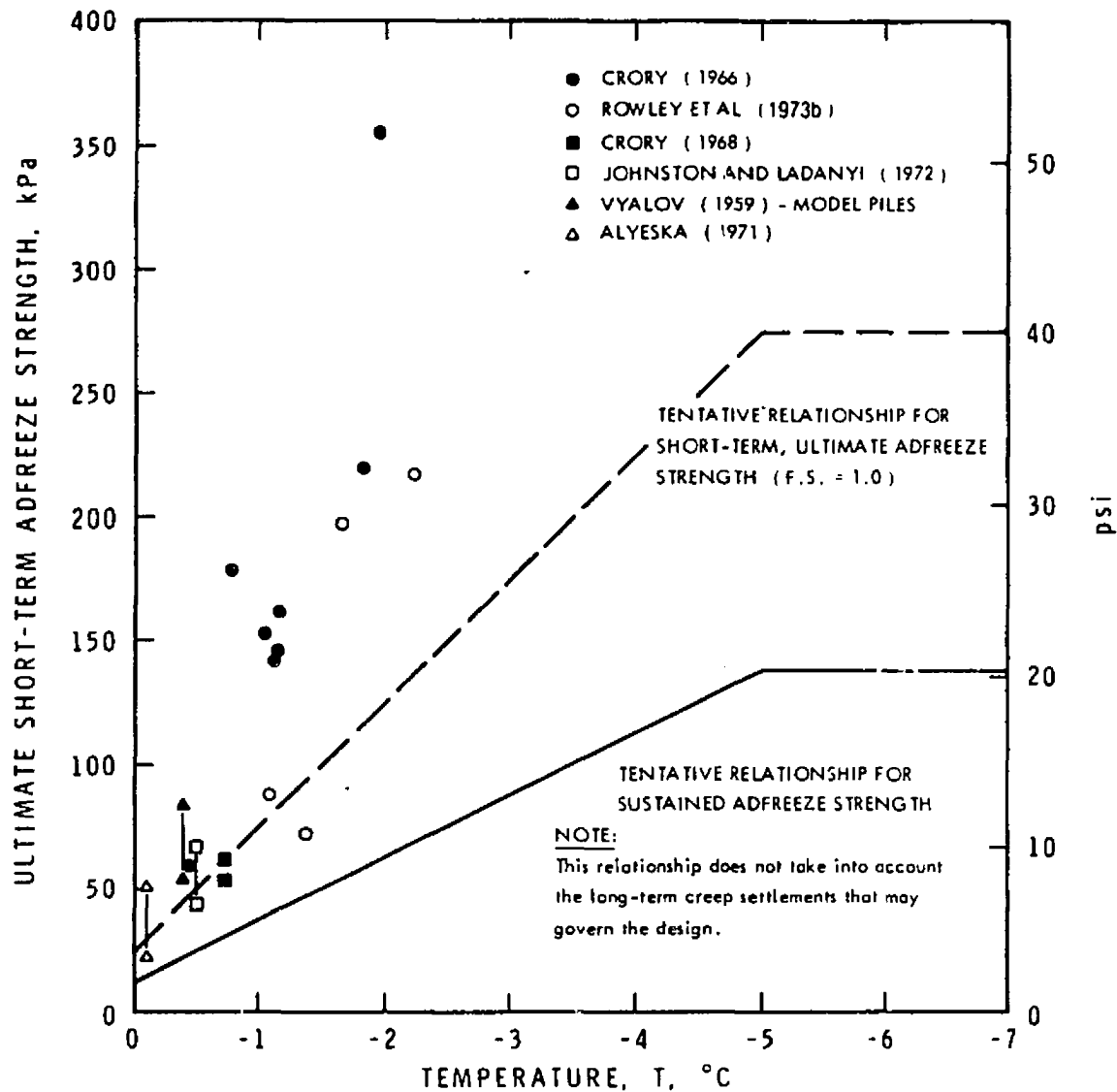


Fig. 6.7 Ultimate Short-Term and Sustained Adfreeze Strengths for Wood and Steel Piles in Frozen Clay and Silts (After Johnston, Edition 1981)

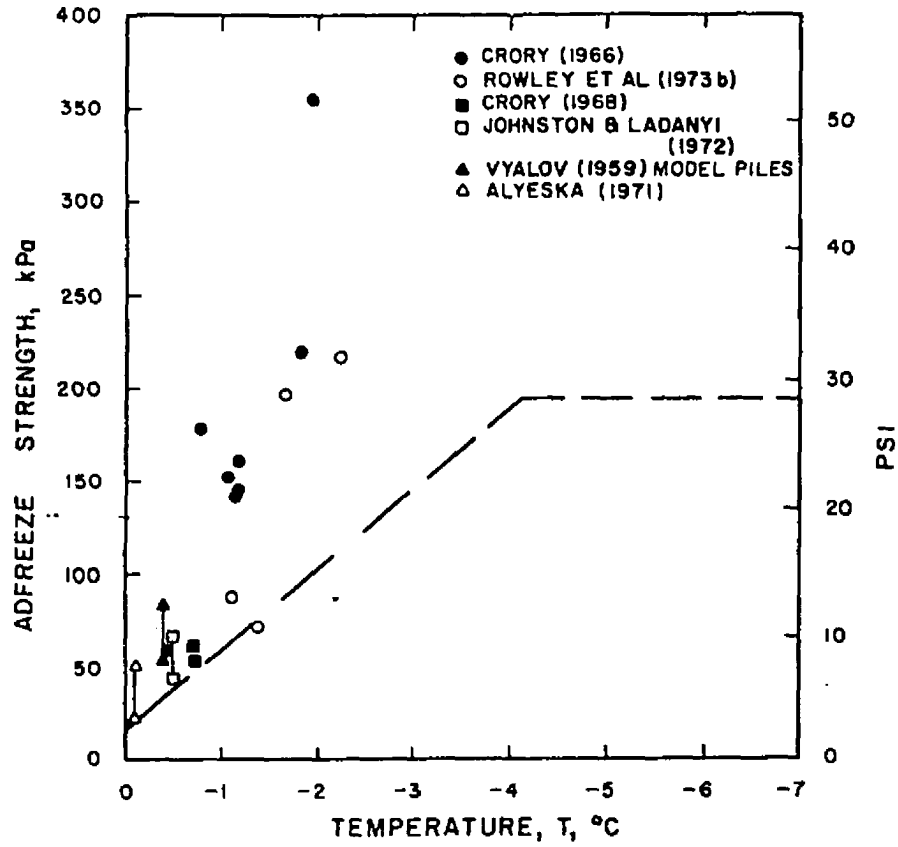


Fig. 6.8 Recommended Adfreeze Strength of Soil Interface, Modified from Johnston, 1981 (After Phukan, 1985)

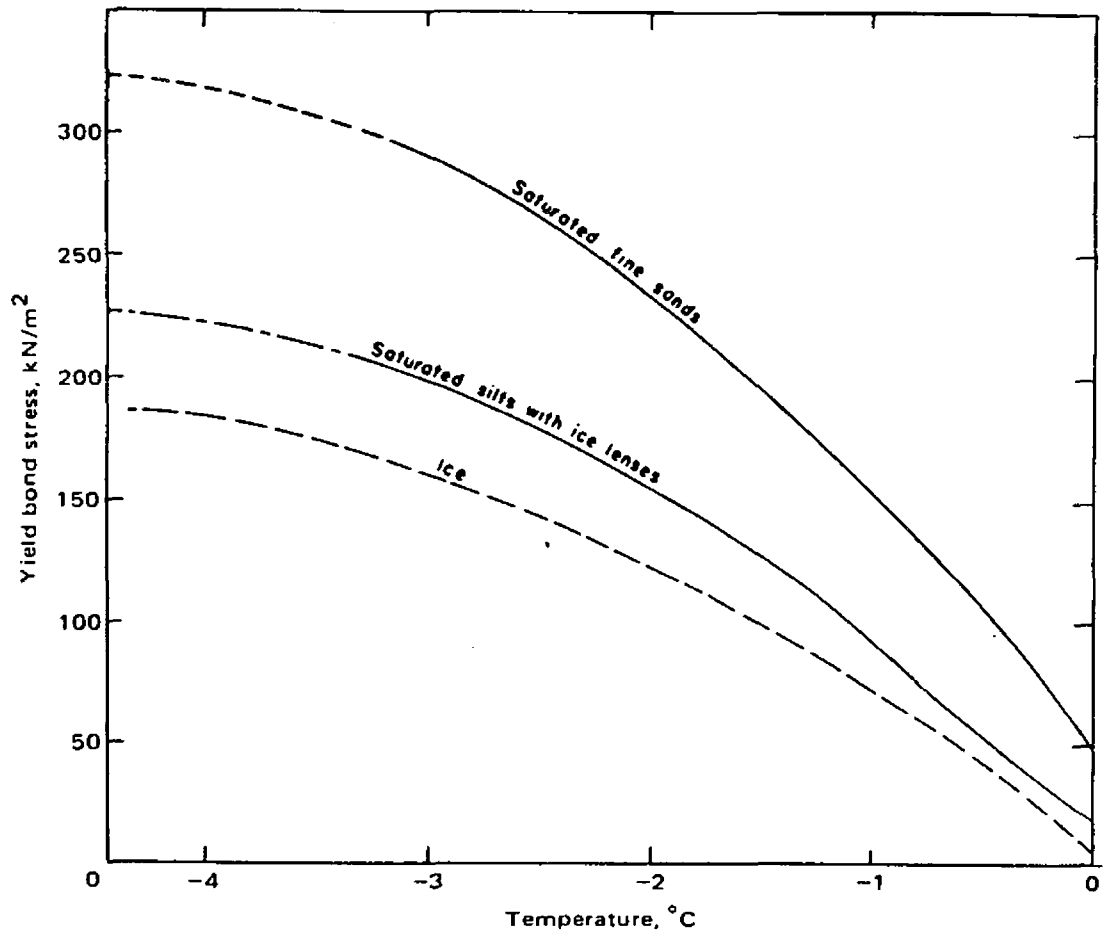


Fig. 6.9 Tentative Ultimate Adfreeze Bond Strength in Creep for Saturated Soils. (*Adapted from Sanger, 1969*)

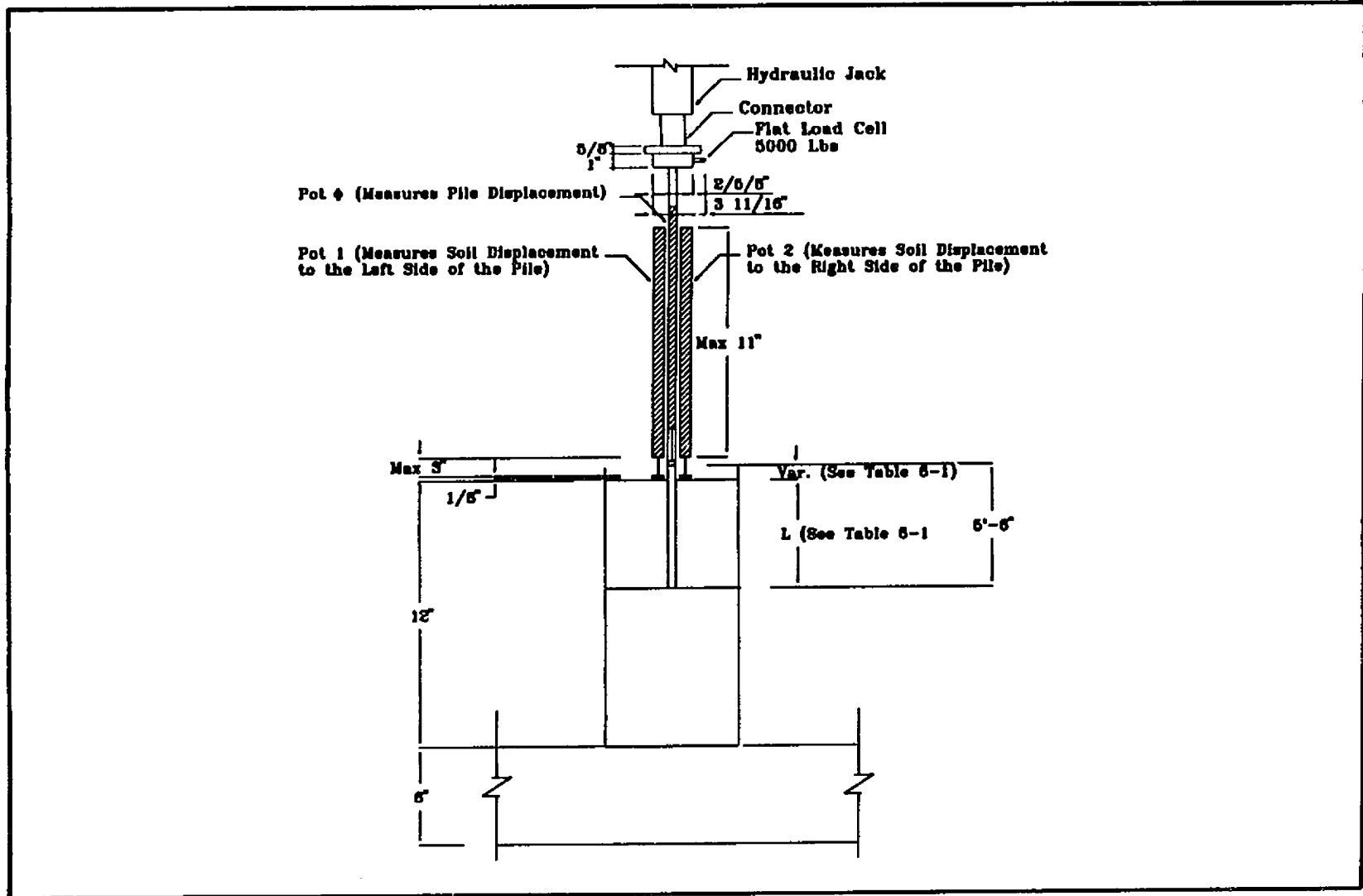


Fig. 6.10 Adfreeze Strength Frame Loading System

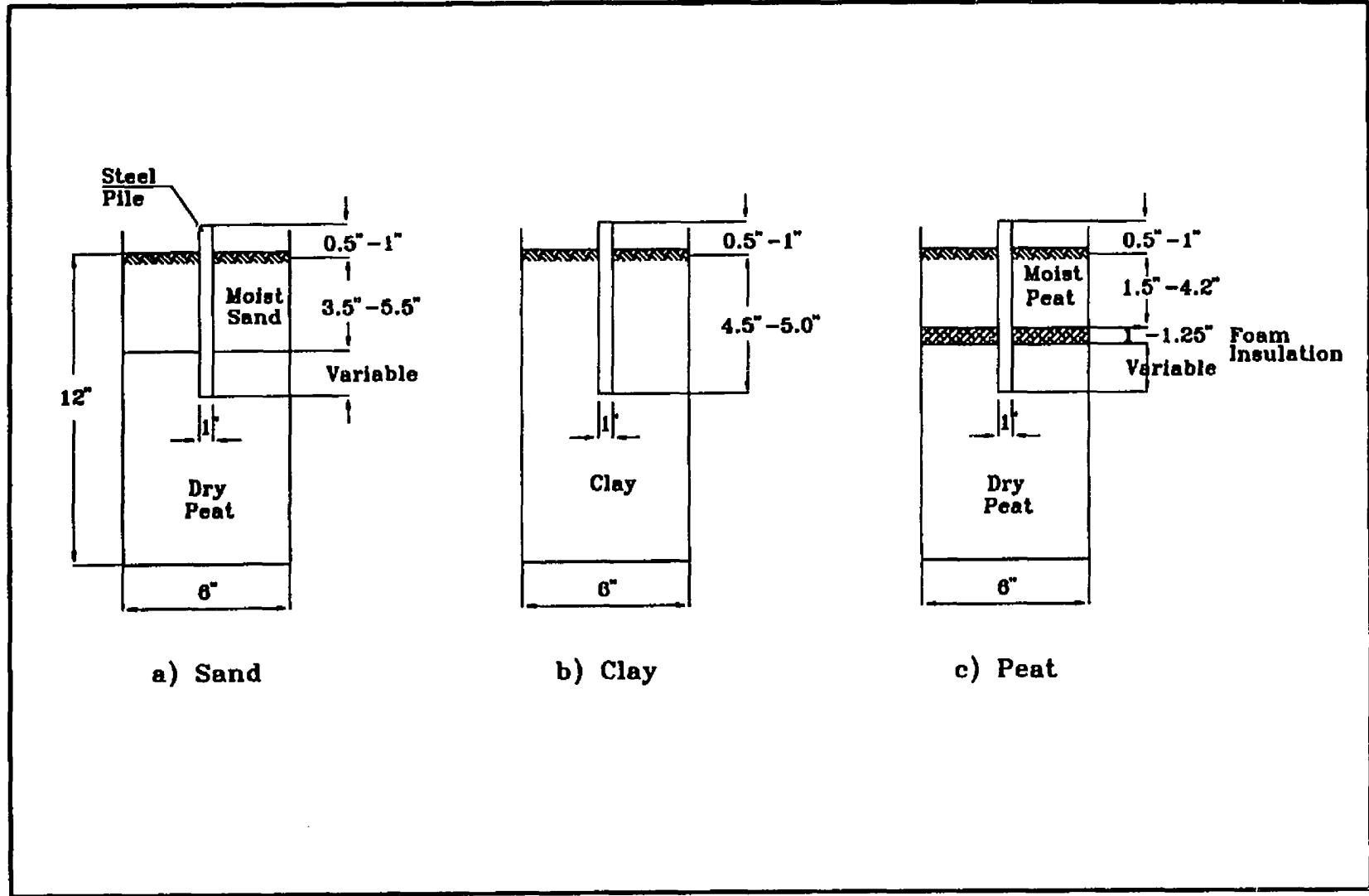


Fig. 6.11 Laboratory Testing Disposition for Pile Embedded in Sand, Clay and Peat Soils

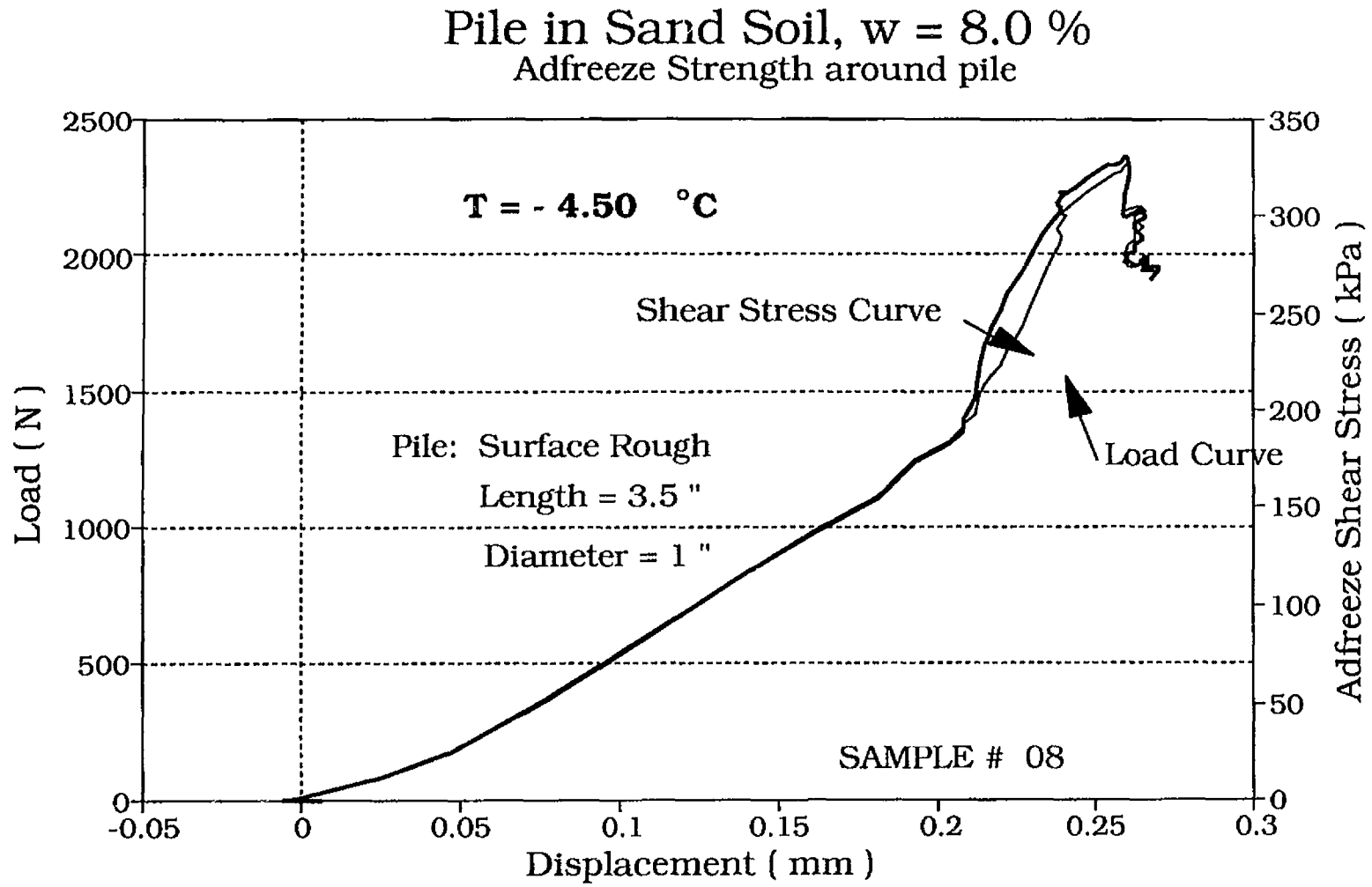


Fig. 6.13 Adfreeze Strength for Sample # 8

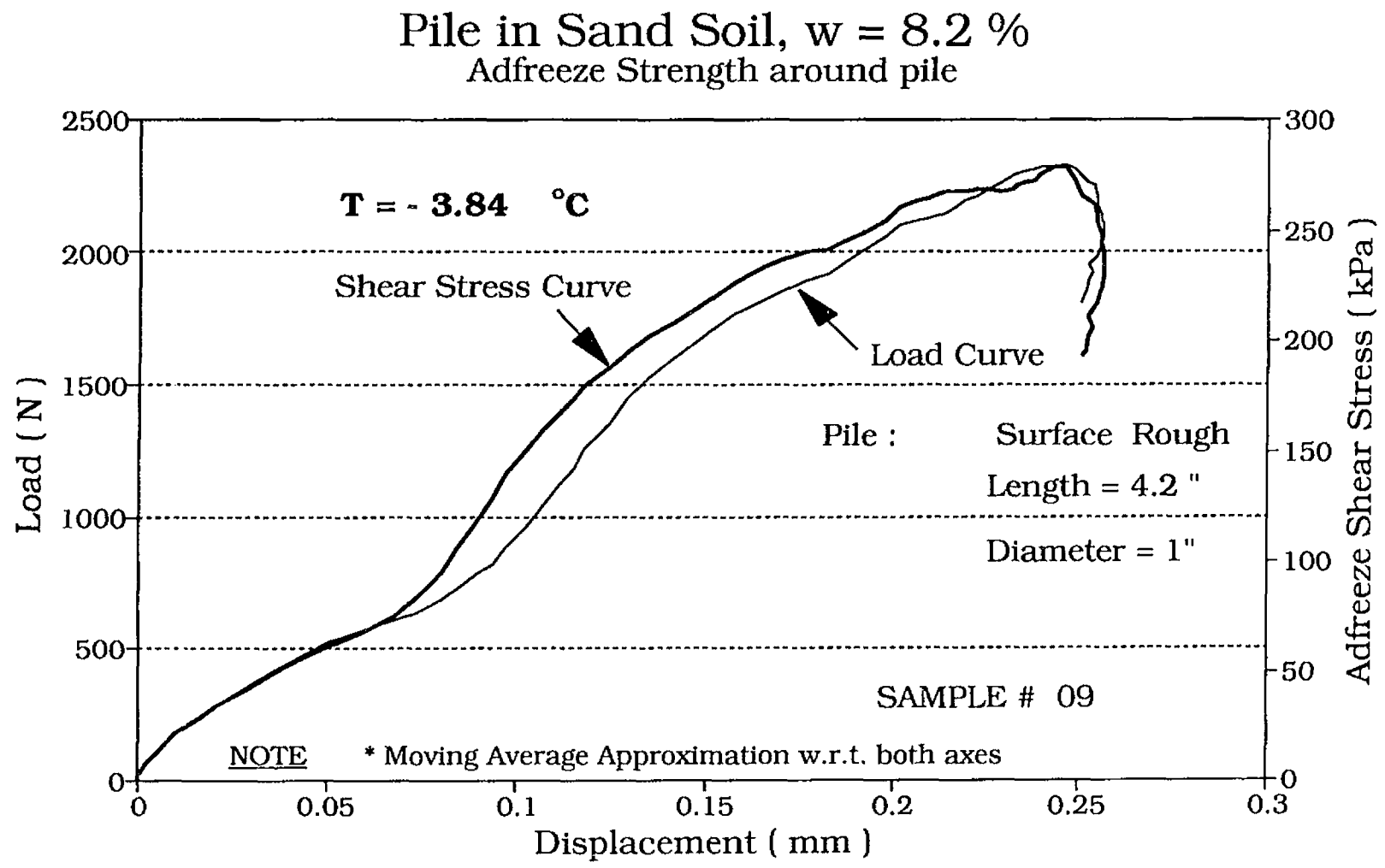


Fig. 6.14 Adffreeze Shear Strength for Sample # 9

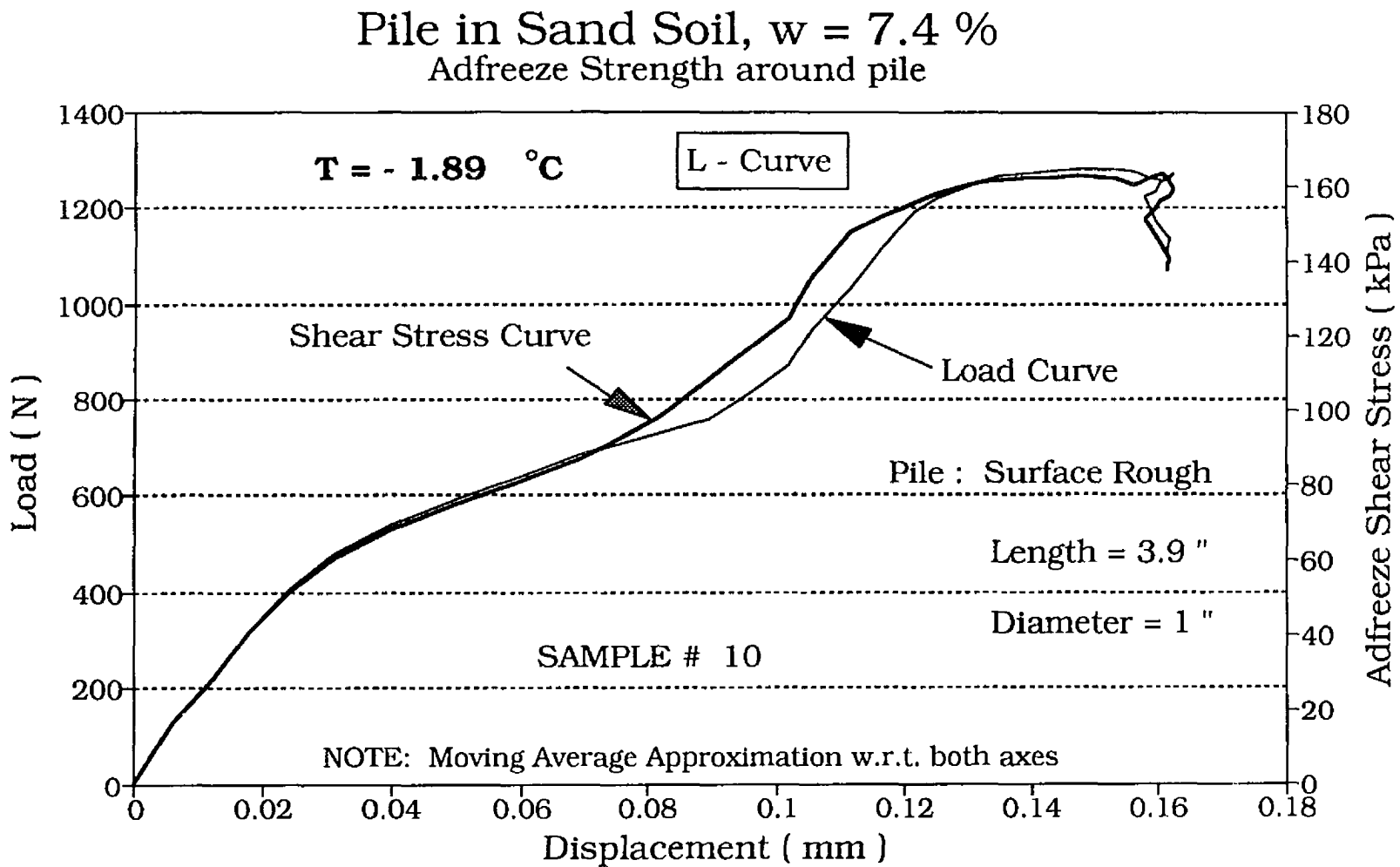


Fig. 6.15 Adfreeze Shear Strength for Sample # 10 - L Curve -

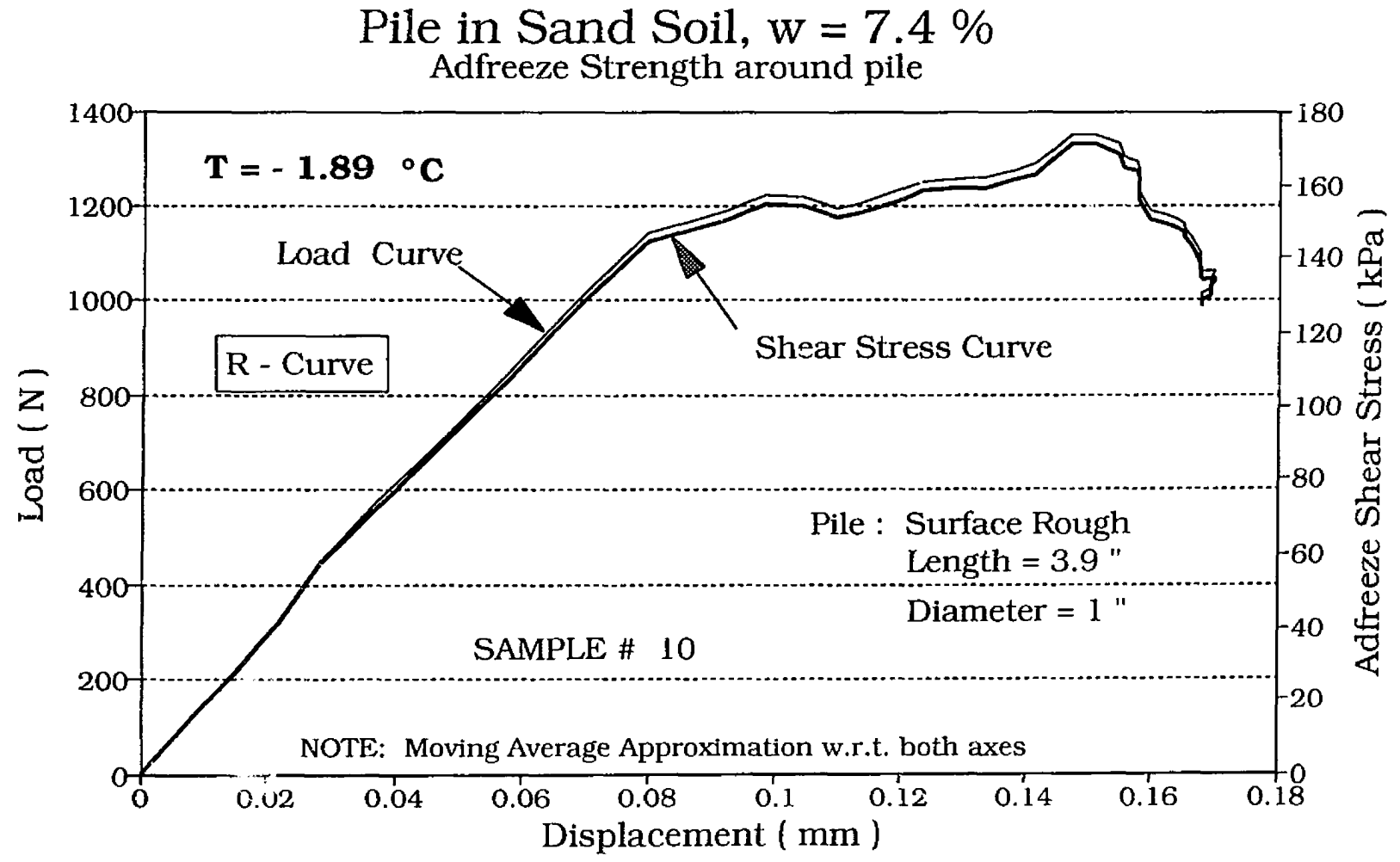


Fig. 6.16 Adfreeze Shear Strength for Sample # 10 - R Curve -

Pile in Sand Soil, $w = 8.0\%$ Adfreeze Strength around pile

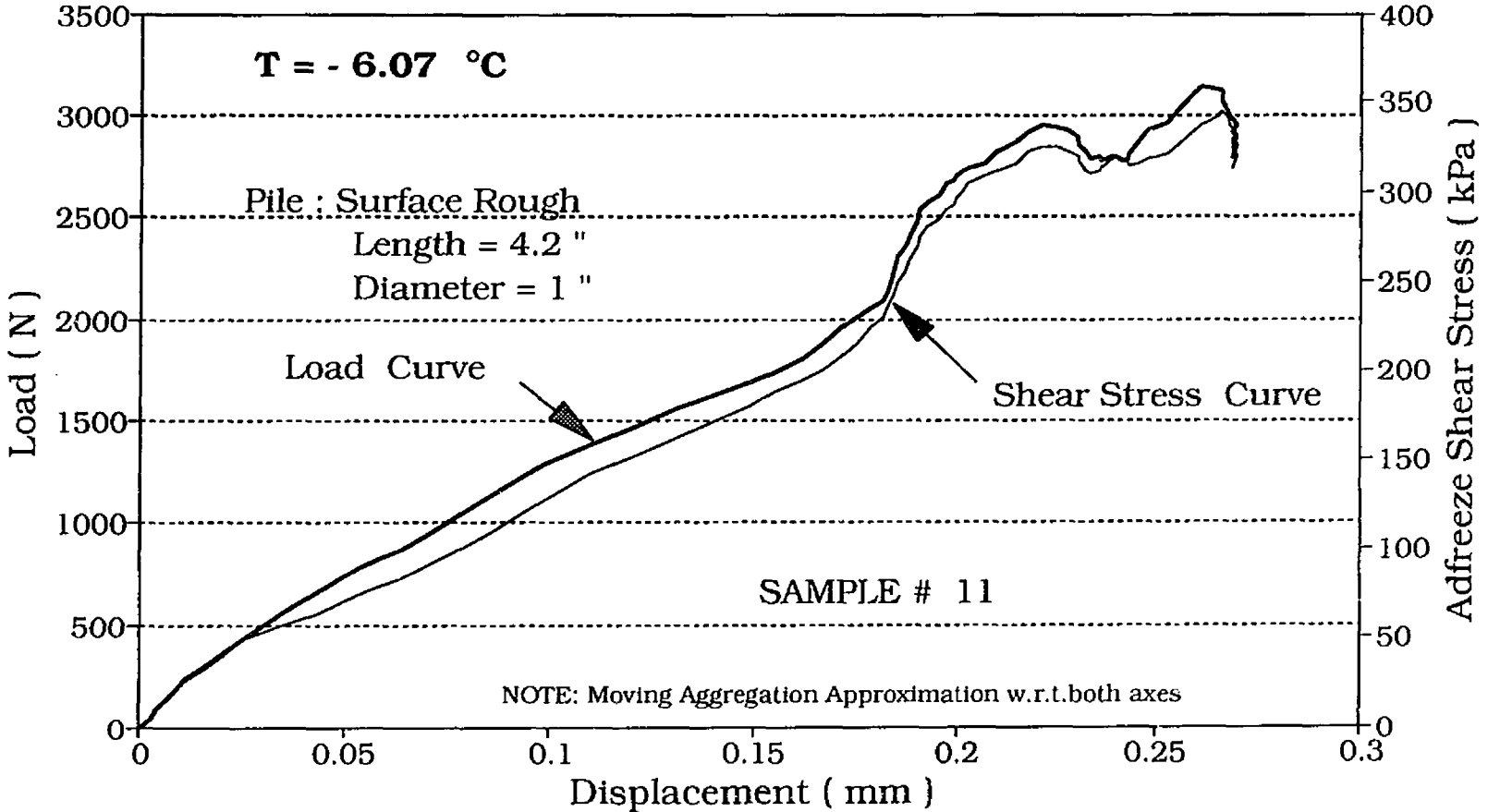


Fig. 6.17 Adfreeze Shear Strength for Sample # 11

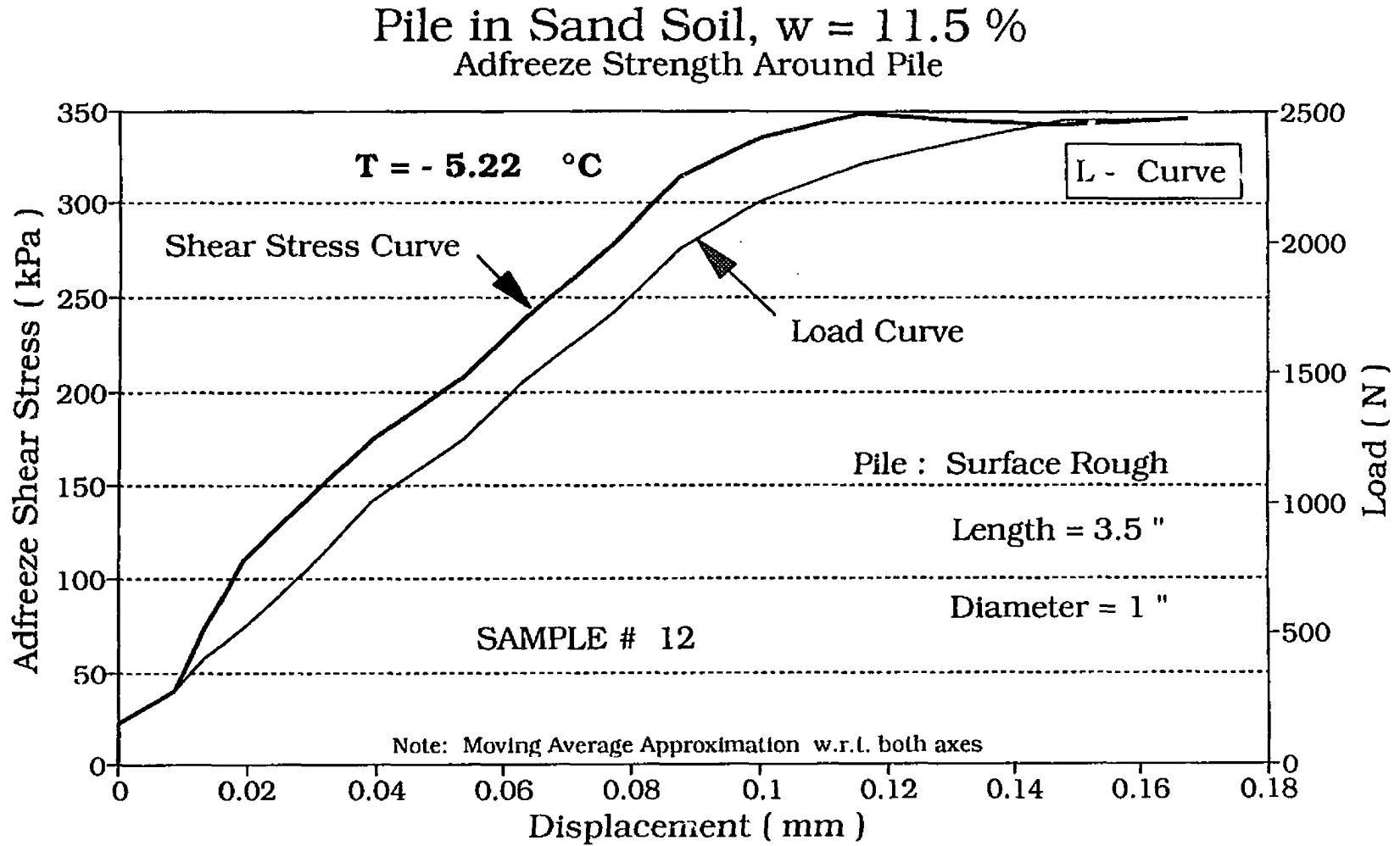


Fig. 6.18 Adfreeze Shear Strength for Sample # 12

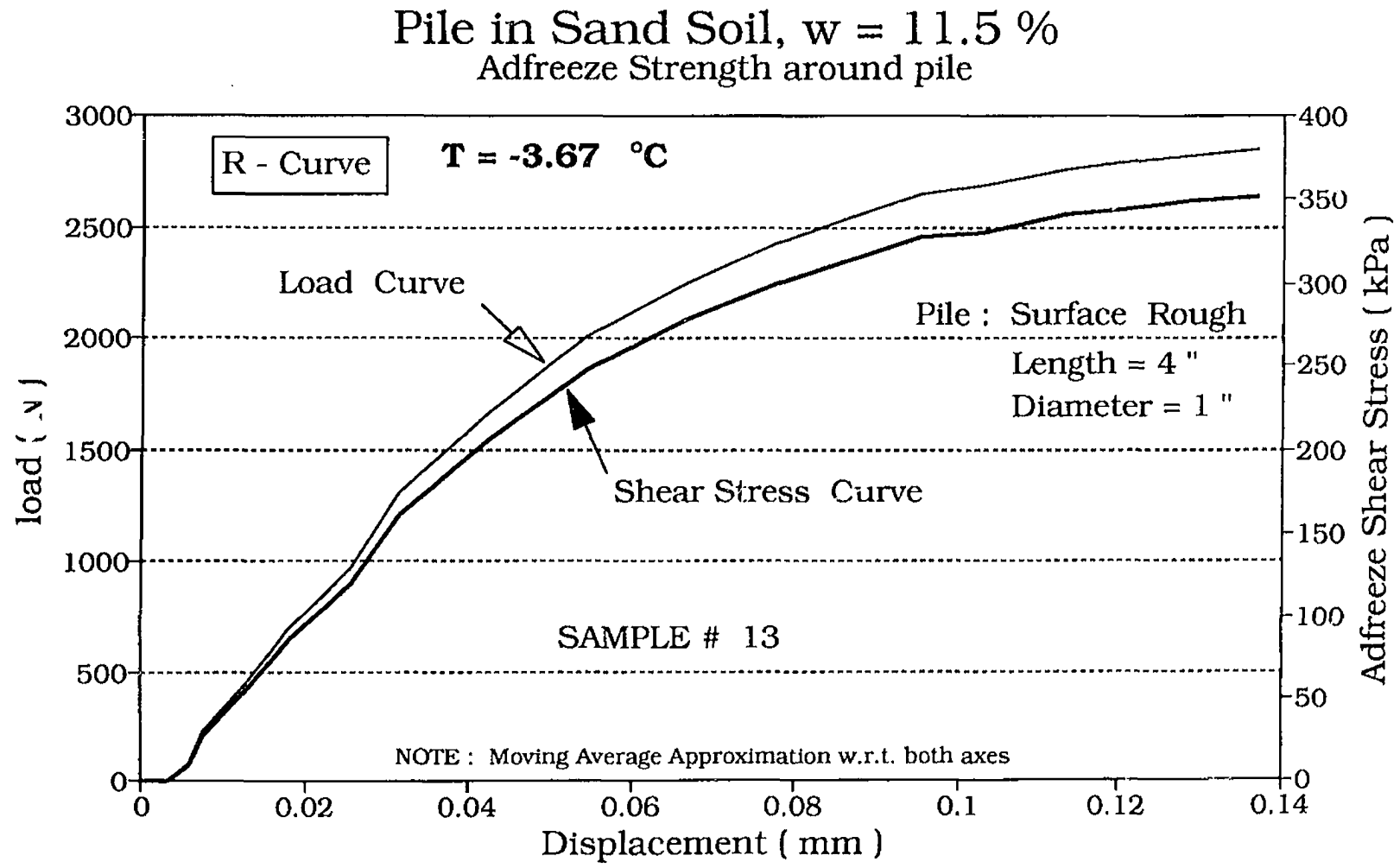


Fig. 6.19 Adfreeze Shear Strength for Sample # 13

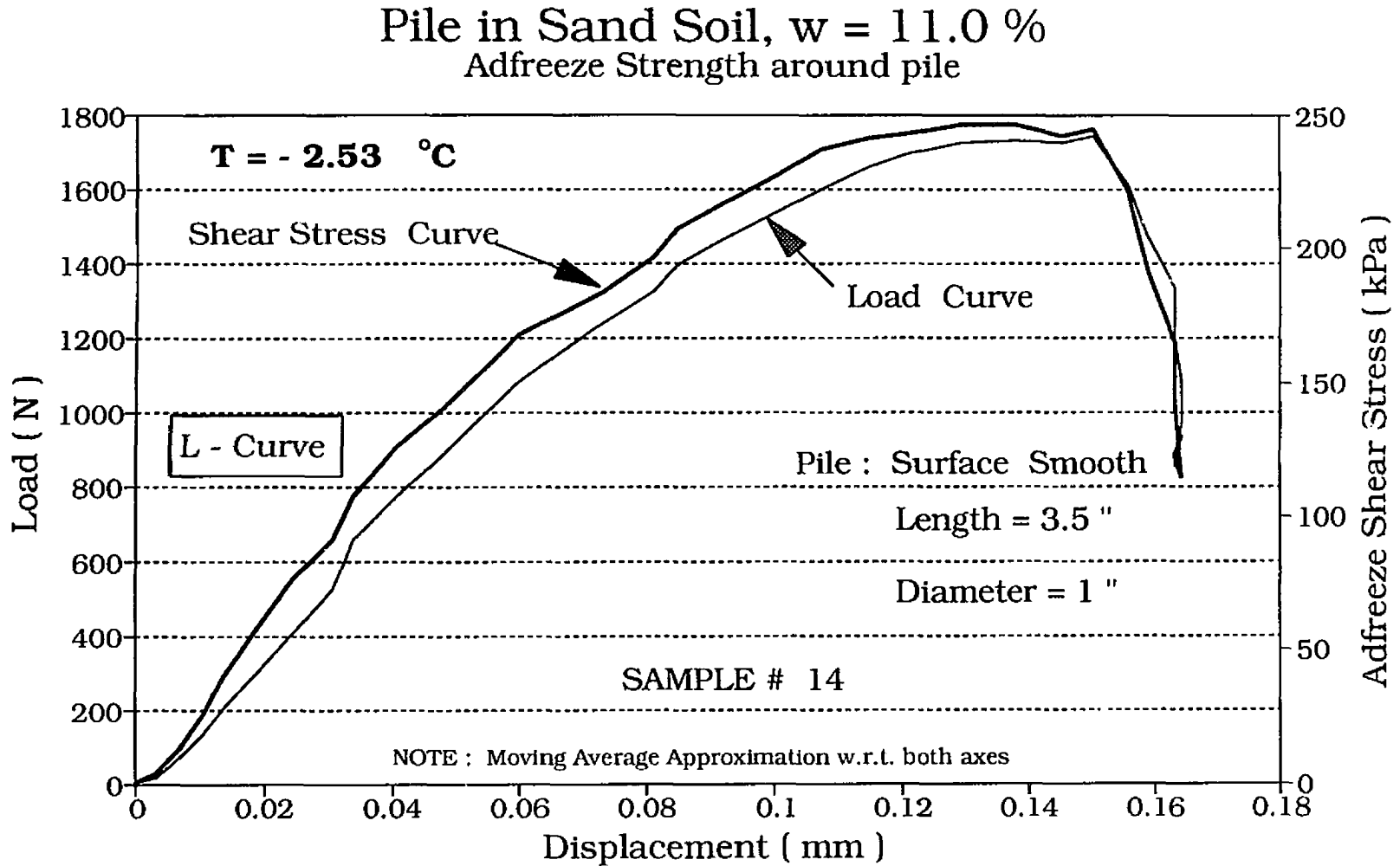


Fig. 6.20 Adfreeze Strength for Sample # 14 - L Curve -

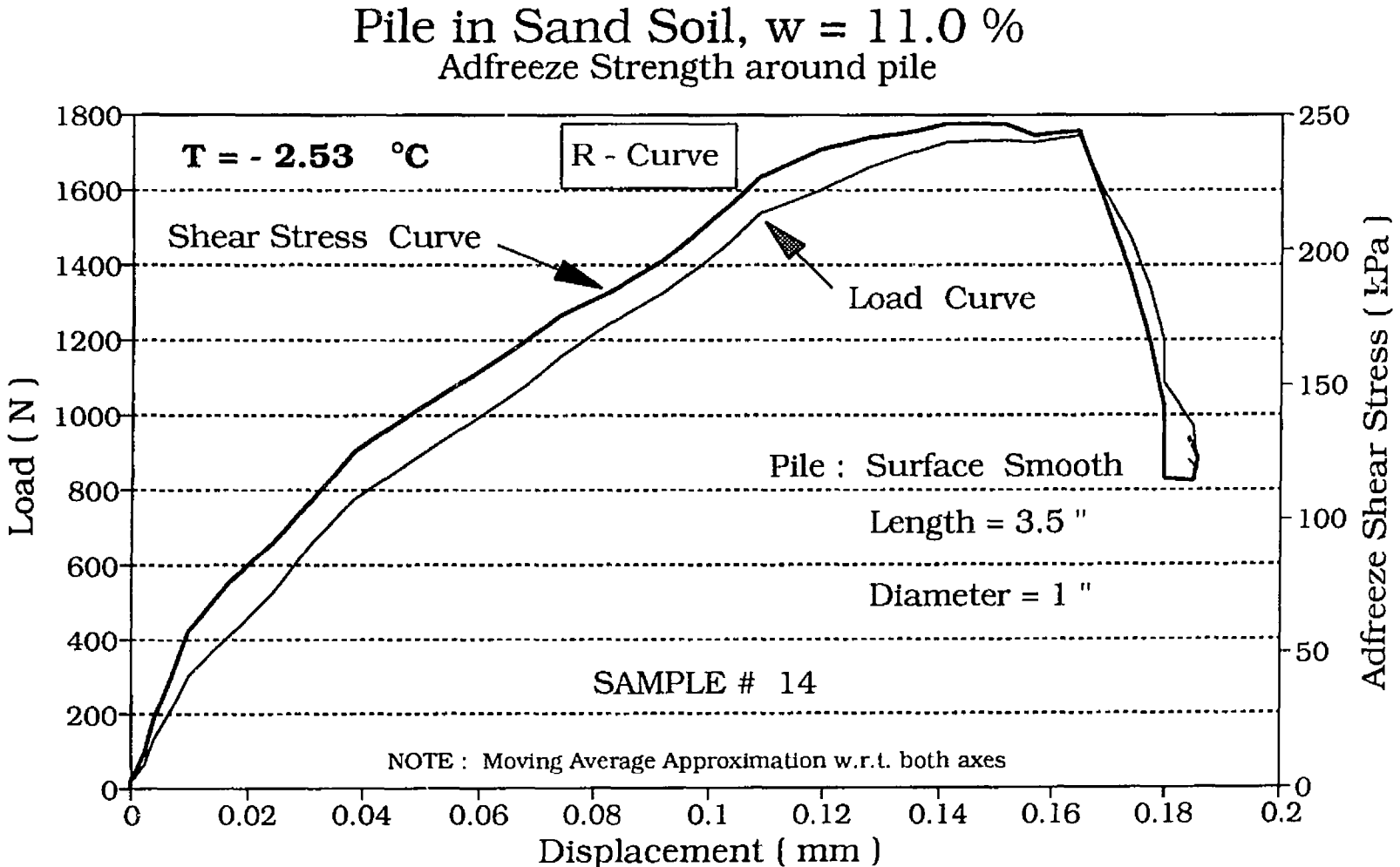


Fig. 6.21 Adfreeze Strength for Sample # 14 - R Curve -

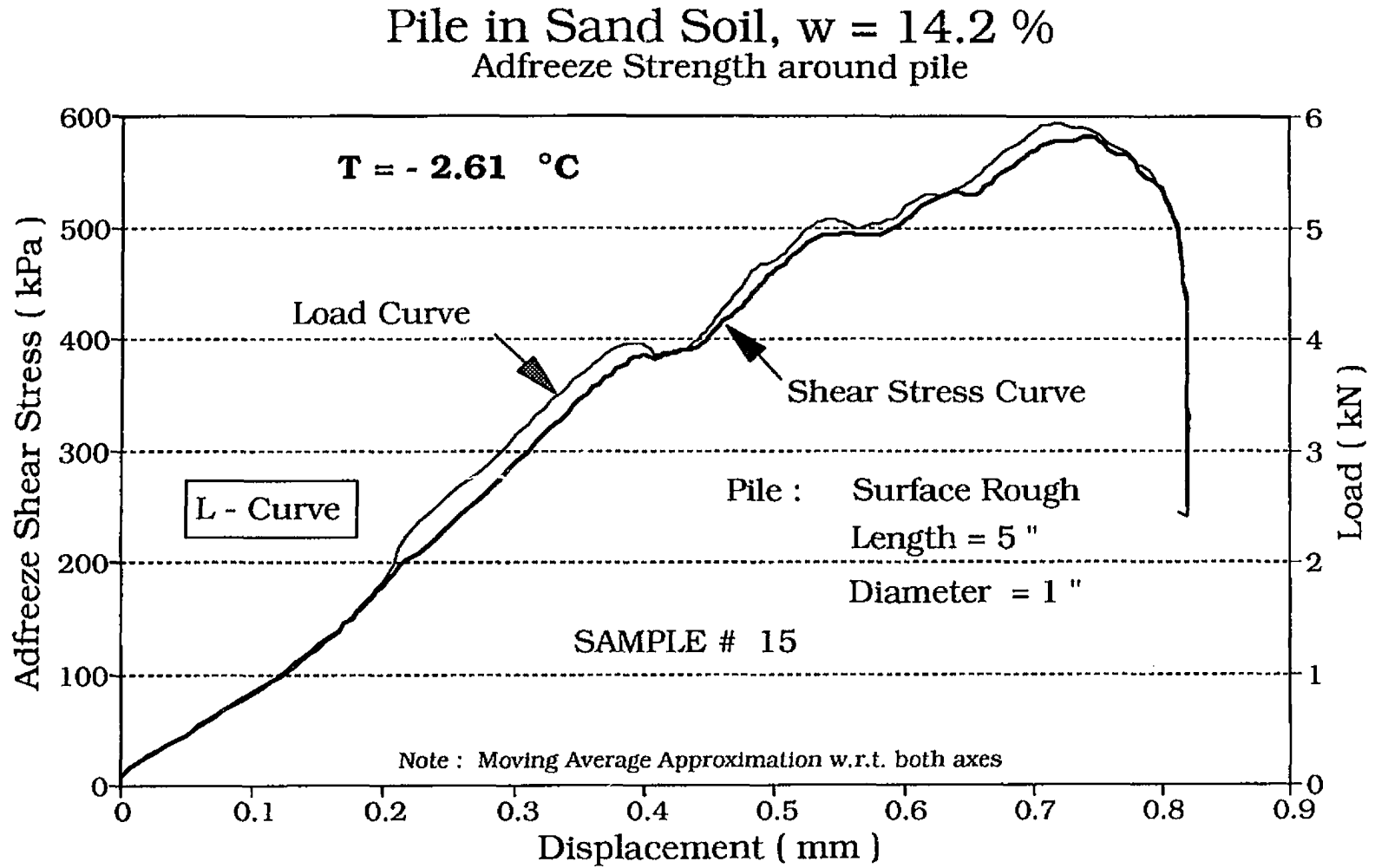


Fig. 6.22 Adfreeze Shear Strength for Sample # 15

Pile in Sand Soil, $w = 14.2\%$ Adfreeze Strength around pile

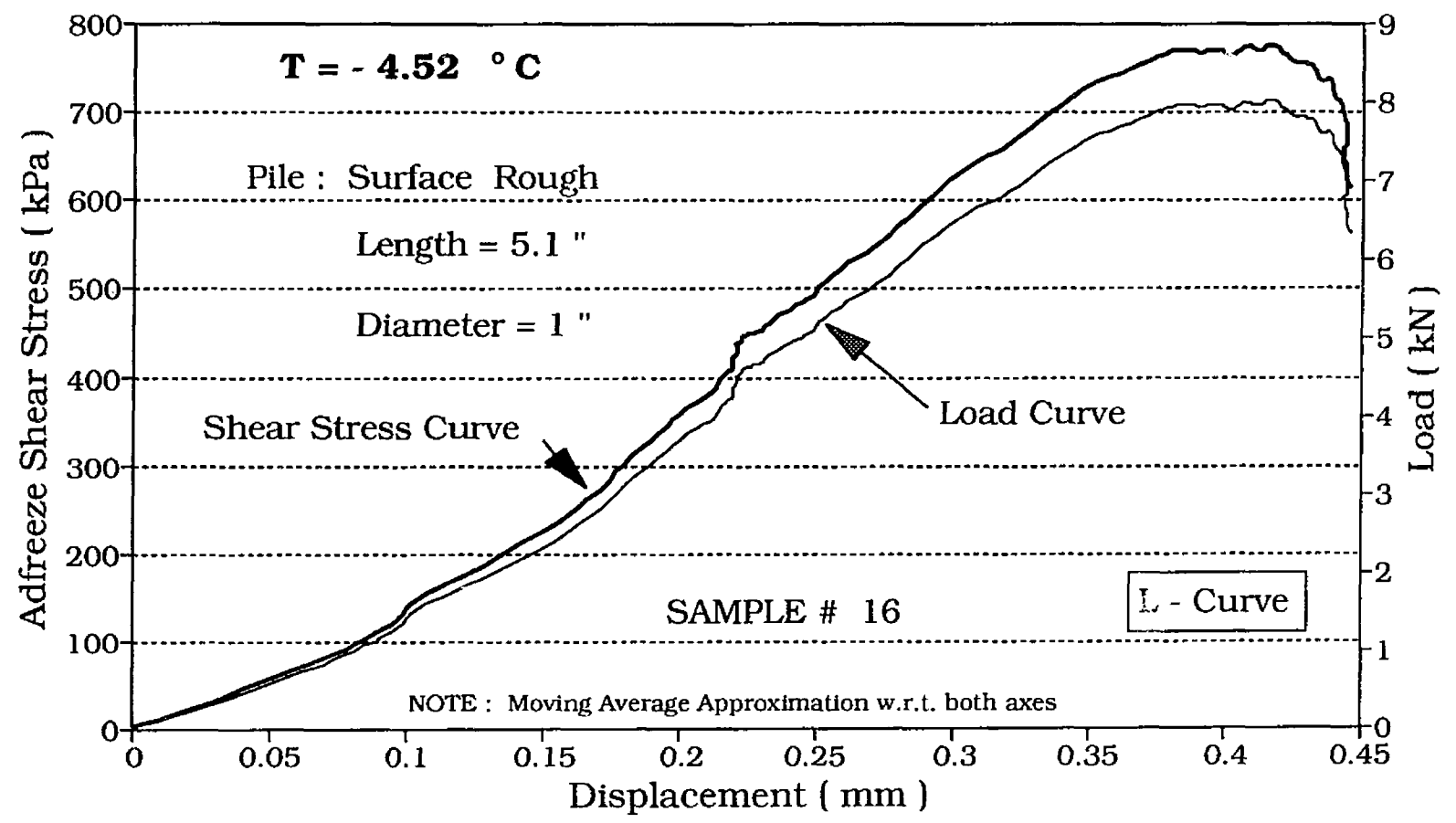


Fig. 6.23 Adfreeze Strength for Sample # 16 - L Curve -

Pile in Sand Soil, $w = 14.2\%$ Adfreeze Strength around pile

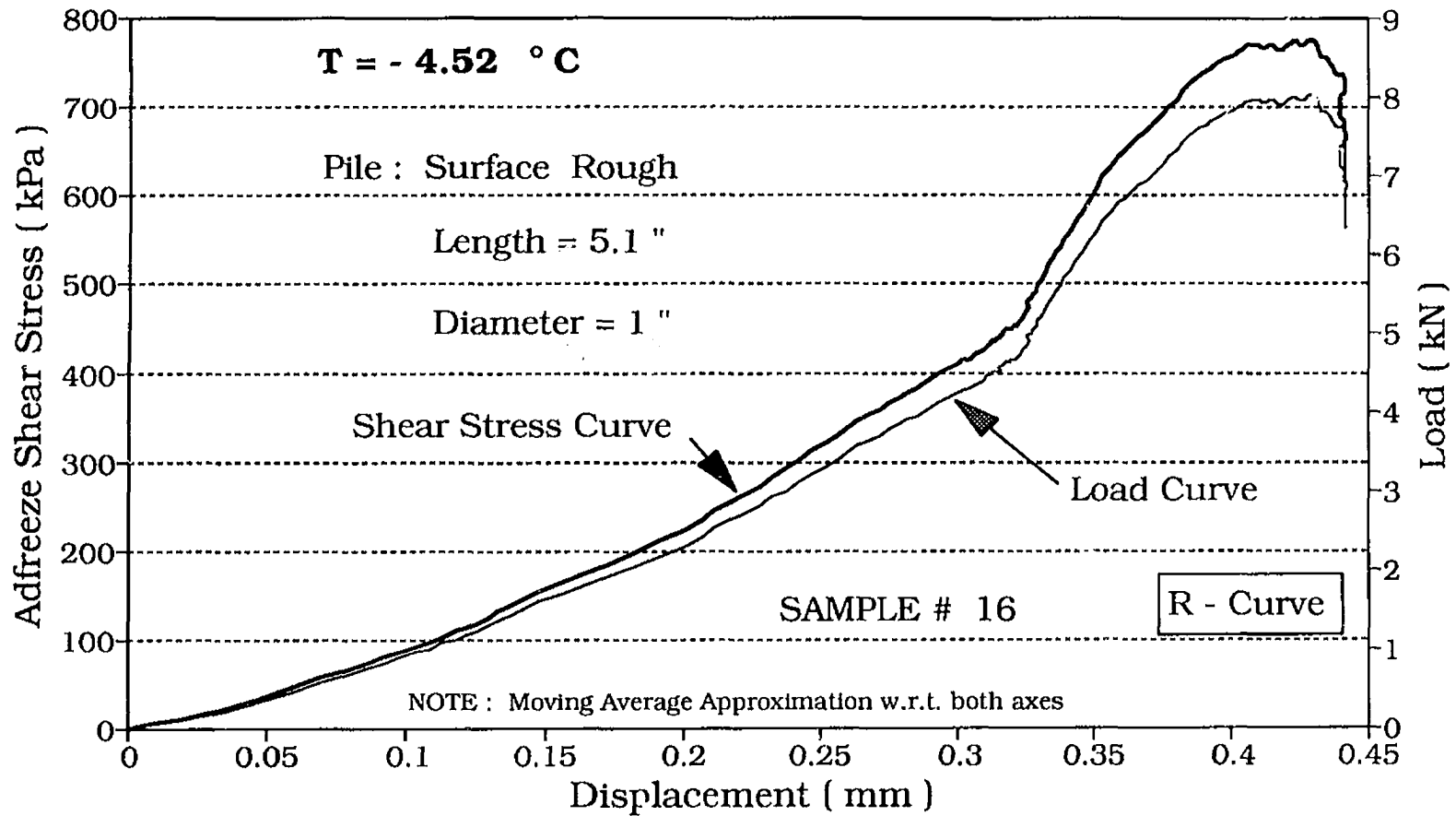


Fig. 6.24 Adfreeze Strength for Sample # 16 - R Curve -

Pile in Sand Soil, $w = 14.0\%$ Adfreeze Strength Around Pile

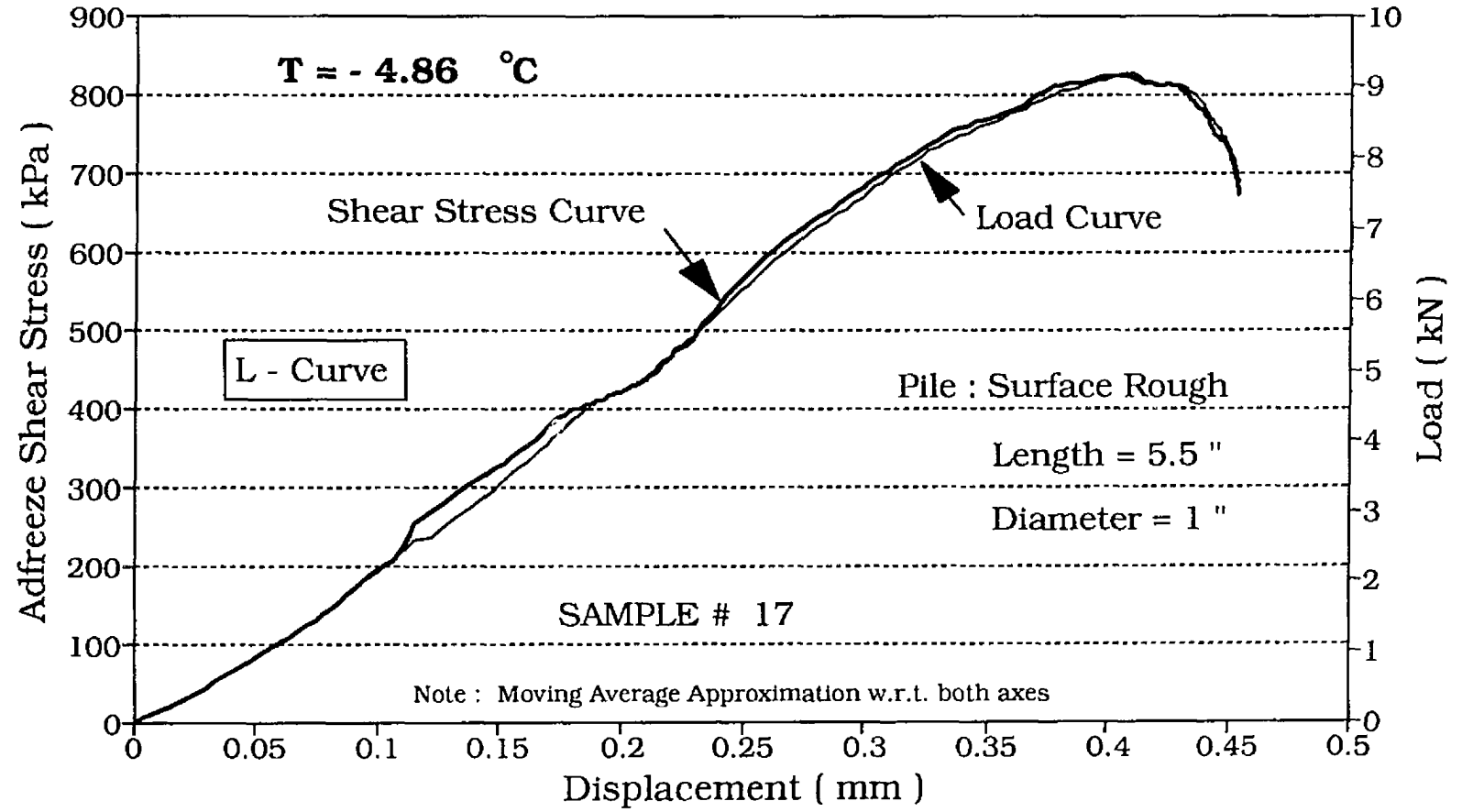


Fig. 6.25 Adfreeze Shear Strength for Sample # 17 - L Curve -

Pile in Sand Soil, $w = 14.0\%$ Adfreeze Strength Around Pile

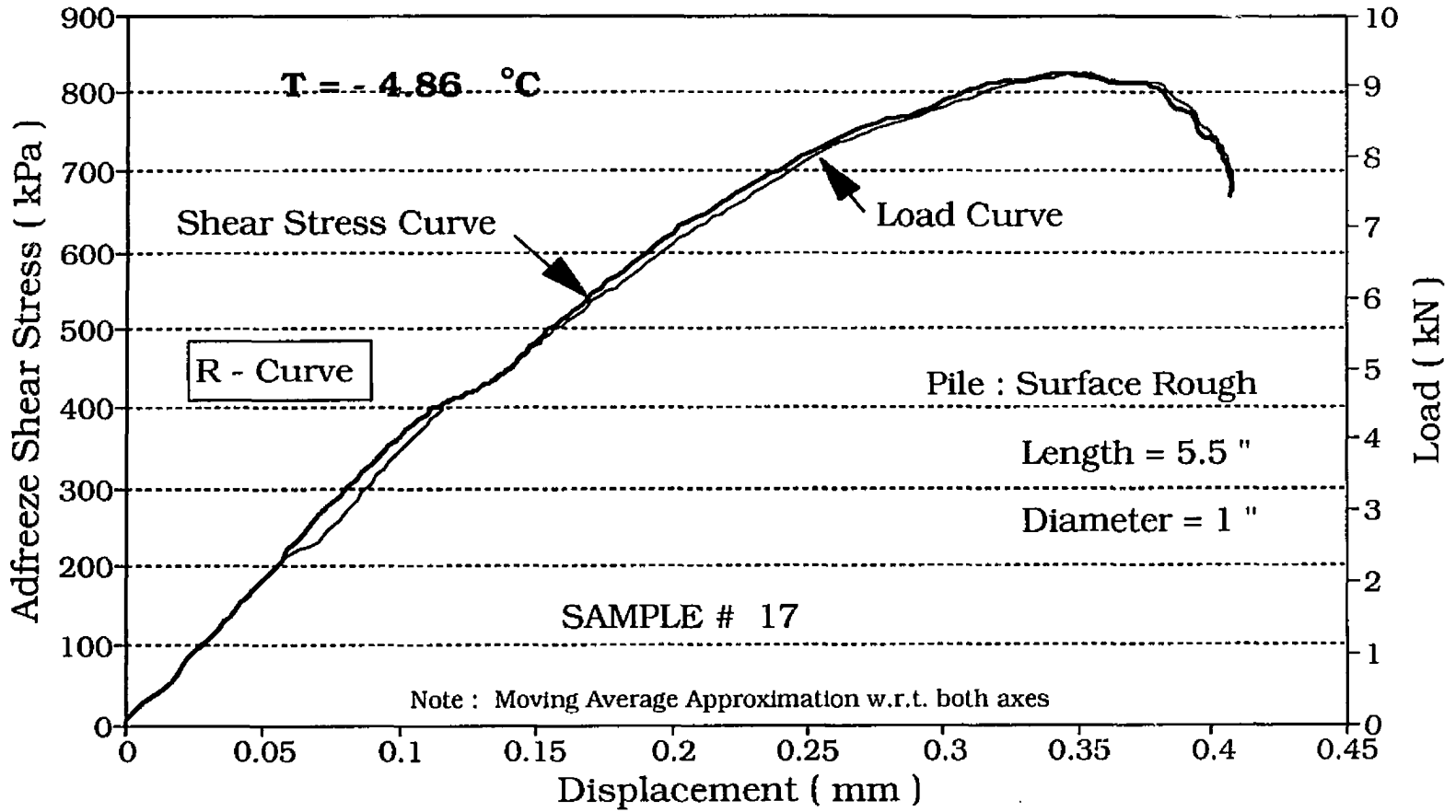


Fig. 6.26 Adfreeze Shear Strength for Sample # 17 - R Curve -

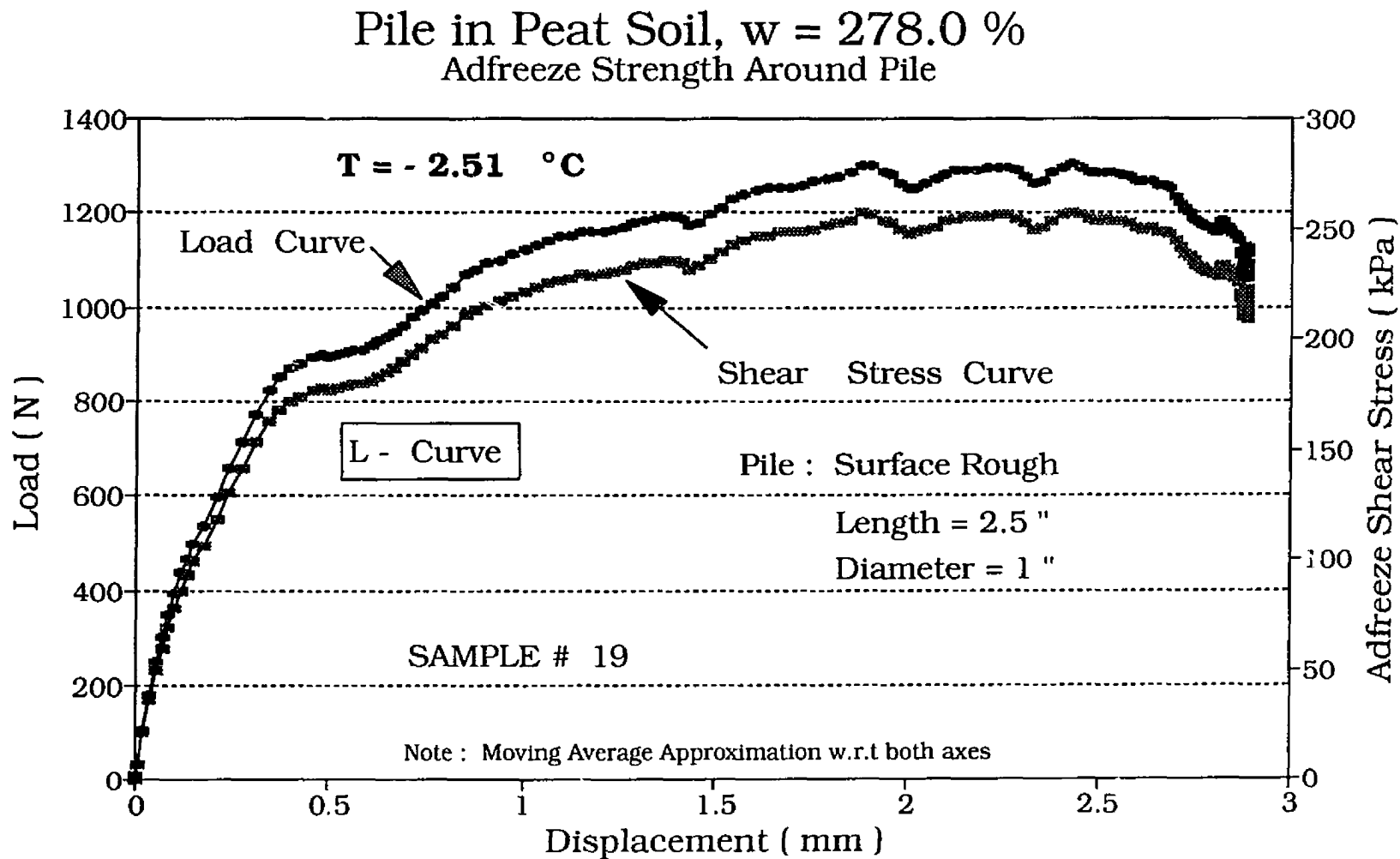


Fig. 6.27 Adfreeze Shear Strength for Sample # 19

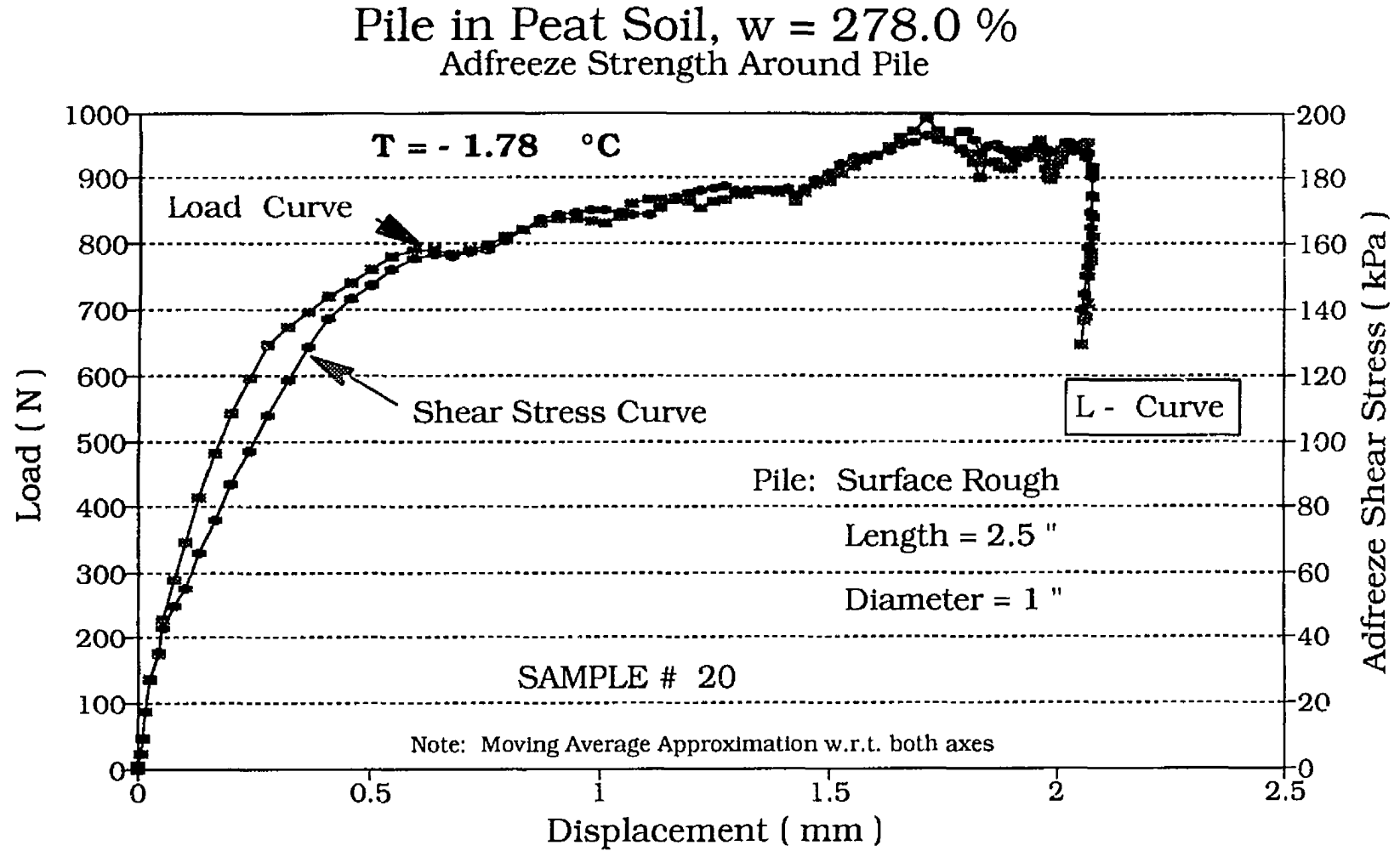


Fig. 6.28 Adfreeze Shear Strength for Sample # 20 - L Curve -

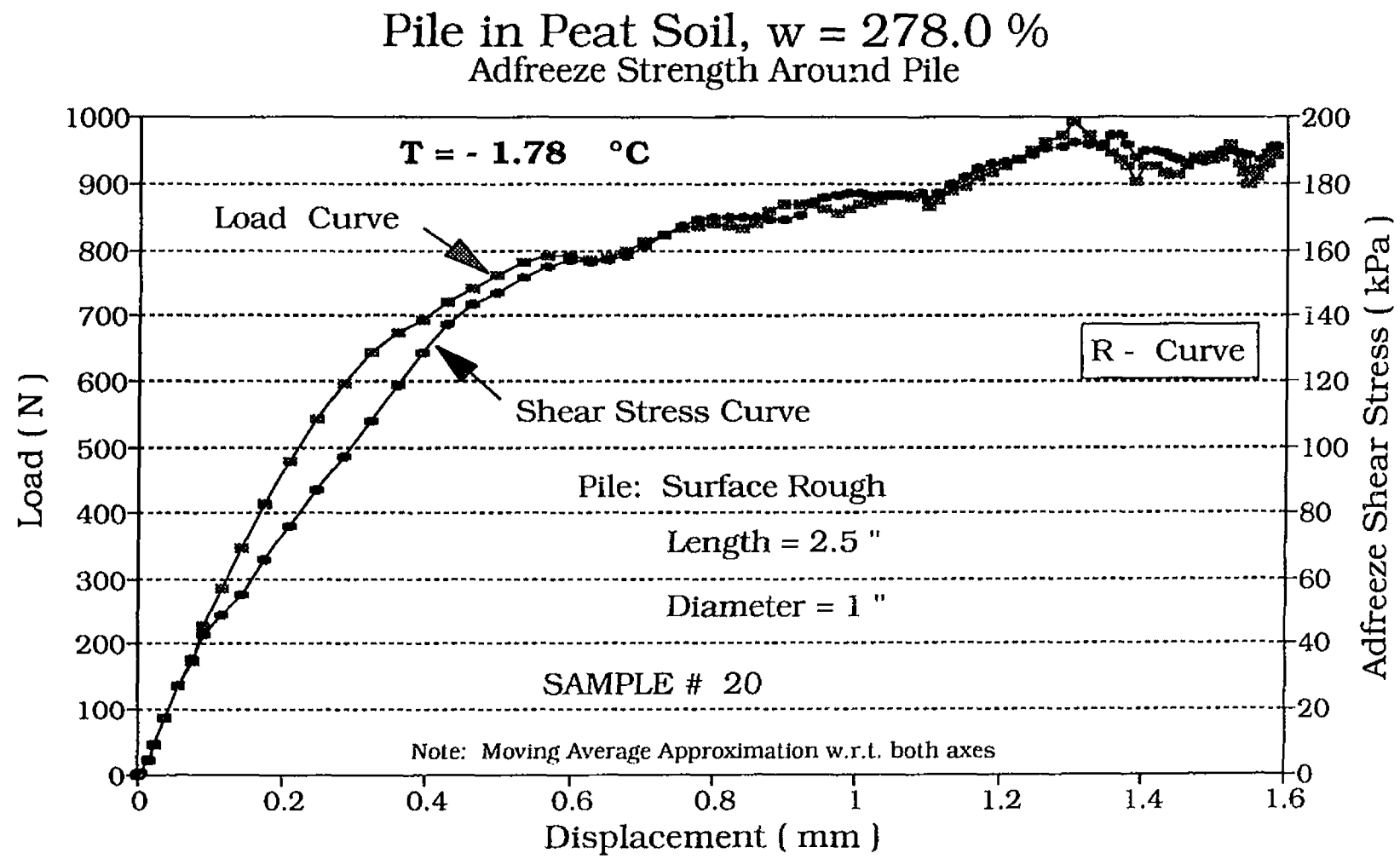


Fig. 6.29 Adfreeze Shear Strength for Sample # 20 - R Curve -

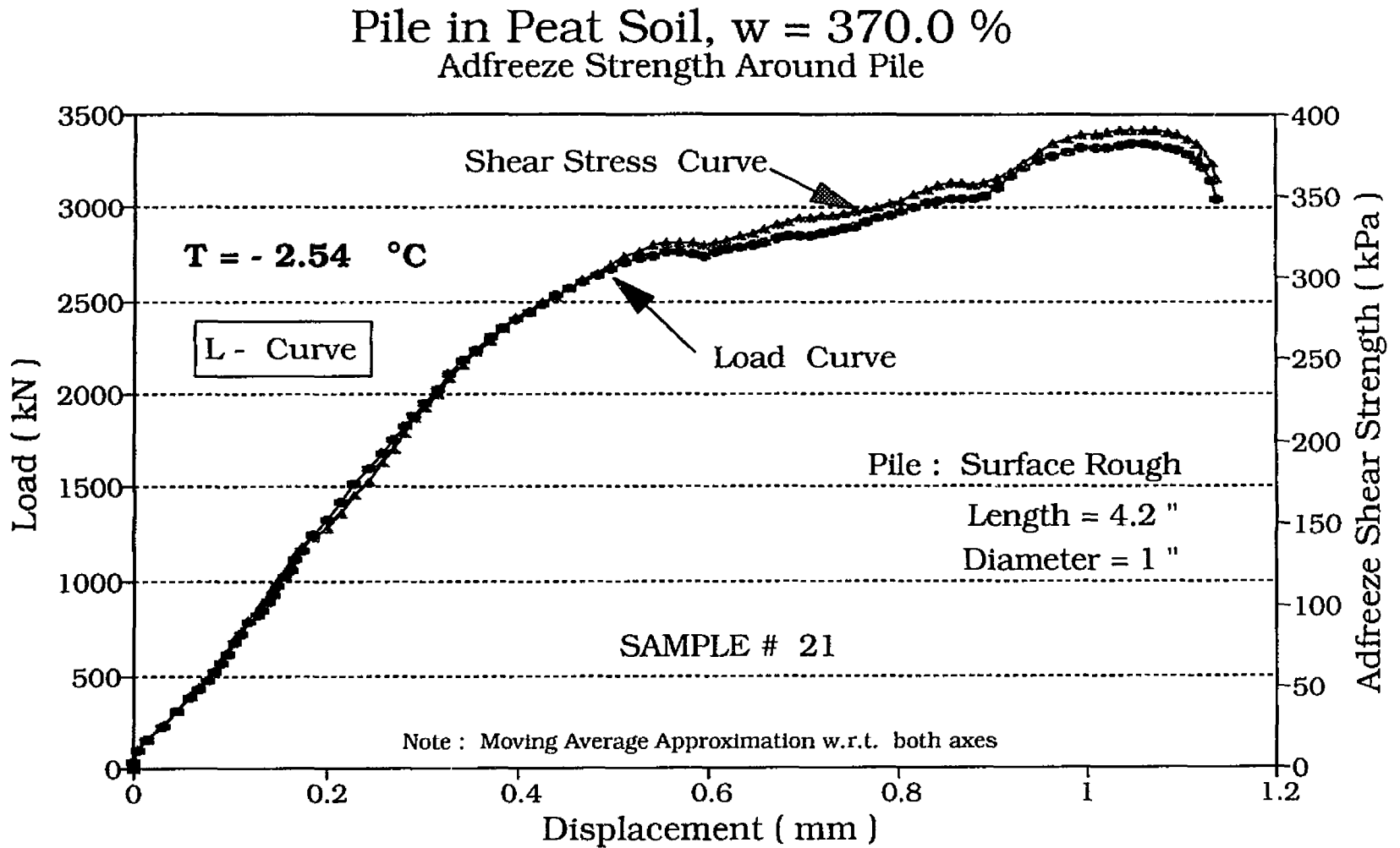


Fig. 6.30 Adfreeze Shear Strength for Sample # 21

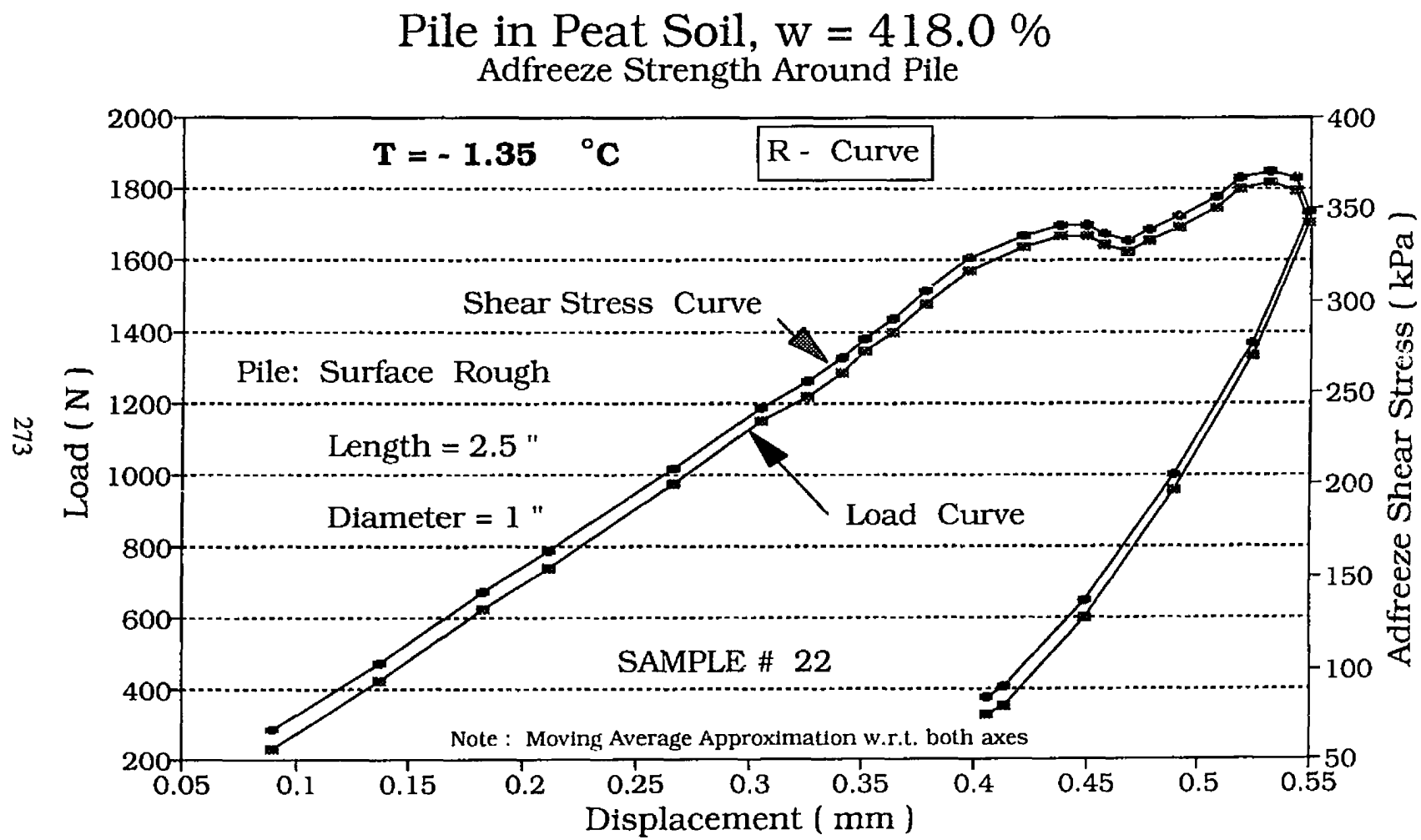


Fig. 6.31 Adfreeze Shear Strength for Sample # 22

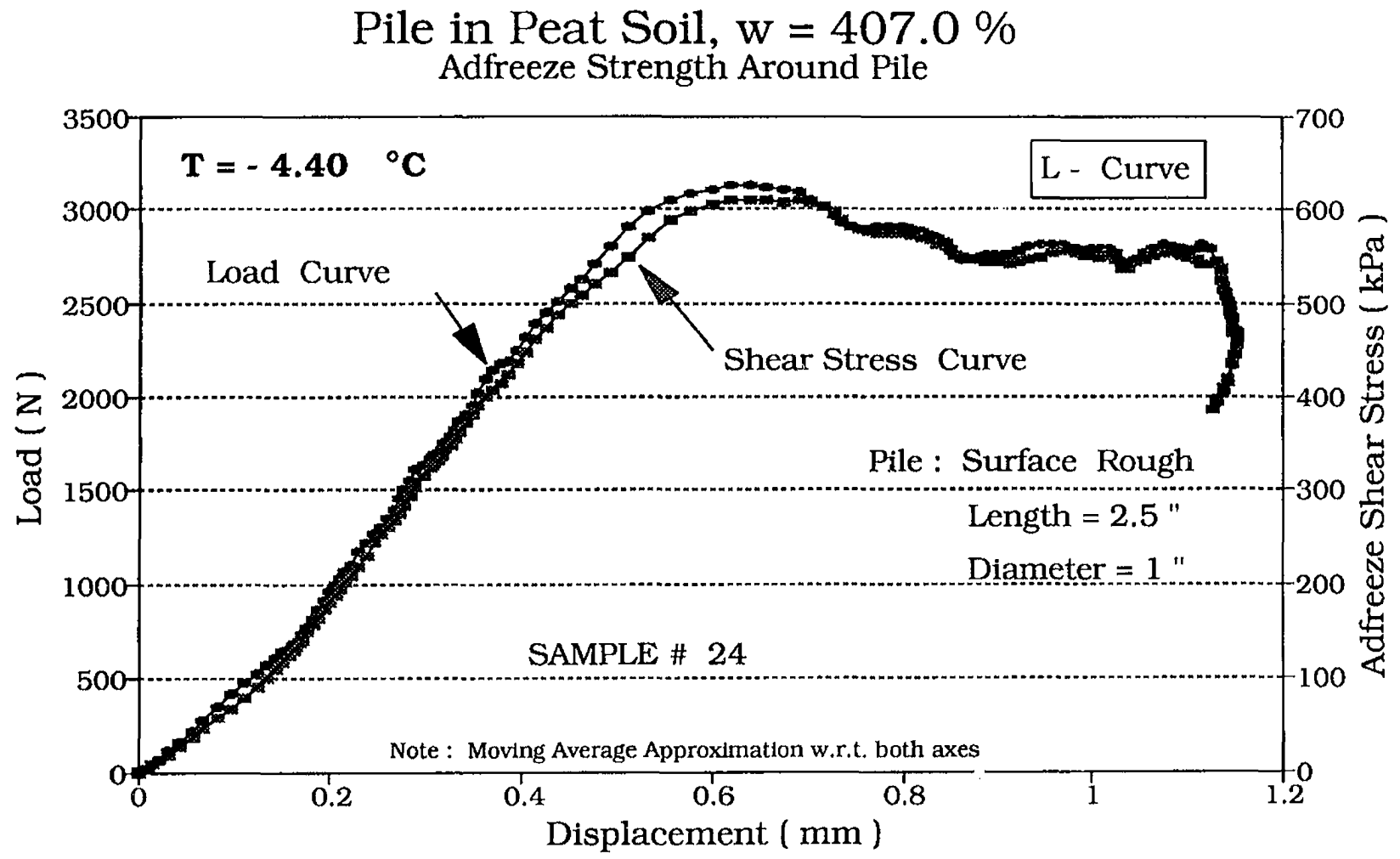


Fig. 6.32 Adfreeze Shear Strength for Sample # 24 - L Curve -

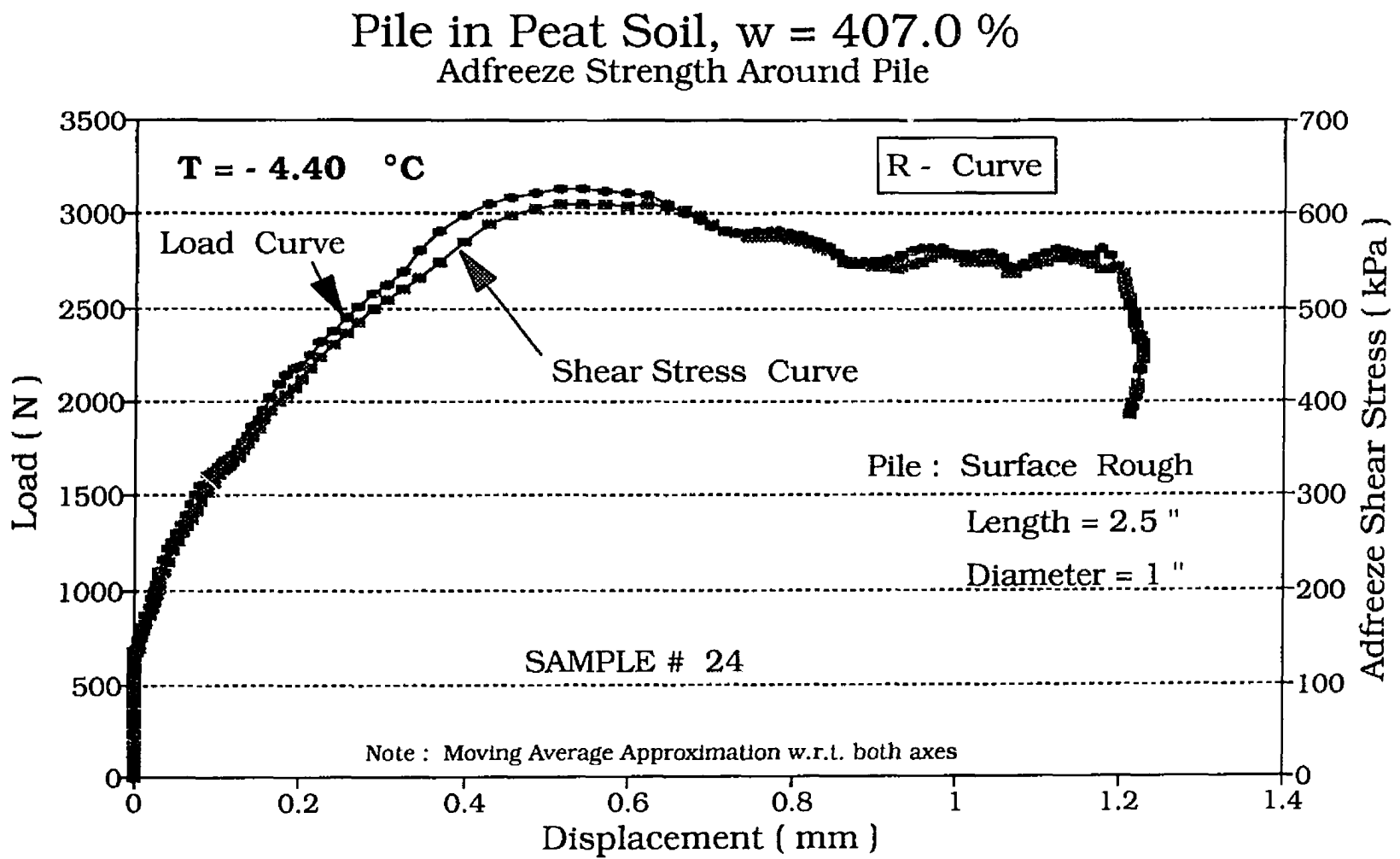


Fig. 6.33 Adfreeze Shear Strength for Sample # 24 - R Curve -

Pile in Peat Soil, $w = 407.0\%$ Adfreeze Strength Around Pile

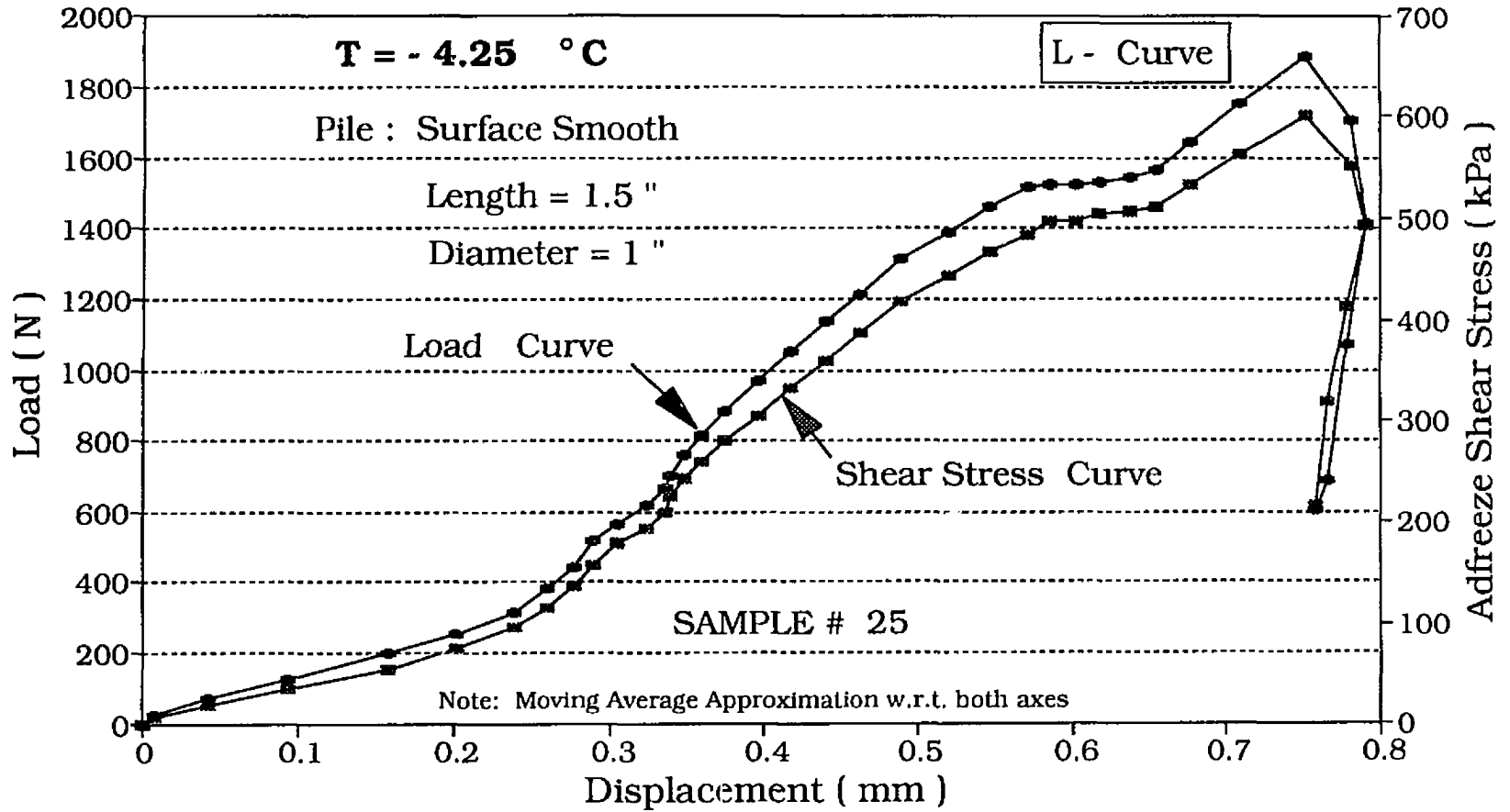


Fig. 6.34 Adfreeze Shear Strength for Sample # 25

Pile in Peat Soil, $w = 272.0\%$ Adfreeze Strength Around Pile

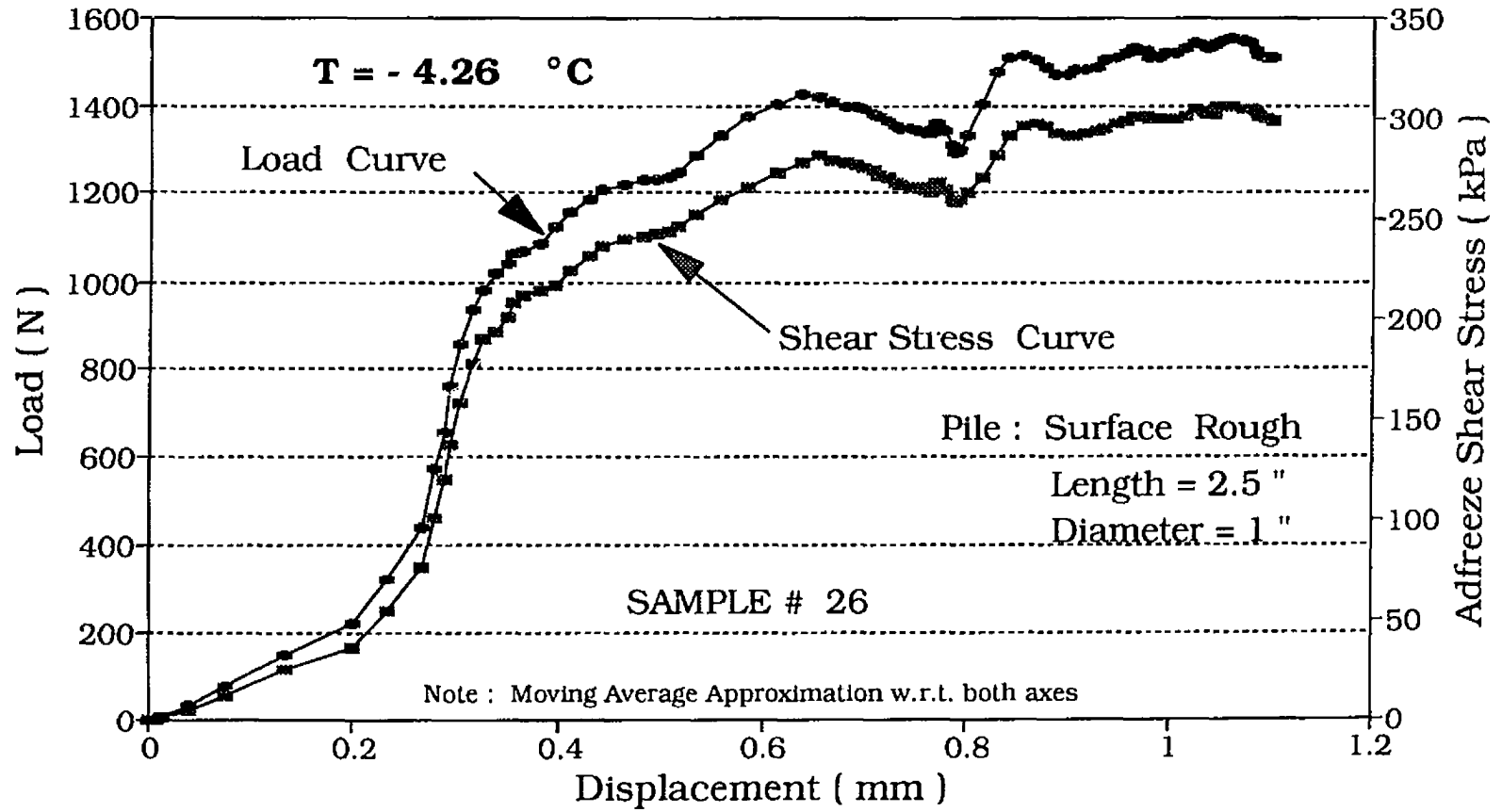


Fig. 6.35 Adfreeze Shear Strength for Sample # 26

Pile in Peat Soil, $w = 273.0\%$ Adfreeze Strength Around Pile

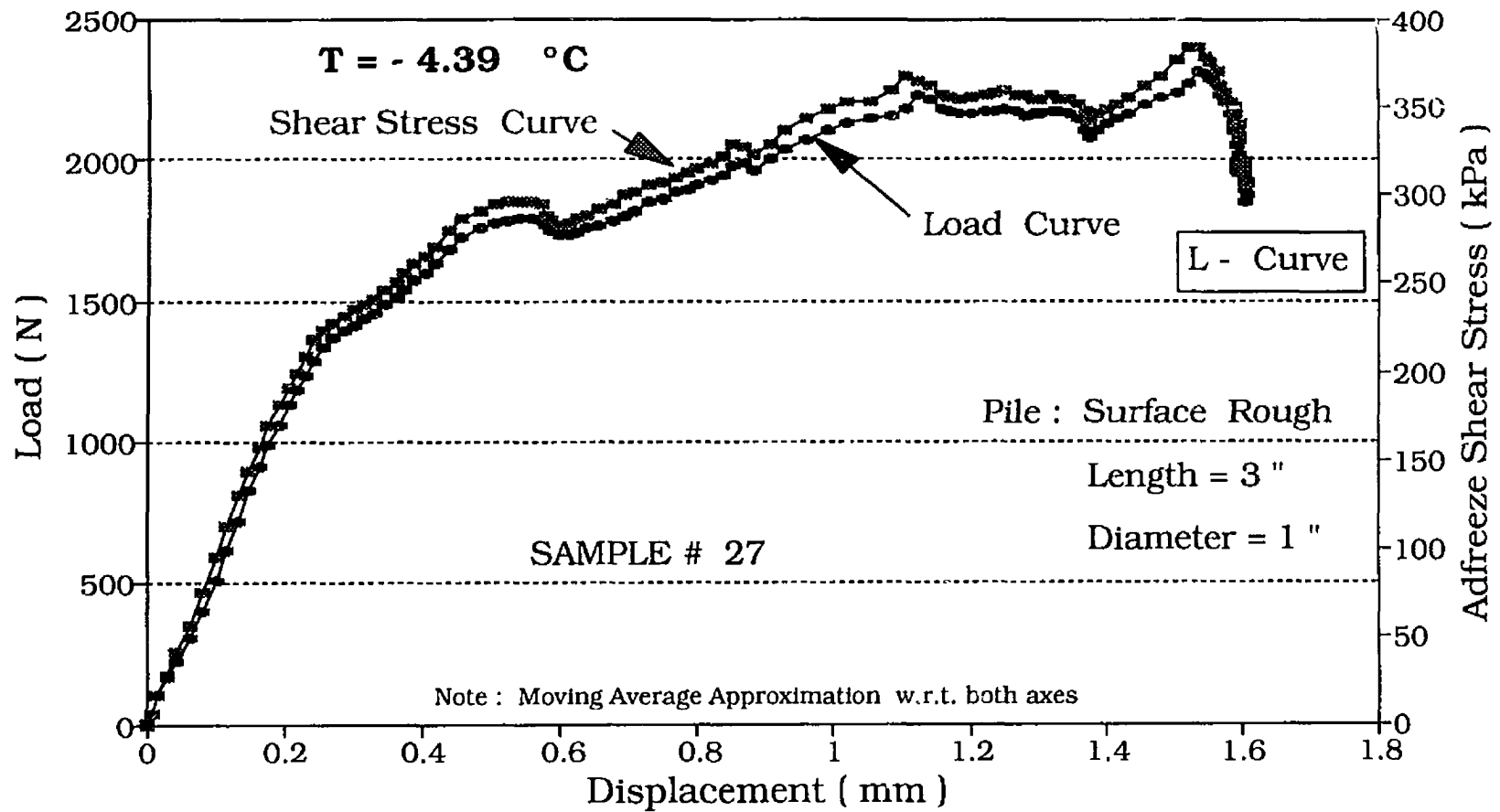


Fig. 6.36 Adfreeze Shear Strength for Sample # 27 - L Curve -

279

Pile in Peat Soil, $w = 273.0\%$ Adfreeze Strength Around Pile

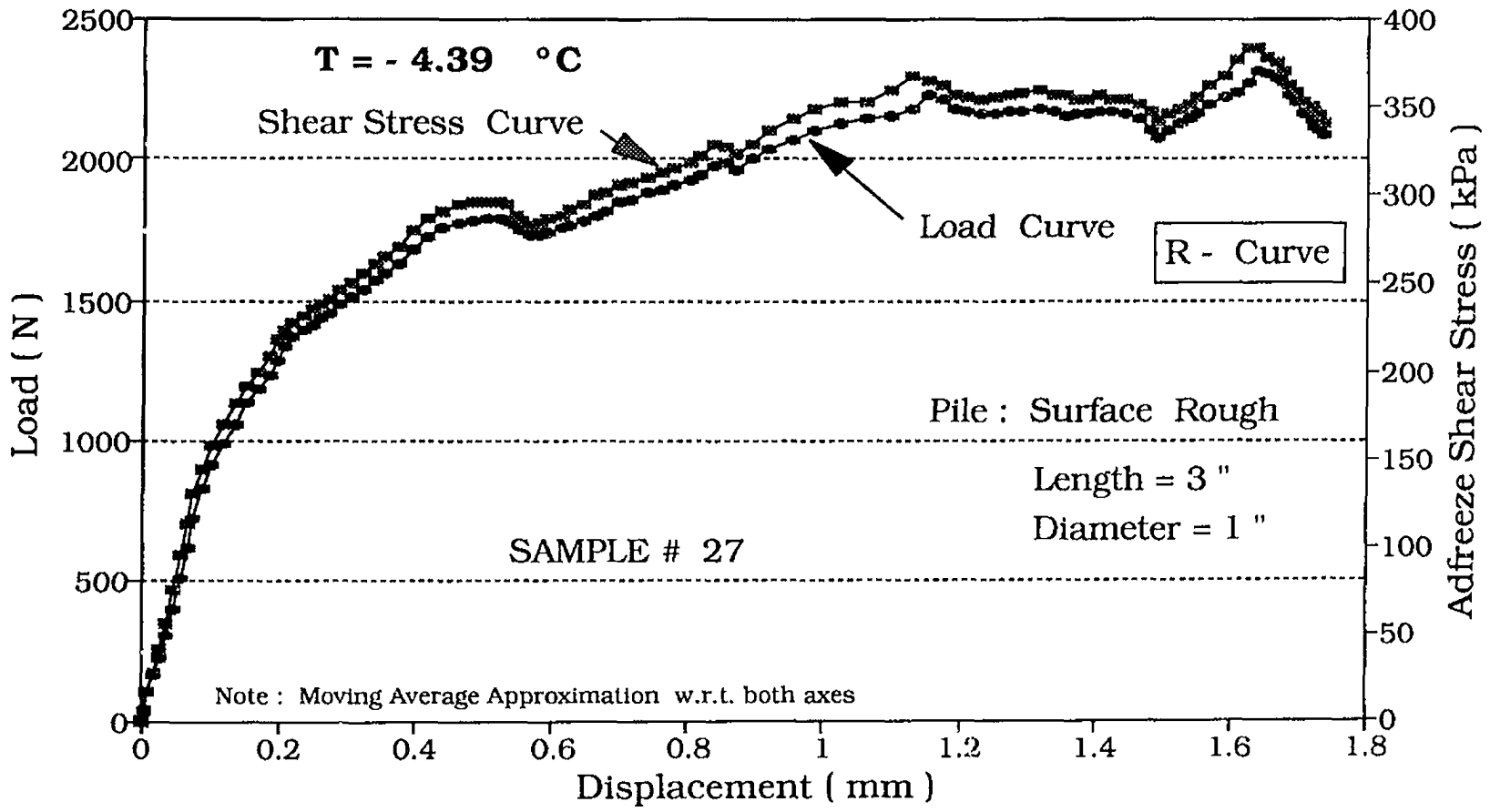


Fig. 6.37 Adfreeze Shear Strength for Sample # 27 - R Curve -

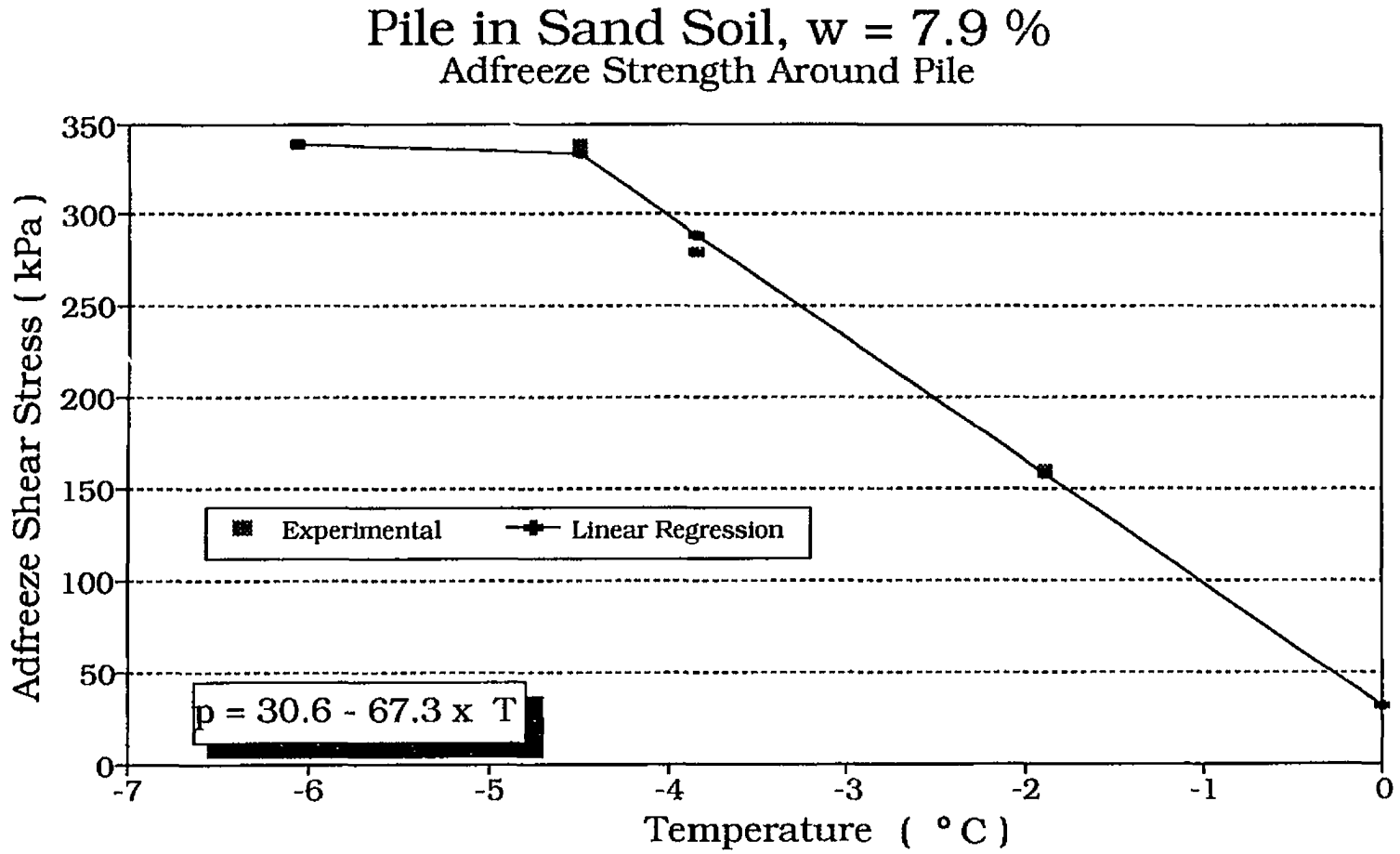


Fig. 6.38 Adfreeze Strength, Function of Temperature, for Sand with $w = 7.9\%$

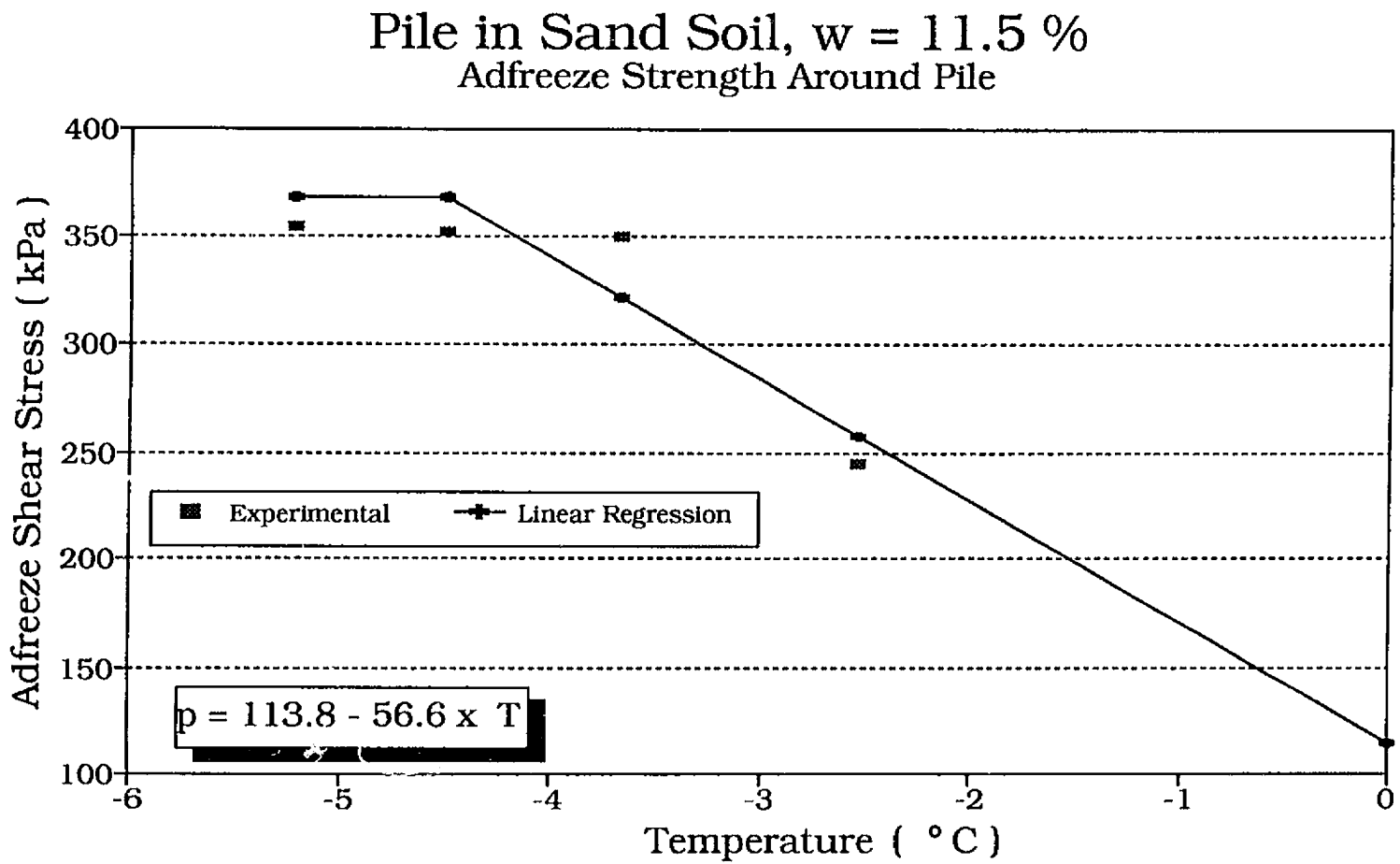


Fig. 6.39 Adfreeze Strength, Function of temperature, for Sand with w = 11.5 %

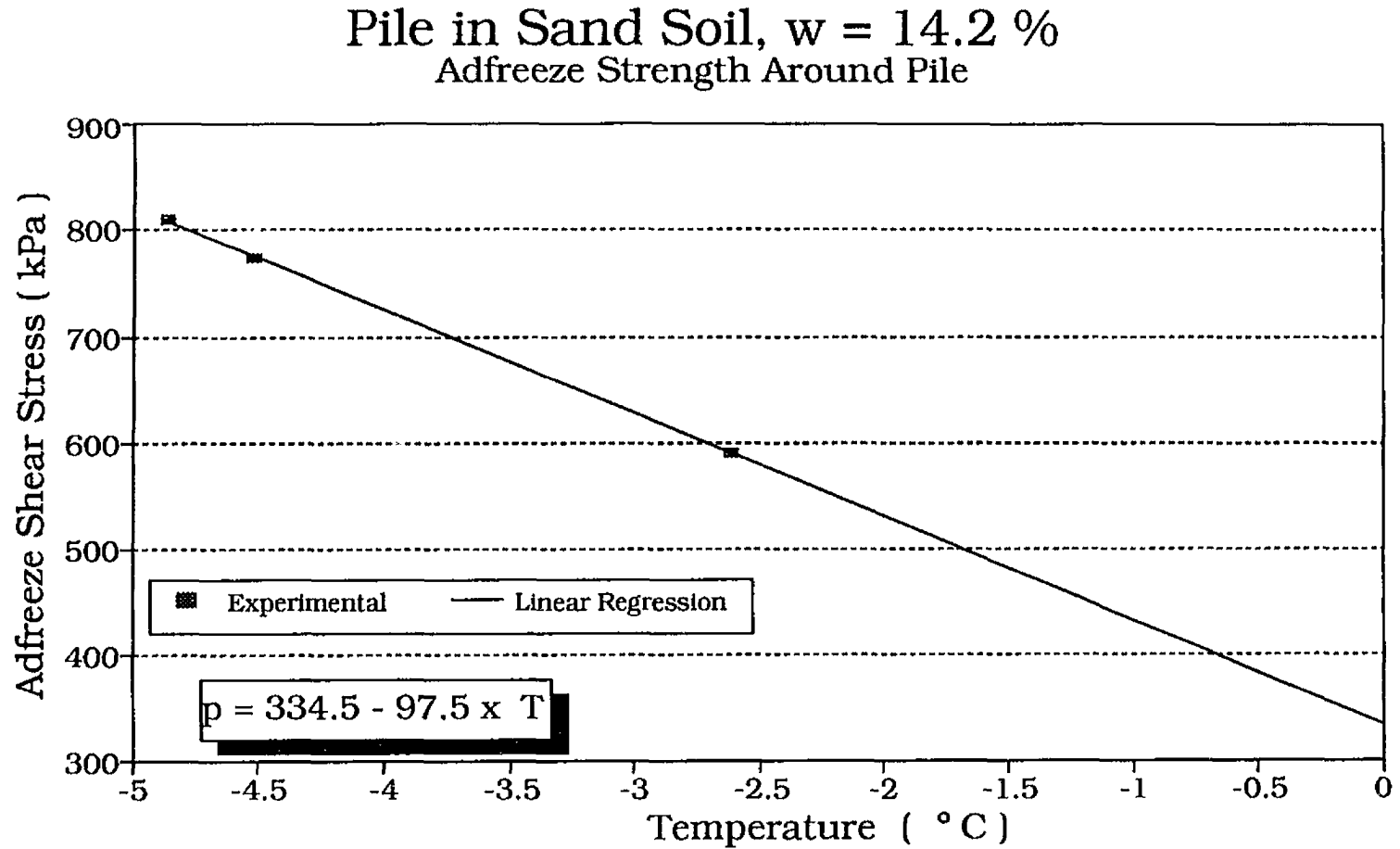


Fig. 6.40 Adfreeze Strength, Function of Temperature, for Sand with $w = 14.2\%$

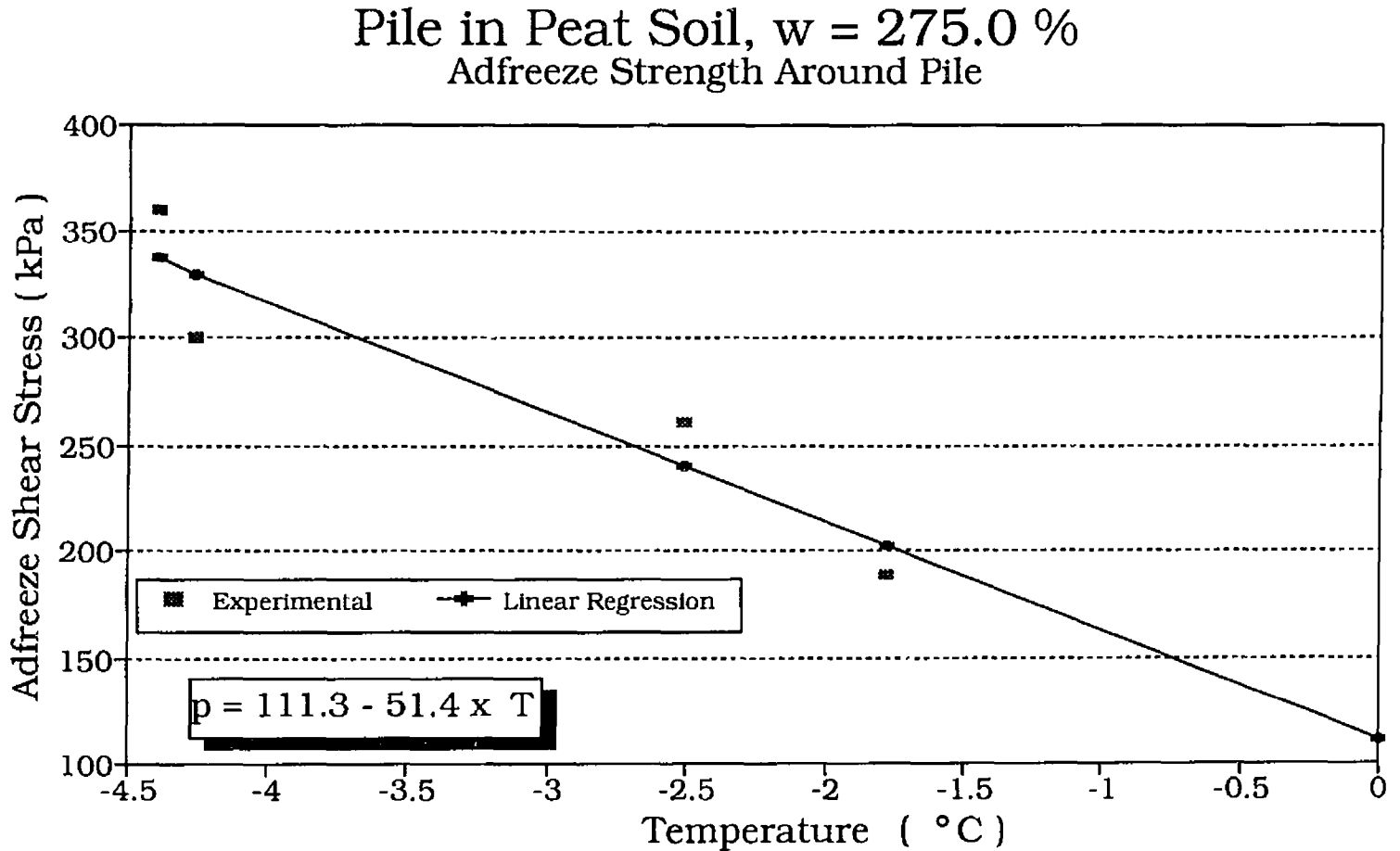


Fig. 6.41 Adfreeze Strength, Function of Temperature, for Peat with $w = 275\%$

Pile in Peat Soil, $w = 412.5 \%$ Adfreeze Strength Around Pile

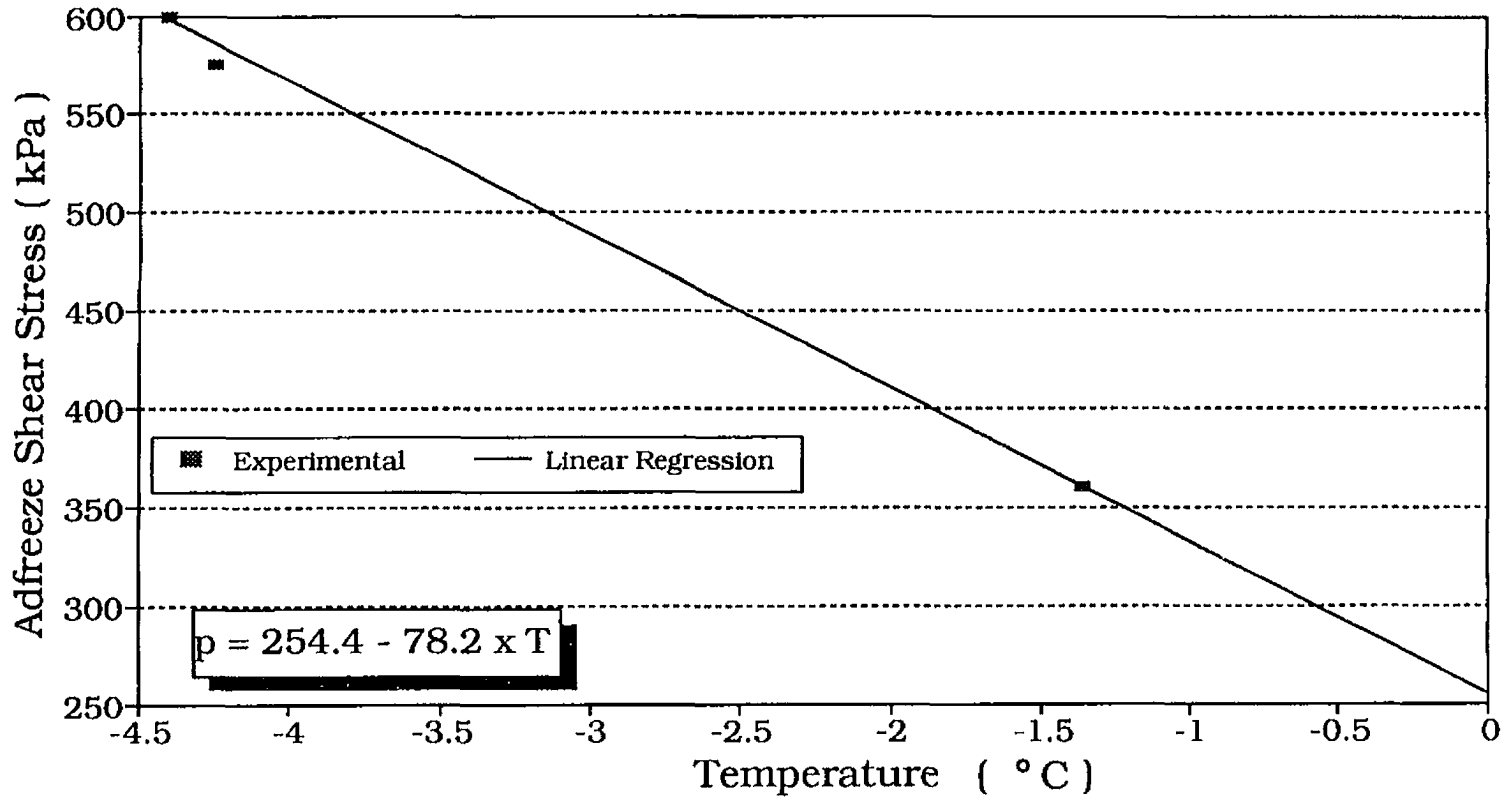


Fig. 6.42 Adfreeze Strength, Function of Temperature, for Peat with $w = 412.5 \%$

Pile in Sand, Variable Water Content Adfreeze Strength Around Pile

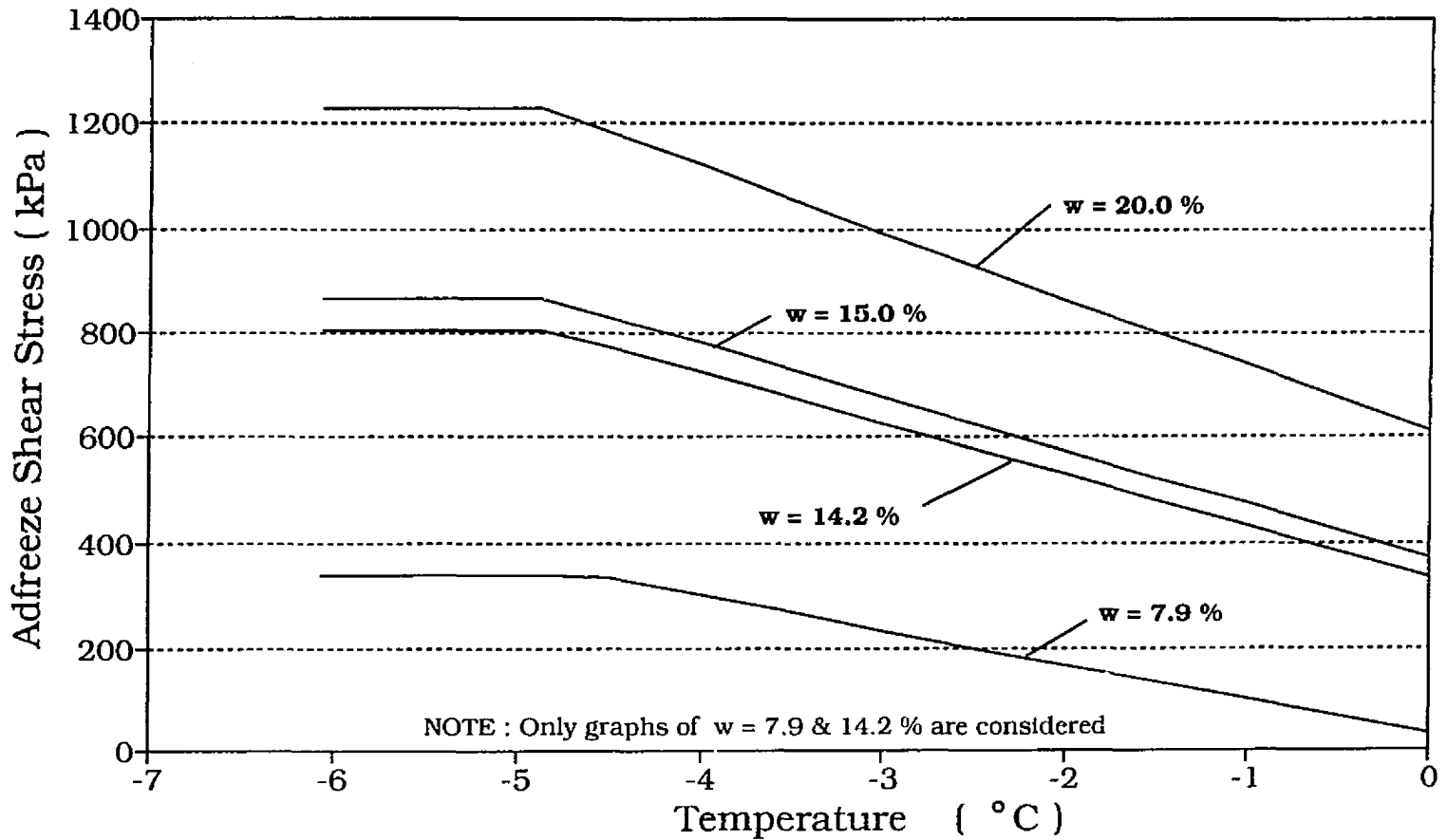


Fig. 6.43 Adfreeze Strength, Function of Temperature, for Sand Soil with Variable Water Contents

Pile in Peat , Variable Water Content Adfreeze Strength Around Pile

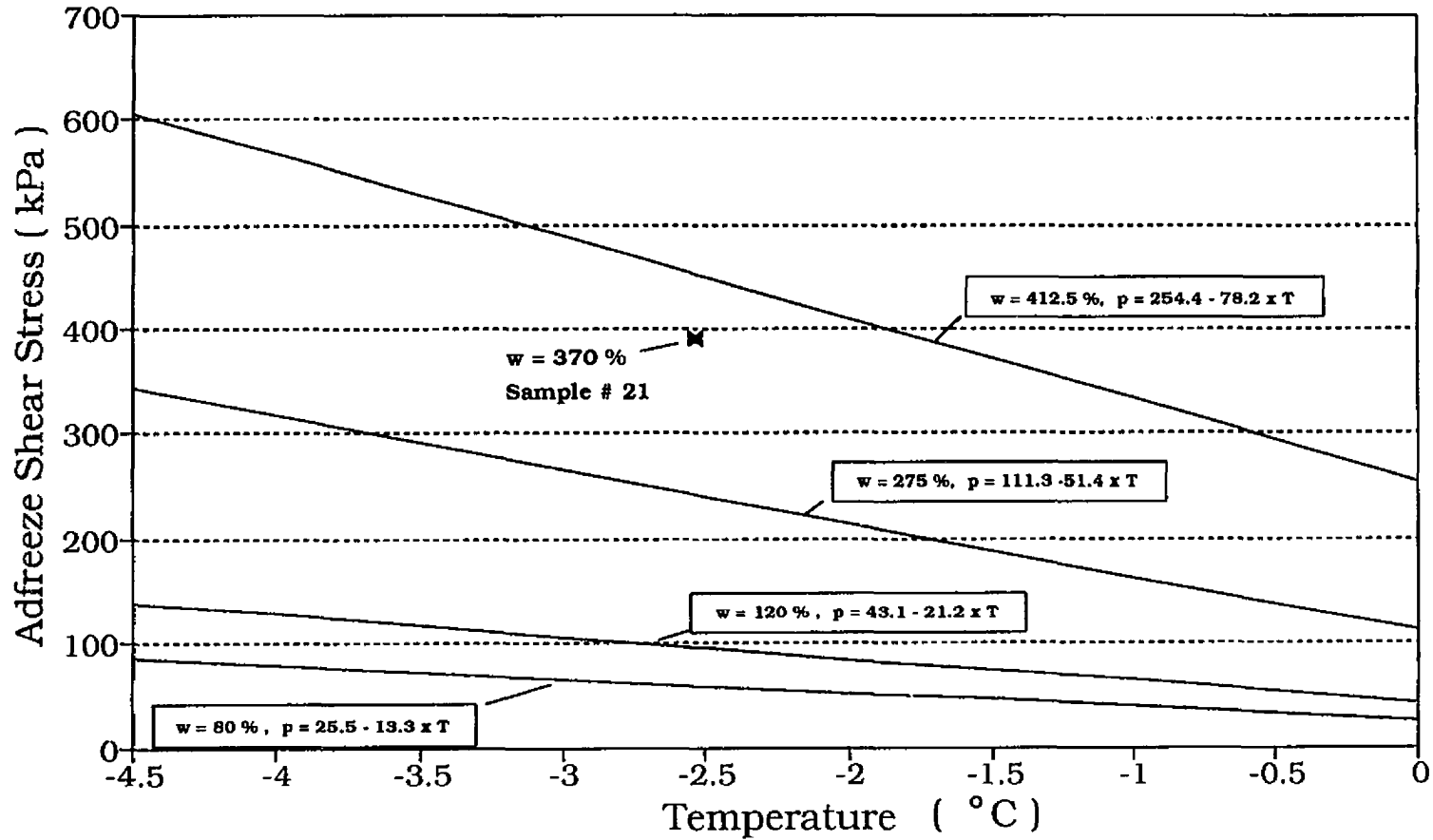


Fig. 6.44 Adfreeze Strength, Function of Temperature, for Peat Soil with Variable Water Contents

Pile in Clay, Variable Water Content Adfreeze Strength vs Temperature

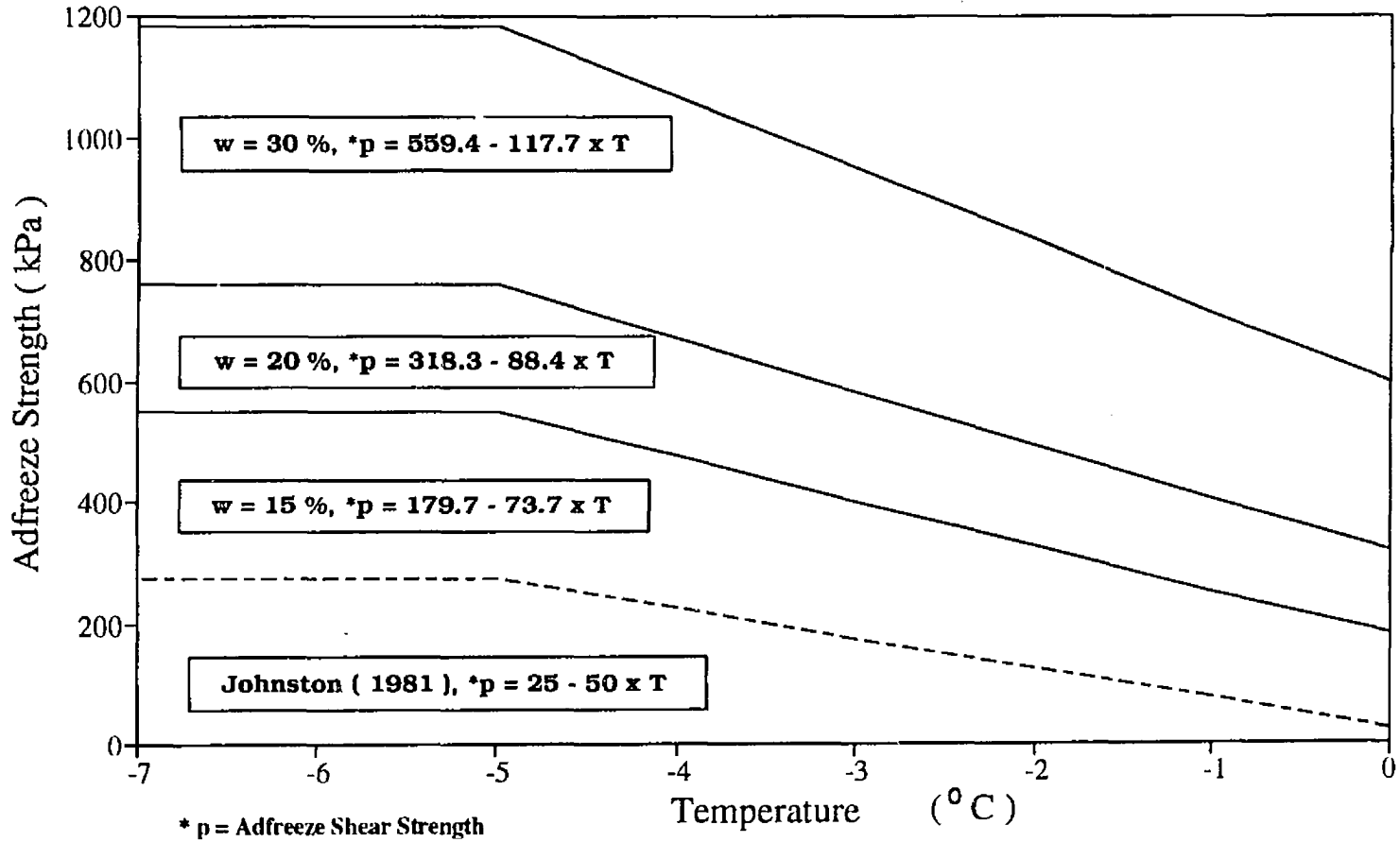


Fig. 6.45 Adfreeze Shear Strength for Pile Foundation Embedded in Clayey Soil with Variable Water Contents

Pile in Sand, Variable Water Content Adfreeze Strength Around Pile

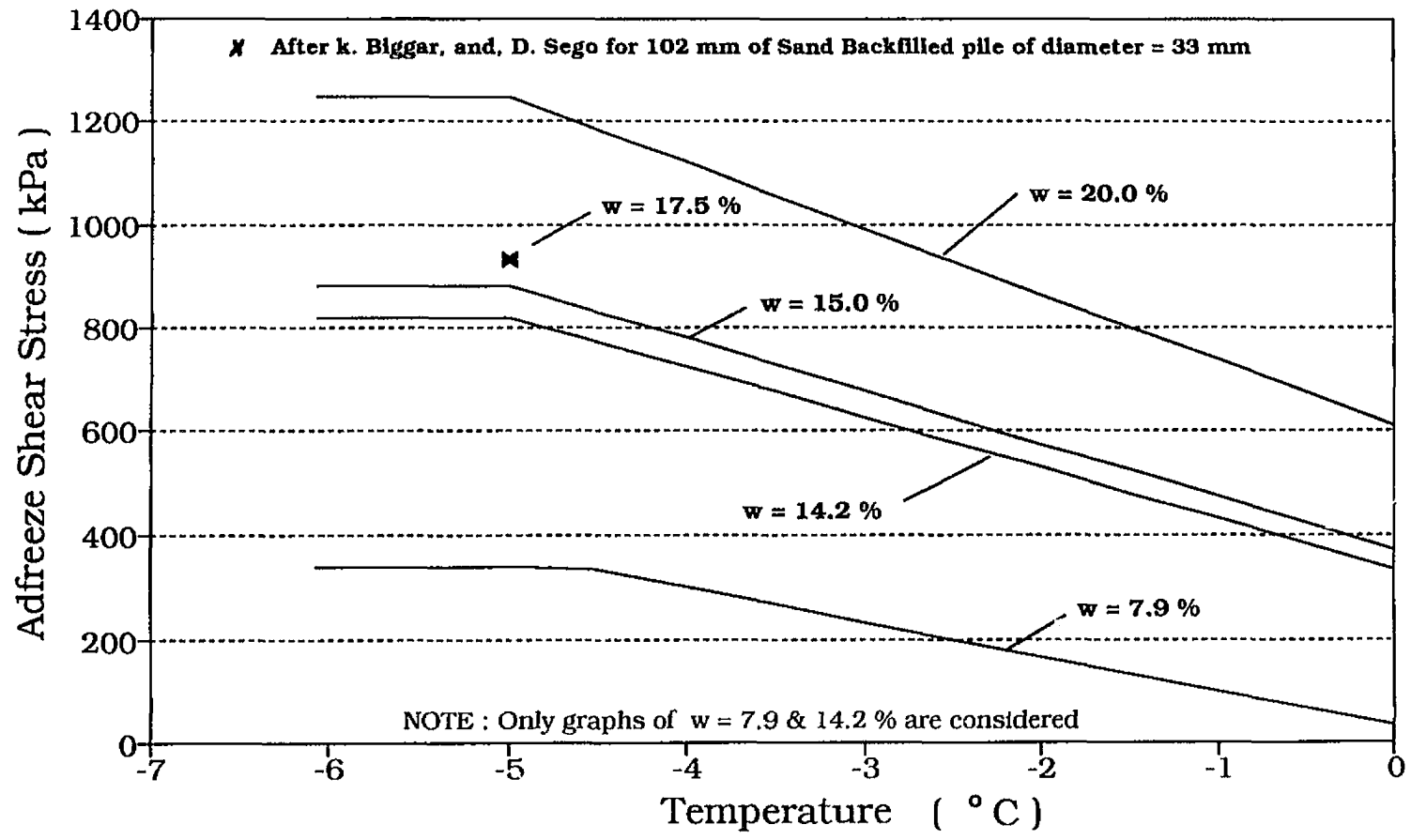


Fig. 6.46 Adfreeze Strength For Sand with Experimental Result after Study done by Biggar, K. and Segó, D. (1993)

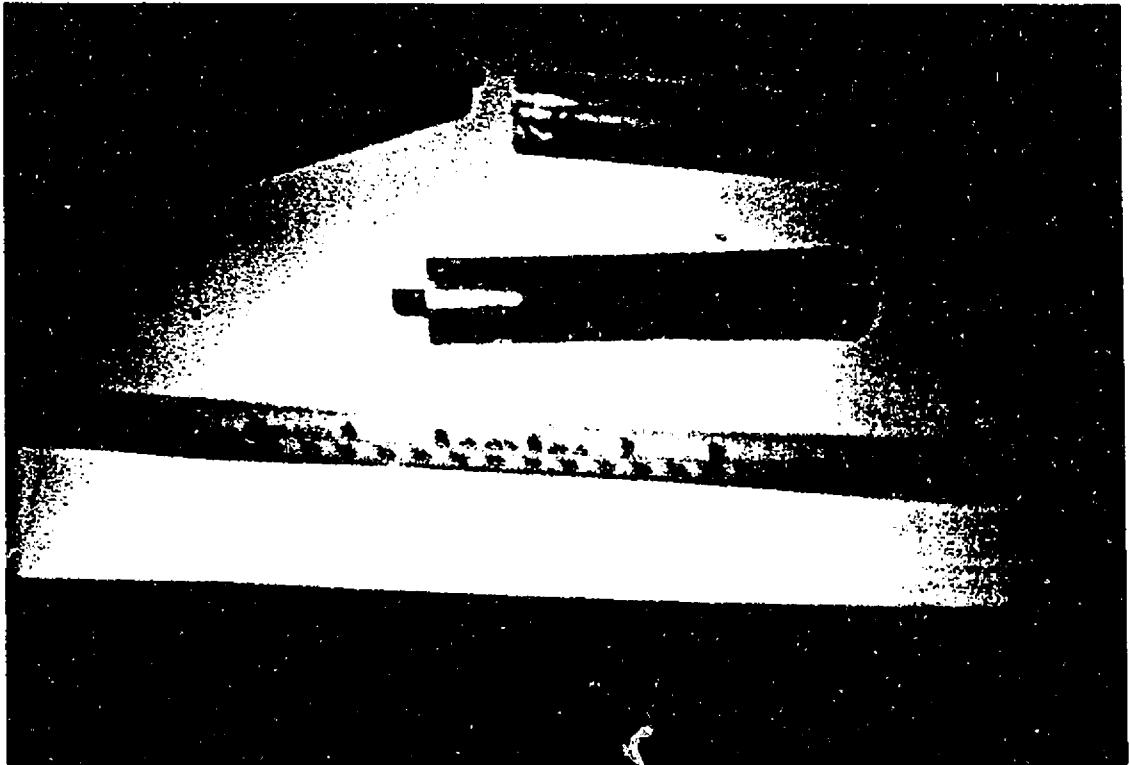
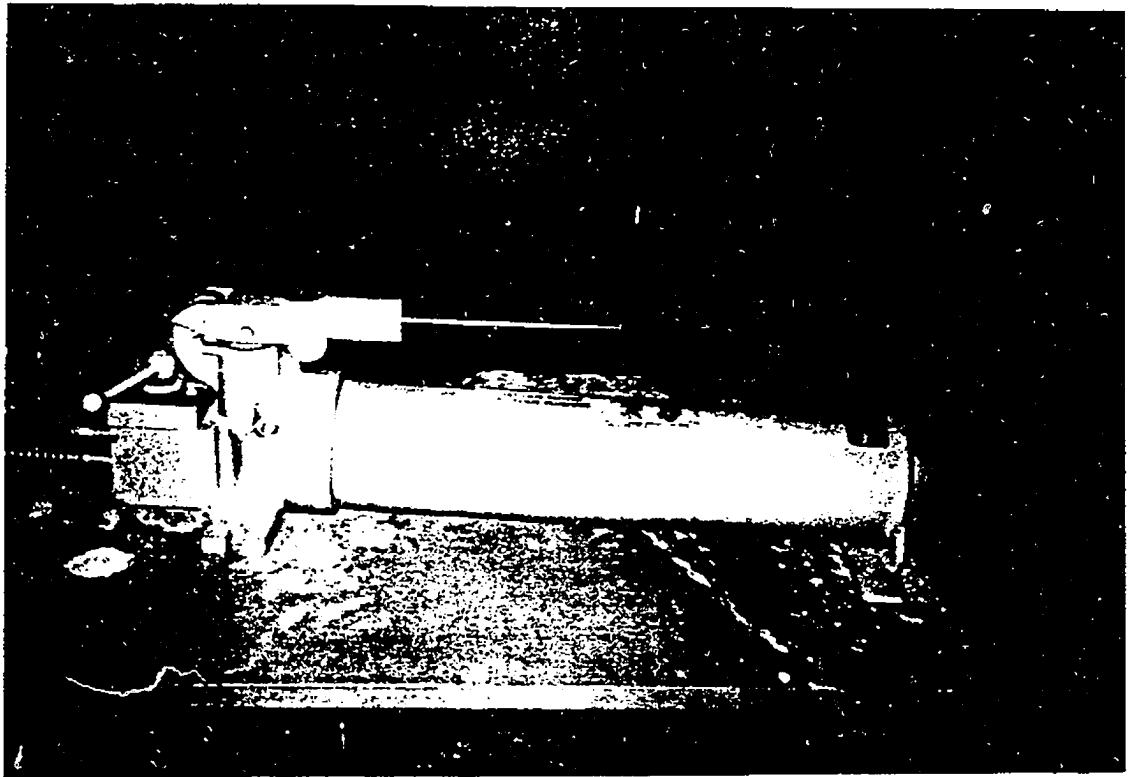


Fig 6.47 Steel Model Piles for Laboratory Testing. Note the Grooves that Hold The Thermocouple Wires Measuring Freezing Temperatures.



**Fig 6.48 High Power Hydraulic Pump with Maximum Pressure 10000 psi.
(700 bars) Used to Transmit Loads on Top of The Pile Through the
Flat Load Cell**

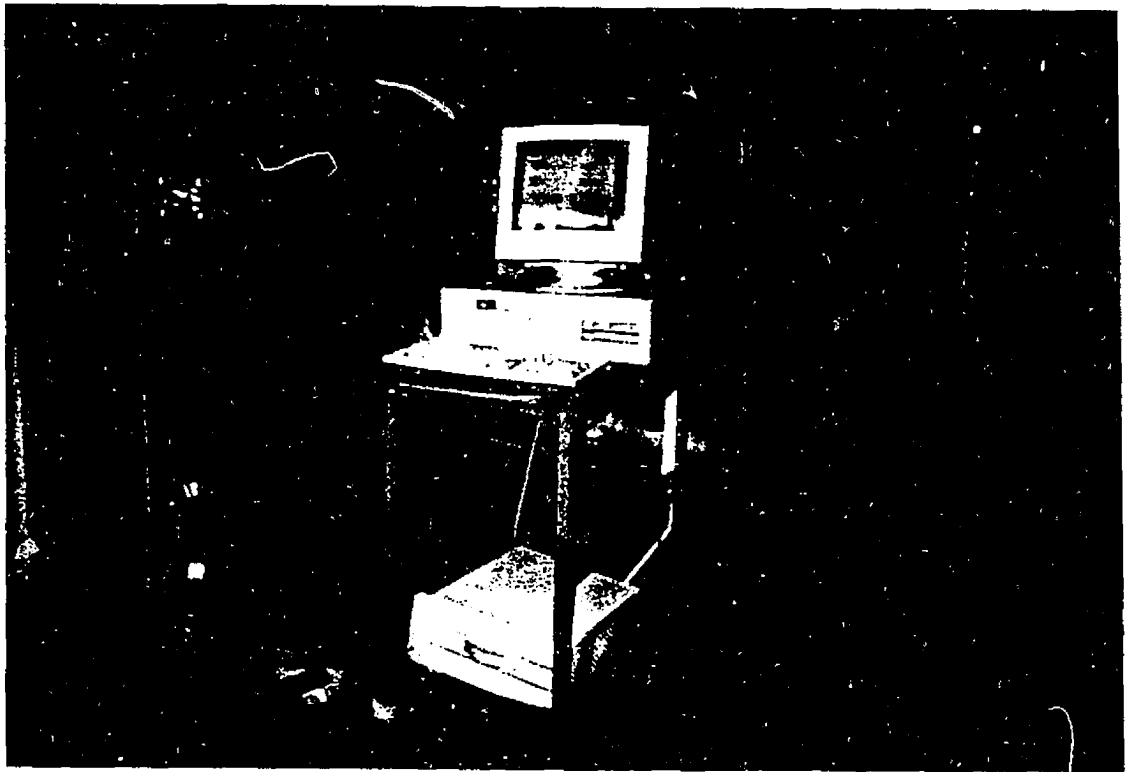


Fig 6.49 Data Acquisition System Used to Monitor Pre-and-Post-Tests Processing Data Including Temperatures, Settlements, and Corresponding Loads. The MEGADAC and the PC Computer are Shown.

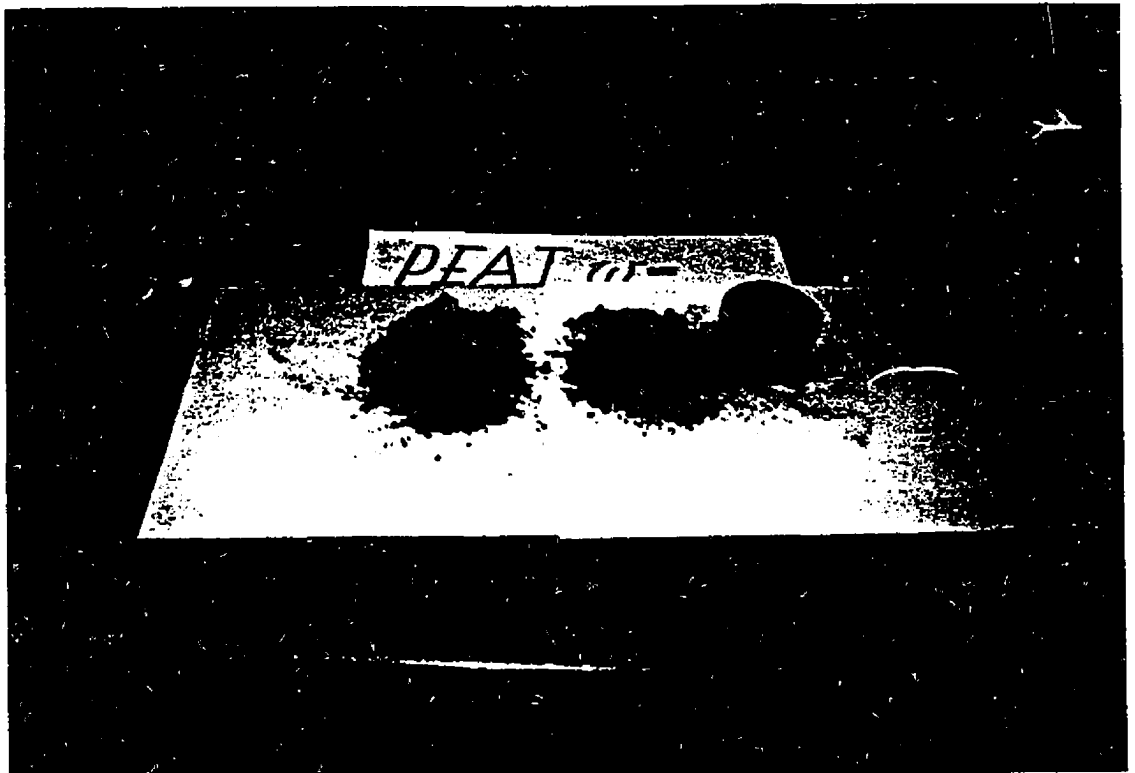


Fig 6.50 Samples of Peat Soil Used for Laboratory Testing. On the Left Side, the Peat Sample is Wet While on The Right Side, it is Dry (Treated in the Oven at $T = 105^{\circ} \text{C}$ for 24 hours).

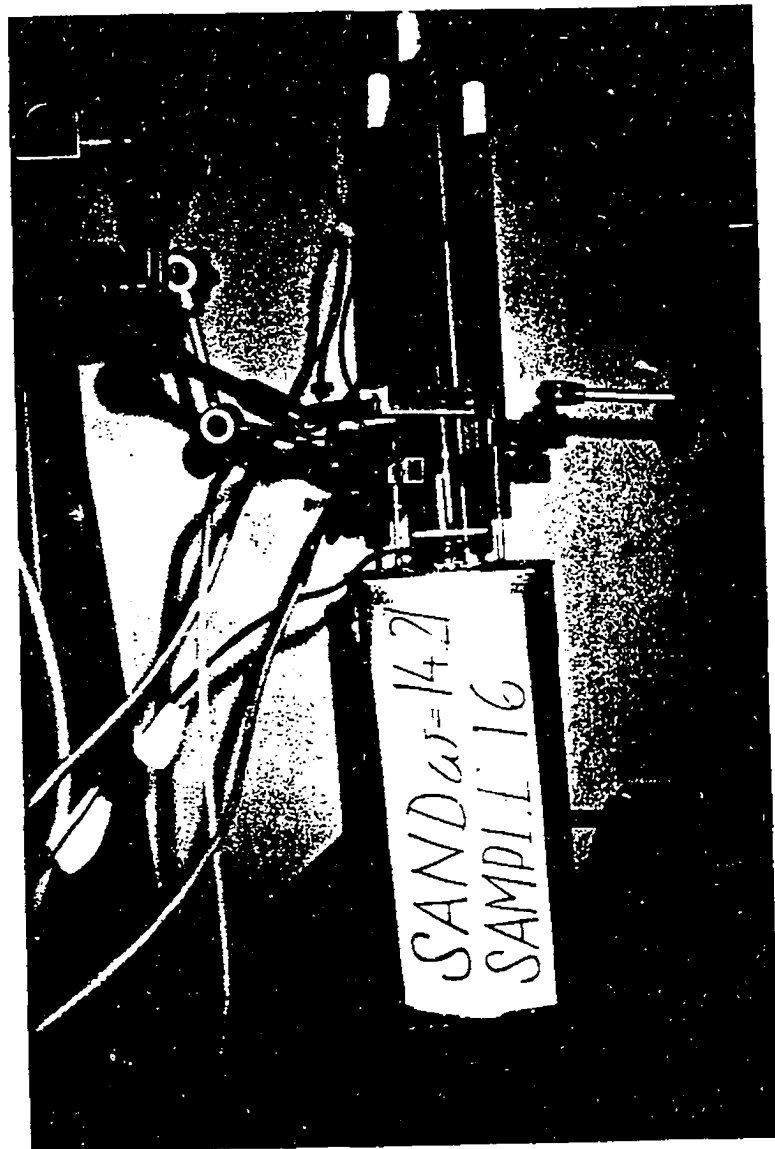


Fig 6.51 Test # 16: Sand Sample With Water Content $w = 14.2\%$, $T = -4.52^{\circ}\text{C}$

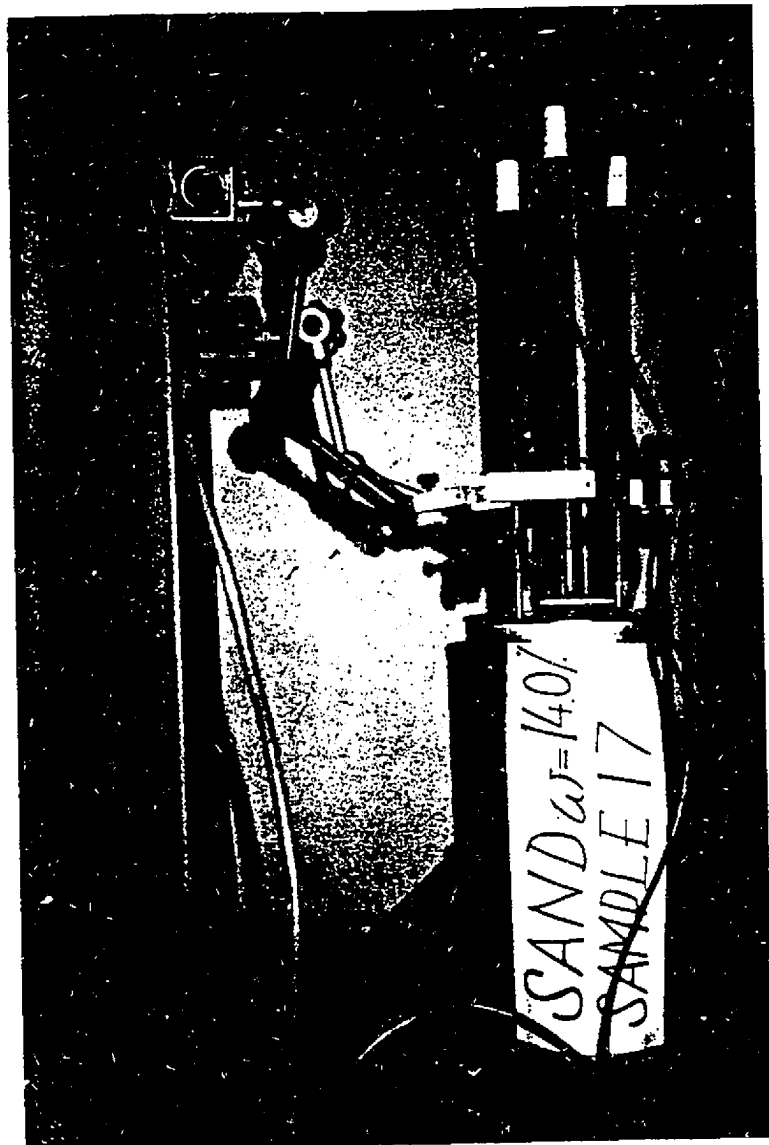


Fig 6.52 Test # 17: Sand Sample With Water Content $w = 14.0\%$, $T = -4.86^\circ\text{C}$

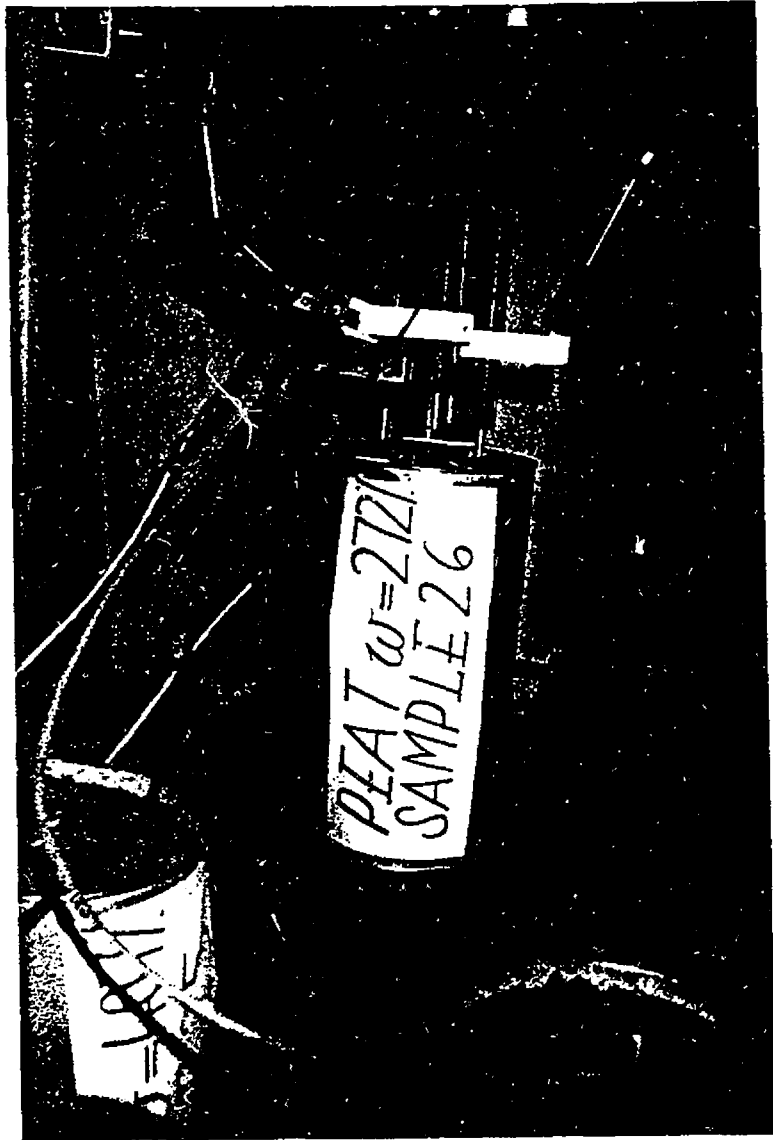


Fig 6.53 Test # 26: Peat Sample With Water Content $w = 272\%$, $T = -4.26^{\circ}\text{C}$



Fig 6.54 Test # 27: Peat Sample With Water Content $w = 273\%$, $T = -4.39^\circ\text{C}$



Fig 6.55 Mode of Failure for Tests # 24 to 27: Concentric Rupture Circles Appearing Around the Pile Surface.

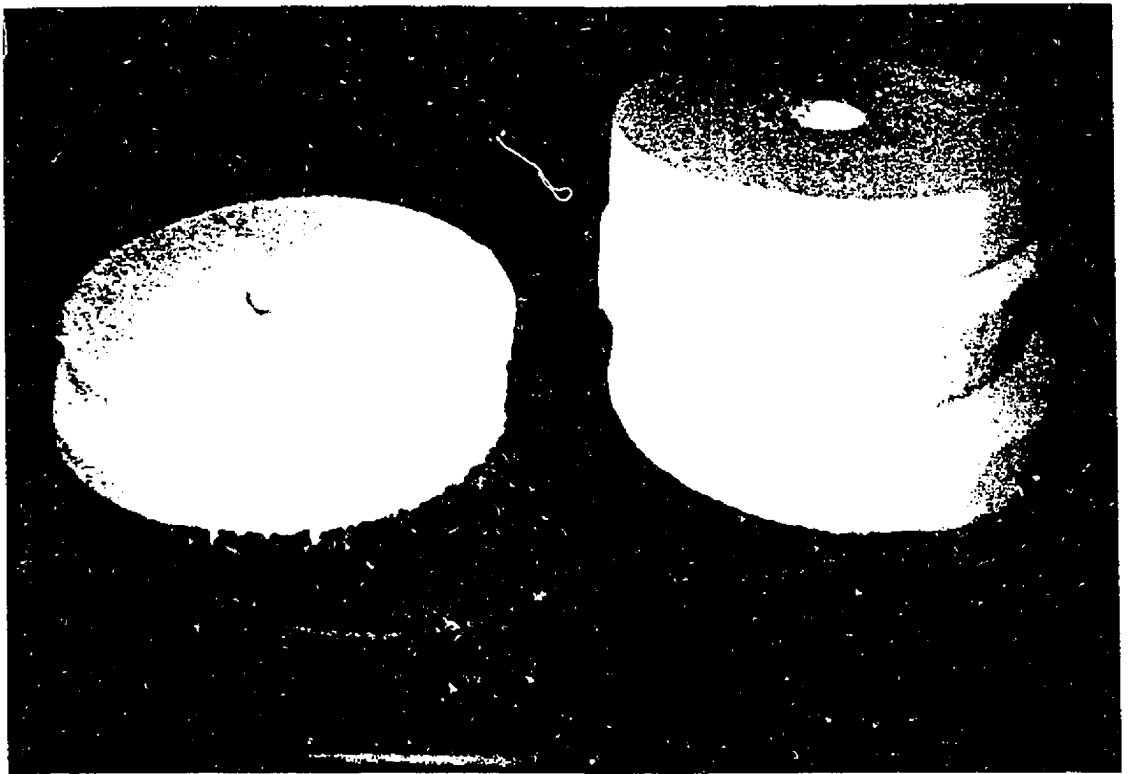


Fig 6.56 Foam Material Used as a Separating Surface Between Wet and Dry Peat Sample for Tests # 19 to 27. The Thickness Varies from One Test to the Other.



Fig 6.57 Disposition Set Up for Tests with Peat. Note the Loose Dry Peat in the Bottom of the Testing Cylinder under the Insulating Surface.

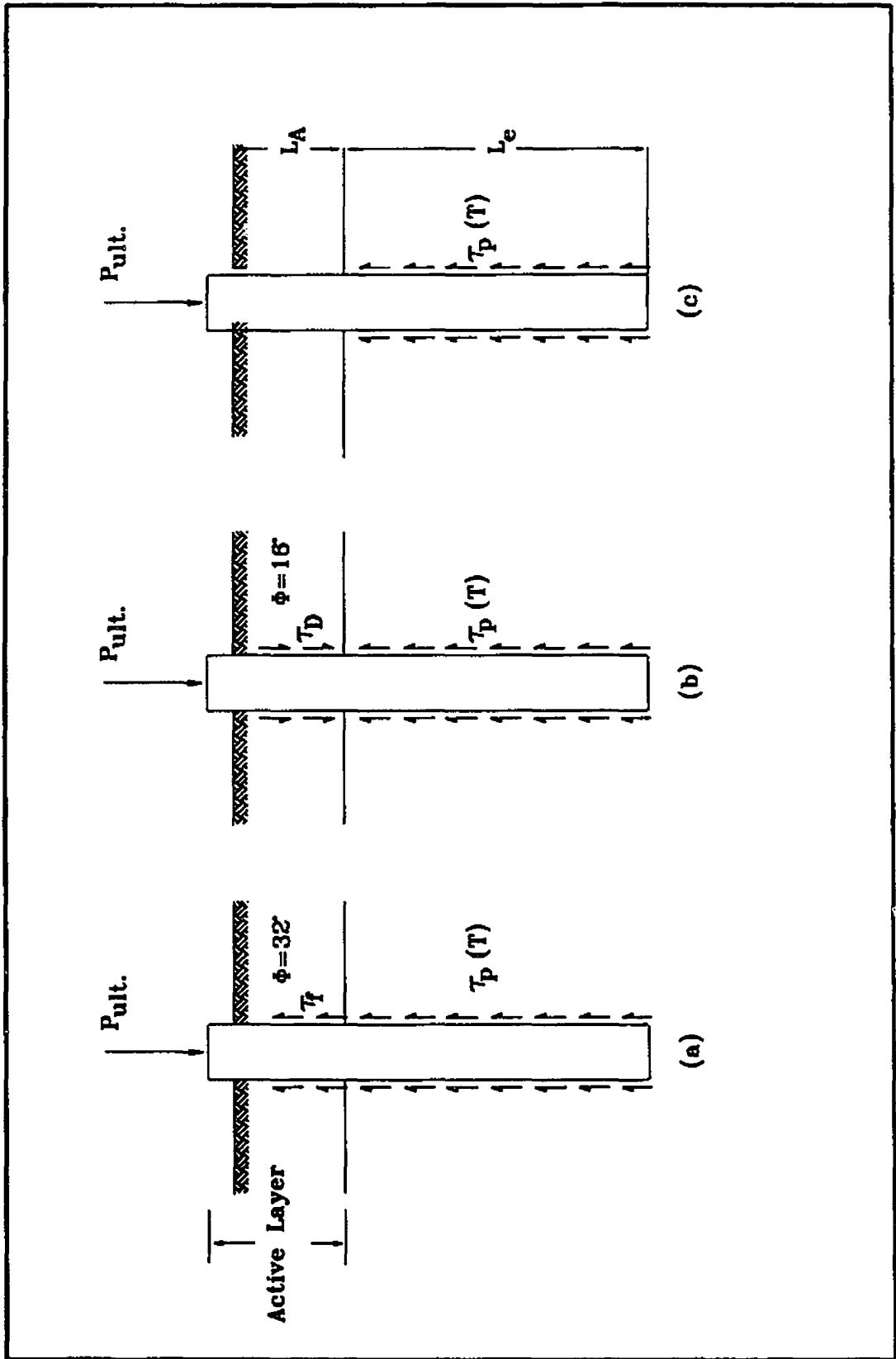


Fig. 7.1 System of FORCES Acting on the Pile Embedded in:
a) Sand, b) Clay, c) Peat.

Pile in Sand Soil, $w = 15\%$, Mesh 1 August 20, Summer Conditions

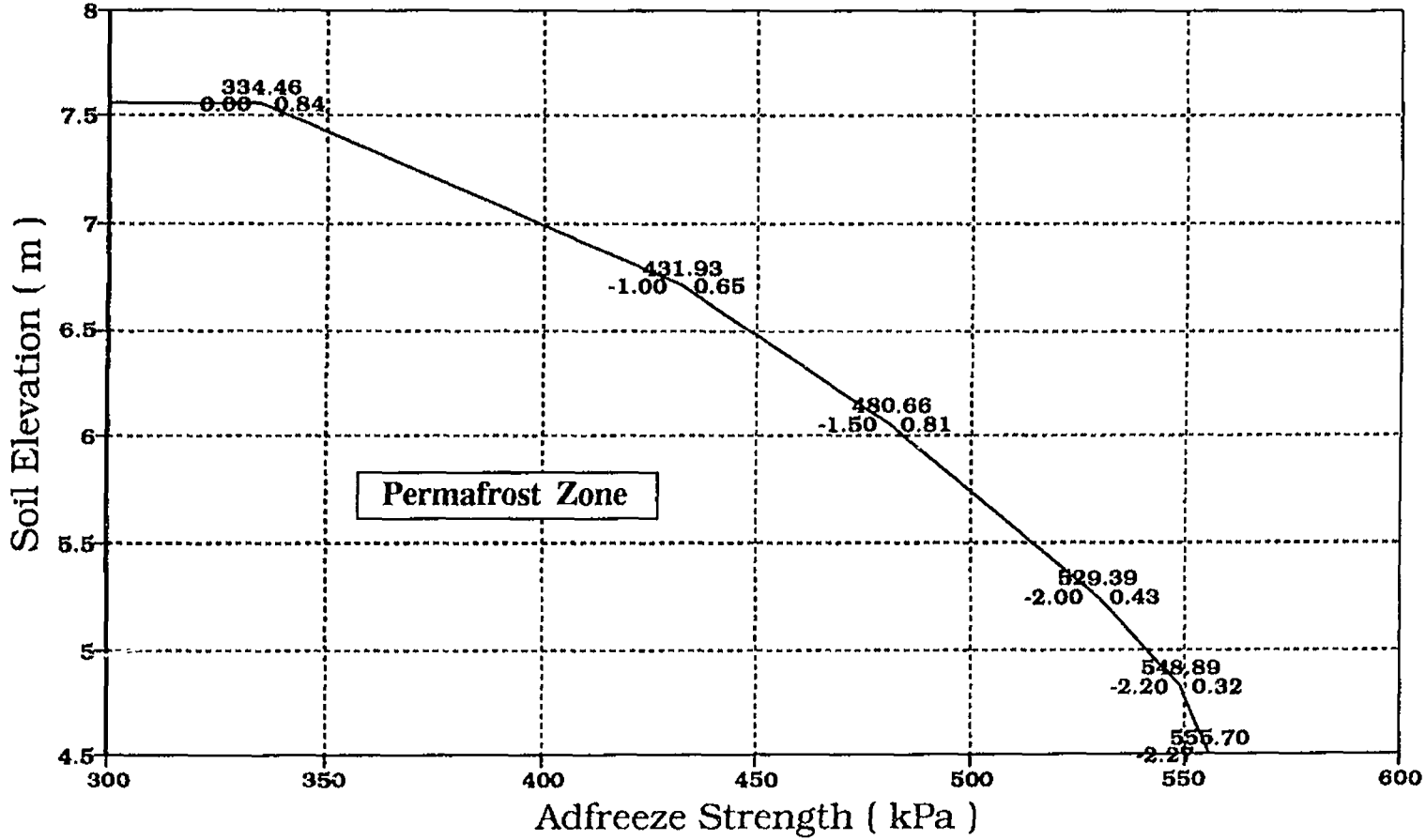


Fig. 7.2 Distribution of the Adfreeze Strength along the Pile Embedded in Sandy Soil with Water Content, $w = 15\%$

Pile in Sand Soil, w= 20 % , Mesh 1 August 20 , Summer Conditions

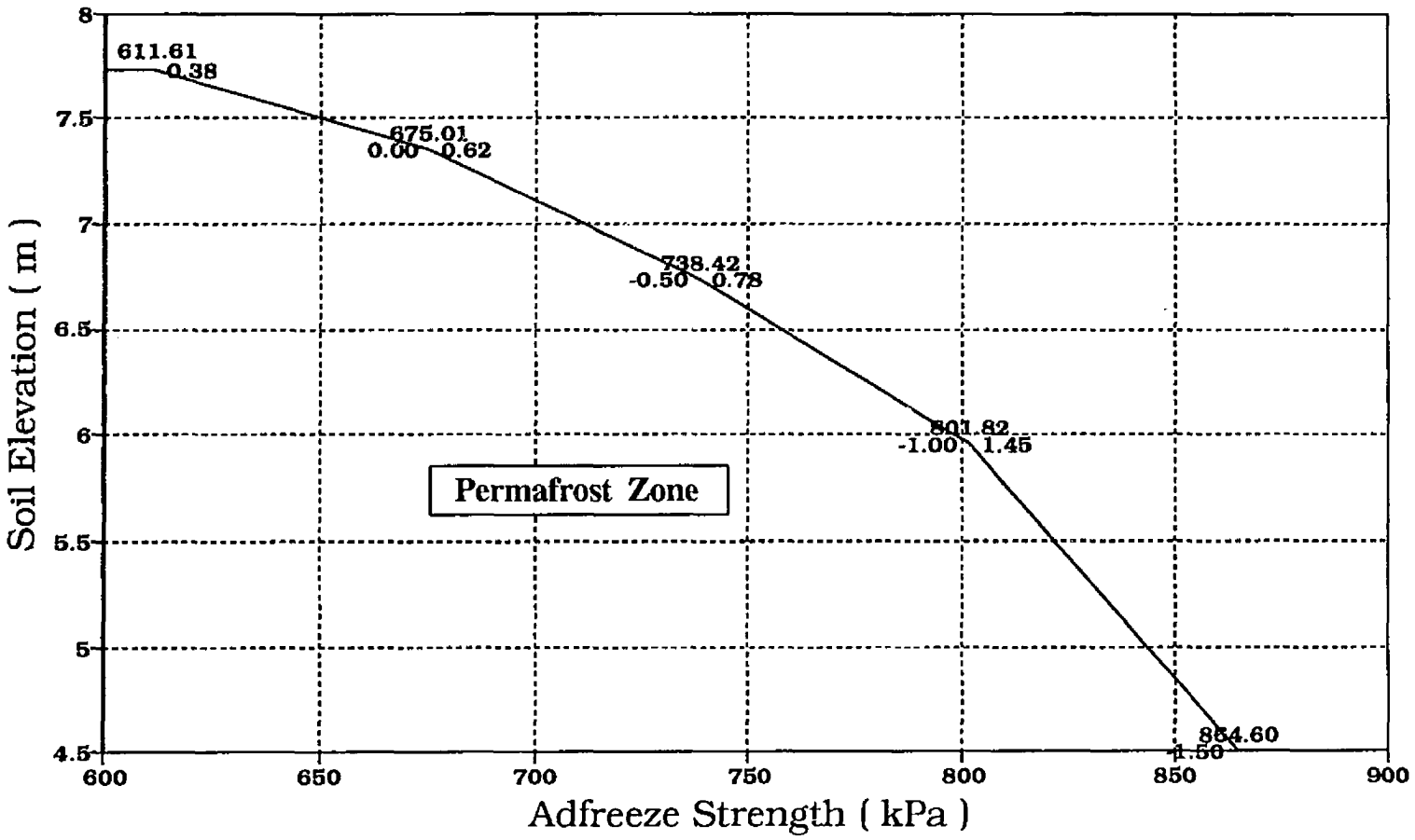


Fig. 7.3 Distribution of the Adfreeze Strength along the Pile Embedded in Sandy Soil with Water Content, w = 20 % , for Summer Condition.

Pile in Clay soil, $w = 15\%$, Mesh -2- August 20, Summer Conditions

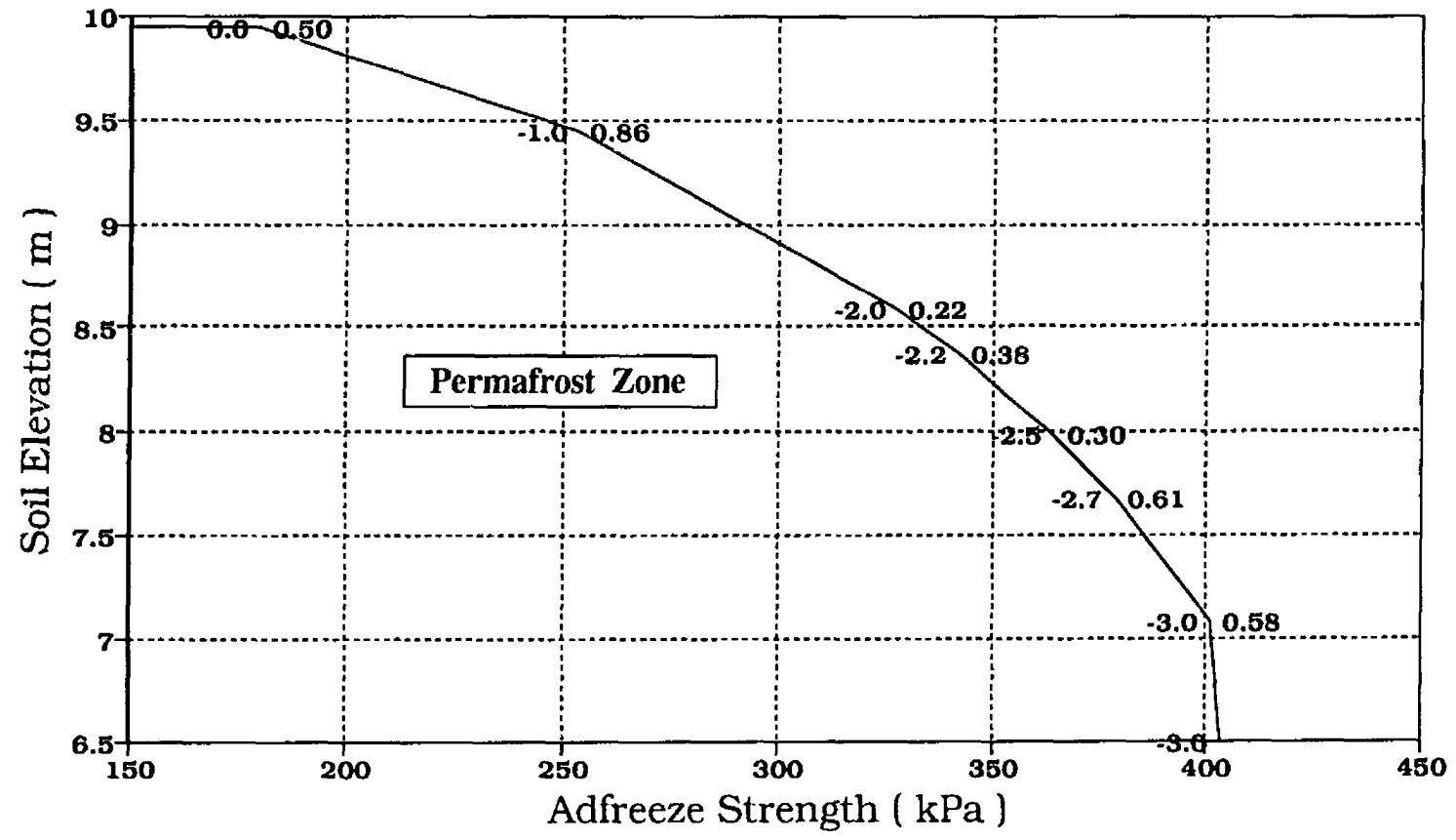


Fig. 7.4 Distribution of the Adfreeze Strength along the Pile Embedded in Clayey Soil with Water Content, $w = 15\%$, for Summer Condition.

Pile in Clay Soil, $w = 30\%$, Mesh -2- August 20, Summer Conditions

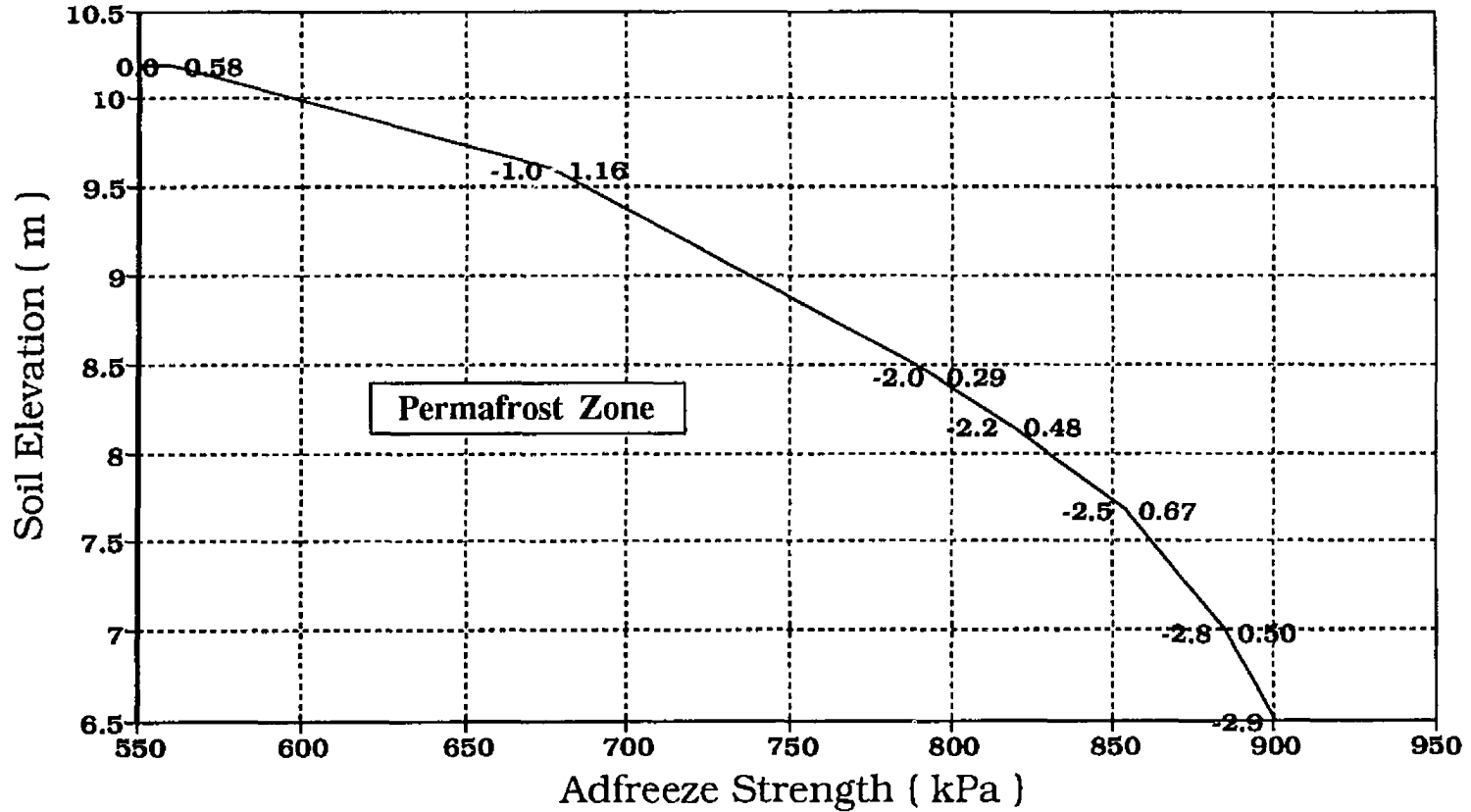
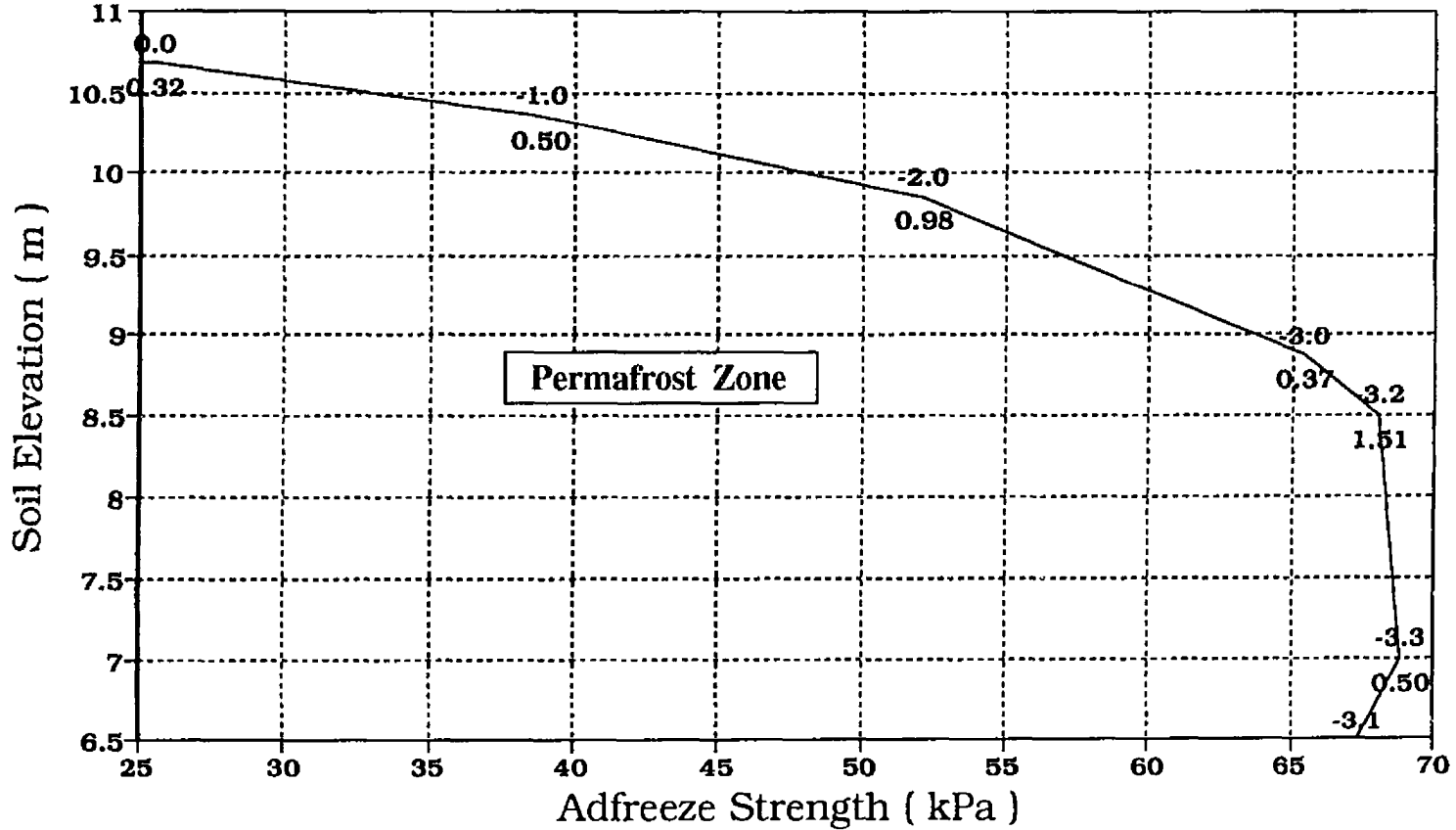


Fig. 7.5 Distribution of the Adfreeze Strength along the Pile Embedded in Clayey Soil with Water Content, $w = 30\%$, for Summer Condition.

Pile in Peat Soil, $w = 80\%$, Mesh -2- August 20, Summer Conditions



305

Fig. 7.6 Distribution of the Adfreeze Strength along the Pile Embedded in Peat Soil with Water Content, $w = 80\%$, for Summer Condition.

Pile in Peat Soil, $w=120\%$, Mesh -2- August 20 , Summer Conditions

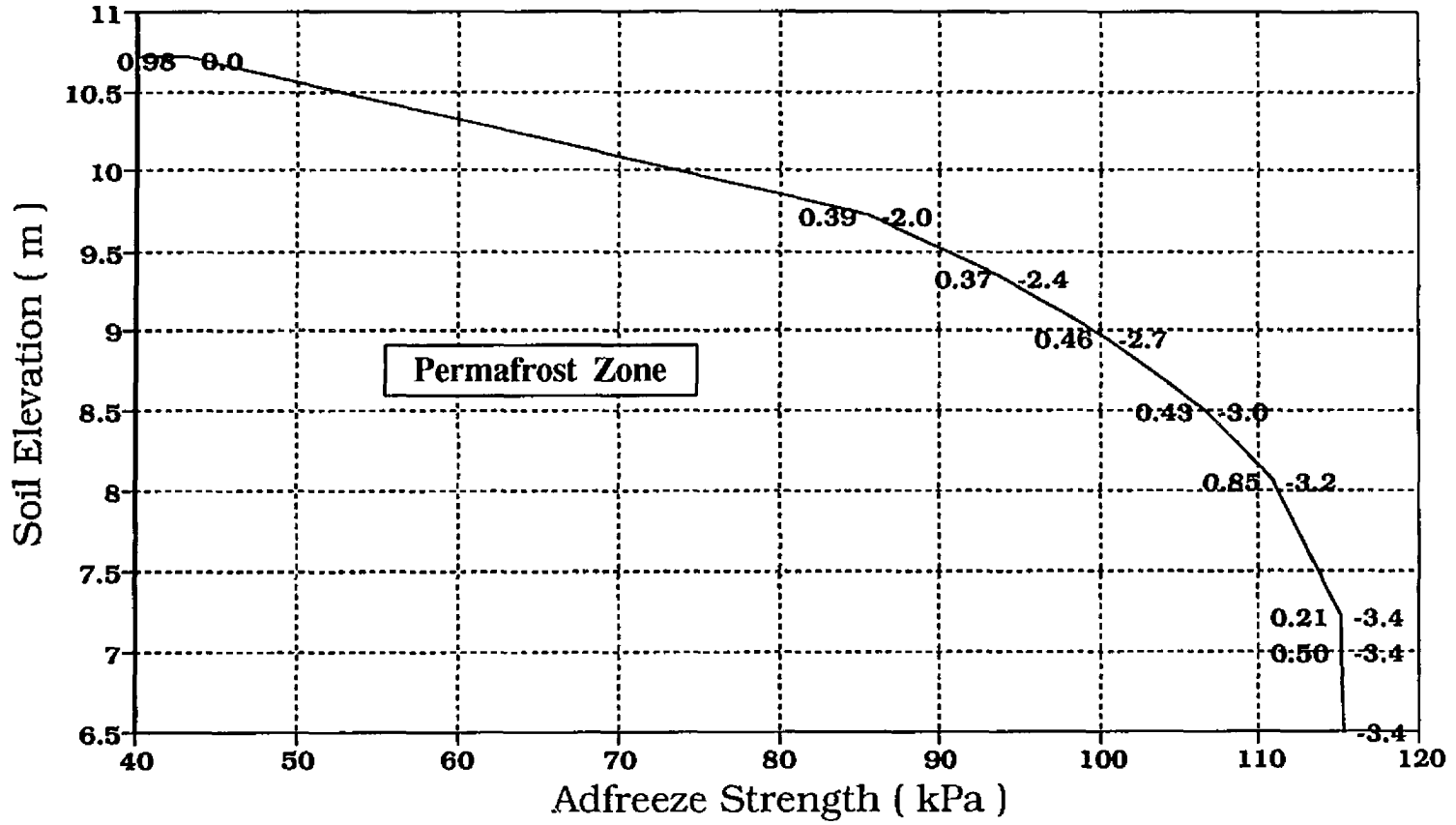


Fig. 7.7 Distribution of the Adfreeze Strength along the Pile Embedded in Peat Soil with Water Content, $w = 120\%$, for Summer Condition.

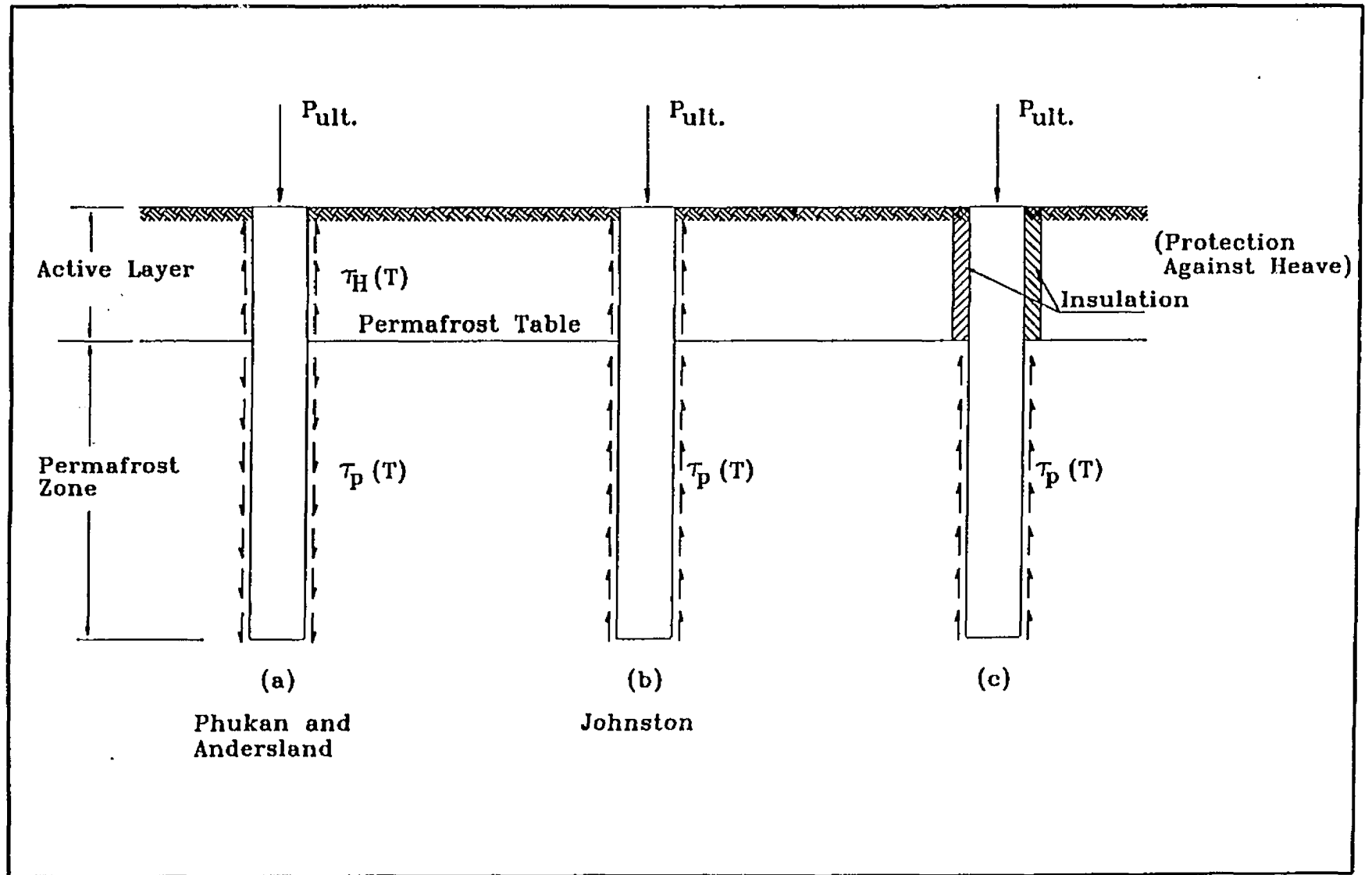


FIG. 7.8 System of FORCES Acting on the Pile Embedded in:
 in Sand, Clay and Peat for Winter Condition:
 a&b) with Heave, and, c) without Heave

Pile in Sand Soil, $w = 15\%$, Mesh 1 Winter Conditions With Heaving

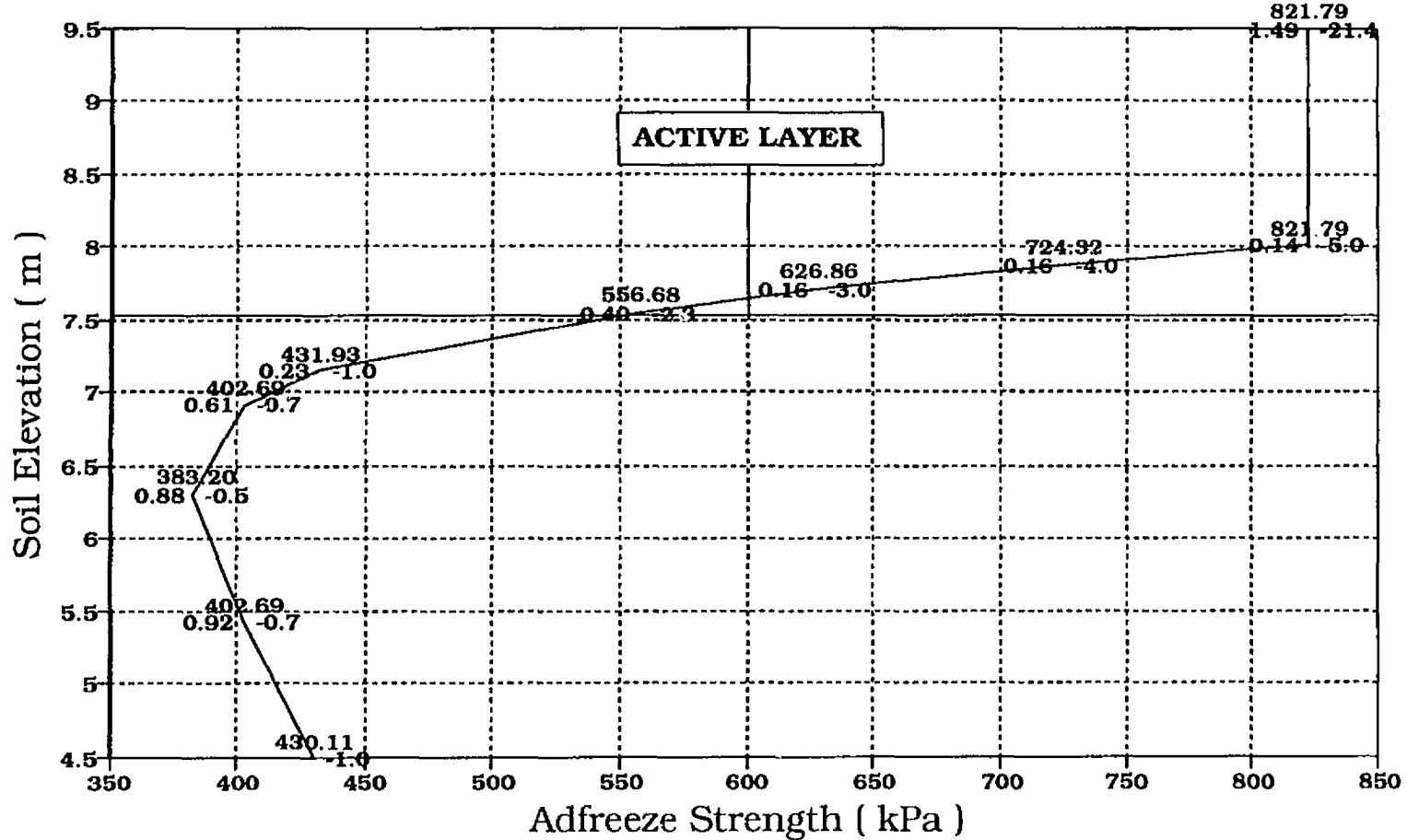


Fig. 7.9 Distribution of the Adfreeze Strength along the Pile Embedded in Sandy Soil with $w = 15\%$, for Winter Condition with Heaving.

Pile in Sand Soil, $w = 15\%$, Mesh 1 Winter Conditions Without Heaving

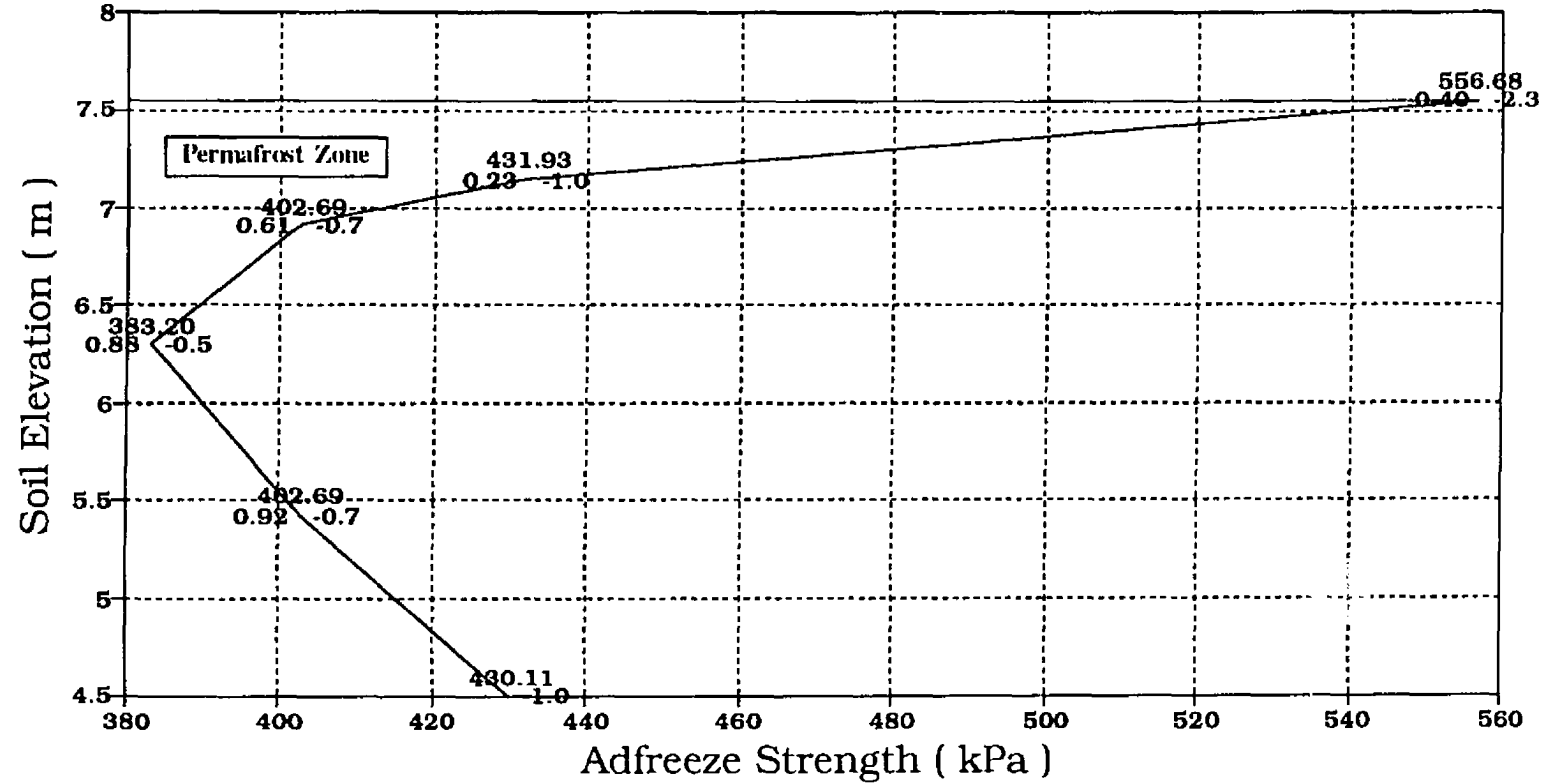


Fig. 7.10 Distribution of the Adfreeze Strength along the Pile Embedded in Sandy Soil with $w = 15\%$, for Winter Condition without Heaving.

Pile in Sand Soil, $w = 20\%$, Mesh -1- Winter Conditions With Heaving

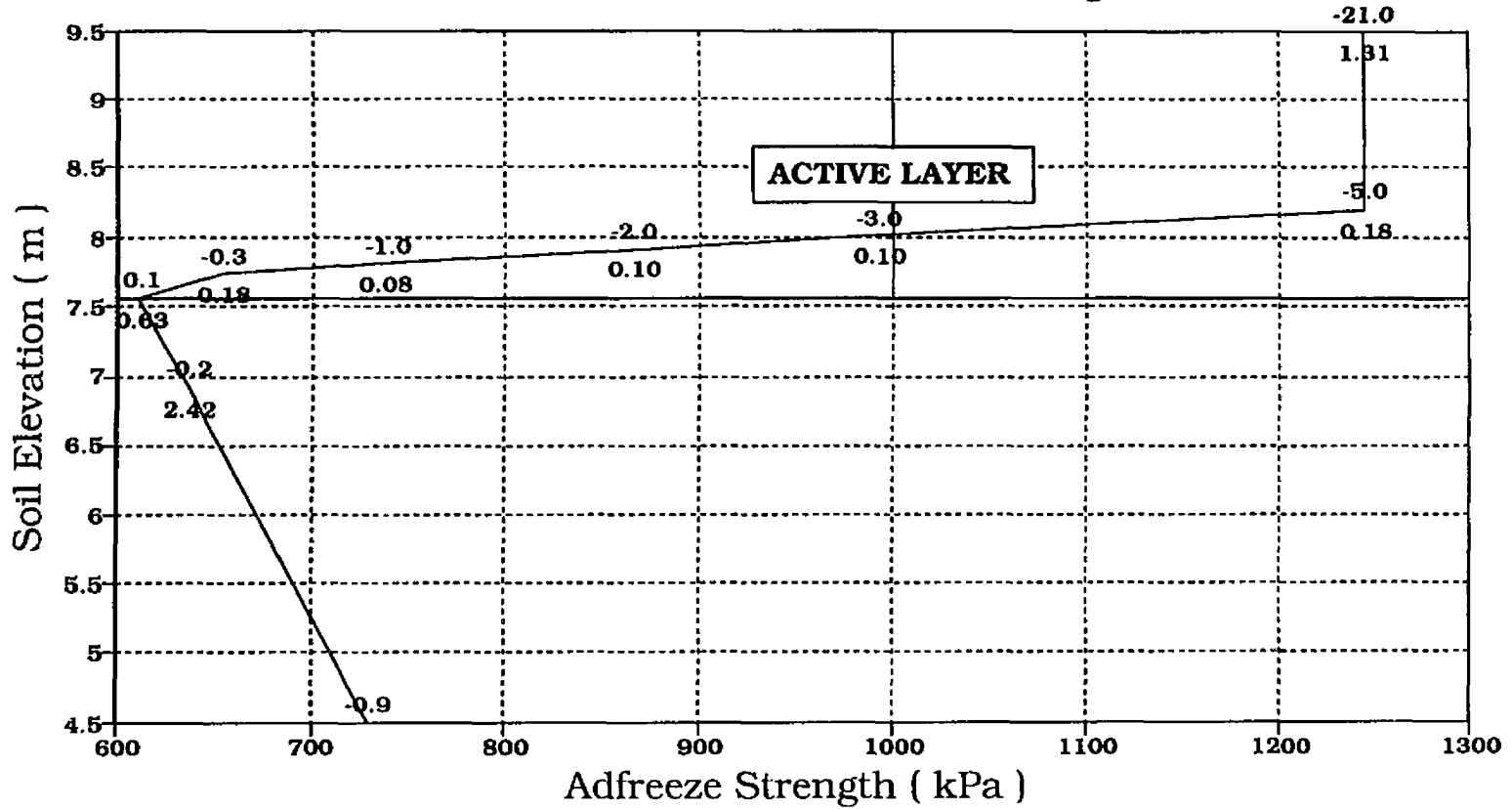


Fig. 7.11 Distribution of the Adfreeze Strength along the Pile Embedded in Sandy Soil with $w = 20\%$, for Winter Condition with Heaving.

Pile in Sand Soil, $w = 20\%$, Mesh -1- Winter Conditions Without Heaving

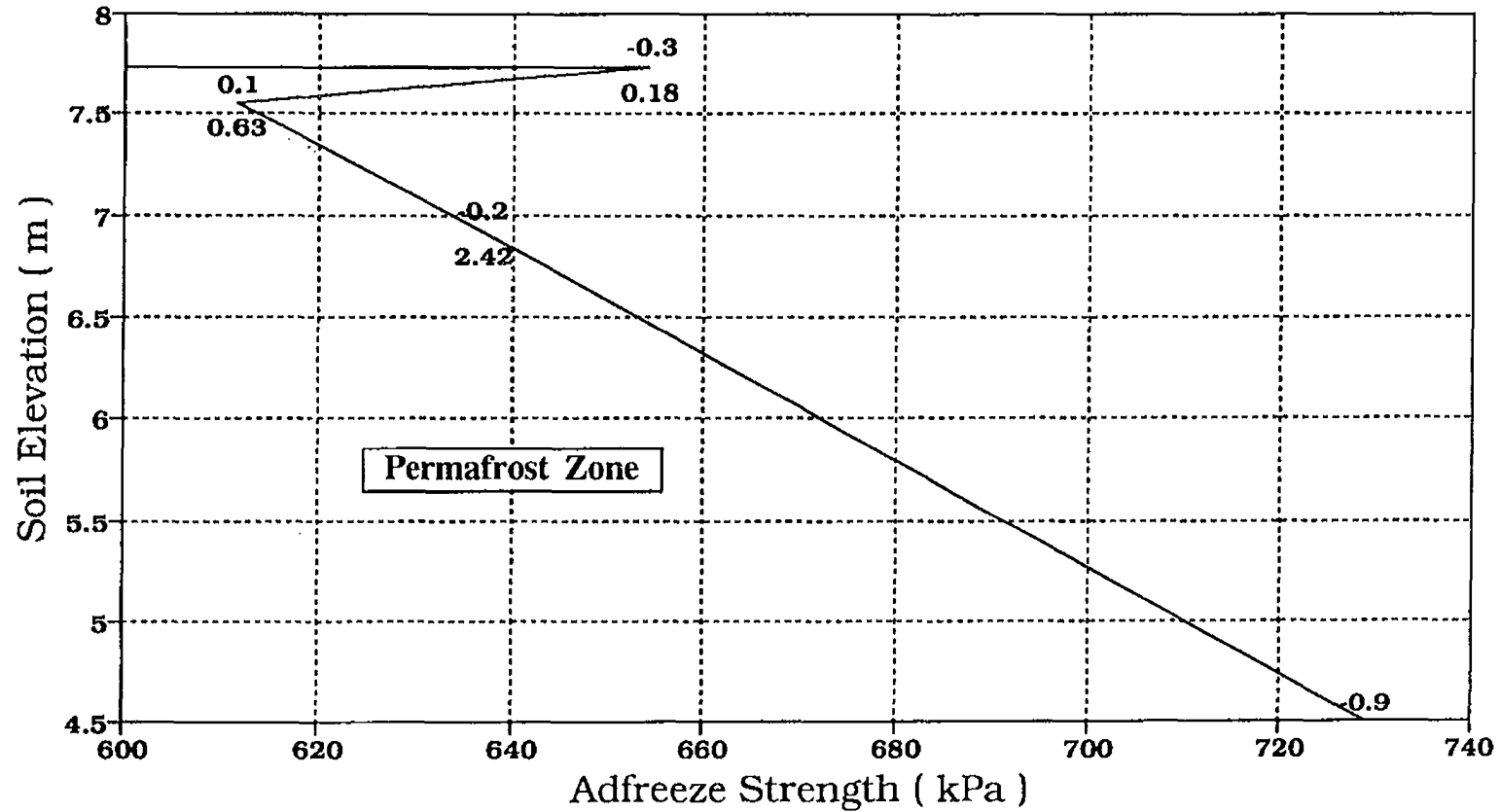


Fig. 7.12 Distribution of the Adfreeze Strength along the Pile Embedded in Sandy Soil with $w = 20\%$, for Winter Condition without Heaving.

Pile in Clay Soil, $w = 15\%$, Mesh -2- Winter Conditions With Heaving

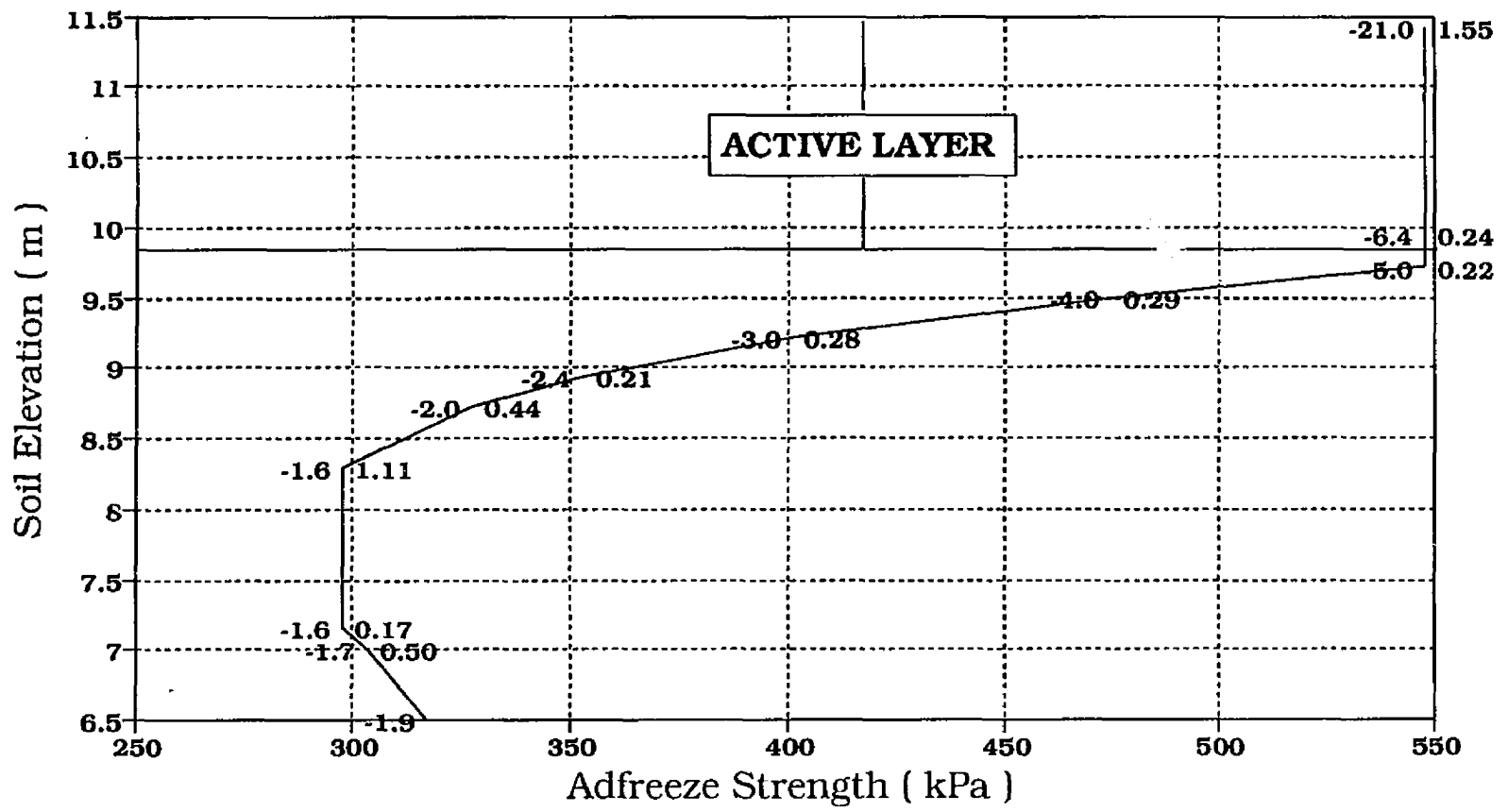


Fig. 7.13 Distribution of the Adfreeze Strength along the Pile Embedded in Clayey Soil with $w = 15\%$, for Winter Condition with Heaving.

Pile in Clay Soil, $w = 15\%$, Mesh -2- Winter Conditions Without Heaving

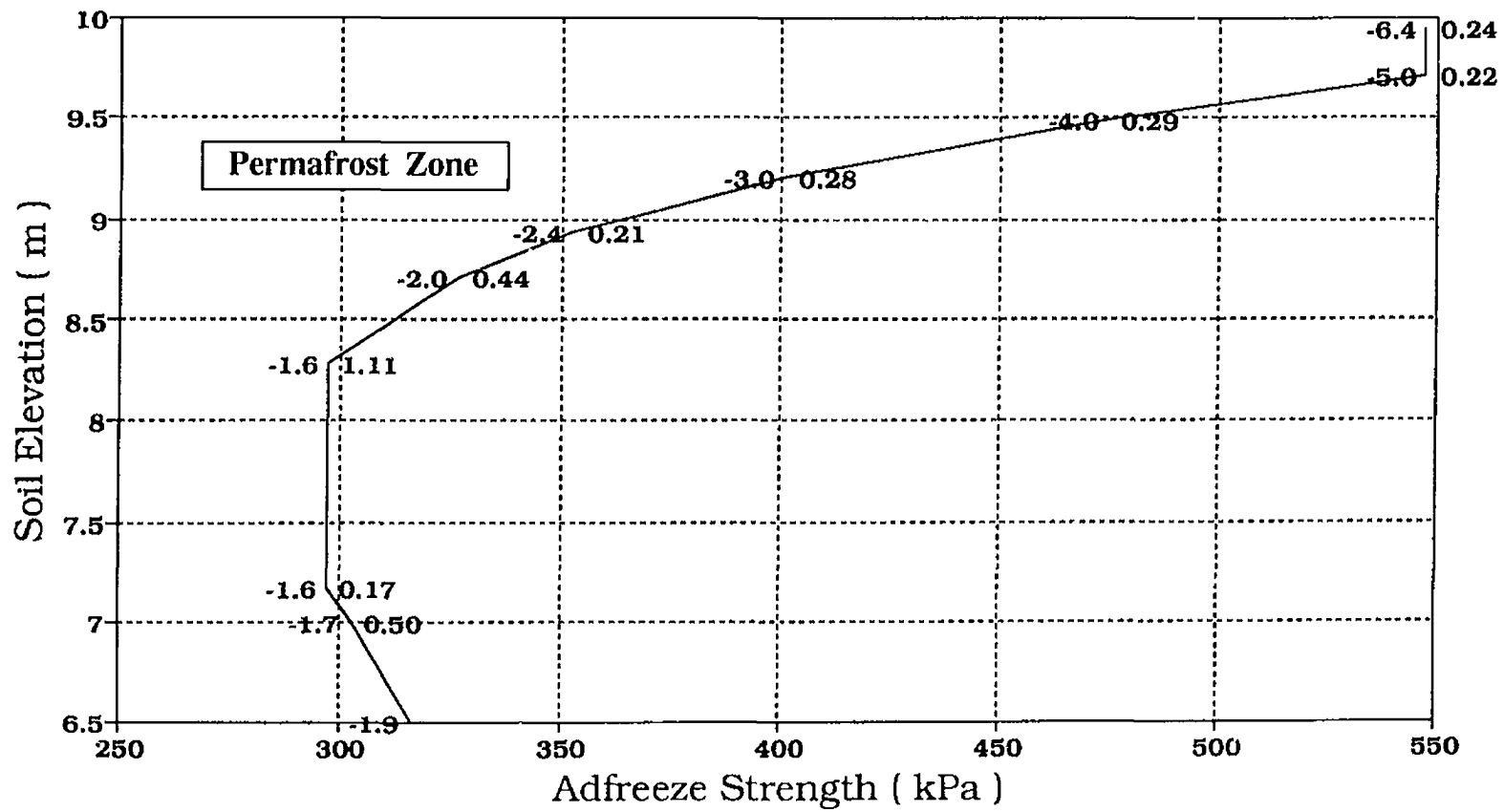


Fig. 7.14 Distribution of Adfreeze Strength along the Pile Embedded in Clayey Soil with $w = 15\%$, for winter Condition without Heaving.

Pile in Clay Soil, $w = 30\%$, Mesh -2- Winter Conditions With Heaving

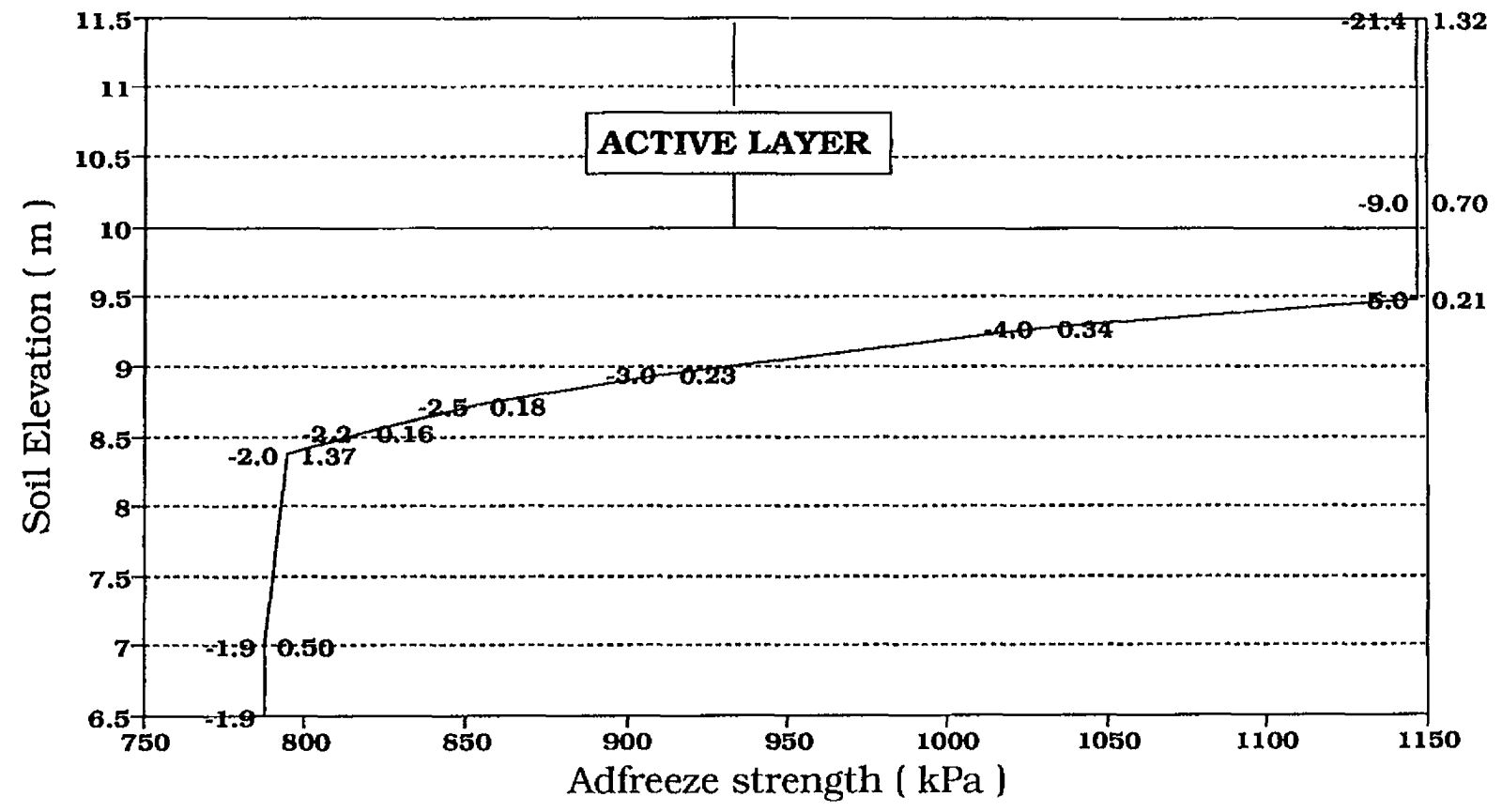


Fig. 7.15 Distribution of the Adfreeze Strength along the Pile Embedded in Clayey Soil with $w = 30\%$, for Winter Condition with Heaving.

Pile in Clay Soil, $w = 30\%$, Mesh -2- Winter Conditions Without Heaving

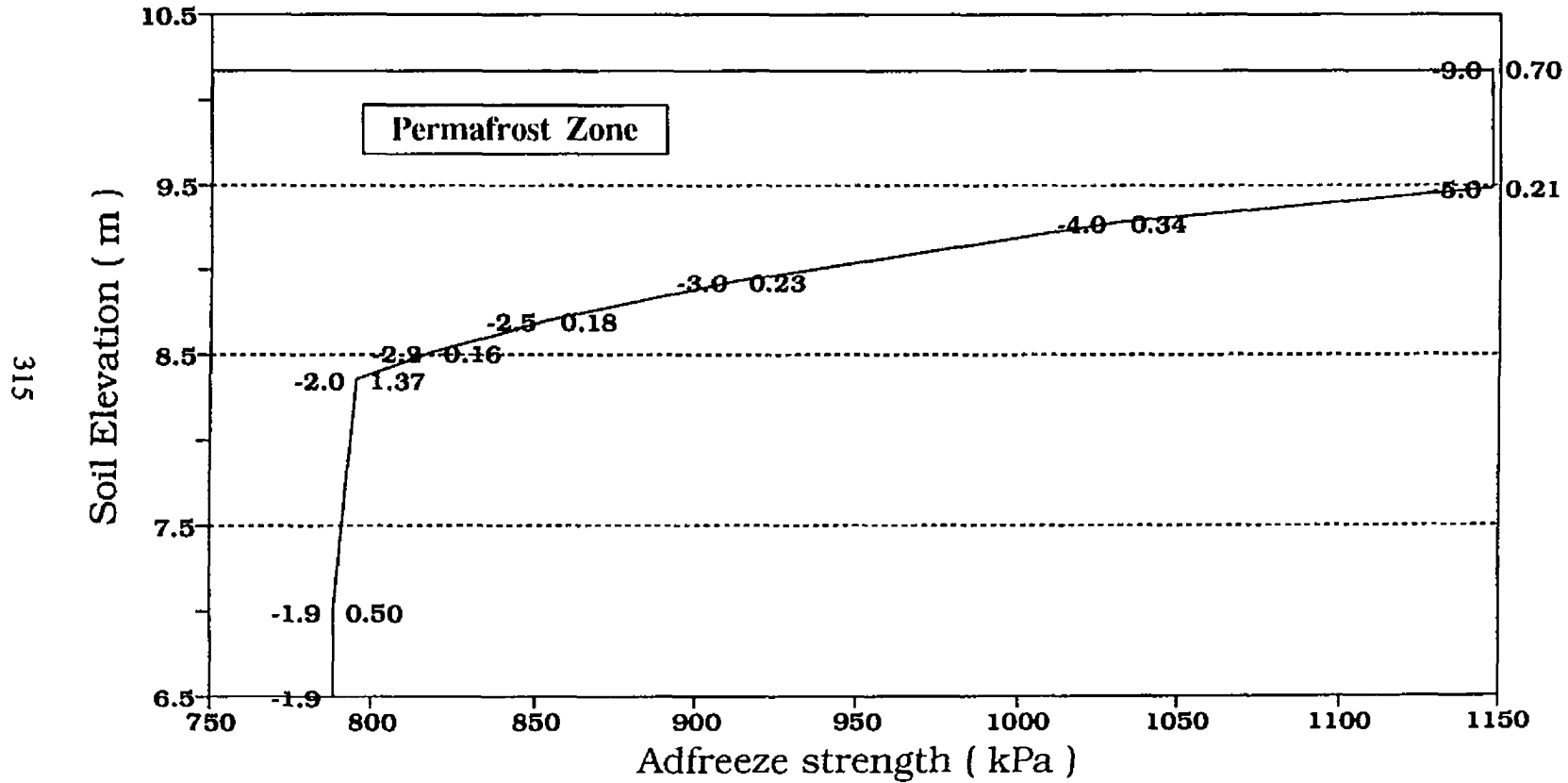


Fig. 7.16 Distribution of the Adfreeze Strength along the Pile Embedded in Clayey Soil with $w = 30\%$, for Winter Condition with Heaving.

Pile in Peat Soil, $w = 80\%$, Mesh 2 Winter Conditions With Heaving

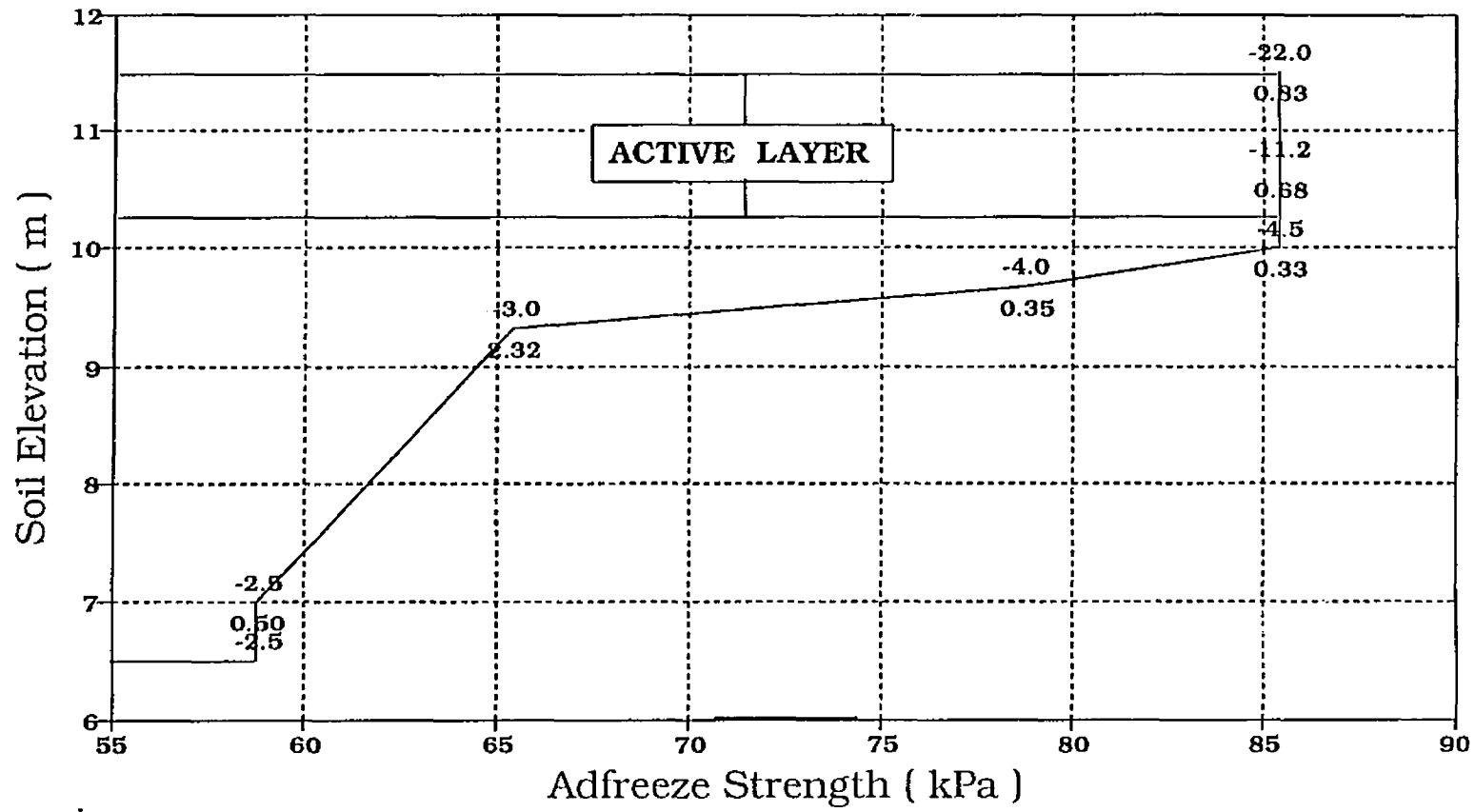


Fig. 7.17 Distribution of the adfreeze Strength along the Pile Embedded in Peat Soil with $w = 80\%$, for Winter Condition with Heaving.

Pile in Peat Soil, $w = 80\%$, Mesh 2 Winter Conditions Without Heaving

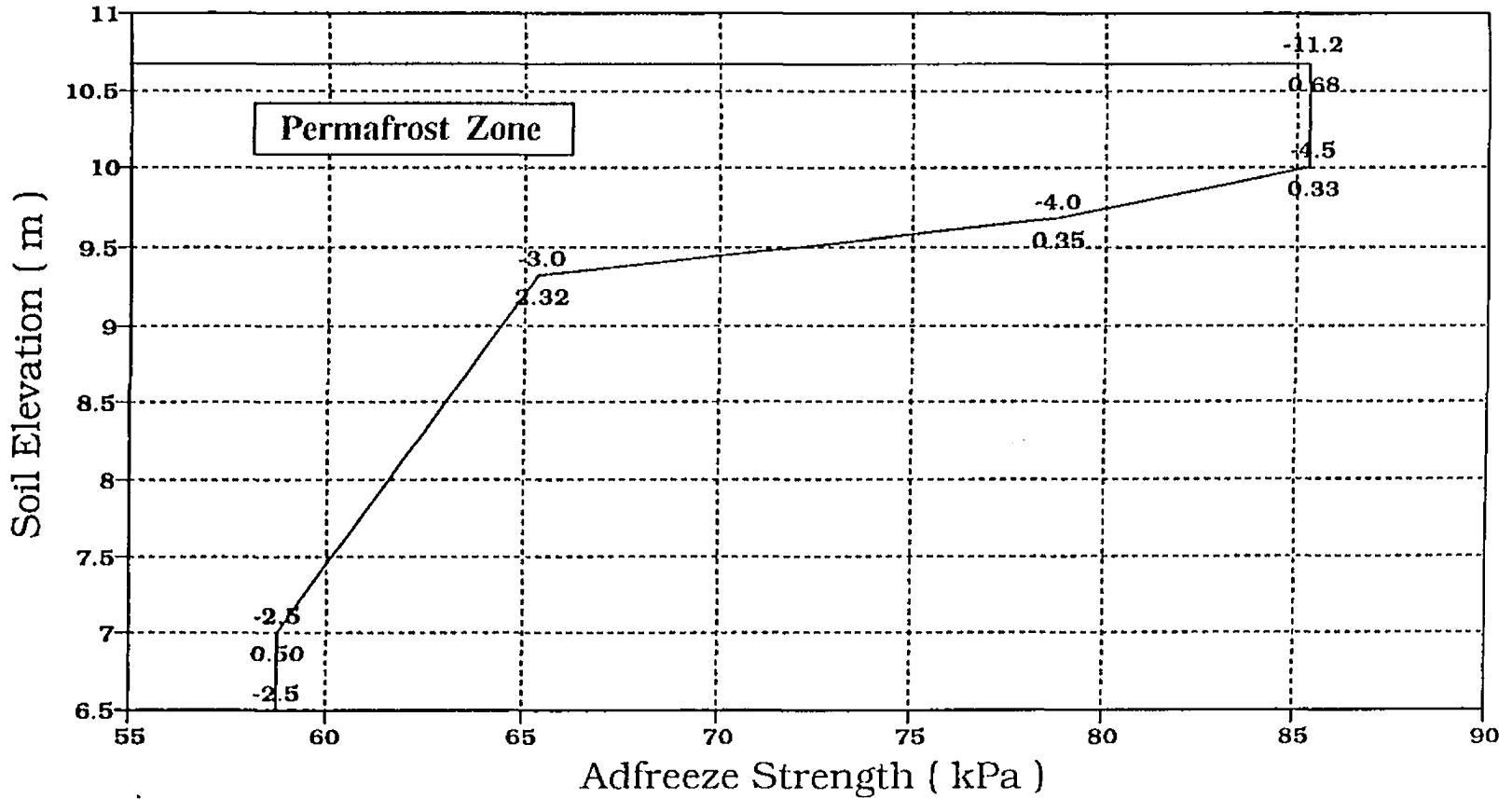


Fig. 7.18 Distribution of the Adfreeze Strength along the Pile Embedded in Peat Soil with $w = 80\%$, for Winter Condition without Heaving.

Pile in Peat Soil, $w=120\%$, Mesh -2- Winter Conditions With Heaving

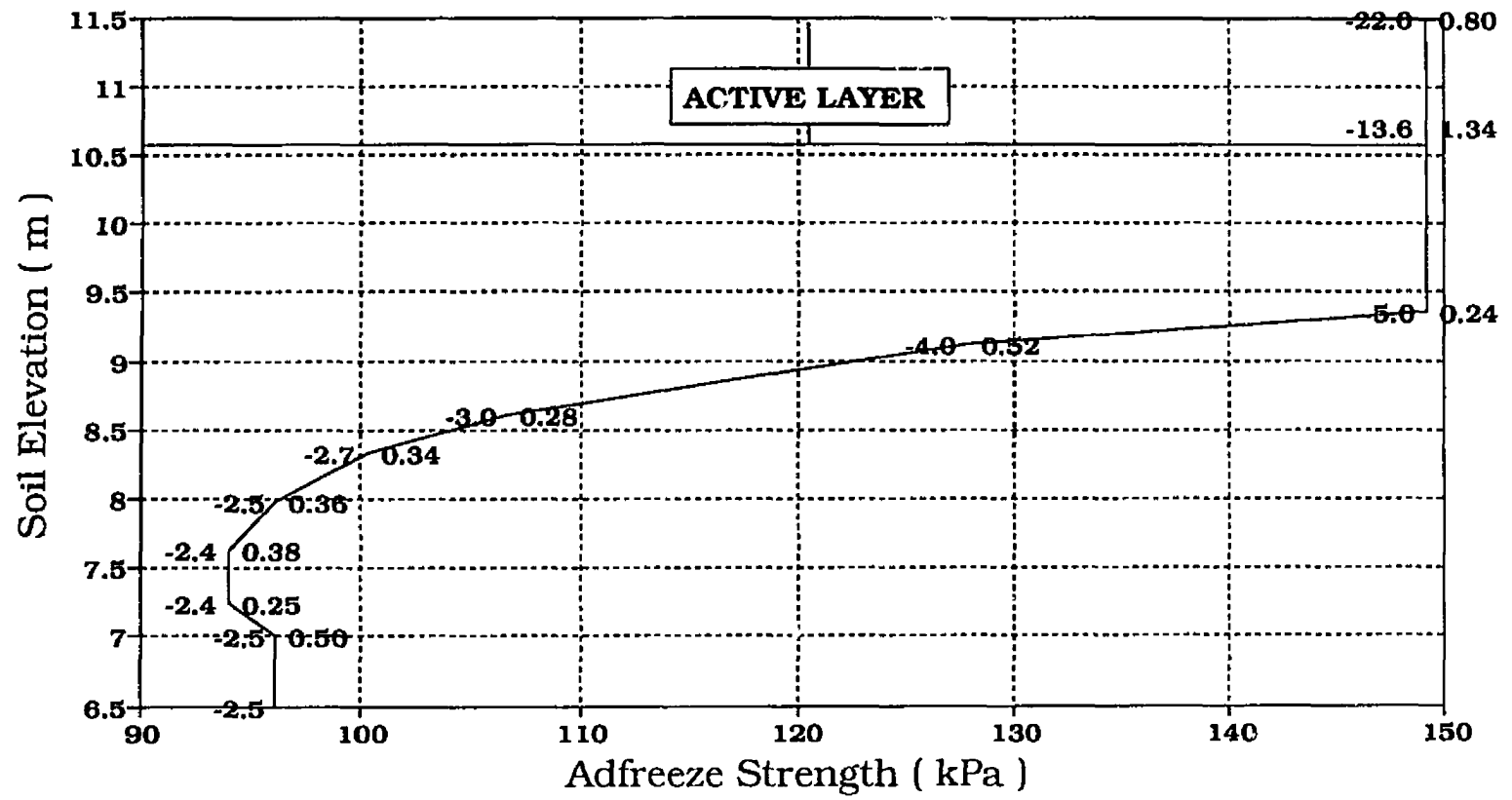


Fig. 7.19 Distribution of the Adfreeze Strength along the Pile Embedded in Peat Soil with $w = 120\%$, for Winter Condition with Heaving.

Pile in Peat Soil, $w=120\%$, Mesh -2- Winter Conditions Without Heaving

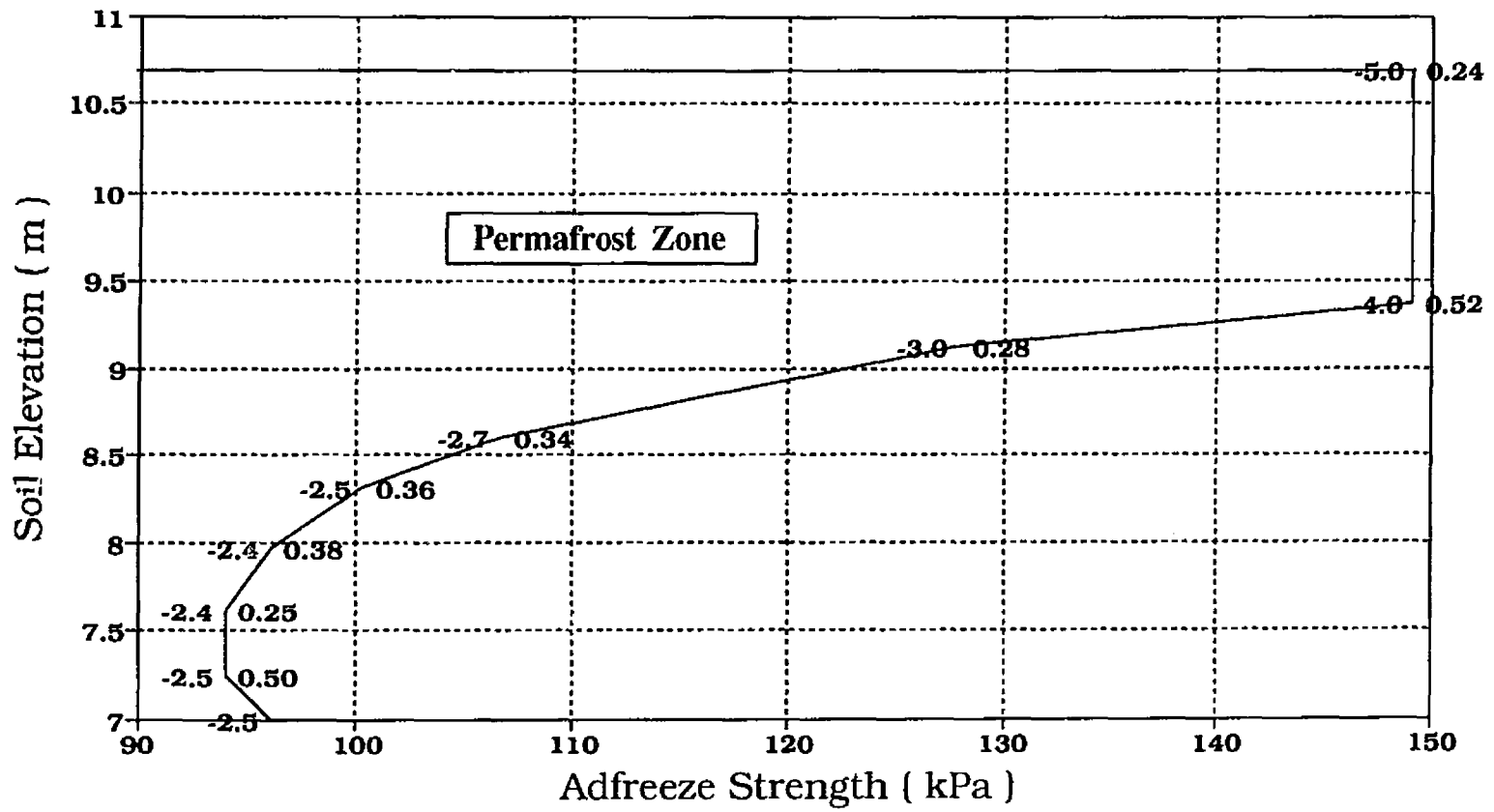


Fig. 7.20 Distribution of the Adfreeze Strength along the Pile Embedded in Peat Soil with $w = 120\%$, for Winter Condition without Heaving.

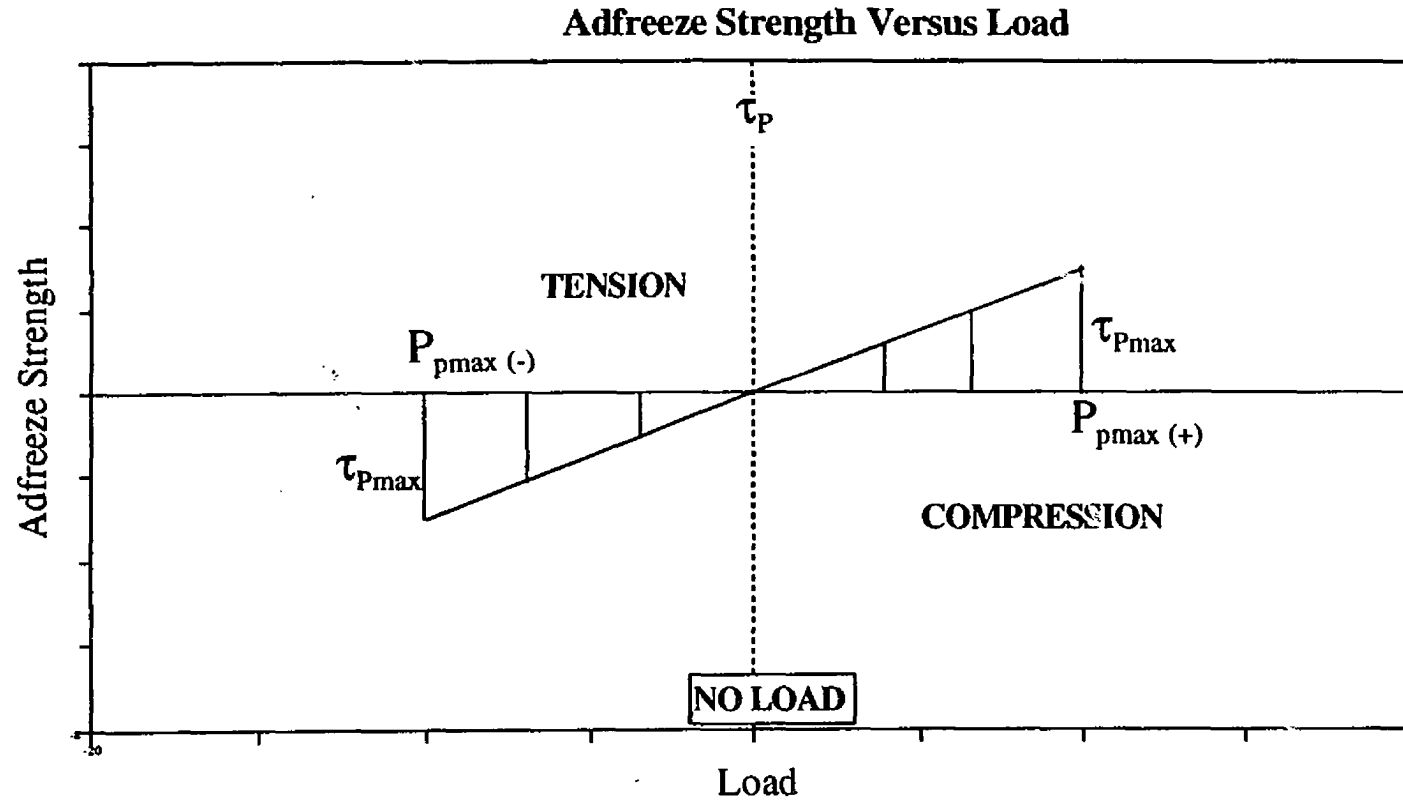


Fig. 7.21 Proposed Linear Adfreeze Strength Versus Load in the Permafrost Zone.

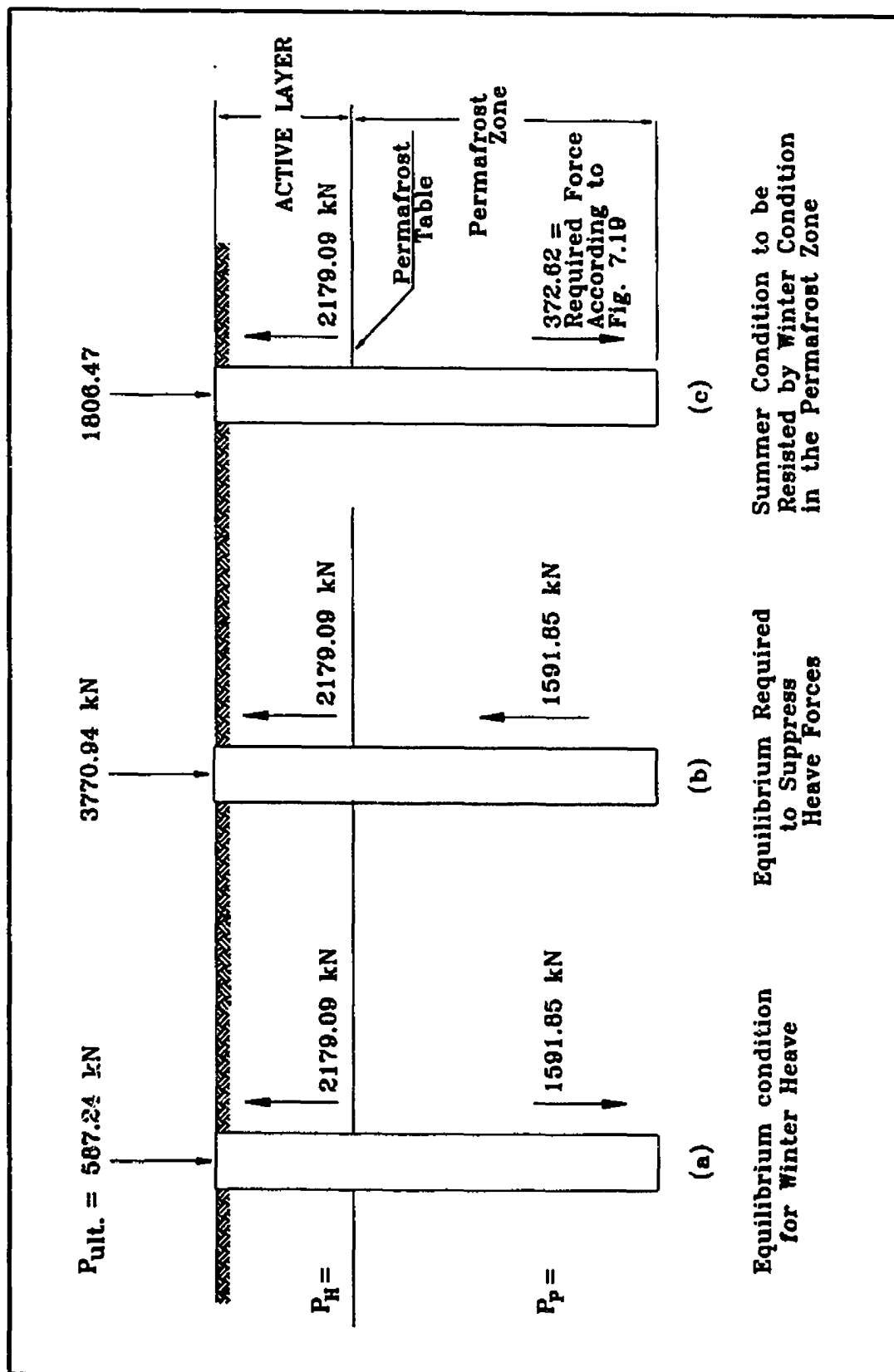


Fig. 7.22 Equilibrium Conditions for Winter

REFERENCES

- 1- Aldrich, H.P. (1956) "*Frost Penetration below Highway and Airfield Pavements*", Highway Research Board Bulletin 135.
- 2- Andersland, O.B. and Anderson, D.M. (1978), "*Geotechnical Engineering for Cold Regions*", McGraw-Hill Book Company, N.Y.
- 3- Bathe, K.J. (1982), "*Finite Element Procedures in Engineering Analysis*", Prentice-Hall Inc., Englewood Cliffs, N.Y.
- 4- Bell, G.E. and Wood, A.S. (1983), "*On the Performance on the Enthalpy Method in the Region of a Singularity*", Int. J. Numer. Methods Engng., Vol. 19, pp. 1583-1592.
- 5- Berggren, W.P., (1943) "*Prediction of Temperature Distribution in Soils*", Transaction, American Geophysical Society, Series C, No. 375.
- 6- Biggar, K.W. and Segoo, D.C. (1989), "*Field Load Testing of Various Pile Configurations in Saline Permafrost and Seasonally Frozen Rock*", Proceeding, 42nd Canadian Geotechnical Conference, Winnipeg, Man., pp. 304-312.
- 7- Biggar, K.W. and Segoo, D.C. (1993), "*The Strength and Deformation Behaviour of Model Adfreeze and Grouted Piles in Saline Frozen Soils*", Canadian Geotechnical Journal, Vol. 30 (2), pp. 319-337.
- 8- Carslaw, H.S. and Jaeger, J.C. (1959), "*Conduction of Heat in Solids*", Oxford University Press.
- 9- Coduto, D.P. (1994), "*Foundation Design, Principle and Practice*", Prentice Hall, Englewood Cliffs, N.J.
- 10- Comini, G., Del Giudice, S., Lewis, R.W. and Zienkiewicz, O.C. (1974), "*Finite Element Solution of Nonlinear Heat Conduction Problems with Special Reference to Phase Change*", Int. J. Numer. Methods Engng, Vol. 8. pp. 613-624.

- 11- Coyle, H.M. and Castello, R.R. (1981), "*New Design Correlations for Piles in Sand*", Journal of the Geotechnical Engineering Division, ASCE. Vol. 107, No. GT7, pp. 965-986.
- 12- Crivelli, L. and Idelsohn S. (1986), "*A Temperature-Based Finite Element Solution for Phase Change Problems*", Int. J. Numer. Methods Engng., Vol. 23, pp. 99-119.
- 13- Crory, F.E. (1966), "*Pile Foundations in Permafrost*", Proceedings of the International Conference on Permafrost, Lafayette, IN, U.S National Academy of Sciences, Publ. 1287, pp. 467-476.
- 14- Dalhuijsen, A.J. and Segal, A (1986), "*Comparison of Finite Element Techniques for Solidification problems*", Int. J. Num. Methods Engng., Vol. 23, pp.,1807-1829.
- 15- Das, B.M. (1990), "*Principle of Foundation Engineering*", Second Edition, PWS-Kent Publishing Company, Boston, U.S.A.
- 16- Eringen, A.C. (1967), "*Mechanics of Continua*", John Wilew & Sons Inc., New York.
- 17- Farouki, O.T. (1981), "*Thermal Properties of Soils*", U.S. Army, CRREL, Monograph, 81-2, U.S.A.
- 18- Frederking, R.M.W. (1979), "*Laboratory Tests on Downdrag Loads Developed by Floating Ice Covers on Vertical Piles*", Proceedings, 5th International Conference on Port and Ocean Engineering under Arctic Conditions, Trondheim, Norway, Vol. 2, pp. 1097-1110
- 19- Goodling, J.S. and Khadar, M.S. (1974), "*Inward Solidification with Radiation-Convection Boundary Conditions*", J. Heat Transfer, Vol. 96(1), pp. 114-115.
- 20- Hughes, T.J.R. (1987), "*The Finite Element Method - Linear Static and Dynamic Finite Element Analysis*", Prentice-Hall, Inc., Englewood Cliffs, New Jersey, U.S.A.
- 21- Incropera, F.P. and Dewitt, D.P. (1985), "*Fundamentals of Heat and Mass Transfer*", John Wiley & Sons Inc., Second Edition, New York, U.S.A.
- 22- Johansen, O. (1975), "*Thermal Conductivity of Soils*", Ph.D. Thesis, Trondheimer, Norway, (CRREL Translation 637, 1977).

- 23- Johnston, G.H. (1981), "*Permafrost: Engineering Design and Construction*", John Wiley & Sons, New York, U.S.A.
- 24- Johnston, G.H. and Ladanyi, B. (1972), "*Field Tests on Grouted Rod Anchors in Permafrost*". Canadian Geotechnical Journal, Vol. 9, pp. 176-194.
- 25- Jumikis, A.R. (1977), "*Thermal Geotechnics*", Rutgers University Press, New Jersey, U.S.A.
- 26- Kaplar, C.W. (1971), "*Some Strength Properties of Frozen Soil and Effect of Loading Rate*". U.S. Army, CRREL, Research Report 159.
- 27- Kersten, M.S. (1949), "*Laboratory Research for the Determination of the Thermal Properties of Soils*", Final Report, Engineering Experimental Station, University of Minnesota.
- 28- Kinoshita, S. and Ono, T. (1963), "*Heaving Force of Frozen Ground: I- Mainly on the Results of Field Researches*", Canada, National research Council, Tech. Transl. TT 1246 (1966), 30 p.
- 29- Kleiber, M. (1985) "*The Finite Element Method in Nonlinear Continuum Mechanics*", Polish Academy of Sciences, PWN, Warsaw-Poznan.
- 30- Linell, K.A. and Johnston, G.H. (1973), "*Engineering Design and Construction in Permafrost Regions*", North Am. Contrib., 2nd Int. Conf. Permafrost, Yakutsk, U.S.S.R. National Academy of Sciences, Washington, pp. 553 - 575.
- 31- Lunardini, V.J. (1981), "*Heat Transfer in Cold Climates*", Van Nostrand Reinhold Co., New York. U.S.A.
- 32- Mackinnon, R.J., and Carey, G.I. (1987), "*Treatment of Material Discontinuities in Finite Element Computations*", Int. J. Numer. Methods Engng., Vol. 24, pp. 397-417.
- 33- McFadden, T.T. and Bennett, F.L. (1991), "*Construction in Cold Region*", John Wiley & Sons Inc., N.Y.
- 34- Ministry of Housing (1990), "*The Ontario Building Code*", Part 9., Ontario, Canada.
- 35- Morgan, K., Lewis, R.W. and Zienkiewicz, O.C. (1978), "*An Improved Algorithm for Heat Conduction Problems with Phase Change*", Int. J. Numer. Methods Engng., Vol. 12, pp. 1191-1195.

- 36- Morgenstern, N.R., Roggensack, W.D. and Weaver J.S. (1980), "*The Behaviour of Friction Piles in Ice and Ice-Rich Soils*", Canadian Geotechnical Journal, Vol. 17, pp. 405-415.
- 37- Myska, A.D. and How, G.T.S. (1978), "*Installation of Pile Foundations for a Microwave Tower System*", Grillam - Churchill, Manitoba, Proceedings, 3rd International Conference on Permafrost, Edmonton, Alta., Canada, National Research Council, Vol. 1, pp. 826 - 832
- 38- Neumann, F. Ca. (1860), "*Lectures Given in 1860's*", See Riemann-Weber. Die Partiellen Differential-Gleichungen. Physik (5th ed., 1912).
- 39- Nixon, J.F. and McRoberts, E.C. (1973), "*A Study of Some Factors Affecting the Thawing of Frozen Soil*", Canadian Geotechnical Journal, Vol. 10, pp. 439-452.
- 40- Nixon, J.F. and McRoberts, E.C. (1976), "*A Design Approach for Pile Foundations in Permafrost*", Canadian Geotechnical Journal, Vol. 13, pp. 40-57.
- 41- O'Neill, K. (1983), "*Fixed Mesh Finite Element Solution for Cartesian Two-Dimensional Phase-Change*", Transactions of ASME, J. Energy Resources Technology, Vol. 15, pp. 436-441.
- 42- Parameswaran, V.R. (1978), "*Adfreeze Strength of Frozen Sand to Model Piles*", Canadian Geotechnical Journal, Vol. 15, pp. 494-500.
- 43- Parameswaran, V.R. (1980) "*Deformation and Strength of Frozen Sand*", Canadian Geotechnical Journal, Vol. 17, pp. 74-88.
- 44- Patankar, S.V. (1980), "*Numerical Heat Transfer and Fluid Flow*", McGraw-Hill Book Company, N.Y., U.S.A.
- 45- Penner, E. (1972), "*Influence of Freezing Rate on Frost Heaving*", U.S. Highway Research Board, Record 393, pp. 36 - 64.
- 46- Penner, E. (1974), "*Uplift Forces on Foundations in Frost Heaving Soils*", Canadian Geotechnical Journal, Vol. 11, (3), pp. 323 - 338.
- 47- Pewe, T.L. and Paige, R.A. (1963), "*Frost Heaving of Piles with an Example from Fairbanks, Alaska, U.S.*", Geol. Surv., Bulletin 1111-1, pp. 333 - 407.
- 48- Ralston, A. (1965), "*A First Course in Numerical Analysis*", McGraw-Hill Book Company, New York, USA.

- 49- Phukan, A. (1985), "*Frozen Ground Engineering*", Prentice-Hall, Inc. New Jersey, U.S.A.
- 50- Robinsky, E.I. and Bespflug, K.E. (1973), "*Design of Insulated Foundations*", ASCE, J. Soil Mech. Found. Div., Vol. 99, No. SM 9, pp. 649 - 667
- 51- Rolph III, W.D. and Bathe, K.J. (1982), "*An Efficient Algorithm for Analysis of Nonlinear Heat Transfer with Phase Changes*", Int. J. Numer. Methods Engng., Vol. 18, pp. 119-134.
- 52- Roose, J. and Storrer, O. (1984), "*Modelization of Phase Changes by Fictitious Heat Flow*", Int. J. Numer. Methods Engng., Vol. 20, pp.217-225.
- 53- Rubinsky, B. and Cravahlo, E.G. (1981), "*A Finite Element method for the Solution of One-Dimensional Phase Change Problems*", Int. J. Heat Mass Transfer, Vol. 24 (12), pp. 1987-1989.
- 54- Sanger, F.J. (1959), "*Discussion of Frost Penetration: Relationship to Air Temperatures and Other Factors*", Kersten, M.S. Highway Research Board Bulletin 225.
- 55- Saeki, H., Ono, T., Takeuchi, T., Kanie, S. and Nakazawa, N., (1986), "*Ice Forces Due to Changes in Water Level and Adfreeze Bond Strength between Sea Ice and Various Materials*", Proceedings, 5th Offshore Mechanics and Arctic Engineering Conference, Tokyo, Japan, Vol. 4, pp. 534 - 540, 1986.
- 56- Stelzer, D.L. and Andersland, O.B. (1991), "*Model Pile-Settlement Behaviour in Frozen Sand*", Journal of Cold regions Engineering, ASCE, Vol. 5, pp. 1-14.
- 57- Stefan, J. Uber (1891), "*Die Theorie des Eisbildung*", Imsbesonder Uber die Eisbildung im Polamere. Ann. Phys. u. Chem. Neue Folge.
- 58- Steven, G.P. (1982), "*Internally Discontinuous Finite Elements for Moving Interface Problems*", Int. J. Numer. Methods Engng., Vol. 18, pp. 569-582.
- 59- Storti, M., Crivelli, L.A. and Idelsohn, S.R. (1988), "*An Efficient Tangent Scheme for Solving Phase-Change Problms*", Computer Methods Appl. Mech. Engng., Vol. 66, pp. 65-86.
- 60- Tacke, K.H. (1985), "*Discretization of the Explicit Enthalpy Method for Planar Phase Change*", Int. J. Numer. Methods Engng., Vol. 21, pp. 543-554.
- 61- Tsyтович, N.A. (1975), "*The Mechanics of Frozen Ground*", McGraw-Hill, New York.

- 62- Velli, Y.Y., Lenzniiep, and Karpunia, A.A. (1973), "***Saline Permafrost as Bearing Ground for Construction***", Proceedings, 2nd International Conference on Permafrost, U.S.S.R. Contribution, Yakutsk, U.S.S.R., pp. 545-550.
- 63- Vyalov, S.S. (1959), "***Rheological Properties and Bearing Capacity of Frozen Soils***", United States Army Corps of Engineers, Cold Region Research and Engineering Laboratory, Hanover, N.H., Translation 74 (Translated in 1965), p. 219.
- 64- Weaver, J.S., and Morgenstern, N.R. (1981), "***Pile Design in Permafrost***", Canadian Geotechnical Journal, Vol. 18, pp. 357-370.
- 65- Zienkiewicz, O.C. (1977), "***The Finite Element Method***", McGraw-Hill, London, Third Edition.

VITA AUCTORIS

ISSA FAWZI ASSALI

The Author was born on 10 January, 1965, in Beirut, Lebanon. In 1982, he completed his high school education at " Mont Lasalle School ", Ain Saadeh, Lebanon. In June 1987, he graduated from the American University of Beirut with a degree of Bachelor of Civil Engineering. In September 1991, he enrolled in M.A.Sc. program in the Department of Civil and Environmental Engineering at the University of Windsor, Windsor, Ontario, Canada, and worked as a teaching and research assistant. He prepared this Thesis in partial fulfilment of the requirements for the degree of Master of Applied Science at the University of Windsor.